CHARACTERIZATION AND MODIFICATION OF SELECTED BIOPLASTICS

A Dissertation

Presented in Partial Fulfillment of the Requirements for the

Degree of Doctor of Philosophy

with a

Major in Natural Resources

in the

College of Graduate Studies

University of Idaho

by

Liqing Wei

Major Professor: Armando McDonald, Ph.D.

Committee Members: Randall Brooks, Ph.D.; Erik Coats, Ph.D.; Mark Roll, Ph.D.

Department Administrator: Anthony Davis, Ph.D.

May 2015

Authorization to Submit

This dissertation of Liqing Wei, submitted for the degree of Doctor of Philosophy and titled "Characterization and modification of selected bioplastics," has been reviewed in final form. Permission, as indicated by the signatures and dates given below, is now granted to submit final copies to the College of Graduate Studies for approval.

Major Professor: _____ Date: _____
Armando G. McDonald, Ph.D.

Committee Members: _____ Date: _____
Randall H. Brooks, Ph.D.

_____ Date: _____
Erik R. Coats, Ph.D.

_____ Date: _____
Mark F. Roll, Ph.D.

Department Administrator: _____ Date: _____
Anthony S. Davis, Ph.D.

Abstract

Bioplastics are becoming increasingly prominent mainly due to the growing environmental pollution caused by non-biodegradable plastics. Polyhydroxybutyrate-co-hydroxyvalerate (PHBV), the major copolymer of polyhydroxyalkanoates (PHAs) family, was biosynthesized (by mixed microbial culture fed with fermented diary manure) and characterized. The monomeric composition (HV% ~ 40%) was determined by GC-MS and NMR. ESI-MS^n and NMR analyses showed these PHBVs had random co-monomeric sequence distribution; meantime, they showed characteristic properties (crystallinity, single melting, and tensile properties) as studied by DSC and DMA. The homopolymer poly(3-hydroxybutyrate) (PHB), typically shows interesting properties such as high crystallinity and multiple melting behaviors. The effect of thermal history, such as crystallization (isothermal (temepratures = 80 to 140℃) and nonisothermal (cooling rates = 2 to 50℃/min)) and melting (heating rates = 5 to 50℃/min), on the multiple melting behavior of PHB has been studied using conventional and temperature modulated DSC (TMDSC) techniques. Results showed PHB multiple melting was ascribed to the melting-recrystallization-remelting mechanism and its crystallization kinetics varied with crystallization temperatures and cooling rates. The brittleness and poor melt strength properties of the bioplastics PHB and poly L-lactic acid (PLLA) were improved by two strategies: (i) to modify polymer structures by cross-linking, (ii) to introduce an external component by grafting, which were initiated by dicumyl peroxide (DCP) via reactive extrusion. In method (i), rheological measurements showed cross-linked PHB and PLLA (0.25 to 1 wt% DCP) separately had higher melting strength than their linear polymers due to the formation of long chain branching. Their brittleness was reduced because smaller crystal sizes were observed by hot-stage polarized microscope (HS-POM), meanwhile the reduction of crystallinity was positively correlated to DCP levels. For case (ii), cellulose (another abundant renewable material) was grafted onto PHB backbone induced by DCP (2 to 5 wt%). The chemical structures of grafted copolymer and grafting mechanism were studied by ESR, NMR, XRD and FTIR. Results suggested both amorphous and crystalline regions of cellulose were involved in the reaction. The characterization and modification approaches discussed in this dissertation provide technical guidance to either researches or industrial processing of these bioplastics.

Acknowledgements

I would like to express the deepest appreciation to my major professor Dr. Armando G. McDonald, who has a positive attitude: he continually and convincingly conveyed a spirit of adventure in regard to research. Without his fatherly guidance and persistent mentoring this dissertation would not have been possible.

I would like to thank my committee members, Drs. Randy Brooks, Erik Coats, and Mark Roll for their time and contribution to this work. Their critical comments through my whole Ph.D. research demonstrated to me that "engagement" in comparative literature will create innovative ideas.

I would like to thank the technical assistance across the University from Drs. Alexander Blumenfeld (Department of Chemistry) and Thomas Williams (University of Idaho Center for Electron Microscopy and Microanalysis), Nick Guho and Andrea Hanson (Department of Civil Engineering). I also would like to thank the faculty and staff from the Department of Forest, Rangeland and Fire Sciences, especially Drs. Thomas Gorman and Carl Morrow, and Brenda Haener. I wish to thank all previous and current graduate and undergraduate students in Renewable Materials Program, Drs. Noridah Osman, Shaobo Liang and Hui Li, Abdulbaset Alayat, Yinglei Han, and David Zack for their daily help and assistance.

Thank you all my friends. I cannot list all your names but you are always in my mind. Your friendship makes my life wonderful.

Finally, I gratefully acknowledge the financial support of Grant number 08-JV-11111133-036.

Dedication

To my beloved parents, Yinfeng Lin (mother) and Zhiguang Wei (father), for their endless love. I thank you and I love you.

To my beloved family members, Liwei and Hongwei (brothers), Shuanye and Caixia (sisters in law), Keke and Shengsheng (my nephews), for their love, encouragement and support throughout my life. I thank you and I love you.

Yours *Liqing Wei*

Table of Contents

List of Abbreviations

AF	Hamilton agreement factor
ATR	Attenuated total reflection
CCD	Chemical compositional distribution
CF	Cellulose fiber
CGP	Cellulose grafted poly(3-hydroxybutyrate)
CPI	Crossover point index
DCP	Dicumyl peroxide
DEPT	Distortionless enhancement by polarization transfer
DMA	Dynamic mechanical analysis
DRI	Dow rheology index
DS	Degree of swelling
DSC	Differential scanning calorimetry
DTG	Derivative thermogravimetry
ESI-MS^n	Electrospray ion trap multistage mass spectrometry
ESR	Electron spin resonance
FTIR	Fourier transform infrared spectroscopy
GC-MS	Gas chromatogram mass spectrometry
GDI	Global distribution index
HB	Hydroxybutyrate
HEI	High elasticity index
HS-POM	Hot-stage polarized microscopy
HSQC	Heteronuclear single quantum coherence
HV	Hydroxyvalerate
LA	Lactic acid
LCB	Long chain branching

MMC	Mixed microbial culture
MRR	Melting recrystallization remelting
MWD	Molecular weight distribution
NMR	Nuclear magnetic resonance
PHA	Polyhydroxyalkanoate
PHB	Poly(3-hydroxybutyrate)
PHBV	Poly(3-hydroxybutyrate-co-3-hydroxyvalerate)
PD	Polydispersity
PDLA	Poly(D-lactic acid)
PLA	Poly(lactic acid)
PLLA	Poly(L-lactic acid)
SEC	Size exclusion chromatography
SEM	Scanning electronic microscopy
TCI	Total crystallinity index
TFAA	Trifluoroacetic anhydride
TGA	Thermogravimetric analysis
TDF	Temperature dependence factor
TMA	Thermal mechanical analysis
TMDSC	Temperature moduluated differential scanning calorimetry
TTS	Time-temperature superposition
VFA	Volatile fatty acid
WAXD	Wide angle X-ray diffraction
XRD	X-ray diffraction

List of Symbols

ΔC_p	Heat capacity
E'	Storage modulus
E''	Loss modulus
E_a	Activation energy
G'	Viscous modulus
G''	Elastic modulus
G_c	Crossover modulus
ΔH_c	Crystallization enthalpy
ΔH_m	Melting enthalpy
ΔH_0	Melting enthalpy of 100% crystalline polymer
M_n	Number average molar mass
M_w	Weight average molar mass
M_z	Z-average molar mass
γ	Shear rates
T_a	Annealing temperature
Tan δ	Damping - the tangent of the phase angle
T_c	Crystalline temperature
T_g	Glass transition temperature
T_m	Melting temperature
V_c	Crystallization rate
ν_e	Cross-linking density
η	Steady shear viscosity
η^*	Complex viscosity
ϕ	Cooling rate
Φ	Heating rate

ω	Angular frequency
X_c %	Degree of crystallinity

List of Figures

List of Tables

Chapter 1. Introduction and literature review

1.1 Background

Strong, lightweight, and moldable plastics are used in thousands of products that improve the quality and bring convenience to our everyday lives. However, about 300 million tons of plastics are produced annually, leading to hundreds of millions of tons of plastic waste (Chen and Patel, 2012). At least 40 % of these conventional plastics are used in short-term applications (e.g. throwaway cups, utensils, and plastic bags) and after being disposed the resulting waste can quickly lead to additional environmental pollution both terrestrial and marine (Chen and Patel, 2012; Halden, 2010). It takes 500-1000 years for these petroleum-based plastics to degrade (TakePart, 2014). These negative impacts could be overcome by using plastics that are biodegradable by microorganisms, but have comparable or superior properties to conventional plastics. In brief, petroleum-based plastics are not sustainable and therefore there is a need to develop various bio-based sustainable plastics. Driven by efforts to develop more environmentally friendly products it is predicted by the European Bioplastics Association (EBA), that the bioplastic market will grow from 1.4 million tons in 2012 to almost 6.2 million tons of biopolymers produced by 2017 (EBA, 2013).

Bioplastics may be bio-based polymers that are derived from renewable feed-stocks and biodegradable that polymer can return to nature. Some of the most commonly known bio-based plastics in today's market place are poly(ethylene terephthalate) (PET), polyethylene (PE), polypropylene (PP), polyamides (PA), poly(trimethylene terephthalate) (PTT), poly(lactic acid) (PLA), polyhydroxyalkanoates (PHAs), poly(propylene carbonate) (PPC), thermoplastic starch, and other biodegradable polyesters [i.e., poly(caprolactone) (PCL), poly(butylene succinate) (PBS) and poly(butylene succinate-co-adipate) (PBSA)], and the most abundant terrestrial polymer on earth, cellulose and its derivatives (Bugnicourt et al., 2014; Chen and Patel, 2012; Garlotta, 2001; Madison and Huisman, 1999; Mekonnen et al., 2013; Ojijo et al., 2013). Except for bio-based PE, PP, PTT, PET, and PA, all other bio-based polymers just mentioned are biodegradable at different levels. The predicted bioplastics production capacities of 2017 is shown in Figure 1.1 (EBA, 2013). Among all of the bioplastics mentioned above, the bio-based PHAs, PLA, PBS/PBSA, and PPC have

gained significantly in interest since they could be completely biodegradable in appropriate environments. Of these PHAs, apart from the good biodegradability, it can be biosynthesized from renewable resources which allows large scale production (Chen and Patel, 2012; Mekonnen et al., 2013).

However, challenges still remain for the commercialization of bioplastics to replace the conventional plastics, including the relative poor performance, variability of product properties associated to different feed stocks, harvest time and locations, and high production cost (Bugnicourt et al., 2014; Mekonnen et al., 2013; Somleva et al., 2013). Ongoing efforts to improve properties and performance of bioplastics are driven by wider market acceptance.

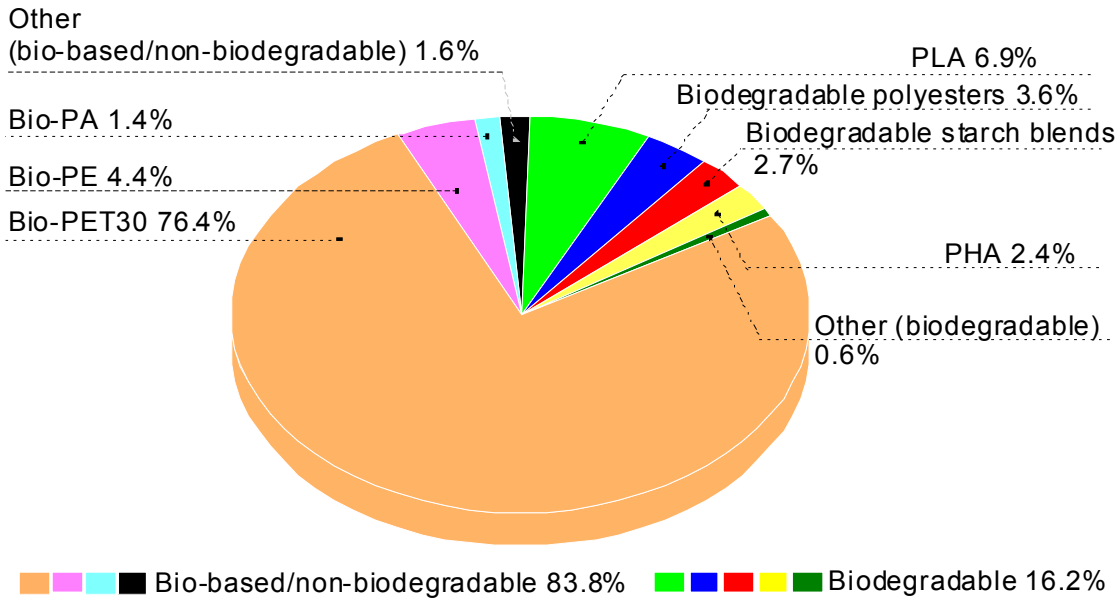

Figure 1.1. Bioplastics production capacities 2017 (by material type) (EBA, 2013).

1.2 Polyhydroxyalkanoate polymers

1.2.1 PHA production

Polyhydroxyalkanoates (PHAs) are a special group of polyesters produced by a wide variety of microorganisms as an internal carbon and energy reservoir as part of their survival

medium to grow. All metabolized carbon sources can be used for the production of PHA such as fatty acids and carbohydrate (Gumel et al., 2013). A large number of literature are available to describe the biosynthesis (Dias et al., 2006; Ienczak et al., 2013; Jendrossek and Pfeiffer, 2014; Khanna and Srivastava, 2005; Reddy et al., 2003; Suriyamongkol et al., 2007; Urtuvia et al., 2014), characterization of the PHA properties (Bugnicourt et al., 2014; Sudesh et al., 2000), opportunities and challenges of PHA products on the global market (Chanprateep, 2010), and applications of PHA (Gumel et al., 2013). Poly(3-hydroxybutyrate) (PHB), Figure 1.2a, is a homopolymer of 3-hydroxybutyrate and was the first discovered member of PHA family in 1925 by Lemoigne, while its copolymer the poly(3-hydroxybutyrate-co-3-hydroxyvalerate) (PHBV, Figure 1.2b) has attracted great attention with improved thermomechanical properties as compared to PHB. This section briefly reviews three subjects in PHA production: biosynthesis mechanism, microbial culture and feed stock.

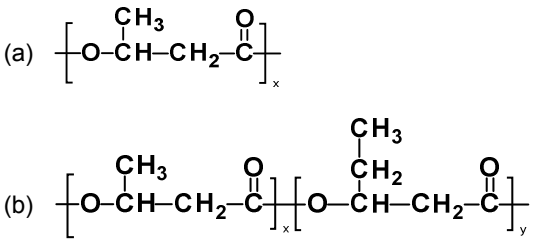

Figure 1.2. Chemical structures of (a) PHB and (b) poly(3-hydroxybutyrate-co-3-hydroxyvalerate) (PHBV).

1.2.1.1 Metabolism of PHA biosynthesis

Based on the number of carbon atoms in the monomeric units, PHA can be classified into two groups: (i) short-chain-length (SCL) consisting of 3-5 carbon atoms, and (ii) medium-chain-length (MCL) which contains 6-14 carbon atoms (Khanna and Srivastava, 2005). The chain length is determined by the characteristic substrate specificity of PHA synthase (PhaC, Figure 1.3) that can accept 3-hydroxyalkanoates (3HAs) with various range of carbon length (Gumel et al., 2013). Low specificity of PhaC can result in the production of PHA with higher diversity (Steinbüchel and Valentin, 1995). For example, the PhaC of *Cupriavidus*

necator can polymerize 3HAs containing 3-5 carbon atoms, while that of *Pseudomonas putida* (KTQQ20) polymerize 3HAs of 6-14 carbons (Khanna and Srivastava, 2005).

There are totally 14 known pathways for the PHA synthesis found to date (Meng et al., 2014). The general metabolic pathways for natural PHA production from sugar and fatty acids are shown in Figure 1.3. If PHA synthesis uses sugar (Pathway I), the pathway starts with the glycolysis of sugar to form pyruvate, and then pyruvate is converted to acetyl-CoA via the pyruvate dehydrogenase (PDH) oxidation pathway followed by the condensation of two units of acetyl-CoA to produce acetoacetyl-CoA with the presence of β-ketothiolase (PhaA). The acetoacetyl-CoA reductase (PhaB) carries out the conversion of acetoacetyl-CoA into 3-hydroxyacetyl-CoA at the expense of NAD(P)H. The final step is the polymerization of the latter monomers into PHA catalyzed by PHA synthase (PhaC). Apart from sugars PHA can also be synthesized from fatty acids (Pathway II), the short chain fatty acids [usually referred to as volatile fatty acids (VFA)], such as acetate, propionate, butyrate, valerate, and caproates (Dias et al., 2006; Pardelha et al., 2012; Riedel et al., 2013; Yu and Si, 2004). This pathway is usually used for the biosynthesis of short-chain-length PHA (SCL-PHA). The general mechanism is outlined in Figure 1.3; while the VFA molecules can be divided into groups with odd or even number of carbons, the metabolic network is schematized in Figure1.4. Simple VFA molecules (i.e., acetate and propionate) are activated directly to form acetyl-CoA and propionyl-CoA molecules, while the remaining VFA pass through β-oxidation to be converted to acetyl-CoA and propionyl-CoA with one more ATP mol is involved. When propionyl-CoA is condensed with acetyl-CoA a hydroxylvalerate (HV, 5 carbons) is generated. In addition, butyrate and valerate can be utilized directly for the respective generation of the hydroxyacyl CoA, the hydroxybutyrate-CoA and hydroxyvalerate-CoA. The latter one can be further synthesized to PHA or partially degraded to produce acetyl-CoA and propionyl-CoA for energy, growth and reducing equivalents. Pathway III directs acetyl-CoA to malonyl-CoA, and then to 3-ketoacyl-ACP to produce 3-hydroxyacyl-CoA monomers, while pathway IV utilizes butyric acid without entering the β-oxidation procedure to generate S-3-hydroxybutyryl-CoA. Other unconventional PHA biosynthesis follows pathways V to XIV.

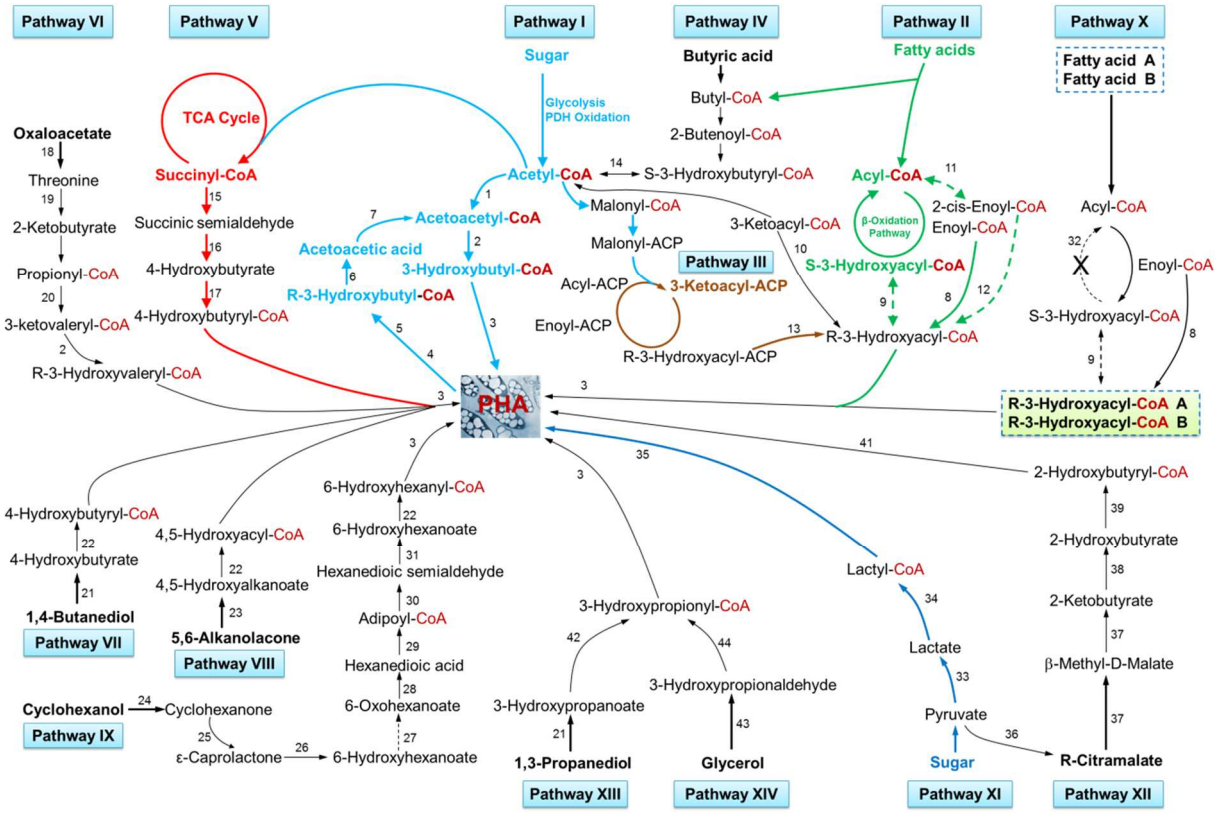

Figure 1.3. Known 14 pathways leading to PHA biosynthesis (Meng et al., 2014). ACP: acyl carrier protein.

1.2.1.2 Microbial cultures

1.2.1.2.1 Pure cultures

Generally, PHA production uses pure cultures and follows a two-stage batch production process. In the first stage, an inoculum of bacteria is introduced into a sterile solution with suitable carbon source and nutrients, and then in the second stage, an essential nutrient (i.e., N, P or O_2) is deliberately limited and the accumulation of PHA would occur (Laycock et al., 2013). To date over 300 species of Gram-positive and Gram-negative bacteria and archaea are known to synthesize PHAs as intracellular insoluble cytoplasmic inclusion bodies under conditions in which growth is restricted by either an external (lack of nutrient or electron acceptor) or an internal limitation arising from the alternate substrate availability (Albuquerque et al., 2011; Janarthanan et al., 2014; Marshall et al., 2013). Only a few

species, such as *Cupriavidus necator* (formerly known as *Ralstonia eutropha* or *Cupriavidus necator*), *Alcaligenes latus*, *Azotobacter vinelandii*, *Pseudomonas oleovorans*, *Paracoccus denitrificans* and *Protomonas extorquens*, are able to produce sufficient PHA for pilot-scale production (Chanprateep, 2010; Dias et al., 2006).

C. necator has been well studied and utilized due to its ability to produce large amount of PHB from simple carbon source. In the 1970s, PHBV was produced and commercialized by Imperial Chemical Industries Ltd. (ICI/Zeneca BioProducts, Bellingham, UK) under the trade name Biopol^{TM} using fed-batch culture of *C. nector* (Holmes, 1985). In 1996 this technology was sold to Monsanto then to Metabolix, Inc. Using *C. nector* Chanprateep et al. (2010) obtained 70% (w/w) yield (based on dry biomass) of MCL poly-3-hydroxybutyrate-*co*-4-hydroxybutyrate (PHB-*co*-4HB) with 38% of 4HB. *A. latus*, similar to *C. nector* in terms of PHA production, was reported to produce SCL-PHA (PHB and PHBV) by Chemie Linz AG, Austria and later also commercialized by Gesellschaft Biotechnologische Forschungs (GBF, Austria), and then Biomers (Germany) (Chen, 2009).

The *Pseudomonas* species is known for MCL-PHA production. It has been reported that more than 150 units of MCL-PHA monomers have been produced by culturing various *Pseudomonas* strains on different carbon substrates (Rai et al., 2011a). *Pseudomonas* species can be grown on both structurally related (i.e., alkanes, alkenes and aldehydes) and unrelated carbon sources providing precursor substrates that are not similar to its structure (Walle et al., 2001). In general, *Pseudomonas* produces MCL-PHA always as a copolymer (Kim et al., 2007), but there are some exceptions, for example *P. mendocina* was able to accumulate a homopolymer poly(3-hydroxyoctanoate) (PHO) of 31% in the dry cell weight if reactor is fed on octanoate (Rai et al., 2011a). Ramalingam et al. attained a 35.6% (w/w) PHA with *P. putida* MTCC 102 (Type B) (Ramalingam et al., 2011). Liu et al. (2011b) reported the use of β-oxidation cycle inhibition to produce MCL-PHA homopolymer by *P. putida* (KTQQ20) fed by fatty acids. When the reactor is fed with dodecanoic acid to the mutant strain the MCL-PHA accumulation could reach to 10% (w/w) in the dry cell. Recent studies on this pathway indicated when the MCL PhaC (C_6-C_{14}) was substituted by a less specific PhaC (*phaPCJAc*) both SCL and MCL monomers (C_3-C_7) could be produced which was the building blocks for the block copolymer polyhydroxybutyrate-block-poly(3-

hydroxyvalerate-co-3-hydroxyheptanoate) (PHB-*b*-PHVHHp) (Li et al., 2011). Through the similar engineering β-oxidation pathway on chromosomes Tripathi et al. (2013a) successfully obtained PHA with polymer content was up to 48.2% (w/w). More recent studies have identified MCL-PHA synthesis specifically follows fatty acid pathway (Pathway II, Figure 1.3) (Cerrone et al., 2013; Jiang et al., 2012; Le Meur et al., 2012). By fed-batch and continuous culture *P. oleovorans* has been used to achieve high concentration and yield of PHA (63%, w/w) grown on n-alkanes (Chen, 2009; Khanna and Srivastava, 2005). It has been reported that *P. oleovorans* and *P. putida* are capable to synthesize over 100 PHAs with various monomer structures. Another MCL-PHA producer is *Aeromonas hydrophila* which was able to produce 47% (w/w) poly(3-hydroxybutyrate-co-3-hydroxyhexanoate) (PHB-*co*-HHx) with the polymer productivity of about 3 g/L in the broth (Liu et al., 2011a). It was seen genetic transformation is associated with fatty acids biosynthesis increased the yield of P(HB-*co*-HHx) by 63% compared to the native strain with only the genes of the acetic acid metabolism deleted.

Advantages of utilizing *Escherichia coli* strains for the PHA production have been well studied and reviewed and in the past few decades (Chen, 2009; Gumel et al., 2013; Khanna and Srivastava, 2005). Microbial metabolic engineering and molecular cloning technologies have enhanced the academic/industrial interest in novel PHA production and the productivity of conventional PHA (Gumel et al., 2013; Meng et al., 2014). For example, *E. coli* strains have been metabolically engineered to regulate the expression of short chain fatty acid catabolism, which significantly enhance the expression of short chain complexed PHB (cPHB) (Filippou et al., 2011; Meng et al., 2014; Theodorou et al., 2011). In addition, the use of recombinant *E. coli* succeeded to produce poly(4-hydroxybutyrate) (P4HB) using glucose as a sole carbon source by the pathway containing genes encoding succinic semialdehyde dehydrogenase and PHB synthase of *R. eutropha* (or *C. necator)* to enhance the carbon flux toward P4HB synthesis (via pathway V in Figure 1.3). The production of PHA by the recombinant *E. coli* harboring *R. eutropha* can reach to 80-90% yield of the cell dry weight (Dias et al., 2006). More recently the engineering of *E. coli* by transforming PHA synthase gene PhaC1 (STQK), SCL-PHA supplying genes (PhaA and PhaB), and MCL-PHA monomer supplying genes (PhaG and PP0763) was successful to obtain the

transformants *(E. coli* LS5218-STQKABGK*),* which was used to improve the production of SCL-*co*-MCL PHA with up to 53% yield (Tappel et al., 2014). In addition, PhbC and orfZ cloned from C. necator H16 and *C. kluyveri* were transformed into a β-oxidation weakened *P. putida* KTOY08ΔGC and a mutant of *P. putida* KT2442 to achieve the mutant KTHH06 which could produce block copolymer PHB-*b*-P4HB (Hu et al., 2011; Wang et al., 2009). Therefore, the cloning technology and metabolic engineering progress to reengineering the central metabolism of PHA producers achieved in recent years have significantly increased the productivity and diversity of PHA.

1.2.1.2.2 Mixed cultures

Commercial PHAs are produced using pure or recombinant cultures at higher cost, which makes it less competitive to conventional petroleum based plastics (e.g. PP and PE) as bulk materials in the point of prices. The use of mixed microbial cultures (MMCs) has been proposed as an ideal alternative to the cost-effective process of PHA production (reviewed by Salehizadeh and Van Loosdrecht (2004), Dias et al. (2006) and Laycock et al. (2013)), since the use of open systems which would not require sterile conditions (Oehmen et al., 2014). Life cycle assessment and financial analysis of PHA production by MMCs were undertaken by Gurieff and Lant (2007). They found that PHA production was more preferable to biogas production and was economically attractive as compared to PHA production with pure cultures, while the environmental impacts involved in this PHA production process were significantly lower than that of HDPE production.

The biosynthesis of PHA in mixed cultures was first discovered in wastewater treatment plants designated for an enhanced biological phosphorus removal (EBPR) when PHA was recovered from the extracts of activated sewage sludge, well-known MMCs (Wallen and Rohwedder, 1974). Wastewater derived PHAs are currently being used for PHA synthesis in an industrial scale (Morgan-Sagastume et al., 2010) and they possess the comparative thermomechanical properties as compared to petroleum base plastics, e.g. PP. Numerous researchers found that most PHA production via MMCs relies on selection cultures that favor organisms with high PHA-storing capacity (Albuquerque et al., 2010a; Kleerebezem and Van Loosdrecht, 2007; Salehizadeh and Van Loosdrecht, 2004). One means of the

enrichment in PHA-accumulating organisms is via subjecting the MMCs to transient conditions of carbon supply when the external substrate is excess (feast) or limited (famine) (feast/famine (FF)) cycles, usually known as aerobic dynamic feeding (ADF) process (Beccari et al., 1998; Beun et al., 2002; Majone et al., 1996). A portion of the consortium is removed or selected during each cycle of ADF, and hence microbial consortium is ecologically engineered. The organisms are able to store carbon during feast phase which occurs immediately after the feeding triggers the bacterial growth and then use that stored carbon to grow during famine phase are selectively enriched. After a long period of starvation, an open MMC system operated under ADF conditions, about 70% of the carbon substrate uptake are towards to PHA storage (Beun et al., 2002).

Another strategy adopted to accumulate PHA is to use alternating aerobic-anaerobic conditions, and this case was that used in EBPR process mentioned above when PHA production by MMC was observed. Two types of microorganisms are anaerobic storage of carbon source in MMC and capable to synthesize PHA: (i) polyphosphate accumulating organisms (PAO) and (ii) the glycogen-accumulating organisms (GAO) (Bengtsson et al., 2010; Kong et al., 2004; Pisco et al., 2009; Salehizadeh and Van Loosdrecht, 2004). During anaerobic phase, PAOs assimilate carbon substrates store them as PHAs (Kong et al., 2004; Sheik et al., 2014). When entered into aerobic conditions, PAOs oxidize PHAs, which provides energy for polyphosphate accumulation, resulting in the P removal from the wastewater. This approach could give PHA yield about 20% (Dias et al., 2006). The higher PHA content (30 and 75%) was achieved in a “PHA accumulating bacteria enhanced reactor” (PABER) process; nonetheless it is difficult to control the PHA yield in this process.

In order to maximize the PHA productivity many research groups have developed various strategies, especially in the final production stage via optimizing the culture enrichment stage under different operating conditions (Albuquerque et al., 2007; Albuquerque et al., 2010b; Jiang et al., 2009; Serafim et al., 2008). As reported 89% and 74% PHA content were obtained by Johnson et al. (2009) and Albuquerque et al. (2010b), respectively, through optimizing the selection efficiency of specific culture in the sequencing batch reactor (SBR).

Although MMC together with the FF operation has been demonstrated to be an effective condition to achieve a high PHA content, the volumetric productivity is still lower than that using pure culture. This was ascribed to the lower cell concentration of ADF processing. It was reported that the cell concentration of MMC PHA-accumulating culture selection reactor was about 10 g/L (Albuquerque et al., 2010a; Albuquerque et al., 2007; Albuquerque et al., 2011; Albuquerque et al., 2010b), while using pure culture this value can be larger than 100 g/L. Therefore, to develop strategies to improve the volumetric productivity of PHA production by MMC is necessary to make it competitive with the pure culture PHA production.

Another advantage to use MMC for PHA biosynthesis is in the term of PHA compositions. Using this approach to produce a wider diversity of HA monomers other than the simple 3HB, such as 3-hydroxy-2-methyl-valerate (3H2MV), 3HHx and other unconventional monomers as the building block of MCL-PHAs, and therefore to meet the increasing demands for different PHA properties would trigger the research interests of this field in the future. To note that the fractions of monomers other than 3HB are greatly higher by using MMC system than that of pure culture which typically incorporated with refined sugars requiring numerous amount of co-substrate (i.e. alcohols and organic acids) but only a small amount of monomers other than 3HB was obtained (Albuquerque et al., 2011). In addition, the composition of monomers is highly dependent on the carbon sources that supplied to the MMC PHA production system.

1.2.1.3 Feed stock

1.2.1.3.1 Pure substrate

One of the major reasons resulting in the high price of PHA is the high cost of carbon source or feed-stock in conjunction with pure culture. A wide range of commercial carbon sources such as sugars (e.g. glucose, fructose, sucrose, xylose, lactose), starch (e.g. cassava starch and potato starch), alcohols (e.g. methanol, n-amyl alcohol, n-pentanol and ethanol), alkanes (e.g. hexane to dodecane), vegetable oils, and short/long chain fatty acids (e.g. butyrate upwards) have been used for PHA industrial production (Chanprateep, 2010; Koller et al., 2010). Although these pure substrates have been used to generate reasonably high PHA

contents (48-77 % in dry cell weight), they are still costly, edible (food crops) and are therefore not competitive for large scale of PHA production (Allen et al., 2014).

1.2.1.3.2 Waste stream as substrate

Selecting the suitable carbon source is one of the important solutions that can reduce the total PHA production cost. Studies have found that substrate cost accounts for 28-50 % of the total cost of PHA production (Sudesh and Abe, 2010). Inexpensive carbon/nitrogen sources such as agricultural residues or industrial waste and by-product streams have become very competitive carbon sources to minimize the production cost of PHA (Koller et al., 2005). The substrate is generally matched to the bacterial culture, for example *C. necator* can utilize organic acids such as lactate, acetate and butyrate, but not glucose, fructose or xylose, whereas *A. latus* is a growth associated producer of PHA to produce PHB by consuming sucrose (Allen et al., 2014). Similarly, wild type *P. oleovorans* is known for MCL-PHA production; however, it does not utilize substrates of fructose or glucose, but grows on substrates such as fatty acids or carbon sources which can undergo fatty acid synthesis (e.g. n-alkanoic acids, n-alkanals and n-alkanes (He et al., 1998). The waste-based feed-stocks have complex composition and comprise more substrates that can be metabolized by wide range of bacteria to PHA. Hence, the idea of utilizing the waste raw materials with higher varieties by a combination of different microbial species, i.e. MMC, was proposed.

Numerous articles have reported to use waste stream successfully to produce PHA of the world; for example, the VFAs from fermented molasses (an industrial by-product of sugar production) have been used to produce PHA (Albuquerque et al., 2010a; Albuquerque et al., 2007; Albuquerque et al., 2010b; Bengtsson et al., 2010; Kulpreecha et al., 2009; Oehmen et al., 2014; Pardelha et al., 2012; Pardelha et al., 2014; Pisco et al., 2009). Corrone et. al. (2013) utilized VFAs derived from the anaerobic digestion of grass, one of the typical lignocellulosic biomass, for the production of MCL-PHA. Recently, another research group successfully utilized lignin derived from corn stover as feedstock subjected to pretreatment to obtain glucose and VFAs and then fed for MCL-PHA production by pure culture *P. putida* KT2440 (Linger et al., 2014). Because VFAs can be readily stored as PHA by

MMCs, so most of these studies reported have been carried out for PHA production by MMCs using organic acids (e.g. acetate, propionate, butyrate, and valerate) as carbon sources. As for the metabolism involved in this process, Oehmen and coworkers (2014) have summarized it into 3-stage process in their recent work: (i) fermentation of the feedstock into a VFA-rich stream that is used as the carbon source for the following stages, (ii) a culture enrichment stage, operated under ADF, and (iii) the PHA production and accumulation stage using the enriched biomass as inoculum. This three-stage process has been demonstrated by other researchers which also employ waste as feed stocks including fermented paper mill effluents (Bengtsson et al., 2008), fermented olive oil mill effluents (Beccari et al., 2009; Dionisi et al., 2005), and even the fermented cheese whey and milk whey (Duque et al., 2014). The metabolic network of VFAs conversion to PHA by MMCs has recently been proposed by dynamic modeling as depicted in Figure 1.4 (Duque et al., 2014; Pardelha et al., 2012; Pardelha et al., 2014). In these studies the VFAs were grouped according to carbon numbers (even or odd).

Waste lipids from a variety of sources, such as used cooking oil (Verlinden et al., 2011), *Vernonia galamensis* oil (Allen et al., 2014) and palm oil (Gumel et al., 2012; Loo et al., 2005), have been directly used for PHA production. The crude by-products (i.e. glycerol) of the process from biodiesel production have also been assessed for PHA production (Dobroth et al., 2011; García et al., 2013). Moita and Lemos (2012) employed poultry waste pyrolysis bio-oil as feed stock to successfully obtain PHBV in high yield (70%) with a 30% HV content.

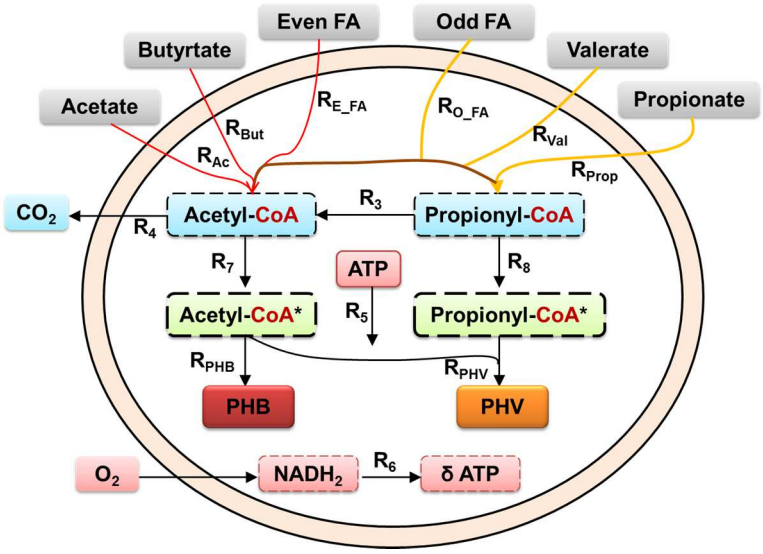

Figure 1.4. Schematic representation of the metabolic model for the PHA production process from VFAs fermented from sugar cane molasses by MMCs under aerobic conditions (Pardelha et al., 2012). Light grey are carbon sources present in fermented molasses, long dash are intermediate metabolites, and R stands for different reaction flux.

Further research is still required to understand the effects of factors such as feeding strategy (continuous/pulse) and pH control in order to achieve higher volumetric productivity and PHA content with MMC (Albuquerque et al., 2011; Villano et al., 2010). With MMC, another obstacle to upscale the PHA production fed with a waste stream is to control the compositional distribution of PHAs.

1.2.2 Diversity of PHA

The kinetics of PHA chain biosynthesis are rapid, and the high degree of diversity present in biological systems indicates a wide range of polymer chains could be synthesized by bacteria (McChalicher and Srienc, 2007). Therefore, the final product could be a complex mixture of random copolymers and/or homopolymers, or even a block copolymer. The majority of documentations related to PHA diversity has been focused on the manipulation of monomeric variations because it is difficult to control the composition of PHA main chain structure (Meng et al., 2014). Most recently PHA compositions, including homopolymers, random copolymers and block copolymers, have been successfully

monitored by engineering the metabolic pathways of the PHA production process (Chung et al., 2011; Liu et al., 2011b; Tripathi et al., 2012; Tripathi et al., 2013a; Tripathi et al., 2013b; Wang et al., 2013a). Therefore, by controlling the polymer microstructures new and favorable PHA properties are expected to be achieved.

1.2.2.1 Homopolymers

As mentioned earlier, PHB was the first and most extensively studied PHA homopolymer. To date only limited types of PHA homopolymers have been synthesized (Table 1.1), such as SCL-PHAs: PHB, P3HP, P4HB, PHV; and other non-fully characterized MCL-PHAs: P3HHx, P3HHp, PHO, P3HD, P3HDD, P3HTD, P3HPhV, P3HPE, PHU, P3H2MV (Chen, 2010; Laycock et al., 2013; Meng et al., 2014). PHA homopolymer with four to ten carbon atoms (C_4-C_{10} PHA homopolymers) have been successfully biosynthesized. With the technological progress in the metabolic engineering area greater varieties of PHA homopolymers will be produced and commercialized.

1.2.2.2 Random copolymers

In a polymer, if the sequence of monomers of the copolymer follows a statistical rule, the polymer is considered to have a random comonomeric distribution. In other words, if the probability of a given monomer at a particular position in the chain is equal to the mole fraction of that monomer along the molecular chain, then the polymer may be referred to as a truly random copolymer. So far most commercially or lab synthesized PHA copolymers are random (Chen, 2009; Laycock et al., 2013). Common random PHAs include PHBV, P(3HB-*co*-4HB), P(3HP-*co*-4HB), etc. (Table 1.1). With the random incorporation of the second monomer into the homopolymer units, the resulting random copolymer shows strongly improved properties, including the melting temperatures, crystallinity, and brittleness, over the homopolymers (Andreeßen and Steinbuchel, 2010). By adjusting the feed substrate compositions the diversity of PHAs can be manipulated. For example, Dai et al. (2008b) reported in a GAO process when the ratio of propionate to acetate in the feed reagent was reduced less 3H2MV and 3H2MB units of the final P(3HB-*co*-3HV-*co*-3H2MV-*co*-3H2MB) copolymer were observed and a mixture of random copolymer was

produced, whereas if propionate was fed alone only a random copolymer was generated. A wild type *Burkholderia sp.* was fed fructose/crude palm kernel oil, sodium valerate and 4-methylvaleric acid as well to successfully produce a blend of copolymer P(3HB-*co*-19mol% 3H4MV) (Lau et al., 2011).

1.2.2.3 Block copolymers

A block copolymer is a polymer consisting of two or more homopolymer subunit blocks connected to each other by covalent bonds (Chen and Thouas, 2014). Block copolymers are classified based on the number of blocks they contain and how the blocks are arranged. For example, block copolymers with two and three distinct blocks are called diblock copolymer (-A-A-A-A-A-A-A-B-B-B-B-B-B-B-B-; A and B are different monomer units) and triblock copolymer (-A-A-A-A-A-A-A-B-B-B-B-B-B-B-A-A-A-A-A-A-A-A-), respectively; and those with more than three blocks are called multiblocks [(-A-B-)*n*: (-A-A-A-A-A-B-B-B-B-B-B-)*n*]. This coblock structure would possess the properties of each block and potentially achieve new properties that cannot be available by polymer blending. Due to the specificity of PHA synthases, the bacterial synthesis of PHA block copolymers is less common. Peterson et al. (2006) reported the first biosynthesized PHA block copolymer of PHB-*b*-PHBV by pure culture (*C. necator*) using periodic substrate addition regime. By employing sequential feeding regime other block PHA copolymers have recently been successfully biosynthesized in lab (Table 1.1), such as PHB-*b*-P3HVHHp (Li et al., 2011), PHB-*b*-4HB (Hu et al., 2011), P3HP-*b*-4HB (Tripathi et al., 2013b), PHB-*b*-3HHx (Tripathi et al., 2012), PHB-*b*-3HP (Wang et al., 2013a), P3HHx-*b*-P(3HD3HDD) (Tripathi et al., 2013a). All these block copolymers showed several improved properties as compared to their homopolymers, random copolymers, and blending of their homopolymer as well. McChalicher and Srienc (2007) produced block copolymer PHB-*b*-PHBV using *C. necator* and compared the properties with random copolymer films with comparable HV content. An alternating feeding strategy (fructose/valeric acid) was developed to obtain a 50/50 block copolymer. Later, Pereira et al. (2008) reported the production of PHB-*b*-PHBV with *C. necator* fed fructose in the first stage and propionic acid in the second stage.

Table 1.1. Biosynthesized PHA homopolymers and different types of copolymers.

PHA classification	Polymers[a]	Literature
Homopolymers	PHB	(Chen et al., 2006; Coats et al., 2007a; Coats et al., 2007b; Dai et al., 2015; Dobroth et al., 2011; Madden et al., 1998)
	P3HP	(Andreeßen and Steinbuchel, 2010)
	P4HB	(Steinbüchel et al., 1994; Zhou et al., 2012)
	P3HV	(Coats et al., 2007b; Steinbüchel et al., 1993)
	P3HHx	(Tripathi et al., 2012; Wang et al., 2010)
	P3HD, P3HDD	(Liu et al., 2011b)
	P3HO	(Rai et al., 2011b)
	P3HPhV, P3HPE, PHU, P3H6PHx, P3HTD, P3H2MV, P3HHp	(Meng et al., 2014)
Random copolymers	PHBV	(Horng et al., 2013; Ishihara et al., 1996; Yang et al., 2013; Yoshie et al., 1995)
	P(HB-*co*-4HB)	(Doi et al., 1988; Li et al., 2010; Mitomoa et al., 2001)
	P(3HP-*co*-4HB)	(Tripathi et al., 2013b)
	P(3HP-*co*-HB)	(Wang et al., 2013b)
	P(HB-*co*-3HHx)	(Loo et al., 2005)
	P(HB-*co*-MCL 3HA)	(Chen et al., 2006)
	P(HB-*co*-3H4MV)	(Tanadchangsaeng et al., 2010)
	P(HB-*co*-LA)	(Jung et al., 2010)
	P(HB-*co*-3HV-*co*-3H2MV-*co*-3H2MB)	(Dai et al., 2008a, b)
Block copolymers	PHB-*b*-PHBV	(Pederson et al., 2006)
	PHB-*b*-4HB	(Hu et al., 2011)
	P3HP-*b*-4HB	(Tripathi et al., 2013b)
	PHB-*b*-P3HVHHp	(Li et al., 2011)
	PHB-*b*-3HHx, PHB-*b*-P(3HV-*co*-3HHp)	(Tripathi et al., 2012)
	PHB-*b*-3HP	(Wang et al., 2013a)
	P3HHx-*b*-P(3HD-*co*-3HDD)	(Tripathi et al., 2013a)

[a] Abbreviations: 3-hydroxybutyrate (HB); 3-hydroxypropionate (3HP); 4-hydroxybutyrate (4HB); 3-hydroxyvalerate (3HV); 3-hydroxyhexanoate (3HHx); 3-hydroxydecanoate (3HD); 3-hydroxydodecanoate (3HDD), 3-hydroxyoctanoate (3HO), 3-hydroxy-5-phenylvalerate (3HPhV); 3-hydroxy-4-pentenoic acid (3HPE); hydroxyundecenoate (HU); 3-hydroxy-6-phenylhexanoate (3H6PHx); 3-hydroxytetradecanoate (3HTD); 3-hydroxy-2-methyl-valerate (3H2MV); 3-hydroxyheptanoate (3HHp); hydroxyalkanoic acid (HA); 3-hydroxy-4-methylvalerate (3H4MV); 3-hydroxy-2-methylvalerate (3H2MV); lactic acid (LA); 3-hydroxy-2-methylbutyrate (3H2MB); *co*: random copolymer; *b*: block copolymer.

1.2.3. Characterization of PHAs

The great diversity of PHAs give it a wide range of properties such as (Bugnicourt et al., 2014): (i) good UV resistance but poor acid/base resistance, (ii) soluble in chloroform and other chlorinated hydrocarbons but insoluble in water, (iii) less "sticky' in the polymer melt than conventional polymers, especially the copolymer (i.e. PHBV with higher HV content), and (iv) nontoxic and biocompatible suitable for biomedical applications. Before stating the applications of PHAs, polymer characterization involved in determining the microstructures and properties are covered in this section.

1.2.3.1 Comonomer compositional distribution

One of the effective approaches to control the chemomechanical properties of PHA copolymers is to manipulate the monomer sequence distribution within the polymer chain. Tanadchangsaeng et al. (2010) postulated that the complex chemical compositional distribution (CCD) can be varied by factors, including bacterial strains, carbon substrates, pH in the fermentation medium, physiological state, and other conditions during cultivation. If the same carbon source is utilized by the same microorganism to synthesize two polymer samples, one of which could be a random copolymer and the other could be a mixture of two random copolymers. The CCD of PHBV and P(HB-*co*-3H4MV) has been investigated by ^{13}NMR (diad and triad analysis) to evaluate the extent of deviation of the comonomeric composition distribution from the statistically random (Bernoullian) distribution. In order to estimate the deviation from Bernoullian statistics, a parameter *D* defined as $D = F_{BB}F_{VV}/F_{BV}F_{VB}$ (B = 3HB, V = 3HV) has been calculated (Žagar et al., 2006), where F_{BB}, F_{VV}, F_{BV}, F_{VB} are the molar fractions of diad BB, VV, BV, and VB, respectively. If D is close to 1.0 the copolymer has completely random distribution; while block copolymers have this value is >> 1.0 and that of alternative copolymers would be close to 0, respectively. The degree of randomness in the copolymer chain based on the triad sequence distribution analysis can be calculated from the coefficient *R* which is defined as $R = L_B^R/L_B^E = L_V^R/L_V^E$ (L_V^E and L_B^E are the experimental number average lengths of 3HV and 3HB blocks in the PHBV copolymers), which is calculated from triad fractions (i.e. VVV, BVB, BVV, and VVB, etc.) (Žagar et al., 2006). The R value is unity for random

copolymers, and 0 for blocky or mixture of polymers (Doi et al., 1988; Kamiya et al., 1989). Except for the Bernoullian Model, the other two models, first-order and second-order Markovian Models were also well developed to assess the randomness of PHA copolymers from NMR diad/triad analysis (Kamiya et al., 1989). Several studies used FT-IR spectroscopy and fast atom bombardment mass spectroscopy (FAB-MS) (Ballistreri et al., 1991) to investigate the randomness of PHA copolymers. Recent research employs multistage electrospray ionization mass spectrometry (ESI-MS^n) to assess the CCD of PHBV oligomers with different HV content (Žagar et al., 2006).

1.2.3.2 Crystalline structures and crystallization kinetics

The PHB homopolymer is a well known semicrsystalline polymer. PHB single crystals have been prepared for surface morphology, crystal structure (X-ray diffraction, XRD) and microscopic (polarized) studies (Hu et al., 2013; Sudesh et al., 2000); while, the crystallization rate and degree of crystallinity of PHAs are generally investigated by well developed techniques, including FTIR, XRD and differential scanning calorimetry (DSC) (Bloembergen et al., 1986). All these PHA analyses are correlated to the crystallization kinetics which are dependent on the nucleation rate and crystal growth rate. Spherulites are formed from molten PHB and lamellar crystals grow radially in axis *a* together with twisting in *b* and *c* axes and rotating about *a*, and hence banded textures are usually seen for these spherulites (Barham et al., 1984; Tanaka et al., 2005). It was also found the banding patterns change with processing temperature and PHA molecular weight (molar mass). If the PHA polymer crystallizes from the melt isothermally the crystal spherulite radians were linearly related to time, meanwhile the growth rate was also correlated to the isothermal crystallization temperatures. The spherulite growth rate of PHB has been studied extensively in a ralative narrow crystallization temperature range, which was similar to PP, nylon 6, and PET. The average thickness of single PHB crystals was in the range of 4 to 10 nm, which was dependent on its molecular weight, casting solvent and crystallization temperature (Fujita et al., 2005). In the review of Laycock et al. (2013) the crystal forms were summarized based on PHA homopolymers or copolymer, the former one having a α- and β-form crystals while the later copolymer (i.e. PHBV) was addressed to be an isodimorphic copolymer.

The crystallization kinetics of PHA polymers are important because these govern commercial processes used and product applications. Crystallization kinetics can be influenced by the thermal history of the polymer which are always investigated by various models derived from DSC data (Gunaratne and Shanks, 2006a; Gunaratne et al., 2004; Hu et al., 2013). Different models/equations are used to describe the crystallization kinetics of isothermal crystallization of PHB using the Avrami equation and nonisothermal crystallization using Tobin and Ozawa method is achieved by plotting the relative degree of crystallinity as function of temperature (Ziaee and Supaphol, 2006). When PHAs are crystallized from the melt at various cooling rates, not only the degree of crystallinity (X_c %) and crystalline temperatures (T_c) will be different, but the subsequent melting behavior will also vary (An et al., 1998; Gunaratne and Shanks, 2006a; Gunaratne et al., 2004). In addition, how fast the sample is being heating until melt also affects the cystallinity and crystallization rate of PHAs. During industrial melt processing (e.g. injection molding and extrusion) the crystallization rate determines the cycle time. If crystallization occurs more slowly the smaller crystal sizes tend to be formed, and therefore less cycle time will be needed for thermal transfer in the process (Sudesh and Abe, 2010). Due to the natural origin of PHB, it is free of heterogeneties, impurities, and catalyst residues that could act as a heterogeneous nucleator. This may also explain why nucleation agents are added to PHA (e.g. boron nitride) to accelerate crystallization and increase the numbers of small crystals formed, especially for PHB based copolymers. To note, the brittleness of PHB is a result of secondary crystallization with aging (or storing time) at room temperature and will be discussed further in relation to its mechanical properties.

1.2.3.3 Thermal properties

1.2.3.3.1 Melting and glass transition temperatures

PHA thermal properties vary based on its origin. The differences would be from variations in the biological system used (e.g. species), biosynthesis conditions (e.g. carbon substrate, pH, etc.), and recovery method used (solvent extraction, mechanical disruption, chemical digestion, or enzymatic digestion, etc.). On average, PHA melting temperature (T_m) ranges from 50 to 180 $^{\circ}$C, which is usually determined by DSC analysis. The typical T_m of solvent

casted films (SCF) is about 180 °C for homopolymer PHB. The T_m of SCF samples of PHA copolymers are highly dependent on the monomer composition. When 3HV content is lower than 42 mol% the T_m is decreased with an increase of HV content; whereas T_m started to increase when HV content is increased from 42 to 88 mol% (Bluhm et al., 1986). PHB usually shows multiple (double) (T_{m1} and T_{m2}, in the order of low to high temperature) melting peaks in the DSC analysis, and this phenomenon is always observed for some of its copolymers (e.g. PHBV) (Table 1.2). The origins for the double melting behavior of PHAs is still being researched, although it was found the endothermic peak associated to T_{m2} becomes smaller in area as the heating rate is increased, and the lower endothermic peak exhibited the opposite trend (Sudesh and Abe, 2010). With the endotherm involved in the melting process, the degree of crystallinity (X_c %) of PHAs is always estimated by using the value of enthalpy (146 J/g) that 100% crystalline PHB is obtained. This value could reach 60 to 80%.

At the same X_c %, the material with a lower glass transition temperature (T_g) is considered to be more flexible due to longer side chains with higher mobility (Laycock et al., 2013). Furthermore, the T_g of PHAs is also usually determined by DSC analysis. The T_g of PHB is in the range of -20 to 10 °C and is also influenced by factors that influence its T_m's. T_g's of PHB based copolymers, such as P(HB-*co*-3HV), P(HB-*co*-3HHx), P(HB-*co*-3HP) and P(HB-*co*-4HB), showed a negative relationship with an increase in the second monomer fraction. This decreasing trend was more apparent if the monomer had a long side chain. Therefore, incorporation of different hydroxy-acid monomer units to the polymer can increase the molecular weight of the resulting copolymer, which can influence its crystallinity and transition temperatures (T_m and T_g) as well as their mechanical properties.

Table 1.2. Thermal properties of selected PHB and PHBV with various 3HV content from literature.

Polymer	T_g (°C)	T_{m1} (°C)	T_{m2} (°C)	X_c (%)	Reference
PHB	-20-10	175-180	175-180	30-60	(Avella et al., 2000)
PHBV					
10mol% 3HV[a]	1.6	-	168	34	(Reis et al., 2003)
12mol% 3HV[b]	-2.8	143	156	5.3	(Modi et al., 2013)
30mol% 3HV	-10	158	172	38.6	(Dagnon et al., 2009)
72mol% 3HV[a]	-30	-	99	7	(Avella et al., 2000)
97mol% 3HV[c]	-44	-	42	8	(Reis et al., 2003)

[a] Sample was produced by mixed culture; [b] commercial sample (Sigma-Aldrich, St Louis, Missouri, USA); [c] sample was produced by pure culture.

1.2.3.3.2 Thermal stability

The thermal processing of PHAs is challenging because of their relative low decomposition temperatures that are close to their melting temperatures, and directly limits applications. A short exposure of PHB to temperature (~180 °C) can result in the generation of primary degradation products such as crotonic acid and various oligomers via cis-elimination of –CH groups and six-member ring transition (Bugnicourt et al., 2014). Further exposure to higher temperature (i.e. >300 °C), secondary products including propene, ketene, ethanol, acetaldehyde and CO_2 are produced due to the decomposition of the primary byproducts. In the practical processing of PHB, additives (i.e. lubricant) are added to reduce the degradation of polymer chains, however, leading to the drop of molecular weight and melt viscosity, and meantime crystallization temperature will be lowered and crystallization will take longer. Compared to PHB, its copolymers showed lower T_m's, and hence less degradation will occur during thermal processing. The thermal stability of PHBV is improved if a higher HV content is introduced. Moderate levels (22 mol%) of MCL-PHAs segments could stabilize the PHO-*co*-MCL-PHAs. Further research is required to develop easy to use technologies to improve the thermal stability of PHAs.

1.2.3.3.3 Melt rheology and processing aids for PHAs

Compared to other polymer characteristics, melt rheological properties of PHA have been less studied, although its rheological properties have significant impact on the processing. One of the key melt flow properties is the viscosity of the polymer melt. Extensional thickening and an increase in the viscosity above its linear viscosity limit is important to stabilize the processing operations with polymer melts that are being stretched and drawn, including film blowing, fiber spinning and melt coating. Production processes used depends on the rheological properties of the polymer which are dependent on its molecular weight and monomer compositions (Modi et al., 2013) (Figure 1.5). Rheological characterization of PHBV showed a dramatic decrease of viscosity with an increasing shear rate (shear thinning) (D'Haene et al., 1999). It was found that an increase in molecular weight resulted in an increase in viscosity. In addition, an increase in polymer polydispersity (M_w/M_n), via modification of PHA structure, could also be an effective means to improve the melt strength and thermal processability accordingly (D'Haene et al., 1999). Various approaches including the addition of nucleating agents and plasticizers (e.g. soybean oil, dibutyl phthalate, and polyester plasticizer (Lapol 108), triethyl citrate) have been shown to improve polymer properties and processability (Abdelwahab et al., 2012; Corrêa et al., 2011; Erceg et al., 2005; Mekonnen et al., 2013; Shen et al., 2009). Alternative approaches to improving PHA properties are currently under investigation.

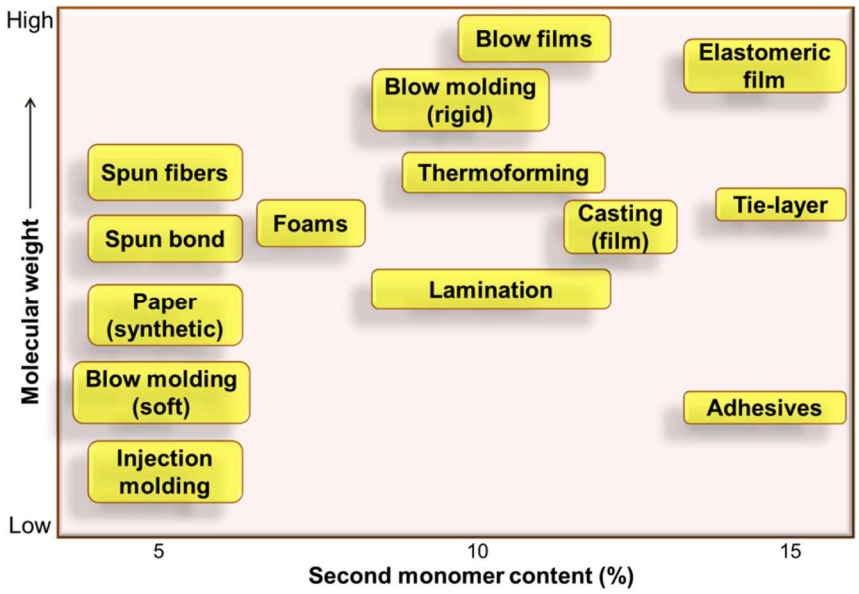

Figure 1.5. General processing technique of different PHB based copolymers vs. molecular weight and the second monomer content (Bugnicourt et al., 2014).

1.2.3.4 Mechanical properties

The monomer composition and distribution, crystallinity, microstructure and molecular weight are key factors affecting the mechanical properties of PHAs. The Young's modulus (stiffness), tensile strength (strength prior to the onset of permanent plastic deformation), and elongation at break (toughness) are standard tests to compare the mechanical properties of homopolymers, random copolymers and block copolymers.

Generally, PHB has a Young's modulus, tensile strength and elongation at break of about 2.9 GPa, 37 MPa and ~ 4%, respectively (De Koning and Lemstra, 1993). The brittleness (poor toughness) of the homopolymers PHB and P4HB is due to their high level of crystallinity, which limits their use in a wider range of applications where flexibility is required. One of the most effective solutions to improve the toughness of PHB was through copolymerization of 3-hydroxybutyrate with other monomeric units, such as 3-hydroxyvalerate (3HV), to form PHBV with higher 3HV content, or preparation of MCL-PHA copolymers (Khanna and Srivastava, 2005; Laycock et al., 2013). These copolymers showed improved mechanical properties as a result of being less crystalline, which is

attributed to the presence of dislocations, crystal strain and smaller crystallite sizes due to the disruption of 3HV unit to PHB crystal lattice (Laycock et al., 2013; Orts et al., 1990). The ductility of these copolymers is highly dependent on the monomer (3HV or 4HB) molar fraction (Khanna and Srivastava, 2005; Sudesh and Abe, 2010). As the 3HV content increases the copolymer PHBV becomes tougher (increase in impact strength) and more flexible (decrease in Young's modulus), and the elongation at break also increases with increasing 3HV content. Laycock et al. (2013) reviewed the mechanical properties of various types of PHAs by classifying PHAs according to the culture (pure or mixed) used for the PHA biosynthesis. The obtained MCL-PHA copolymers, such as PHB-*b*-P(3HV-*co*-3HHp) (Table 1.3) are expected to be more flexible as compared to PHBV copolymers. Similar to PHBV copolymer, the mechanical properties (elongation at break) of copolymer PHB-*b*-P(3HV-*co*-3HHp) is positively correlated to 3HV content.

Table 1.3. Effect of microstructure (block/random) on the mechanical properties of selected PHAs. abstracted from Li et al. (2011).

Polymer	3HB mol%	3HV mol%	3HHp mol%	Young's modulus (GPa)	Tensile strength (MPa)	Elongation at break (%)
PHB homopolymer	100	0	0	1.47	18	3.0
Random copolymer	60.9	18.5	20.6	25.0	0.03	498
Random copolymer	72.9	13.1	14.0	0.13	7.0	462
Random copolymer	77.0	12.3	10.7	0.10	4.5	224
Block copolymer	71.5	10.2	16.5	0.37	7.5	63
Blend	71.5	10.2	16.5	0.26	5.3	24
PHV homopolymer	0	100	0	0.39	6.6	3.5

In addition to the monomeric composition mentioned above that would influence the mechanical properties of PHAs, the microstructure (random or block copolymers) can also affect their mechanical performance. McChalicher et al. (2007) found the random copolymer PHB-*co*-PHBV showed 20% less elongation at break as compared to the block copolymer

PHB-*b*-PHBV with comparable monomer composition after being annealed for several days. Whereas the block copolymer still showed 100% elongation at break after being stored for 3 months after annealing. This phenomenon was attributed to the lower degree of crystallinity and slower crystallization rate for the block copolymer with different phases of monomer blocks. Li et al. (2011) successfully obtained a block copolymer PHB-*b*-P(3HV-*co*-3HHp) by removing the random copolymer with ethanol and then compared the properties with PHB and the random copolymer of 3HV and 3HHp, and blends of PHB, P3HV and P3HHp as well. As shown in Table 1.3, the Young's modulus of block copolymer was higher than the blend and random copolymers, while the tensile strength was higher than the blend, and elongation at break (%) was lower than the random copolymers. However, conflicting results have been reported (Laycock et al., 2013) and further work is required to resolve this matter. In addition to composition, the mechanical properties of PHAs are also highly dependent on processing and annealing history.

1.2.3.5 Influence of processing conditions and annealing on properties of PHAs

Generally, PHA processing conditions influence the thermal and mechanical properties of PHAs. The T_m, T_g and tensile properties of more commonly characterized PHB, PHBV, P(HB-*co*-4HB), and some petroleum based plastic films/sheets from literature are given in Table 1.4. Solvent cast films of PHBV (5% HV) had a higher T_m and lower T_g than those prepared from melting processed sheet and were all annealed the same (time and temperature). It was pointed out by Holmes (1988) that solvent casted films of PHB and its copolymer showed higher elongation at break (flexibility) and impact strength (toughness) than samples prepared from melting mixing and casting, because solvent casted films possess fine spherulitic morphology due to reduced crystallization temperature (high nucleation density). According to Jiang and coworkers findings (Jiang et al., 2008), PHBV (12% HV) compounded by extrusion and injection molding processing showed higher Young's modulus and tensile strength as compared to samples that prepared by solvent casting (Table 1.4). In addition, different melting processing can lead to differences among properties of final products. As shown in Table 1.4, PHBV with same HV content (13%), the melt processed sheet samples showed higher T_g and Young's modulus, but lower T_m and strength than the injection molded samples. Fewer studies have been carried out to compare

variations within the properties of end PHA products that produced by extrusion (sheet) and injection molding.

Nonetheless, all these thermomechanical values were significantly influenced by factors as stated above, including annealing conditions. PHA tensile property changes with aging/annealing time after samples were prepared as presented in Table 1.4. As an example, melt processed PHB samples have improved mechanical properties if being annealed for 3 weeks when comparing with samples annealed for only 1 week. Due to PHB secondary crystallization with aging/annealing time, hence the crystallinity and mechanical properties will change with time. It was found that PHB samples stored at room temperature for 60 days have lower elongation at break values than samples stored for 30 days (Bugnicourt et al., 2014). In the industrial processing, whether processing aid (i.e. talc) being used in the compounding also affects the properties. For example, with the addition of a small amount of talc, the stiffness (tensile strength) was increased significantly for PHBV (20% HV) prepared by melt processing if annealing condition was ignored.

Table 1.4. Mechanical properties of PHB and some copolymers prepared by different means and aged for different time abstracted from Laycock et al. (2013), Bugnicourt et al. (2014), Jiang et al. (2008), and some petroleum based plastics (Chanprateep and Kulpreecha, 2006).

Polymer	Sample preparation method[a]	Aging conditions	Young's modulus (GPa)	Tensile strength (MPa)	Elongation at break (%)	T_m (°C)	T_g (°C)
PHB	MPS	1 w	1-2	8-20	0.8	-	-
	MPS	3 w	2.99	36.4	2.1	181	17.7
	SCF	60°C, 20h	3.6	44	3	175	9
	SCF	"Several d's"	2.1	28	3.6	-	-
PHBV							
1mol% 3HV	MPS	24°C, 1 d	3.65	19.7	0.17	158	-
5mol% 3HV	MPS	25°C, 2 w; 60°C, 2 w, vacuum	13	22.1	1.39	171	-0.4
5mol% 3HV	SCF	25°C, 2 w; 60°C, 2 w, vacuum	-	-	-	166	2
8mol% 3HV	IM	90°C, 12h	3.5	27.1	3.6	153	-
10mol% 3HV	SCF	224 d	-	19.3	25	163	1.7
12mol% 3HV	EX/IM	Unspecified	~1.7	~29.0	~6.5	-	-
12mol% 3HV	SCF	Unspecified	0.82	14.1	12.4	154	~0
13mol% 3HV	SCF	224 d	-	18.8	48	161	-0.9
13mol% 3HV	MPS	Unspecified	1.07	12.7	-	157	2.9
13mol% 3HV	IM	Unspecified	1.0	26	-	157.3	0.3
20mol% 3HV	MPS	25°C, 2 w; 60°C, 2 w, vacuum	8.37	15.2	1.26	132	-0.05
20mol% 3HV	MPS	Small amount of talc; 60°C, 24h	1.2	32	-	145	-1
36mol% 3HV	MPS	Unspecified	0.5	16.6	70	166	0
50mol% 3HV	MPS	Unspecified	0.41	13.4	230	162	0
P(3HB-co-4HB)							
3mol% 4HB	SCF	3 w	-	28	45	166	-
10mol% 4HB	SCF	3 w	-	24	242	159	-
16mol% 4HB	SCF	3 w	-	26	444	150	-7
64mol% 4HB	SCF	3 w	0.03	17	591	50	-35
90mol% 4HB	SCF	3 w	0.1	65	1080	50	-42
Petroleum based plastics							
Plastic bag (HDPE)	Sheet	Unspecified	0.64	19	576	-	-
Plastic bag (PP)	Sheet	Unspecified	0.59	27	435	-	-
Plastic bag (LDPE)	Sheet	Unspecified	0.16	13	126	-	-
UV degradable bag	Sheet	Unspecified	0.67	24	384	-	-

[a] SCF: solvent casted film; MPS: melting pressed sheet; IM: injection molded; EX/IM: extrusion followed by injection molded; w, weeks; d, days; h, hours.

1.2.4 Applications of PHA

1.2.4.1 PHA as packaging materials

Packaging is the largest plastic processing and consuming sector. However, plastics used for this application have short service time and are discarded in environment and remain for over hundreds of years before it's decomposed (Merton-Council, 2013). Biodegradable polymers offered an effective solution to this issue, and PHAs gained much attention among biodegradable polymers due to their promising biodegradability in different environment (dos Santos Rosa et al., 2001; dos Santos Rosa et al., 2004; Tsuji and Suzuyoshi, 2002). In addition, as compared to other biopolymers, due to their good thermomechanical and barrier properties, PHAs offer a great potential for packaging materials. PHAs were first used in bottles and carrier bags and later developed for other consumable materials including razors, utensils, diapers, feminine hygiene products, cosmetic containers, disposable cups, and cutlery, although occupying a limited market share (Chen, 2010). Disposable medical devices and products are now being manufactured from PHAs (Bugnicourt et al., 2014; Chen, 2010). Despite the great potential use of PHAs as packaging materials, PHA thermal processing issues (e.g in foaming and film forming) in relevance to their rheological properties (poor melt strength or low viscosity when melt) are a major limitation.

1.2.4.2 PHA as biomedical implant materials

Due to good biocompatibility PHAs, such as PHB, PHBV, P(3HB-*co*-3HHx) and PHO have been developed for biomedical implant materials. PHB and/or its blends or composites (i.e. hydroxyapatite/PHB) have been used as bone replacement materials (Ramakrishna et al., 2001). Monofilament sutures made of PHB and PHBV showed comparable interaction between tissue and the implanted plastics as to silk (Shishatskaya et al., 2004). PHAs can also be applied as wider ranges of devices that have been listed in literatures (Chen, 2009, 2010; Ramakrishna et al., 2001). With greater diversity of PHA materials synthesized and characterized; it is believed that PHAs will become a family of bio-implant materials with richer applications in the future.

1.3 Poly(lactic acid) (PLA)

1.3.1 Production of PLA

Another major bioplastic on the market is polylactic acid (PLA). PLA is a synthetically produced biodegradable plastic from bioderived monomers from renewable resources. PLA can be synthesized via different polymerization routes, which is shown in Figure 1.6. Based on the stereochemistry of lactic acid (LA) and lactide monomers (Figure 1.6a), several distinct forms of PLA exist: poly(L-lactic acid) (PLLA) is the product resulting from polymerization of L-lactide (also known as (S,S) or L-lactide), while poly(D-lactic acid) (PDLA) is synthesized from D-lactide (also known as (R,R)-lactide). Commercial PLA homopolymer is generally prepared from L-lactide (LLA) which can be derived from corn starch fermentation with relatively high enantiomeric purity (Södergård and Stolt, 2002; Sun, 2011). Polymerization of a racemic mixture of L- and D-lactides (known as (R,S) or meso-lactide) usually results to the synthesis of poly-D, L-lactide (PDLLA), which is amorphous. High molecular weight PLA (weight average molar mass, M_w > 100,000 g/mol) is most commonly obtained by ring-opening polymerization (ROP) of the cyclic dimer 3,6-dimethyl-1,4-dioxane-2,5-dione commonly referred to as lactide in the presence of various metal catalyst (commonly tin octoate) (Groot et al., 2010). This route involves two steps of reaction that results in additional purification and therefore significant cost will be required. PLA prepared via polycondensation route has lower M_w due to the low equilibrium constant of lactic acid esterification and the difficulty to remove the by-product, H_2O, in the viscous reaction mixture. Interest in commercial PLA manufactured from lactic acid to develop effective cost approach from LA increased. In addition to LA and lactide, the five-membered cyclic lactic acid *O*-carboxyanhydride has been attempted for PLA synthesis (He et al., 2013). This compound is found to be more reactive than lactide. The direct biosynthesis of PLA which is similar to the PHAs has been reported (Jung et al., 2010). To date, the major PLA suppliers have been Cargill (in USA known as Ingreo^{TM}, under trade name Nature Works), Mitsui Chemicals, Inc. (Japan), Purac (The Netherlands), and Teijin Limited (Japan). The increased productivity of PLA facilitated an increased in its research and development activities. The number of publications related to PLA increased dramatically over the past decade, which is due to the increasing demands of sustainable and

eco-efficient bioplastics. A viable end-of-life option of PLA is chemically recycling back to monomers through hydrolysis into lactic acid which will enter into the polycondensation step (Witzke et al., 1997), or reversible polymerization to lactide monomer using catalytic thermal depolymerization (Narayan et al., 2012). To upscale the depolymerizatin of PLA back to lactide is under progress, which is believed to reduce the market prices of PLA significantly.

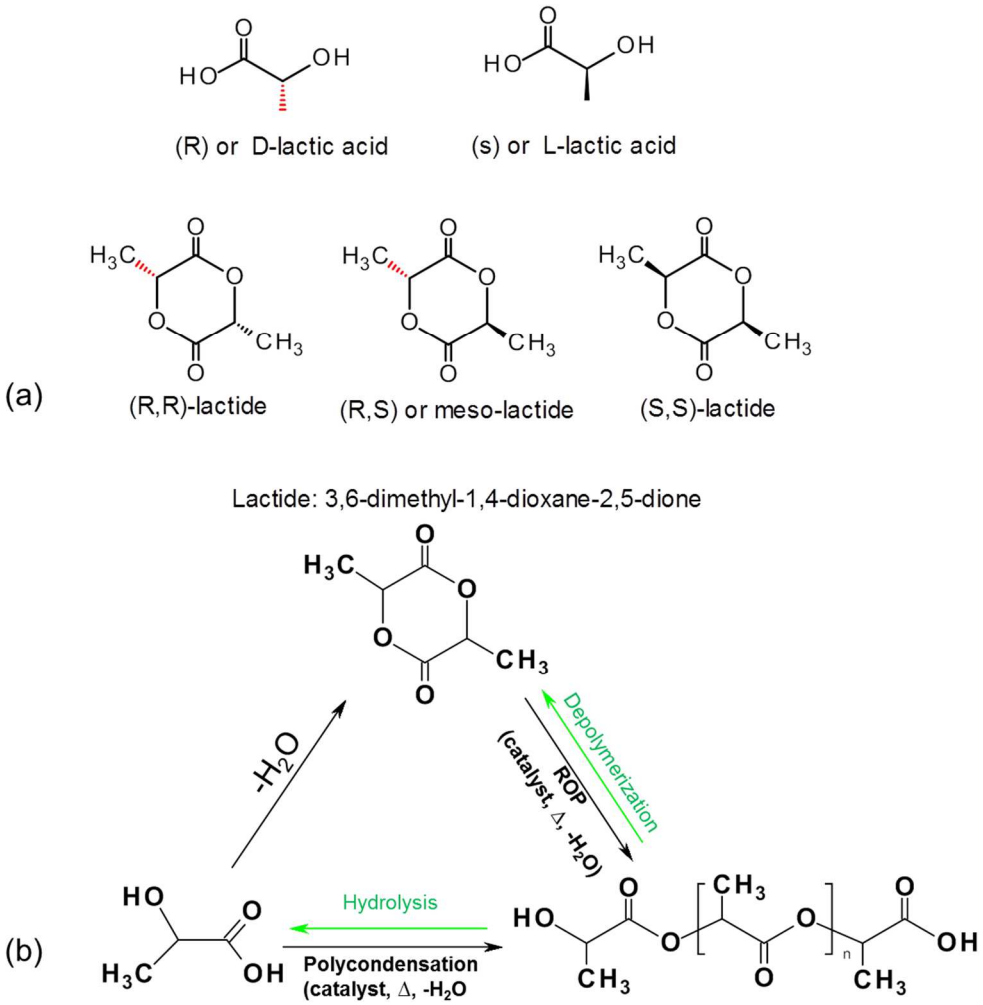

Figure 1.6. Stereochemistry of the lactic acid (LA) and lactide monomers (a) and chemistry of the interconversion between LA, lactide and PLA (b). Note: Reversible depolymerization and hydrolysis steps are highlight in green color (Narayan et al., 2013).

1.3.2 Crystallization and thermomechanical properties

Processing conditions and final thermomechanical properties are highly influenced by the crystalline structure of PLA. PLLA and PDLA are semicrystalline material; while PDLLA is an equimolar random copolymer L- and D-lactide, which is fully amorphous because of its irregular structure. Pure PLLA and PDLA have similar thermal properties, for example, T_g, T_m and X_c % are always in the range of 50-70 ˚C, 170-190 ˚C, and 35%, respectively (Garlotta, 2001). These values can be determined from DSC, which is highly dependent on the polymer M_w, polymerization conditions, processing (thermal) history, etc. During the first heating scan in DSC analysis, T_g values are relatively higher than expected due to high crystallinity content (X_c %), which was caused by the restriction of crystalline domains that hinder the mobility of amorphous polymer chains. It is worth noting in the cooling scan after full melting of PLLA, crystallization is inhibited by the high content of terminal groups with low M_w (2,000 g/mol) and by the low mobility of the long PLLA (200,000 g/mol) polymer chains (Fambri and Migliaresi, 2010). During the second heating scan, when M_w was increased from 2,000 to 200,000 g/mol, X_c % was increased from 10 to 28 %, which is also proportionally depending on the mobility of respective short and long polymer chains; meantime, their T_g was increased from 43 to 64 ˚C, respectively (Fambri and Migliaresi, 2010). This increase in T_g values was again contributed to the hindering effect introduced to the amorphous chain mobility by the crystalline regions. Similar trend for melting was observed with T_m was increased from 130 to 180 ˚C with increasing molecular weight (number average molecular weight, M_n) (Jamshidi et al., 1988).

The mechanical properties of PLA are significantly influenced by stereochemistry used for sample preparation. Both PLLA and PDLA are hard materials with modulus about 2.7 GPa, tensile strength of 50-70 MPa, elongation at break of 4 %, flexural modulus of 5 GPa, and flexural strength of 100 MPa (Albertsson et al., 2010). Similar to PHA, annealing (temperature and time) is also an important factor affecting mechanical properties of PLA (Park et al., 2004). Although PLA is considered as a good substitution to conventional plastics, the low elongation at break and higher glass transition make it brittle at room

temperature. Current research is focused on PLA blends to improve its ductility (Abdelwahab et al., 2012; Zhao et al., 2013).

1.3.3 Melt rheological properties and processing aids for PLA

The base properties of PLA are extensively available in the literature, only a few publications have been found on melt rheological properties of PLA (Dorgan et al., 1999; Lehermeier and Dorgan, 2001; Palade et al., 2001). In these studies, PLA melt also showed shear thinning as that of PHA melts. Blending of linear and branched PLA was effective to increase the shear viscosity and elasticity with increasing branched PLA. Another important concern in the melt rheological study is the melt stability of PLA in the temperature range below its thermal degradation onset. Dorgan and coworkers used tris(nonylphenyl)phosphate (TNPP) as stabilizer to investigate the melt rheological properties of PLA with temperature extended to 200 ˚C (Dorgan et al., 1999). Similar to PHAs, melt processing is the most widely adopted to process PLA into different end products. High M_w PLA particularly can be processed using conventional plastic equipment, such as injection molding, extrusion and melt spinning. Different processing requires carefully controlled processing temperatures, for example, injection molding, extrusion, inflation molding, spinning and lamination at 170-200 ˚C, 180-240 ˚C, 170-190 ˚C, 180-240 ˚C, and 200-240 ˚C, respectively (Groot et al., 2010).

However, brittleness of PLA leads to relatively poor performance and particularly thermal processing difficulty. Different types of additives such as ethylene copolymer additives and impact modifier have been used to improve the toughness for rigid applications subjected to thermoforming (cast sheet) and injection molding (Mekonnen et al., 2013). The poor melt strength of PLA leads to polymer melt necking and poor drawability, and therefore reduces throughput which will cause processing difficulties during blown film extrusion, film and sheet extrusion, and foaming. Additives such as acrylics and polymer extenders (i.e. Clariant's Cesa-Extend) have been employed to improve PLA melt strength by improving chain entanglement and reducing breakage in the melt (Groot et al., 2010). Apart from low flexibility and melt strength, similar to homopolymer PHB, the PLA melt is sticky because of their high surface coefficient of friction. Other additives such as fatty acid amides are the

most widely used slip additives to solve the issue (Markarian, 2007; Yu et al., 2008). For instance, $CaCO_3$ was added to reduce the thermal degradation of PLA, but meantime the biodegradation rate was reduced (Renstad et al., 1998). Similar to the modification of PHAs, more effective strategies are required to improve PLA processability and properties. Recently, Dean et al. (2012) modified PLA via alkyl radical-based at high temperature proposed a feasible solution to the issues of low melt strength of PLAs without using external additives; nonetheless, in their studies the chemistry and properties changes were failed to be characterized and addressed in detail.

1.3.4 Applications of PLA

As the most promising synthetic biodegradable biomaterial, PLA has been widely used in medical applications due to its good mechanical properties and relative long-term biocompability as implant material. PLA with enhanced toughness can be used in bone fixation that requires strength and elasticity similar to native bone tissue. When PLA experiences degradation by hydrolytic scission of ester bonds, LA will be produced. LA is a natural product associated with muscle in animals and humans, which can join into body's normal metabolic activities; namely, it is nontoxic to the body. To note, L-LA is a naturally occurring stereoisomer of LA; hence, PLLA is more commonly used for medical applications than PDLA. Except for implants, PLA can be applied as various medical devices, such as sutures, biodegradable stents, mesh (performing as membrane), chondral plug, and other surgical devices (e.g. screws, pins, rods, plates, microspheres, microcapsules, and thin coatings, etc.).

Apart from medical uses, PLA has been widely used fields of packaging and containers, compost, agricultural and civil engineering (Chiellini, 2008; Jandas et al., 2013). PLA is very transparent and can be used as vegetable packaging, food trays, films (shrink, overlap), paper lamination, cutting blade for wrapping film, and clear windows for envelopes. Biodegradable PLA can be used in products such as compost bags, kitchen net, mulch film, nonwoven nursery pots, sandbags, and drainage devices (Obuchi and Ogawa, 2010). Durable PLA materials have been used in automobile and electrical applications (Obuchi and Ogawa, 2010). However, as compared to conventional polyolefins (PE/PP) that have

been used as flexible film materials for packaging (i.e. bags), oriented films of PLA will give a rustling sound when being used as packaging materials due to its brittleness (Chiellini, 2008; Groot et al., 2010). To improve the flexibility of PLA films, as mentioned above plasticization could be a potential means; however, it was found the significant increase of elongation at break (flexibility) always showed an expense of strength (Mekonnen et al., 2013). Therefore, options to modify PLA to broaden its applications are in need.

1.4 Blending of PHAs and PLA with other polymers

1.4.1 Aliphatic polyester blends

As discussed in sections 1.2 and 1.3, both PHB and PLA are brittle plastics and have low thermal stability and blending the polymers offers promise to improve their properties. Ikada and coworkers studied stereocomplexed PLLA/PDLA blends to improve their thermal properties (Ikada et al., 1987). The blends showed a significant increase in T_m and improved hydrolysis resistance as compared to pure PLLA and PDLA alone. The PLLA/PDLLA (40/60) blend was shown to have a higher elongation at break and elastic modulus (Chen et al., 2003a).

Because PHAs are known for their good biocompatibility, blends of different PHAs have attracted considerable research interest associated with their medical applications. It was shown the PHB/PHBHHx blends become an attractive candidate for tissue engineering and scaffold materials due to improved biocompatibility and promotion to the growth for cell L929 (Yang et al., 2002). PHB based blends are compatible and co-crystallization exist. For example, PHB/PHBV blends were shown to have a completely PHB-rich crystalline phase with a thicker amorphous layer than that of PHBV copolymer (Saito et al., 2001). Through blending of these two polyesters, the cyrstallinity, mechanical properties (flexibility), and processability are expected to be improved.

In addition to PLA/PLA and PHA/PHA blends, the blends of PLA and PHA (PLA/PHA: PLA/PHB and PLA/PHBV) have provided a practical approach of improving/tailoring the structures and properties of either phase, but without compromising their biodegradability (Bliimm and Owen, 1995; Loureiro et al., 2013; Wagner et al., 2014; Zhao et al., 2013).

Zhang et al. (1995) showed the crystallinity was reduced due to being blended with PLA, which is affected by the PLA ratio. Solution blends PLA/PHBV were electrospun to prepare fiber samples which have potential applications that need a high surface to volume ratio such as filtration, biomedical, and energy storage devices (Wagner et al., 2014). PLA/PHBV blend prepared by injection molding indicated that the blend had larger elasticity with increasing PHBV content, whereas PLA and PHBV were immiscible when the content of PHBV exceeded 30% (Zhao et al., 2013). The miscibility highly influences the biodegradability of the blends (Yu et al., 2006). A careful control of the PLA/PHA formulation is required in order to achieve a complete miscibility.

1.4.2 Biocomposites

A composite is usually defined as the combination of two or more different components, in which one plays the role of filler or reinforcement while the other performs as matrix material. If both the filler/reinforcement material (i.e. biofibers) and the polymer matrix are bio-based (PHAs and PLA), resulting in a biocomposite that is always classified into green composite in the perspective of sustainability (Mohanty et al., 2002; Terzopoulou et al., 2014). Green composites are advantageous materials as they can decompose in the environment without any environmental impact at the end of life cycle. According to market data reported by Bioplastic Magazine, 352,000 tons of the wood- (74% of the market share) and natural fibers (26% of the market share) based composites were produced in 2012 in the European Union, and the wood plastic composites (WPC) will increase to 350,000 tons by 2015 (Anonymous, 2014). About 38% of WPC was used for automotive industry in 2012, majorly for rear shelves and trims for trunks and spare wheels, as well as in interior trims for doors; while natural fibers based composites are mainly used for interior trims for high value doors and dashboards. North America is the leading production region of biocomposites, followed by China and Europe.

1.4.2.1 Fibers and cellulose

Natural fibers are used as reinforcement in biocomposites and have been recently reviewed (Faruk et al., 2012). Fibers were catagorized into six types: bast fibers (jute, flax, hemp,

kenaf and ramie), leaf fibers (abaca, sisal and pineapple), seed fibers (coir, cotton and kapok), core fibers (kenaf, hemp and jute), grass and reed fibers (wheat, corn and rice) and other types (wood, bamboo and roots). Each fibril has a complex and layered structure as shown in Figure 1.7 (John and Thomas, 2008). The middle lamella performs as glue between two adjacent cells as tissue. The primary wall is the first layer deposited during the formation of cell. Three layers, outer layer (S1), middle layer (S2), and inner layer (S3), compose the secondary cell wall (Rowell, 2005; Terzopoulou et al., 2014). In the primary wall the orientation of cellulose microfibrils is random from 0 to 90^{o} relative to long axial direction of cell. For wood fibers the angle (microfibrillar angle) between microfibrils direction and long axis is between 50 to 70^{o} for S1 layer (Rowell, 2005). These microfibrils have diameter in the range of 10-30 nm and are typically made up of 30-100 cellulose molecules in extended chain conformation, which dominants the mechanical strength of the fibers (John and Thomas, 2008).

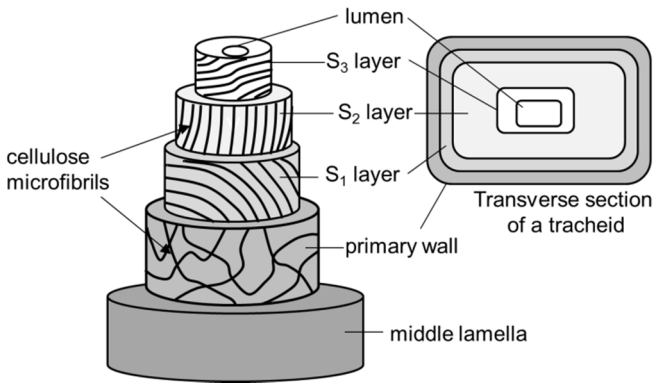

Figure 1.7. Three-dimensional structure of the secondary cell wall of a xylem cell.

All these fibers contain a high proportion of cellulose (40-90 %) (Figure 1.8) (Hon and Shiraishi, 2001); a hydrophilic polysaccharide consists of a linear macromolecular chain of 1→4 linked β-D-glucopyranosyl units (Kadla and Gilbert, 2000). The numerous hydroxyl groups on the glucose ring contribute to extensive intra- and inter-molecular C−H···O hydrogen bonds (Figure 1.9) (Klemm et al., 2005; Roy et al., 2009). The hydrogen bonding within and between cellulose chains are responsible for its high strength, crystallinity and durability, biocompatibility and hydrophilicity (Carlmark et al., 2012; Klemm et al., 2005;

Roy et al., 2009). Furthermore, natural fibers also contain hemicellulose (branched polysaccharide) and lignin.

Biocomposite properties can be improved via exchanging wood fiber with cellulose fibers based on its improved thermal stability and mechanical properties. Such biocomposites will have great potential to be used in the automobile industry with increasing demands for recyclable new cars (Pilla, 2011; Terzopoulou et al., 2014).

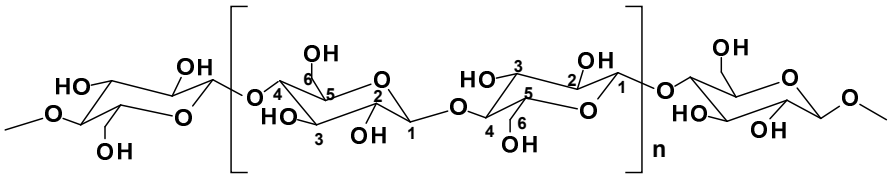

Figure 1.8. The molecular structure of cellulose (n=DP, degree of polymerization; the carbon positions of the ring structure are marked).

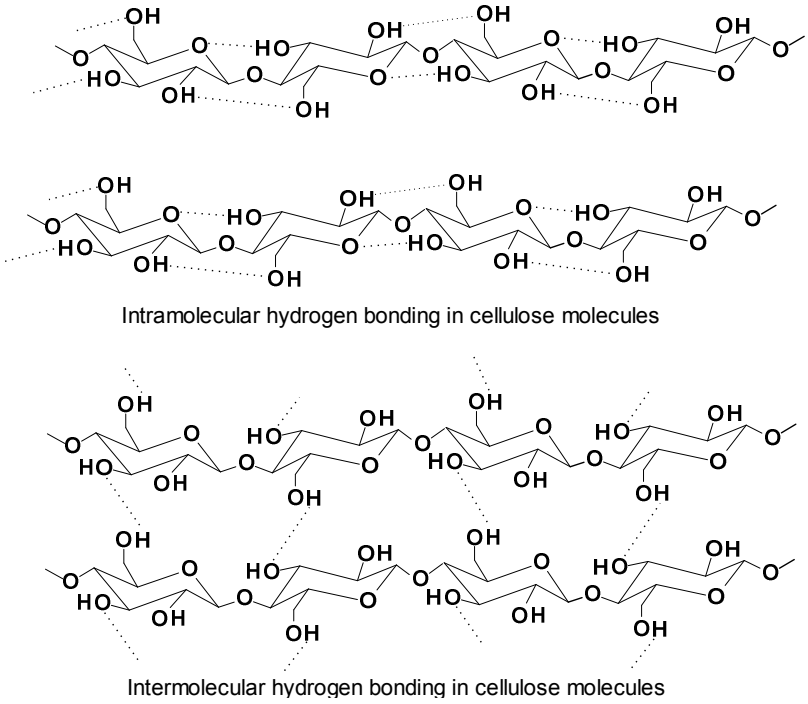

Figure 1.9. (Top) Intra- and (bottom) inter-molecular hydrogen bonding in cellulose molecules.

1.4.2.2 PHA based biocomposites

Bio/natural fibers have been incorporated into the PHA polymer matrix to improve its thermomechanical properties and cost reduction of the final products (biocomposites) (Mohanty et al., 2002; Yu et al., 2006). PHB/PHBV based biocomposites reinforced with kenaf fibers (Avella et al., 2007), straw/hemp fibers (Avella et al., 2000) and bamboo fibers (Singh et al., 2008) have been reported. In these cases, the thermal stability was increased by addition of fibers, while Shanks et al. (2004) showed improvement in bending/storage modulus by addition of flax fibers. Barkoula and collegues (2010) studied properties of flax fibers reinforced PHB composites and showed that PHB was toughened in these biocomposites. Furthermore, the presence of fibers stimulated the initial biodegradation of these biocomposites by its moisture uptake. Srithep et al. (2013) prepared nanocomposites with PHBV reinforced with nanofibrillated cellulose (NFC). Addition of NFC increased the tensile modulus significantly because it served as nucleation agent that facilitated PHBV crystallization. Coats et al. (2008) prepared biocomposites with PHB-rich biomass compounded to pine wood fibers and compared properties with purified PHB based composites. The former composites exhibited comparable strength to the later type. This proposed another strategy to utilize PHA biomass without further purification of PHA polymers from bacterial cells, which could reduce the cost of the biocomposite.

1.4.2.3 PLA based biocomposites

Similar to PHAs based biocomposites, PLA is another attractive biodegradable polymer matrix. Various properties for different biofibers, such as hemp, flax, coir, and wood fibers as well as cellulose and lignin have been used as reinforcement have been widely studied (Dong et al., 2014; Liu et al., 2014; Masirek et al., 2007; Oksman et al., 2003; Wong et al., 2004), and reviewed (Faruk et al., 2012; Satyanarayana et al., 2009).

1.4.2.4 Improvement of biocomposites performance by modification

Although biofibers are good candidates for biocomposites production, they also bring about challenges. Biofibers have a large number of hydroxyl groups (Figures 1.8 and 1.9) resulting in a polar fiber surface, and this can result in poor interfacial bonding between the cellulose

and the, generally hydrophobic, polymer matrix. The relative poor stress transfer from matrix to filler is strongly dependent on the degree of bonding between the two phases (Dufresne et al., 1999). The poor interfacial adhesion at the two interfaces means that the full capabilities of the composite cannot be exploited, resulting in the cellulose being a filler and not a true reinforcement, which could weaken its mechanical properties, and thus reducing its life span (Kalia et al., 2011). To reduce the hydrophilicity of cellulose fiber surface this can be achieved either through a physical treatment (e.g. cold plasma treatment) (Bledzki and Gassan, 1999) or chemical treatment (e.g. maleic anhydride, organosilanes, isocyanates, etherification and esterification) (Gassan and Bledzki, 1999; Joseph and Thomas, 1996; Lu et al., 2000; McDonald and Ma, 2010; Wei et al., 2013), and therefore to improve the interfacial adhesion between the two phases. These modifications result in a decrease in moisture absorption and an increase in mechanical properties, biodurability and weatherability (Kalia et al., 2011). However, the processes used for cellulose modification are costly and could be a deterrent to its use in pilot scale. As for the polymer matrix, to render the surface hydrophobic, the introduction of hydrophilic groups by transesterification with ethylene glycol, sulfonic acid and poly(ethylene glycol) (PEG), can improve PHBVs biocompatibility and broaden its applications such as emulsifiers, foams, thickeners and compatibilizer, beyond biomedical implantable materials (Förster and Antonietti, 1998; Hadjichristidis et al., 2001; Hazer, 2010). An alternate approach to obtain an amphiphilic type PHB is through grafting and copolymerization onto chitosan and cellulose/ethyl cellulose (Samain et al., 2011; Yu et al., 1999; Yu et al., 2012). Graft-copolymerization has been demonstrated to be an effective approach to modify the hydrophobicity of cellulose (Saad, 2001; Samain et al., 2011; Yu et al., 2012). Therefore, grafting bioplastics (PHAs or PLA) onto cellulose will retain the stiffness of cellulose and the thermoplasticity of the polymer matrix but with excellent stress-transfer and hydrophobicity-hydrophilicity between the two phases in the biocomposite. The applications of biocomposites are expected to be broadened accordingly.

1.5 Research goal and objectives

The aims of this dissertation are to improve the properties and melt processability of selected bioplastics, including PHB homopolymers, PHBV copolymer and PLA. The

brittleness (especially for PHB), poor thermostability/melt processability are the typical shortcomings of these bioplastics, and therefore to understand the relations between their chemical structures and thermophysical properties seems urgent. The specific objectives to overcome some of the inherent material limitations of PHB (or PLA) bioplastics include:

1. Biosynthesis the copolymer PHBV with higher HV content, and investigation the relationship between its chemical structures and properties.

2. Modeling studies of PHB crystallization process and multiple melting behavior by DSC, TMDSC, and TMA to provide theoretical guidance to its melt processing manipulation of its thermophysical properties.

3. Cross-linking modification of PHB (and PLA) properties (e.g. brittleness, thermodegradability) and processability as well through changing their structures via *in-situ* reactive extrusion.

4. Modification of PHB by grafting onto cellulose, as a reinforcement, to improve its properties via *in-situ* reactive extrusion.

Figure 1.10 summarizes the overall structure of this dissertation which is focused on characterization and modification of selective bio-based polymers. Chapter 1 is a general introduction and reviews of PHAs and PLA in the point of synthesis/production, properties, melt processing, applications, and strategies to improve processability and properties. Chapter 2 covers the isolation and characterization of PHBV biosynthesized by mixed microbial consortia fed fermented dairy manure. Chapter 3 delivers the effect of thermal history on crystallization and multiple melting behaviors of PHB studied by conventional DSC, TMDSC and TMA in order to understand the origins of PHB multiple melting behaviors. Chapter 4 discusses peroxide induced cross-linking by reactive melt processing of PHB and PLLA to improve their melt strength, thermostability, and flexibility, especially focusing on the molecular weight distribution changes from rheology test of resulting polymers. Chapter 5 covers grafting of bacterial PHB onto cellulose via *in-situ* reactive extrusion with dicumyl peroxide to tune the PHB/cellulose properties. Chapter 6

summarizes the conclusions and potential further work beyond this dissertation. Chapters 2 through 5 were written as separate journal manuscripts.

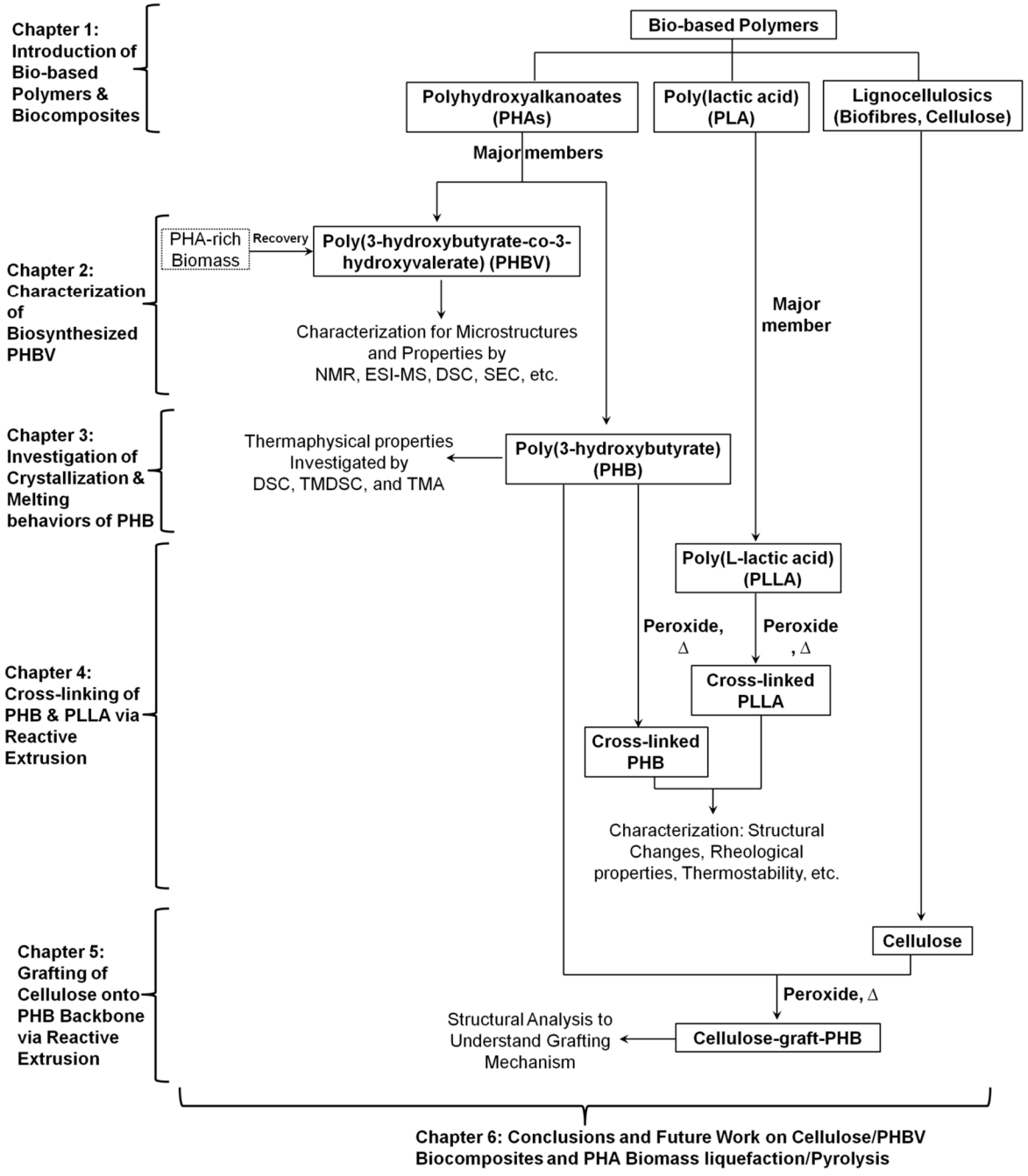

Figure 1.10. Schematic diagram showing the outline of each chapter of this dissertation.

1.6 References

Abdelwahab, M.A., Flynn, A., Chiou, B.-S., Imam, S., Orts, W., Chiellini, E., 2012. Thermal, mechanical and morphological characterization of plasticized PLA–PHB blends. Polymer Degradation and Stability 97, 1822-1828.

Albertsson, A.C., Varma, I.K., Lochab, B., Finne-Wistrand, A., Kumar, K., 2010. Design and synthesis of different types of poly(lactic acid), in: Auras, R., Lim, L.-T., Selke, S.E.M., Tsuji, H. (Eds.), Poly(Lactic Acid): Synthesis, Structures, Properties, Processing, and Applications. John Wiley & Sons, Inc.: Hoboken, New Jersey, Chap.4, pp. 43-58.

Albuquerque, M.G.E., Concas, S., Bengtsson, S., Reis, M.A.M., 2010a. Mixed culture polyhydroxyalkanoates production from sugar molasses: The use of a 2-stage CSTR system for culture selection. Bioresource Technology 101, 7112-7122.

Albuquerque, M.G.E., Eiroa, M., Torres, C., Nunes, B.R., Reis, M.A.M., 2007. Strategies for the development of a side stream process for polyhydroxyalkanoate (PHA) production from sugar cane molasses. Journal of Biotechnology 130, 411-421.

Albuquerque, M.G.E., Martino, V., Pollet, E., Avérous, L., Reis, M.A.M., 2011. Mixed culture polyhydroxyalkanoate (PHA) production from volatile fatty acid (VFA)-rich streams: Effect of substrate composition and feeding regime on PHA productivity, composition and properties. Journal of Biotechnology 151, 66-76.

Albuquerque, M.G.E., Torres, C.A.V., Reis, M.A.M., 2010b. Polyhydroxyalkanoate (PHA) production by a mixed microbial culture using sugar molasses: Effect of the influent substrate concentration on culture selection. Water Research 44, 3419-3433.

Allen, A.D., Ayorinde, F.O., Eribo, B.E., 2014. Non-edible vernonia galamensis oil and mixed bacterial cultures for the production of polyhydroxyalkanoates. Modern Chemistry and Applications 2, 38-42.

An, Y., Dong, L., Mo, Z., Liu, T., Feng, Z., 1998. Nonisothermal crystallization kinetics of poly(β-hydroxybutyrate). Journal of Polymer Science Part B: Polymer Physics 36, 1305-1312.

Andreeßen, B., Steinbuchel, A., 2010. Biosynthesis and biodegradation of 3-hydroxypropionate-containing polyesters. Applied and Environmental Microbiology 76, 4919-4925.

Anonymous, 2014. European and global markets: 2012 and future trends, Bioplastics Magazine. Polymedia Publisher GmbH, Mönchengladbach, Germany.

Avella, M., Bogoeva-Gaceva, G., Buzõarovska, A., Emanuela Errico, M., Gentile, G., Grozdanov, A., 2007. Poly(3-hydroxybutyrate-co-3-hydroxyvalerate)-based biocomposites reinforced with kenaf fibers. Journal of Applied Polymer Science 104, 3192-3200.

Avella, M., Martuscelli, E., Raimo, M., 2000. Properties of blends and composites based on poly(3-hydroxy)butyrate (PHB) and poly(3-hydroxybutyrate-hydroxyvalerate) (PHBV) copolymers. Journal of Matererials Science 35, 523-545.

Ballistreri, A., Montaudo, G., Garozzo, D., Giuffrida, M., Montaudo, M.S., 1991. Microstructure of bacterial poly(β-hydroxybutyrate-co-β-hydroxyvalerate) by fast atom bombardment mass spectrometry analysis of the partial pyrolysis products. Macromolecules 24, 1231-1236.

Barham, P.J., Keller, A., Otun, E.L., 1984. Crystallization and morphology of a baterial thermoplastic: poly-3-hydroxybutyrate. Journal of Matererials Science 19, 2781-2794.

Barkoula, N.M., Garkhail, S.K., Peijs, T., 2010. Biodegradable composites based on flax/polyhydroxybutyrate and its copolymer with hydroxyvalerate. Industrial Crops and Products 31, 34-42.

Beccari, M., Bertin, L., Dionisi, D., Fava, F., Lampis, S., Majone, M., Valentino, F., Vallini, G., Villano, M., 2009. Exploiting olive oil mill effluents as a renewable resource for production of biodegradable polymers through a combined anaerobic-aerobic process. Journal of Chemical Technology & Biotechnology 84, 901-908.

Beccari, M., Majone, M., Massanisso, P., Ramadori, R., 1998. A bulking sludge with high storage response selected under intermittent feeding. Water Research 32, 3403-3413.

Bengtsson, S., Pisco, A.R., Reis, M.A.M., Lemos, P.C., 2010. Production of polyhydroxyalkanoates from fermented sugar cane molasses by a mixed culture enriched in glycogen accumulating organisms. Journal of Biotechnology 145, 253-263.

Bengtsson, S., Werker, A., Christensson, M., Welander, T., 2008. Production of polyhydroxyalkanoates by activated sludge treating a paper mill wastewater. Bioresource Technology 99, 509-516.

Beun, J.J., Dircks, K., Van Loosdrecht, M.C.M., Heijnen, J.J., 2002. Poly-β-hydroxybutyrate metabolism in dynamically fed mixed microbial cultures. Water Research 36, 1167-1180.

Bledzki, A.K., Gassan, J., 1999. Composites reinforced with cellulose based fibres. Progress in Polymer Science 24, 221-274.

Bliimm, E., Owen, A.J., 1995. Miscibility, crystallization and melting of poly(3-hydroxybutyrate)/poly(L-lactide) blends. Polymer 36, 4077-4081.

Bloembergen, S., Holden, D.A., Hamer, G.K., Bluhm, T.L., Marchessault, R.H., 1986. Studies of composition and crystallinity of bacterial poly(β–h-ydroxybutyrate-co-β-hydroxyvalerate). Macromolecules 19, 2865-2871.

Bluhm, T.L., Hamer, G.K., Marchessault, R.H., Fyfe, C.A., Veregin, R.P., 1986. Isodimorphism in bacterial poly(β-hydroxybutyrate-co-β-hydroxyvalerate). Macromolecules 19, 2871-2876.

Bugnicourt, E., Cinelli, P., Lazzeri, A., Alvarez, V., 2014. Polyhydroxyalkanoate (PHA): Review of synthesis, characteristics, processing and potential applications in packaging. Express Polymer Letters 8, 791-808.

Carlmark, A., Larsson, E., Malmström, E., 2012. Grafting of cellulose by ring-opening polymerisation – A review. European Polymer Journal 48, 1646-1659.

Cerrone, F., Choudhari, S.K., Davis, R., Cysneiros, D., O'Flaherty, V., Duane, G., Casey, E., Guzik, M.W., Kenny, S.T., Babu, R.P., O'Connor, K., 2013. Medium chain length polyhydroxyalkanoate (mcl-PHA) production from volatile fatty acids derived from the anaerobic digestion of grass. Applied Microbiology and Biotechnology 98, 611-620.

Chanprateep, S., 2010. Current trends in biodegradable polyhydroxyalkanoates. Journal of Bioscience and Bioengineering 110, 621-632.

Chanprateep, S., Buasri, K., Muangwong, A., Utiswannakul, P., 2010. Biosynthesis and biocompatibility of biodegradable poly(3-hydroxybutyrate-co-4-hydroxybutyrate). Polymer Degradation and Stability 95, 2003-2012.

Chanprateep, S., Kulpreecha, S., 2006. Production and characterization of biodegradable terpolymer poly(3-hydroxybutyrate-co-3-hydroxyvalerate-co-4-hydroxybutyrate) by Alcaligenes sp. A-04. Journal of Bioscience and Bioengineering 101, 51-56.

Chen, C.-C., Chueh, J.-Y., Tseng, H., Huang, H.-M., Lee, S.-Y., 2003. Preparation and characterization of biodegradable PLA polymeric blends. Biomaterials 24, 1167-1173.
Chen, G.-Q., 2009. A microbial polyhydroxyalkanoates (PHA) based bio- and materials industry. Chemical Society Reviews 38, 2434.

Chen, G.-Q., 2010. Plastics completely synthesized by bacteria: polyhydroxyalkanoates, in: Chen, G.Q. (Ed.), Plastics from bacteria. Natural functions and applications. . Springer-Verlag: Berlin Heidelberg, pp.17-37.

Chen, G.-Q., Patel, M.K., 2012. Plastics derived from biological sources: present and future: A technical and environmental review. Chemical Reviews 112, 2082-2099.

Chen, J.-Y., Song, G., Chen, G.-Q., 2006. A lower specificity PhaC2 synthase from Pseudomonas stutzeri catalyses the production of copolyesters consisting of short-chain-length and medium-chain-length 3-hydroxyalkanoates. Antonie van Leeuwenhoek 89, 157-167.

Chen, Q., Thouas, G., 2014. Biomaterials: A basic introduction. CRC Press, Boca Raton.

Chiellini, E., 2008. Environmentally compatible food packaging. Elsevier., Boca Raton, FL.

Chung, A.-L., Jin, H.-L., Huang, L.-J., Ye, H.-M., Chen, J.-C., Wu, Q., Chen, G.-Q., 2011. Biosynthesis and characterization of poly(3-hydroxydodecanoate) by *β*-oxidation inhibited mutant of *Pseudomonas Entomophila* L48. Biomacromolecules 12, 3559-3566.

Coats, E.R., Loge, F.J., Smith, W.A., Thompson, D.N., Wolcott, M.P., 2007a. Functional stability of a mixed microbial consortium producing PHA from waste carbon sources. Applied Biochemistry and Biotechnology 136-140, 909-925.

Coats, E.R., Loge, F.J., Wolcott, M.P., Englund, K., McDonald, A.G., 2007b. Synthesis of polyhydroxyalkanoates in municipal wastewater treatment. Water Environment Research 79, 2396-2403.

Coats, E.R., Loge, F.J., Wolcott, M.P., Englund, K., McDonald, A.G., 2008. Production of natural fiber reinforced thermoplastic composites through the use of polyhydroxybutyrate-rich biomass. Bioresource Technology 99, 2680-2686.

Corrêa, M.C.S., Branciforti, M.C., Pollet, E., Agnelli, J.A.M., Nascente, P.A.P., Avérous, L., 2011. Elaboration and characterization of nano-biocomposites based on plasticized poly(Hydroxybutyrate-Co-Hydroxyvalerate) with organo-modified montmorillonite. Journal of Polymers and the Environment 20, 283-290.

D'Haene, P., Remsen, E.E., Asrar, J., 1999. Preparation and characterization of a branched bacterial polyester. Macromolecules 32, 5229-5235.

Dagnon, K.L., Chen, H.H., Innocentini-Mei, L.H., D'Souza, N.A., 2009. Poly[(3-hydroxybutyrate)-co-(3-hydroxyvalerate)]/layered double hydroxide nanocomposites. Polymer International 58, 133-141.

Dai, J., Gliniewicz, K., Settles, M.L., Coats, E.R., McDonald, A.G., 2015. Influence of organic loading rate and solid retention time on polyhydroxybutyrate production from hybrid poplar hydrolysates using mixed microbial cultures. Bioresource Technology 175, 23-33.

Dai, Y., Lambert, L., Yuan, Z., Keller, J., 2008a. Characterisation of polyhydroxyalkanoate copolymers with controllable four-monomer composition. Journal of Biotechnology 134, 137-145.

Dai, Y., Lambert, L., Yuan, Z., Keller, J., 2008b. Microstructure of copolymers of polyhydroxyalkanoates produced by glycogen accumulating organisms with acetate as the sole carbon source. Process Biochemistry 43, 968-977.

De Koning, G.J.M., Lemstra, P.J., 1993. Crystallization phenomena in bacterial poly[(R)-3-hyd roxybutyrate]: 2. Embrittlement and rejuvenation. Polymer 34, 4089-4094.

Dean, K.M., Petinakis, E., Meure, S., Yu, L., Chryss, A., 2012. Melt strength and rheological properties of biodegradable poly(lactic acid) modified via alkyl radical-based reactive extrusion processes. Journal of Polymers and the Environment 20, 741-747.

Dias, J.M.L., Lemos, P.C., Serafim, L.S., Oliveira, C., Eiroa, M., Albuquerque, M.G.E., Ramos, A.M., Oliveira, R., Reis, M.A.M., 2006. Recent advances in polyhydroxyalkanoate production by mixed aerobic cultures: from the substrate to the final product. Macromolecular Bioscience 6, 885-906.

Dionisi, D., Carucci, G., Papini, M.P., Riccardi, C., Majone, M., Carrasco, F., 2005. Olive oil mill effluents as a feedstock for production of biodegradable polymers. Water Research 39, 2076-2084.

Dobroth, Z.T., Hu, S., Coats, E.R., McDonald, A.G., 2011. Polyhydroxybutyrate synthesis on biodiesel wastewater using mixed microbial consortia. Bioresource Technology 102, 3352-3359.

Doi, Y., Kunioka, M., Nakamura, Y., Soga, K., 1988. Nuclear magnetic resonance studies on unusual bacterial copolyesters of 3-hydroxybutyrate and 4-hydroxybutyrate. Macromolecules 21, 2722-2727.

Dong, Y., Ghataura, A., Takagi, H., Haroosh, H.J., Nakagaito, A.N., Lau, K.-T., 2014. Polylactic acid (PLA) biocomposites reinforced with coir fibres: Evaluation of mechanical performance and multifunctional properties. Composites Part A: Applied Science and Manufacturing 63, 76-84.

Dorgan, J.R., Williams, J.S., Lewis, D.N., 1999. Melt rheology of poly (lactic acid): Entanglement and chain architecture effects. Journal of Rheology 43, 1141-1155.

dos Santos Rosa, D., Calil, M.R., Guedes, C.d.G.a.F., Santos, C.E.O., 2001. The effect of UV-B irradiation on the biodegradability of poly-β-hydroxybutyrate (PHB) and poly-ε-caprolactone (PCL). Journal of Polymers and the Environment 9, 109-113.

dos Santos Rosa, D., Calil, M.R., Guedes, C.d.G.F., Rodrigues, T.C., 2004. Biodegradability of Thermally Aged PHB, PHB-V, and PCL in Soil Compostage. Journal of Polymers and the Environment 12, 239-245.

Dufresne, A., Kellerhals, M.B., Witholt, B., 1999. Transcrystallization in Mcl-PHAs/cellulose whiskers composites. Macromolecules 32, 7396-7401.

Duque, A.F., Oliveira, C.S.S., Carmo, I.T.D., Gouveia, A.R., Pardelha, F., Ramos, A.M., Reis, M.A.M., 2014. Response of a three-stage process for PHA production by mixed microbial cultures to feedstock shift: impact on polymer composition. New Biotechnology 31, 276-288.

EBA, 2013. Bioplastics market grows above average between 2012 and 2017: European Boplastics publishes market data update. European Bioplastics, Marienstr, Berlin.

Erceg, M., Kovačić, T., Klarić, I., 2005. Thermal degradation of poly(3-hydroxybutyrate) plasticized with acetyl tributyl citrate. Polymer Degradation and Stability 90, 313-318.

Fambri, L., Migliaresi, C., 2010. Crystalliation and thermal properties, in: Auras, R., Lim, L.-T., Selke, S.E.M., Tsuji, H. (Eds.), Poly(Lactic Acid): Synthesis, Structures, Properties, Processing, and Applications. John Wiley & Sons, Inc.: Hoboken, New Jersey, Chap.9, pp.113-124.

Faruk, O., Bledzki, A.K., Fink, H.-P., Sain, M., 2012. Biocomposites reinforced with natural fibers: 2000–2010. Progress in Polymer Science 37, 1552-1596.

Filippou, P.S., Koini, E.N., Calogeropoulou, T., Kalliakmani, P., Panagiotidis, C.A., Kyriakidis, D.A., 2011. Regulation of the Escherichia coli AtoSC two component system by synthetic biologically active 5;7;8-trimethyl-1;4-benzoxazine analogues. Bioorganic & Medicinal Chemistry 19, 5061-5070.

Förster, B.S., Antonietti, M., 1998. Amphiphilic block copolymers in structure-controlled nanomaterial hybrids. Advanced Materials 10, 195-217.

Fujita, M., Sawayanagi, T., Tanaka, T., Iwata, T., Abe, H., Doi, Y., Ito, K., Fujisawa, T., 2005. Synchrotron SAXS and WAXS studies on changes in structural and thermal properties of poly[(R)-3-hydroxybutyrate] single crystals during heating. Macromolecular Rapid Communications 26, 678-683.

García, I.L., López, J.A., Dorado, M.P., Kopsahelis, N., Alexandri, M., Papanikolaou, S., Villar, M.A., Koutinas, A.A., 2013. Evaluation of by-products from the biodiesel industry as fermentation feedstock for poly(3-hydroxybutyrate-co-3-hydroxyvalerate) production by Cupriavidus necator. Bioresource Technology 130, 16-22.

Garlotta, D., 2001. A literature review of PLA. Journal of Polymers and the Environment 9, 63-84.

Gassan, J., Bledzki, A.K., 1999. Effect of cyclic moisture absorption desorption on the mechanical properties of silanized jute-epoxy composites. Polymer Composites 20, 604-611.

Groot, W., van Krieken, J., Sliekersi, O., de Vos, A.S., 2010. Production and purification of lactic acid and lactide, in: Auras, R., Lim, L.-T., Selke, S.E.M., Tsuji, H. (Eds.), Poly(Lactic Acid): Synthesis, Structures, Properties, Processing, and Applications. John Wiley & Sons, Inc.: Hoboken, New Jersey, Chap.1, pp. 3-18.

Gumel, A.M., Annuar, M.S.M., Chisti, Y., 2013. Recent advances in the production, recovery and applications of polyhydroxyalkanoates. Journal of Polymers and the Environment 21, 580-605.

Gumel, A.M., Annuar, M.S.M., Heidelberg, T., 2012. Effects of carbon substrates on biodegradable polymer composition and stability produced by Delftia tsuruhatensis Bet002 isolated from palm oil mill effluent. Polymer Degradation and Stability 97, 1224-1231.

Gunaratne, L.M.W.K., Shanks, R.A., 2006. Isothermal crystallisation kenetics of poly(3-hydroxybutyrate) using step-scan DSC. Journal of Thermal Analysis and Calorimetry 83, 313-319.

Gunaratne, L.M.W.K., Shanks, R.A., Amarasinghe, G., 2004. Thermal history effects on crystallisation and melting of poly(3-hydroxybutyrate). Thermochimica Acta 423, 127-135.

Gurieff, N., Lant, P., 2007. Comparative life cycle assessment and financial analysis of mixed culture polyhydroxyalkanoate production. Bioresource Technology 98, 3393-3403.

Hadjichristidis, N., Pitsikalis, M., Pispas, S., Iatrou, H., 2001. Polymers with complex architecture by living anionic polymerization. Chemical Reviews 101, 3747-3792.

Halden, R.U., 2010. Plastics and health risks. Annual Review of Public Health 31, 179-194.

Hazer, B., 2010. Amphiphilic poly(3-hydroxy alkanoate)s: Potential candidates for medical applications. International Journal of Polymer Science 2010, 1-8.

He, W., Tian, W., Zhang, G., Chen, G.Q., Zhang, Z., 1998. Production of novel polyhydroxyalkanoates by Pseudomonas stutzeri 1317 from glucose and soybean oil. FEMS Microbilogy Letters 169, 45-49.

He, Z., Jiang, L., Chuan, Y., Li, H., Yuan, M., 2013. Ring-opening polymerization of L-lactic acid *O*-carboxyanhydrides initiated by alkoxy rare earth compounds. Molecules 18, 12768-12776.

Holmes, P.A., 1985. Applications of PHB-a microbially produced biodegradable thermoplastic. Physics in Technology 16, 32-36.

Holmes, P.A., 1988. Biologically produced (R)-3-hydroxyalkanoate polymers and copolymers, in: Bassett, O.C. (Ed.), Developments in crystalline polymers-2. Elsevier Applied Science Publishers Ltd.: Essex, UK, pp. 1-65.

Hon, D.N.-S., Shiraishi, N., 2001. Wood and cellulosic chemistry, Second Edition, Revised, and Expanded. Marcel Dekker, Inc., New York.

Horng, Y.T., Chien, C.C., Huang, C.T., Wei, Y.H., Chen, S.Y., Lan, J.C.W., Soo, P.C., 2013. Biosynthesis of poly(3-hydroxybutyrate-co-3-hydroxyvalerate) with co-expressed propionate permease (prpP), beta-ketothiolase B (bktB), and propionate-CoA synthase (prpE) in Escherichia coli. Biochemical Engineering Journal 78, 73-79.

Hu, D., Chung, A.-L., Wu, L.-P., Zhang, X., Wu, Q., Chen, J.-C., Chen, G.-Q., 2011. Biosynthesis and characterization of polyhydroxyalkanoate block copolymer P3HB-b-P4HB. Biomacromolecules 12, 3166-3173.

Hu, S., McDonald, A.G., Coats, E.R., 2013. Characterization of polyhydroxybutyrate biosynthesized from crude glycerol waste using mixed microbial consortia. Journal of Applied Polymer Science 129, 1314-1321.

Ienczak, J.L., Schmidell, W., de Aragão, G.M.F., 2013. High-cell-density culture strategies for polyhydroxyalkanoate production: a review. Journal of Industrial Microbiology & Biotechnology 40, 275-286.

Ikada, Y., Jamshidi, K., Tsuji, H., Hyon, S.H., 1987. Stereocomplex formation between enantiomeric poly(lactides). Macromolecules 20, 904-906.

Ishihara, Y., Shimizu, H., Shioya, S., 1996. Mole fraction control of poly(3-Hydroxbutyric-co-3-Hydroxyvaleric) acid in fed-batch culture of *Alcaligenes eutrophus*. Journal of Fermentation and Bioengineering 81, 422-428.

Jamshidi, K., Hyon, S.-H., Ikada, Y., 1988. Thermal characterization of polylactides. Polymer 29, 2229-2234.

Janarthanan, O.M., Yu, Y., Laycock, B., Werker, A., Pratt, S., 2014. Fractionation of microbial populations in a PHA accumulating mixed culture and associated PHA content and composition. International Journal of Biological Macromolecules.

Jandas, P.J., Mohanty, S., Nayak, S.K., 2013. Sustainability, compostability, and specific microbial activity on agricultural mulch films prepared from poly(lactic acid). Industrial and Engineering Chemistry Research 52, 17714-17724.

Jendrossek, D., Pfeiffer, D., 2014. New insights in the formation of polyhydroxyalkanoate granules (carbonosomes) and novel functions of poly(3-hydroxybutyrate). Environmental Microbiology 16, 2357-2373.

Jiang, L., Morelius, E., Zhang, J., Wolcott, M., Holbery, J., 2008. Study of the poly(3-hydroxybutyrate-co-3-hydroxyvalerate)/cellulose nanowhisker composites prepared by solution casting and melt processing. Journal of Composite Materials 42, 2629-2645.

Jiang, X., Sun, Z., Marchessault, R.H., Ramsay, J.A., Ramsay, B.A., 2012. Biosynthesis and properties of medium-chain-length polyhydroxyalkanoates with enriched content of the dominant monomer. Biomacromolecules 13, 2926-2932.

Jiang, Y., Chen, Y., Zheng, X., 2009. Efficient polyhydroxyalkanoates production from a waste-activated sludge alkaline fermentation liquid by activated sludge submitted to the aerobic feeding and discharge process. Environmental science & technology 43, 7734-7741.

John, M., Thomas, S., 2008. Biofibres and biocomposites. Carbohydrate Polymers 71, 343-364.

Johnson, K., Jiang, Y., Kleerebezem, R., Muyzer, G., Van Loosdrecht, M.C.M., 2009. Enrichment of a mixed bacterial culture with a high polyhydroxyalkanoate storage capacity. Biomacromolecules 10, 670-676.

Joseph, K., Thomas, S., 1996. Effect of chemical treatment on the tensile properties of short sisal fibre-reinforced polyethylene composites. Polymer 37, 5139-5149.

Jung, Y.K., Kim, T.Y., Park, S.J., Lee, S.Y., 2010. Metabolic engineering of Escherichia coli for the production of polylactic acid and its copolymers. Biotechnology and Bioengineering 105, 161-171.

Kadla, J.F., Gilbert, R.D., 2000. Cellulose structure: A review. Cellulose Chemistry and Technology, 197-216.

Kalia, S., Dufresne, A., Cherian, B.M., Kaith, B.S., Avérous, L., Njuguna, J., Nassiopoulos, E., 2011. Cellulose-based bio- and nanocomposites: A review. International Journal of Polymer Science 2011, 1-35.

Kamiya, N., Yamamoto, Y., Inoue, Y., Chujo, R., Doi, Y., 1989. Microstructure of bacterially synthesized poly(3-hydroxybutyrate-*co*-3-hydroxyvalerate). Macromolecules 22, 1676-1682.

Khanna, S., Srivastava, A.K., 2005. Recent advances in microbial polyhydroxyalkanoates. Process Biochem. 40, 607-619.

Kim, D.Y., Kim, H.W., Chung, M.G., Rhee, Y.H., 2007. Biosynthesis, modification, and biodegradation of bacterial medium-chain-length polyhydroxyalkanoates. The Journal of Microbiology 45, 87-97.

Kleerebezem, R., Van Loosdrecht, M.C.M., 2007. Mixed culture biotechnology for bioenergy production. Current Opinion in Biotechnology 18, 207-212.

Klemm, D., Heublein, B., Fink, H.-P., Bohn, A., 2005. Cellulose: fascinating biopolymer and sustainable raw material. Angewandte Chemie International Edition 44, 3358-3393.

Koller, M., Atlic, A., Dias, M., Reiterer, A., Braunegg, G., 2010. Microbial PHA production from waste raw materials, in: Chen, G.Q. (Ed.), Plastics from bacteria. Natural functions and applications. Springer-Verlag, Berlin, pp. 85-119.

Koller, M., Bona, R., Braunegg, G., Hermann, C., Horvat, P., Kroutil, M., Martinz, J., Neto, J., Pereira, L., Varila, P., 2005. Production of polyhydroxyalkanoates from agricultural waste and surplus materials. Biomacromolecules 6, 561-565.

Kong, Y., Nielsen, J.L., Nielsen, P.H., 2004. Microautoradiographic study of rhodocyclus-related polyphosphate-accumulating bacteria in full-scale enhanced biological phosphorus removal plants. Applied and Environmental Microbiology 70, 5383-5390.

Kulpreecha, S., Boonruangthavorn, A., Meksiriporn, B., Thongchul, N., 2009. Inexpensive fed-batch cultivation for high poly(3-hydroxybutyrate) production by a new isolate of Bacillus megaterium. Journal of Bioscience and Bioengineering 107, 240-245.

Lau, N.-S., Tsuge, T., Sudesh, K., 2011. Formation of new polyhydroxyalkanoate containing 3-hydroxy-4-methylvalerate monomer in Burkholderia sp. Applied Microbiology and Biotechnology 89, 1599-1609.

Laycock, B., Halley, P., Pratt, S., Werker, A., Lant, P., 2013. The chemomechanical properties of microbial polyhydroxyalkanoates. Progress in Polymer Science 38, 536-583.

Le Meur, S., Zinn, M., Egli, T., Thöny-Meyer, L., Ren, Q., 2012. Production of medium-chain-length polyhydroxyalkanoates by sequential feeding of xylose and octanoic acid in engineered Pseudomonas putida KT2440. BMC Biotechnology 12, 53-64.

Lehermeier, H.J., Dorgan, J.R., 2001. Melt rheology of poly(lactic acid): Consequences of blending chain architectures. Polymer Engineering and Science 41, 2172-2184.

Li, S.Y., Dong, C.L., Wang, S.Y., Ye, H.M., Chen, G.-Q., 2011. Microbial production of polyhydroxyalkanoate block copolymer by recombinant Pseudomonas putida. Applied Microbiology and Biotechnology 90, 659-669.

Li, Z.-J., Shi, Z.-Y., Jian, J., Guo, Y.-Y., Wu, Q., Chen, G.-Q., 2010. Production of poly(3-hydroxybutyrate-co-4-hydroxybutyrate) from unrelated carbon sources by metabolically engineered Escherichia coli. Metabolic Engineering 12, 352-359.

Linger, J.G., Vardon, D.R., Guarnieri, M.T., Karp, E.M., Hunsinger, G.B., Franden, M.A., Johnson, C.W., Chupka, G., Strathmann, T.J., Pienkos, P.T., Beckham, G.T., 2014. Lignin valorization through integrated biological funneling and chemical catalysis. Proceedings of the National Academy of Sciences 111, 12013-12018.

Liu, F., Jian, J., Shen, X., Chung, A., Chen, J., Chen, G.-Q., 2011a. Metabolic engineering of Aeromonas hydrophila 4AK4 for production of copolymers of 3-hydroxybutyrate and medium-chain-length 3-hydroxyalkanoate. Bioresource Technology 102, 8123-8129.

Liu, Q., Luo, G., Zhou, X.R., Chen, G.-Q., 2011b. Biosynthesis of poly(3-hydroxydecanoate) and 3-hydroxydodecanoate dominating polyhydroxyalkanoates by β-oxidation pathway inhibited Pseudomonas putida. Metabolic Engineering 13, 11-17.

Liu, R., Peng, Y., Cao, J., Chen, Y., 2014. Comparison on properties of lignocellulosic flour/polymer composites by using wood, cellulose, and lignin flours as fillers. Composites Science and Technology 103, 1-7.

Loo, C.-Y., Lee, W.-H., Tsuge, T., Doi, Y., Sudesh, K., 2005. Biosynthesis and characterization of poly(3-hydroxybutyrate-co-3- hydroxyhexanoate) from palm oil products in a Wautersia eutropha mutant. Biotechnology Letters 27, 1405-1410.

Loureiro, N.C., Esteves, J.L., Viana, J.C., Ghosh, S., 2013. Mechanical characterization of polyhydroxyalkanoate and poly(lactic acid) blends. Journal of Thermoplastic Composite Materials.

Lu, J.Z., Wu, Q., McNabb, H.S., 2000. Chemical coupling in wood fiber and polymer composites: A review of coupling agents and treatments. Wood and Fiber Science 32, 88-104.

Madden, L.A., Anderson, A.J., Asrar, J., 1998. Synthesis and characterization of poly(3-hydroxybutyrate) and poly(3-hydroxybutyrate-co-3-hydroxyvalerate) polymer mixtures produced in high-density fed-batch cultures of Ralstonia eutropha (Alcaligenes eutrophus). Macromolecules 31, 5660-5667.

Madison, L., Huisman, G.W., 1999. Metabolic engineering of poly(3-Hydroxyalkanoates): from DNA to plastic. Microbiology and Molecular Biology Reviews 63, 21-53.

Majone, M., Masanisso, P., Carucci, A., Lindrea, K., Tandoi, V., 1996. Influence of storage on kinetic selection to control aerobic filamentous bulking. Water Science and Technology 34, 223-232.

Markarian, J., 2007. Slip and antiblock additives: surface medication for film and sheet. Plastics, Additives and Compounding 9, 32-35.

Marshall, C.W., LaBelle, E.V., May, H.D., 2013. Production of fuels and chemicals from waste by microbiomes. Current Opinion in Biotechnology 24, 391-397.

Masirek, R., Kulinski, Z., Chionna, D., Piorkowska, E., Pracella, M., 2007. Composites of poly(L-lactide) with hemp fibers: Morphology and thermal and mechanical properties. Journal of Applied Polymer Science 105, 255-268.

McChalicher, C., Srienc, F., 2007. Investigating the structure–property relationship of bacterial PHA block copolymers. Journal of Biotechnology 132, 296-302.

McDonald, A.G., Ma, L., 2010. Plastic moldable pine fiber by benzylation, in: Botannini, L.F. (Ed.), Wood: Types, Properties, and Uses (Environmental Science, Engineering and Technology) Nova Science Publishers, Inc., pp.181-192.

Mekonnen, T., Mussone, P., Khalil, H., Bressler, D., 2013. Progress in bio-based plastics and plasticizing modifications. Journal of Materials Chemistry 1, 13379-13398.

Meng, D.-C., Shen, R., Yao, H., Chen, J.-C., Wu, Q., Chen, G.-Q., 2014. Engineering the diversity of polyesters. Current Opinion in Biotechnology 29, 24-33.

Merton-Council, 2013. Landfill site: what happens to your waste? Merton Council and its licensors. http://www.merton.gov.uk/environment/waste/recycling/whyrecycle/landfill.htm.

Mitomoa, H., Hsieha, W.-C., Nishiwakia, K., Kasuyaa, K., Doi, Y., 2001. Poly(3-hydroxybutyrate-co-4-hydroxybutyrate) produced by *Comamonas acidovorans*. Polymer 42, 3455-3461.

Modi, S., Koelling, K., Vodovotz, Y., 2013. Assessing the mechanical, phase inversion, and rheological properties of poly-[(R)-3-hydroxybutyrate-co-(R)-3-hydroxyvalerate] (PHBV) blended with poly-(l-lactic acid) (PLA). European Polymer Journal 49, 3681-3690.

Mohanty, A.K., Misra, M., Drzal, L.T., 2002. Sustainable bio-composites from renewable resources: opportunities and challenges in the green materials world. Journal of Polymers and the Environment 10, 19-26.

Moita, R., Lemos, P.C., 2012. Biopolymers production from mixed cultures and pyrolysis by-products. Journal of Biotechnology 157, 578-583.

Morgan-Sagastume, F., Karlsson, A., Johansson, P., Pratt, S., Boon, N., Lant, P., Werker, A., 2010. Production of polyhydroxyalkanoates in open, mixed cultures from a waste sludge stream containing high levels of soluble organics, nitrogen and phosphorus. Water Research 44, 5196-5211.

Narayan, R., Shi, X., Graiver, D., 2013. PLA recycling via thermal depolymerization, Bioplastics Magazine. Polymedia Publisher GmbH, Mönchengladbach, Germany.

Narayan, R., Wu, W.M., Criddle, C.S., 2012. Lactide production from thermal depolymerization of PLA with applications to production of PLA or other bioproducts. U.S. Patent Application 13/421780 3/, p. 780.

Obuchi, S., Ogawa, S., 2010. Packaging and other commercial applications, in: Auras, R., Lim, L.-T., Selke, S.E.M., Tsuji, H. (Eds.), Poly(Lactic Acid): Synthesis, Structures, Properties, Processing, and Applications. John Wiley & Sons, Inc.: Hoboken, New Jersey, Chap.28, pp.457-467.

Oehmen, A., Pinto, F.V., Silva, V., Albuquerque, M.G.E., Reis, M.A.M., 2014. The impact of pH control on the volumetric productivity of mixed culture PHA production from fermented molasses. Engineering in Life Sciences 14, 143-152.

Ojijo, V., Sinha Ray, S., Sadiku, R., 2013. Toughening of biodegradable polylactide/poly(butylene succinate-co-adipate) blends via in situ reactive compatibilization. ACS Applied Materials & Interfaces, 130510085040001.

Oksman, K., Skrifvars, M., Selin, J.F., 2003. Natural fibres as reinforcement in polylactic acid (PLA) composites. Composites Science and Technology 63, 1317-1324.

Orts, W.J., Marchessault, R.H., Bluhm, T.L., Hamer, G.K., 1990. Observation of strain-induced β-form in poly(β-hydroxyalkanoates). Macromolecules 23, 5368-5370.

Palade, L.-I., Lehermeier, H.J., Dorgan, J.R., 2001. Melt rheology of high $_{L}$-content poly(lactic acid). Macromolecules 34, 1384-1390.

Pardelha, F., Albuquerque, M.G.E., Reis, M.A.M., Dias, J.M.L., Oliveira, R., 2012. Flux balance analysis of mixed microbial cultures: Application to the production of polyhydroxyalkanoates from complex mixtures of volatile fatty acids. Journal of Biotechnology 162, 336-345.

Pardelha, F., Albuquerque, M.G.E., Reis, M.A.M., Oliveira, R., Dias, J.M.L., 2014. Dynamic metabolic modelling of volatile fatty acids conversion to polyhydroxyalkanoates by a mixed microbial culture. New Biotechnology 31, 335-344.

Park, S.D., Todo, M., Arakawa, K., 2004. Effect of annealing on the fracture toughness of poly(lactic acid). Journal of Materials Science 39, 1113-1116.

Pederson, E.N., McChalicher, C.W.J., Srienc, F., 2006. Bacterial synthesis of PHA block copolymers. Biomacromolecules 7, 1904-1911.

Pereira, S.M.F., Sánchez, R.J., Rieumont, J., Cabrera, J.G., 2008. Synthesis of biodegradable polyhydroxyalcanoate copolymer from a renewable source by alternate feeding. Polymer Engineering & Science 48, 2051-2059.

Pilla, S., 2011. Handbook of bioplastics and biocomposites engineering applications, Vol 81. John Wiley & Sons, Inc., Inc. Hoboken, New Jersey.

Pisco, A.R., Bengtsson, S., Werker, A., Reis, M.A.M., Lemos, P.C., 2009. Community structure evolution and enrichment of glycogen-accumulating organisms producing polyhydroxyalkanoates from fermented molasses. Applied and Environmental Microbiology 75, 4676-4686.

Rai, R., Keshavarz, T., Roether, J.A., Boccaccini, A.R., Roy, I., 2011a. Medium chain length polyhydroxyalkanoates, promising new biomedical materials for the future. Materials Science and Engineering: R: Reports 72, 29-47.

Rai, R., Yunos, D.M., Boccaccini, A.R., Knowles, J.C., Barker, I.A., Howdle, S.M., Tredwell, G.D., Keshavarz, T., Roy, I., 2011b. Poly-3-hydroxyoctanoate P(3HO), a medium chain length polyhydroxyalkanoate homopolymer from *Pseudomonas mendocina*. Biomacromolecules 12, 2126-2136.

Ramakrishna, S., Mayer, J., Wintermantel, E., Leong, K.W., 1189-1224., 2001. Biomedical applications of polymer-composites materials: A review. Composites Science and Technology.

Ramalingam, S., Vikram, M., Vigneshbabu, M.P., Sivasankari, M., 2011. Flux balance analysis for maximizing polyhydroxyalkanoate production in Pseudomonas putida. Indian Journal of Biotechnology 10, 70-74.

Reddy, C.S.K., Rashmi, R.G., Kalia, V.C., 2003. Polyhydroxyalkanoates: an overview. Bioresource Technology 87, 137-146.

Reis, M.A.M., Serafim, L.S., Lemos, P.C., Ramos, A.M., Aguiar, F.R., Van Loosdrecht, M.C.M., 2003. Production of polyhydroxyalkanoates by mixed microbial cultures. Bioprocess and Biosystems Engineering 25, 377-385.

Renstad, R., Karlsson, S., Sandgren, Å., Albertsson, A.C., 1998. Influence of processing additives on the degradation of melt-pressed films of poly (ε-caprolactone) and poly (lactic acid). Journal of environmental polymer degradation 6, 209-221.

Riedel, S.L., Lu, J., Stahl, U., Brigham, C.J., 2013. Lipid and fatty acid metabolism in Ralstonia eutropha: relevance for the biotechnological production of value-added products. Applied Microbiology and Biotechnology 98, 1469-1483.

Rowell, R., 2005. Handbook of wood chemistry and wood composites. CRC Press, Boca Raton, Florida.

Roy, D., Semsarilar, M., Guthrie, J.T., Perrier, S., 2009. Cellulose modification by polymer grafting: A review. Chemical Society Reviews 38, 2046.

Saad, G.R., 2001. Calorimetric and dielectric study ofthe segmented biodegradable ooly(ester-urethane)s based on bacterial poly[(R)-3-hydroxybutyrate]. Macromolecular Bioscience 1, 387-396.

Saito, M., Inoue, Y., Yoshie, N., 2001. Cocrystallization and phase segregation of blends of poly(3-hydroxybutyrate) and poly(3-hydroxybutyrate-co-3-hydroxyvalerate). Polymer 42, 5573-5580.

Salehizadeh, H., Van Loosdrecht, M.C.M., 2004. Production of polyhydroxyalkanoates by mixed culture: recent trends and biotechnological importance. Biotechnology Advances 22, 261-279.

Samain, X., Langlois, V., Renard, E., Lorang, G., 2011. Grafting biodegradable polyesters onto cellulose. Journal of Applied Polymer Science 121, 1183-1192.

Satyanarayana, K.G., Arizaga, G.G.C., Wypych, F., 2009. Biodegradable composites based on lignocellulosic fibers—an overview. Progress in Polymer Science 34, 982-1021.

Serafim, L.S., Lemos, P.C., Albuquerque, M.G.E., Reis, M.A.M., 2008. Strategies for PHA production by mixed cultures and renewable waste materials. Applied Microbiology and Biotechnology 81, 615-628.

Shanks, R.A., Hodzic, A., Wong, S., 2004. Thermoplastic biopolyester natural fiber composites. Journal of Applied Polymer Science 91, 2114-2121.

Sheik, A.R., Muller, E.E.L., Wilmes, P., 2014. A hundred years of activated sludge: time for a rethink. Frontiers in Microbiology 5.

Shen, L., Haufe, J., Patel, M., 2009. Product overview and market projection of emerging bio-based plastics PRO-BIP 2009. Report for European Polysaccharide Network of Excellence (EPNOE) and European Bioplastics.

Shishatskaya, E.I., Volova, T.G., Puzyr, A.P., Mogilnaya, O.A., Efremov, S.N., 2004. Tissue response to the implantation of biodegradable polyhydroxyalkanoate sutures. Journal of Materials Science: Materials in Medicine 15, 719-728.

Singh, S., Mohanty, A.K., Sugie, T., Takai, Y., Hamada, H., 2008. Renewable resource based biocomposites from natural fiber and polyhydroxybutyrate-co-valerate (PHBV) bioplastic. Composites Part A: Applied Science and Manufacturing 39, 875-886.

Södergård, A., Stolt, M., 2002. Properties of lactic acid based polymers and their correlation with composition. Progress in Polymer Science 27, 1123-1163.

Somleva, M.N., Peoples, O.P., Snell, K.D., 2013. PHA bioplastics, biochemicals, and energy from crops. Plant Biotechnology Journal 11, 233-252.

Srithep, Y., Ellingham, T., Peng, J., Sabo, R., Clemons, C., Turng, L.-S., Pilla, S., 2013. Melt compounding of poly (3-hydroxybutyrate-co-3-hydroxyvalerate)/nanofibrillated cellulose nanocomposites. Polymer Degradation and Stability 98, 1439-1449.

Steinbüchel, A., Debzi, E.M., Marchessault, R.H., Timm, A., 1993. Synthesis and production of poly (3-hydroxyvaleric acid) homopolyester by Chromobacterium violaceum. Applied microbiology and biotechnology 39, 443-449.

Steinbüchel, A., Valentin, H.E., 1995. Diversity of bacterial polyhydroxyalkanoic acids. FEMS Microbilogy Letters 128, 219-228.

Steinbüchel, A., Valentin, H.E., Schönebaum, A., 1994. Application of recombinant gene technology for production of polyhydroxyalkanoic acids: biosynthesis of poly (4-hydroxybutyric acid) homopolyester. Journal of environmental polymer degradation 2, 67-74.

Sudesh, K., Abe, H., 2010. Practical guide to microbial polyhydroxyalkanoates. ISmithers, Shawbury, United Kingdom.

Sudesh, K., Abe, H., Doi, Y., 2000. Synthesis, structure and properties of polyhydroxyalkanoates: biological polyesters. Progress in Polymer Science 25, 1503-1555.

Sun, X.S., 2011. Plastics derived from starch and poly(lactic acids), in: Wool, R., Sun, X.S. (Eds.), Bio-based polymers and composites. Elsevier Academic Press: Burlington, MA, Chap. 11, pp.369-410.

Suriyamongkol, P., Weselake, R., Narine, S., Moloney, M., Shah, S., 2007. Biotechnological approaches for the production of polyhydroxyalkanoates in microorganisms and plants — A review. Biotechnology Advances 25, 148-175.

TakePart, 2014. Oceans/Plastic-Pollution., TakePart, Participant Media, Beverly Hills, CA.

Tanadchangsaeng, N., Tsuge, T., Abe, H., 2010. Comonomer compositional distribution, physical properties, and enzymatic degradability of bacterial poly(3-hydroxybutyrate-co-3-hydroxy-4-methylvalerate) copolyesters. Biomacromolecules 11, 1615-1622.

Tanaka, T., Fujita, M., Takeuchi, A., Suzuki, Y., Uesugi, K., Doi, Y., Iwata, T., 2005. Structure investigation of narrow banded spherulites in polyhydroxyalkanoates by microbeam X-ray diffraction with synchrotron radiation. Polymer 46, 5673-5679.

Tappel, R.C., Pan, W., Bergey, N.S., Wang, Q., Patterson, I.L., Ozumba, O.A., Matsumoto, K.i., Taguchi, S., Nomura, C.T., 2014. Engineering *Escherichia coli* for improved production of short-chain-length-co-medium-chain-length poly[(R)-3-hydroxyalkanoate] (SCL-co-MCL PHA) copolymers from renewable nonfatty acid feedstocks. ACS Sustainable Chemistry & Engineering 2, 1879-1887.

Terzopoulou, Z.N., Papageorgiou, G.Z., Elektra Papadopouloub, Athanassiadou, E., Alexopoulou, E., Bikiaris, D.N., 2014. Green composites prepared from aliphatic polyesters and bast fibers. ndustrial Crops and Products. DOI: 10.1016/j.indcrop.2014.08.034, in press.

Theodorou, E.C., Theodorou, M.C., Kyriakidis, D.A., 2011. AtoSC two-component system is involved in cPHB biosynthesis through fatty acid metabolism in E. coli. Biochimica et Biophysica Acta (BBA) - General Subjects 1810, 561-568.

Tripathi, L., Wu, L.-P., Chen, J., Chen, G.-Q., 2012. Synthesis of diblock copolymer poly-3-hydroxybutyrate-block-poly-3-hydroxyhexanoate [PHB-b-PHHx] by a β-oxidation weakened *Pseudomonas putida* KT2442. Microbial Cell Factories 11, 44.

Tripathi, L., Wu, L.-P., Dechuan, M., Chen, J., Wu, Q., Chen, G.-Q., 2013a. Pseudomonas putida KT2442 as a platform for the biosynthesis of polyhydroxyalkanoates with adjustable monomer contents and compositions. Bioresource Technology 142, 225-231.

Tripathi, L., Wu, L.-P., Meng, D., Chen, J., Chen, G.-Q., 2013b. Biosynthesis and characterization of diblock copolymer of P(3-Hydroxypropionate)-block-P(4-hydroxybutyrate) from Recombinant Escherichia coli. Biomacromolecules 14, 862-870.

Tsuji, H., Suzuyoshi, K., 2002. Environmental degradation of biodegradable polyesters 1. Poly(e-caprolactone), poly[(R)-3-hydroxybutyrate], and poly(L-lactide) films in controlled static seawater. Polymer Degradation and Stability 75, 347-355.

Urtuvia, V., Villegas, P., González, M., Seeger, M., 2014. Bacterial production of the biodegradable plastics polyhydroxyalkanoates. International Journal of Biological Macromolecules 70, 208-213.

Verlinden, R.A., Hill, D.J., Kenward, M.A., Williams, C.D., Piotrowska-Seget, Z., Radecka, I.K., 2011. Production of polyhydroxyalkanoates from waste frying oil by Cupriavidus necator. AMB Express 1, 1-8.

Villano, M., Beccari, M., Dionisi, D., Lampis, S., Miccheli, A., Vallini, G., Majone, M., 2010. Effect of pH on the production of bacterial polyhydroxyalkanoates by mixed cultures enriched under periodic feeding. Process Biochemistry 45, 714-723.

Wagner, A., Poursorkhabi, V., Mohanty, A.K., Misra, M., 2014. Analysis of porous electrospun fibers from poly(l-lactic acid)/poly(3-hydroxybutyrate-co-3-hydroxyvalerate) blends. ACS Sustainable Chemistry & Engineering 2, 1976-1982.

Walle, G.A.M.V.d., Koning, G.J.M.d., Weusthuis, R.A., Eggink, G., 2001. Properties, modifications and applications of biopolyesters. Advances in Biochemical Engineering/Biotechnology 71, 263-291.

Wallen, L.L., Rohwedder, W.K., 1974. Poly-β-hydroxyalkanoate from activated sludge. Environmental Science and Technology 8, 576-579.

Wang, H.-h., Li, X.-t., Chen, G.-Q., 2009. Production and characterization of homopolymer polyhydroxyheptanoate (P3HHp) by a fadBA knockout mutant Pseudomonas putida KTOY06 derived from P. putida KT2442. Process Biochemistry 44, 106-111.

Wang, H.-h., Zhou, X.-r., Liu, Q., Chen, G.-Q., 2010. Biosynthesis of polyhydroxyalkanoate homopolymers by Pseudomonas putida. Applied Microbiology and Biotechnology 89, 1497-1507.

Wang, Q., Yang, P., Xian, M., Liu, H., Cao, Y., Yang, Y., Zhao, G., 2013a. Production of block copolymer poly(3-hydroxybutyrate)-block-poly(3-hydroxypropionate) with adjustable structure from an inexpensive carbon source. ACS Macro Letters 2, 996-1000.

Wang, Q., Yang, P., Xian, M., Yang, Y., Liu, C., Xue, Y., Zhao, G., 2013b. Biosynthesis of poly(3-hydroxypropionate-co-3-hydroxybutyrate) with fully controllable structures from glycerol. Bioresource Technology 142, 741-744.

Wei, L., McDonald, A.G., Freitag, C., Morrell, J.J., 2013. Effects of wood fiber esterification on properties, weatherability and biodurability of wood plastic composites. Polymer Degradation and Stability 98, 1348-1361.

Witzke, D.R., Narayan, R., Kolstad, J.J., 1997. Reversible kinetics and thermodynamics of the homopolymerization of L-lactide with 2-ethylhexanoic acid Tin(II) salt. Macromolecules 30, 7075-7085.

Wong, S., Shanks, R., Hodzic, A., 2004. Interfacial improvements in poly(3-hydroxybutyrate)-flax fibre composites with hydrogen bonding additives. Composites Science and Technology 64, 1321-1330.

Yang, J.E., Choi, Y.J., Lee, S.J., Kang, K.-H., Lee, H., Oh, Y.H., Lee, S.H., Park, S.J., Lee, S.Y., 2013. Metabolic engineering of *Escherichia coli* for biosynthesis of poly(3-hydroxybutyrate-co-3-hydroxyvalerate) from glucose. Applied Microbiology and Biotechnology 98, 95-104.

Yang, X., Zhao, K., Chen, G., 2002. Effect of surface treatment on the biocompatibility of microbial polyhydroxyalkanoates. Biomaterials 23, 1391-1397.

Yoshie, N., Menju, H., Sato, H., Inoue, Y., 1995. Complex composition distribution of poly(3-hydroxybutyrate-co-3-hydroxyvalerate). Macromolecules 28, 6516-6521.

Yu, G.-e., Morin, F.G., Nobes, G.A.R., Marchessault, R.H., 1999. Degree of acetylation of chitin and extent of grafting PHB on chitosan determined by solid state 15N NMR. Macromolecules 32, 518-520.

Yu, H.-Y., Qin, Z.-Y., Wang, L.-F., Zhou, Z., 2012. Crystallization behavior and hydrophobic properties of biodegradable ethyl cellulose-g-poly(3-hydroxybutyrate-co-3-hydroxyvalerate): The influence of the side-chain length and grafting density. Carbohydrate Polymers 87, 2447-2454.

Yu, J., Si, Y., 2004. Metabolic carbon fluxes and biosynthesis of polyhydroxyalkanoates in Ralstonia eutropha on short chain fatty acids. Biotechnology Progress 20, 1015-1024.

Yu, L., Dean, K., Li, L., 2006. Polymer blends and composites from renewable resources. Progress in Polymer Science 31, 576-602.

Yu, L., Liu, H., Xie, F., Chen, L., Li, X., 2008. Effect of annealing and orientation on microstructures and mechanical properties of polylactic acid. Polymer Engineering & Science 48, 634-641.

Žagar, E., Kržan, A., Adamus, G., Kowalczuk, M., 2006. Sequence distribution in microbial poly(3-hydroxybutyrate-co-3-hydroxyvalerate) co-polyesters determined by NMR and MS. Biomacromolecules 7, 2210-2216.

Zhang, L., Xiong, C., Deng, X., 1995. Biodegradable polyesters blends for biomedical application. Journal of Applied Polymer Science 56, 103-112.

Zhao, H., Cui, Z., Sun, X., Turng, L.-S., Peng, X., 2013. Morphology and oroperties of injection molded solid and microcellular polylactic acid/polyhydroxybutyrate-valerate (PLA/PHBV) blends. Industrial and Engineering Chemistry Research 52, 2569-2581.

Zhou, X.-Y., Yuan, X.-X., Shi, Z.-Y., Meng, D.-C., Jiang, W.-J., Wu, L.-P., Chen, J.-C., Chen, G.Q., 2012. Hyperproduction of poly (4-hydroxybutyrate) from glucose by recombinant Escherichia coli. Microbial Cell Factories 11, 54.

Ziaee, Z., Supaphol, P., 2006. Non-isothermal melt- and cold-crystallization kinetics of poly(3-hydroxybutyrate). Polymer Testing 25, 807-818.

Chapter 2. Characterization of poly(3-hydroxybutyrate-co-3-hydroxyvalerate) biosynthesized by mixed microbial consortia fed fermented dairy manure

2.1 Abstract

The bioplastic poly(3-hydroxybutyrate-*co*-3-hydroxyvalerate) (PHBV), was isolated from a bioreactor using mixed microbial consortia fed volatile fatty acids (VFA), from fermented dairy manure, as the carbon source. The molar fraction of 3-hydroxyvalerate (3HV) amounted to 0.33 mol/mol for two isolated PHBV samples as determined by GC-MS and ^{1}H-NMR spectroscopy. The chemical, thermal and mechanical properties were determined. The PHBVs had relatively high M_w (~790,000 g/mol). Only a single glass transition temperature (T_g) and melting point (T_m) were observed. Isolated PHBVs showed acceptable flexibility and elongation to break as compared with commercial PHBVs with lower HV. The diad and triad sequence distributions of the monomeric units were determined by ^{13}C-NMR spectroscopy and followed Bernoullian statistics suggesting that the PHBVs were random. The PHBV sequence distribution was also characterized by electrospray ionization-mass spectrometry (ESI-MS^n) after partial alkaline hydrolysis to oligomers showing a random HV distribution.

2.2 Introduction

Polyhydroxyalkanoates (PHAs) are a class of renewable bioplastics which can be produced by microbial biosynthesis as intracellular granules. Poly-3-hydroxybutyrate (PHB) is the most common PHA and as a consequence has been studied most extensively (Madison and Huisman, 1999; Yu et al., 2006). The primary limitation of PHB as a thermoplastic material is its brittleness upon crystallization due to large spherulites which exhibit inter-spherulitic cracks (Sudesh et al., 2000). However, the copolymer of hydroxyvalerate (HV) with hydroxybutyrate (HB) to form poly(hydroxybutyrate-*co*-hydroxyvalerate) (PHBV) has improved ductility as a result of being less crystalline and can be used in various applications such as flexible packaging materials (Madison and Huisman, 1999). The ductility of PHBVs is positively dependent on HV content which inhibits crystallization (Bauer and Owen, 1988).

Current commercial production of PHB and PHBV uses pure culture bacteria and expensive refined substrate, e.g. glucose, resulting in high production costs. An alternative, the use of open, mixed consortia and waste feedstocks have been proposed as a potential technique to reduce these production costs. Recent work has shown that PHB and PHBV can be produced using mixed microbial consortia from organic waste streams such as crude glycerol from biodiesel production and volatile fatty acids (VFA) (Coats et al., 2007a; Hu et al., 2013). The advantage of PHBV over PHB is that the chemical microstructures can be regulated (such as HV/HB ratio and sequence distribution) which alters the physical and mechanical properties, melting and co-crystallization behavior, and biodegradability (Bauer and Owen, 1988; Doi et al., 1990; Feng et al., 2004; Kamiya et al., 1991; Kunioka et al., 1989; Mitomo et al., 1993; Žagar et al., 2006). Regulating the feed carbon source/composition and the timing of its addition to the biosynthesis process has been shown to be one strategy of varying the HB and HV monomer distribution and sequence (Ishihara et al., 1996; Madison and Huisman, 1999). It has been suggested that the tensile properties of co-block PHBV films were different from the random copolymers if HV contents are comparable (McChalicher and Srienc, 2007; Pederson et al., 2006). Therefore, it is important to be able to determine the composition and HB/HV distribution in PHBVs during the biosynthesis as a function of bioreactor operating parameters to manipulate polymer properties.

Current methods to analyze PHA, such as methanolysis and subsequent analysis by GC-FID, the first method used for PHB analysis, and GC-MS or directly by ^{1}H-NMR spectroscopy, provide limited information such as composition (Bloembergen et al., 1986; Bluhm et al., 1986; Braunegg et al., 1978; Kamiya et al., 1989; Yoshie et al., 1995). To obtain more detailed chemical information such as 3HV and 3HB sequence information in PHBVs ^{13}C-NMR spectroscopy has been applied to look at diad (e.g. 3HB*HV) and 3HV-centered triad (e.g. 3HB-3HV*3HV) sequences of 3HB and 3HV units and establish whether the copolymer is a co-block polymer or randomly distributed or not based on statistical models (Feng et al., 2004; Inoue et al., 1989; Lemos et al., 1998; Montaudo and Montaudo, 1992). However, it is difficult for NMR spectroscopy to discern higher levels than the triad segmentation. Thus, in practice mass spectrometry (MS) provides an alternative technique for the analysis of oligomers formed by partial degradation of copolymers as compared to

NMR analysis (Adamus et al., 2000; Montaudo and Montaudo, 1992). Partial degradation can be achieved by methanolysis, hydrolysis, pyrolysis, and aminolysis of copolymer chains (Ballistreri et al., 1991; Montaudo, 2002; Montaudo et al., 1991; Montaudo et al., 1998). Therefore, it is feasible to determine the sequence distribution of oligomers and construct the sequence in the copolymer.

Recently, bacterial PHBV copolymers were studied using electrospray ionization mass spectrometry (ESI-MS) for the determination of the comonomer sequence distribution of their corresponding oligomers obtained by controlled partial alkaline hydrolysis (Adamus et al., 2000; Žagar et al., 2006). The PHBV oligomers with the same composition and sequence distribution as the starting copolymer contained carboxylic and olefinic end groups (Adamus et al., 2000; Žagar et al., 2006). Controlled depolymerization of PHB and PHBV was achieved through partial saponification of ester linkage which was catalyzed by a KOH/18-crown-6 ether complex (Iwata et al., 1997; Jedlinski et al., 1999). ESI-MS was then used to characterize the oligomeric PHB/PHBV products by the analysis of the pseudomolecular ions (Adamus et al., 2000; Žagar et al., 2006). MS-MS analysis provided further detailed chemical structural information of individual PHBV chains and mixtures of PHBV copolymers containing varying levels of 3HV and sequence distributions of 3HB and 3HV repeats.

The aim of this study was to characterize PHBV isolated from a bioreactor fed VFAs, from fermented dairy manure, using mixed microbial consortia. The PHBV samples were compared with commercial samples, for composition, 3HB and 3HV sequence, and mechanical and thermal properties.

2.3 Experimental

2.3.1 Materials

Laboratory PHBV samples (PHBV-1 and PHBV-2) were biosynthesized in a 20L scale bioreactor inoculated with activated sludge (mixed microbial consortia) obtained from the Moscow, Idaho wastewater treatment plant. The aerated bioreactor was run continuously for 1 year and was fed a mixture of VFAs (Table 2.1). The bioreactor was operated under a 24 h

cycle time for feeding and wasting with solid (SRT) and hydraulic retention times (HRT) of 4 d. The feed for the reactor was centrifuged fermented dairy manure (VFAs summarized in Table 2.1). Manure was collected from the University of Idaho North Farm Dairy biweekly, stored at 4 °C, and fed each day to a continuously operated 20 L anaerobic fermenter (4 day SRT; organic volatile solids loading rate = 10.8 g/L/d) (Coats et al., 2011). The wasted 5 L was centrifuged at 8000 rpm for 5 min and the recovered centrate was stored at 4 °C prior to use. The laboratory PHBV samples were obtained 5 months apart and prewashed with acetone (24h), and then dried followed by extraction from lyophilized biomass with $CHCl_3$ and concentrated to dryness (Hu et al., 2013). The yields of crude PHBV-1 and PHBV-2 from biomass were 42 and 36 %, respectively. The PHBV extract was dissolved in a minimum volume of $CHCl_3$ and then precipitated in cold petroleum ether (boiling point range 35-60 $^{\circ}$C), collected by filtration and dried under vacuum with an average recovery > 98%. HV/HB ratio was determined by GC-MS (Finnigan PolarisQ) as their methyl ester derivatives as described by Hu et al. 2013.(Hu et al., 2013) Commercial PHBV-C1 (Biopol D300G, Monsanto), PHBV-C2 (Biopol D600G, Monsanto) and PHB-C (T_m = 172 $^{\circ}$C, Sigma-Aldrich) were used for comparison (Bauer and Owen, 1988).

2.3.2 Size exclusion chromatography (SEC)

The number- and weight-average molar mass (M_n andM_w, respectively) and the dispersity (M_w/M_n) of all commercial PHB (PHB-C) and PHBV (PHBV-C1, PHBV-C2) and laboratory PHBVs (PHBV-1, PHBV2) were determined by size exclusion chromatography (SEC). A Jordi DVB linear mixed bed column (7.8 mm x 300 mm) column was used for the separation of polymers at 40 $^{\circ}$C. 100 µL samples (2 mg/mL) were injected on elution with HPLC grade $CHCl_3$ at 1 mL/min and detected with triple detector array (refractive index (RI), Waters model 2478), low- and right-angle laser light scattering (LALLS, RALLS), and differential viscometer (Viscotek model 270, Viscotek Corporation). Data were analyzed by OminiSEC 4.1 (Viscotek) software. The system was calibrated using a narrow polystyrene standard (Viscotek, M_w = 98,946 g/mol).

2.3.3 Differential scanning colorimetry (DSC)

Differential scanning calorimetry (DSC) was performed on all samples (4-6 mg, in duplicate) using a TA Instruments model Q200 DSC with refrigerated cooling. The samples were (i) equilibrated at 40˚C (3 min) then ramped to 180˚C at 10 ˚C/min to destroy any prethermal history, held isothermally for 3 min, (ii) cooled to -50˚C at -10 ˚C/min and held isothermally for 3 min and the cycles repeated. The T_m and the T_g were determined from the peak maximum and the inflection point of the second heating scan, respectively. The degree of crystallization (X_c %) of samples were calculated from the ratio of the melting enthalpy (ΔH_f) of the sample to (ΔH_f^0) of 100% crystalline polymers (146 J/g for PHB) (Barham et al., 1984; Hu et al., 2013; Wei et al., 2013). Data were analyzed using TA Universal Analysis v4.4A software.

2.3.4 Tensile properties

PHBV and PHB films were solvent cast from a $CHCl_3$ solution (10 mg/mL) using a Teflon mold, air dried and vacuum dried prior to use. Samples were cut into 10 x 3 x 0.05 mm^3 sized specimens. Tensile testing was performed on a DMA Q800 (TA instruments) with controlled force of 3 N/min until yield. Tensile strength, Young's modulus, and elongation to break were determined from the constructed stress-strain curve using Universal Analysis v4.4A software.

2.3.5 NMR spectroscopy

Samples were dissolved in $CDCl_3$ and ^{1}H- and ^{13}C-NMR spectra were recorded on an Advance Bruker 300 MHz spectrometer at 27 ˚C. Spectra were analyzed using SpinWorks v3.1.7 software. The 3HV molar fraction was determined by the ratio of the integrated ^{1}H peak areas due to the 3HV methyl resonance and the sum of 3HB + 3HV methyl resonance corresponding to B_4 and V_5, respectively (Scheme 1) (Kamiya et al., 1989; Kulkarni et al., 2011). ^{13}C-NMR spectra were obtained using a Lorentz-Gauss transformation of the free induction decay (FID) with a line broadening of 1 Hz and Gaussian multiplication factor of 0.3.

2.3.6 Partial hydrolysis and analysis by ESI-MS^n

PHB and PHBV samples were each dissolved in $CHCl_3$ (10 mg/mL) and subjected to controlled alkaline hydrolysis in 5 M KOH containing 18-crown-6 ether complex (5 mg/mL) at 35 °C with constant stirring for 16 h (Iwata et al., 1997). After filtering, the oligomers were recovered and dried over anhydrous sodium sulfate prior to analysis. Negative ion ESI-MS^n analysis was performed using a Finnigan LCQ-Deca ion trap mass spectrometer. The oligomers were dissolved in $CHCl_3$/methanol mixture (1:1, volumetric) to a concentration of 1-2 mg/mL. The sample was introduced to the ESI source at 5 µL/min. The ESI source was operated at 4.5 kV and capillary heater was set at 275 °C. MS data were collected and analyzed using Xcalibur v2 software.

2.4 Results and discussion

2.4.1 Compositional analysis

The ^{1}H-NMR spectrum of PHBV-2 is shown in Figure 2.1. The triplet CH_3-proton resonance at δ=0.92 ppm corresponds to the methyl groups of 3HV monomer unit (Figure 2.1a; Figure 2.2, V5), while the doublet CH_3-proton resonance at δ=1.29 ppm was assigned to methyl group of 3HB monomer (Figure 2.1a, B4, Figure 2.2). The molar fraction of 3HV was determined from the integrated areas of V5 and B4, which were 0.34and 0.335 mol/mol, for samples PHBV-1 and PHBV-2, respectively. These values were close to the result that was 0.341 and 0.324 mol/mol of 3HV for isolated PHBVs, respectively, as determined by GC-MS (Dobroth et al., 2011). Replicate analyses on the same sample were within ±0.004 mol/mol 3HV and using the commercial PHBV sample for the compositional calibration with an R^2 of 0.99. All commercial PHB, PHBV-C1, and PHBV-C2 compositions determined by both methods were close (Table 2.1). These PHBVs have relatively high 3HV fraction as compared with the literature using mixed microbial consortia (Avella et al., 2000). As polymer composition is directly influenced by the carbon source, with even-carbon VFAs (e.g., acetic, butyric) generating 3HB and odd-carbon VFAs (e.g., propionic and valeric) being the source of 3HV, the high 3HV fraction can be attributed to the substrate (Madison and Huisman, 1999).

While the VFA composition in the fermenter dairy manure used to produce PHBV-1 and PHBV-2 varied in relative magnitude (Table 2.1), the ratio of odd- to even-carbon VFAs was comparable between the two (0.457 and 0.453 for PHBV-1 and PHBV-2, respectively), which contributed to the similar 3HV molar fractions observed.

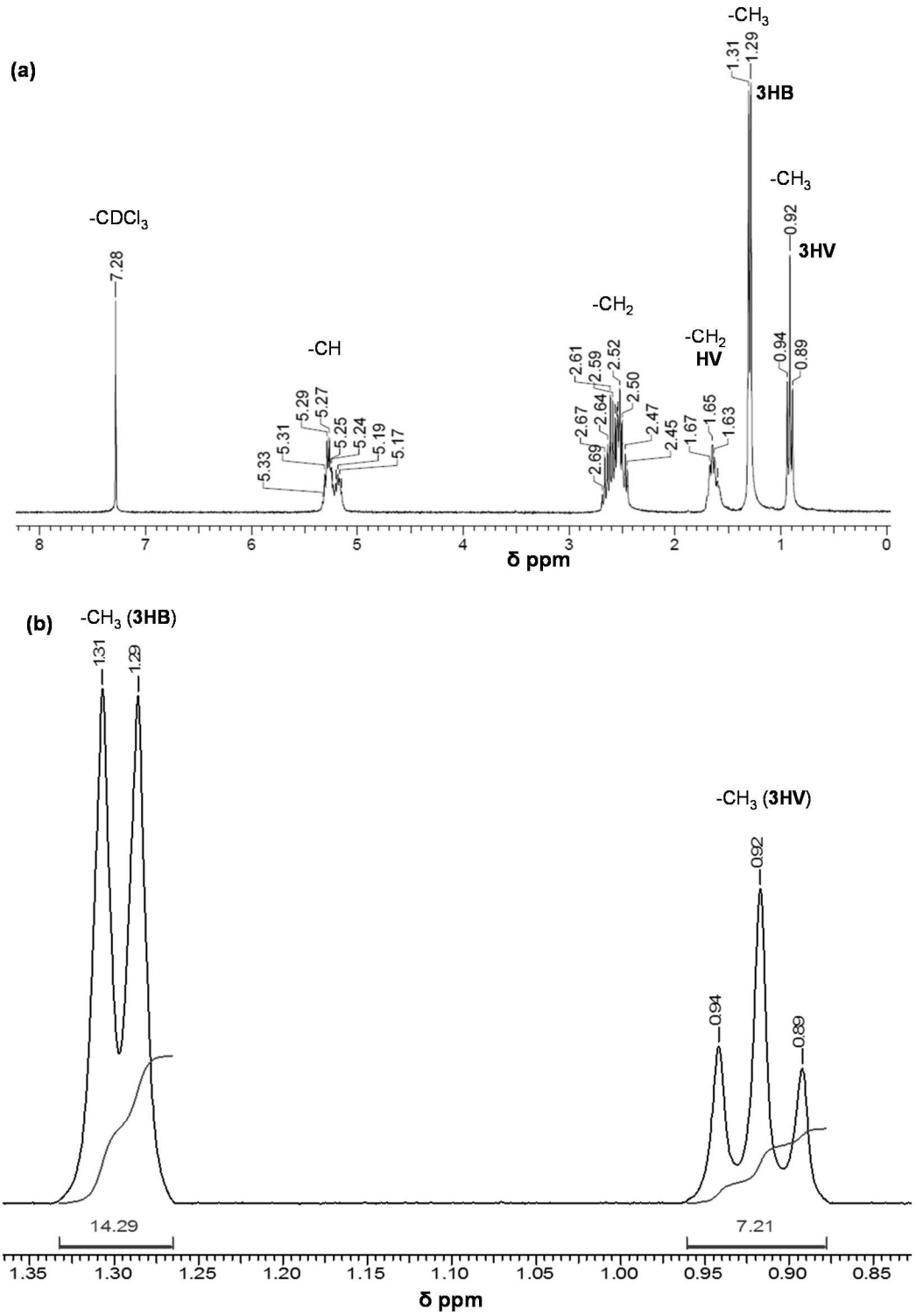

Figure 2.1 (a) 300 MHz ^{1}H-NMR spectrum of PHBV-2, and (b) –CH_3 groups for 3HB and 3HV.

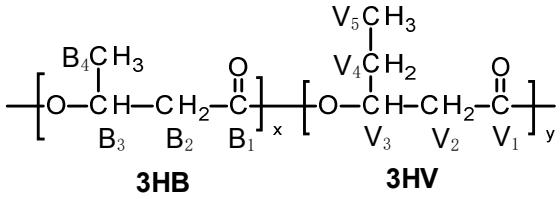

Figure 2.2. Structure of PHBV showing NMR assigned protons and carbons.

Table 2.1. Average composition of VFA deed (mg/L) from fermented dairy manure used for the production of PHBV-1 and PHBV-2

VFA	Concentration (mg/L)	
	PHBV-1	PHBV-2
Acetic	3420	3740
Propionic	1320	1590
Butyric	746	145
Isobutyric	108	120
Valeric	220	420
Isovaleric	153	157
Caproic	90	159
Odd:Even VFAs (unitless)	0.457	0.453

2.4.2 Polymer properties

The physicochemical properties of PHBVs with lower 3HV molar fraction (<0.30 mol/mol) have been widely studied and reviewed (Avella et al., 2000; Dias et al., 2006; Doi, 1990; Sudesh et al., 2000). However, the documentation on higher HV based PHBVs is limited, especially from mixed microbial consortia (Reis et al., 2003). The properties of laboratory and commercial PHB and PHBVs, and PHBVs cited from the literature (denoted by PHBV-R's) with a variable molar fraction of 3HV as well, are given in Table 2.2. The M_w and dispersity of the laboratory PHBVs and commercial PHB and PHBVs were obtained by SEC. The dispersity values of PHBV-1 and PHBV-2 were respectively, 2.2 and 2.1. The M_w of PHBV-1 (790,000 g/mol) and PHBV-2 (770,000 g/mol) were higher than PHBV with 0.45

mol/mol HV prepared using mixed cultures fed on substrates of acetate, propionate and butyrate.(Lemos et al., 1998) These M_w's are comparable to samples reported in the literature for PHBVs with higher 3HV molar fraction (see Table 2.2, samples PHBV-R3 and PHBV-R5) (Dias et al., 2006; Doi, 1990). For comparison, the M_w for PHBV-C1 (0.056 mol/mol HV) and PHBV-C2 (0.197 mol/mol HV) were low at 300,000 and 420,000 g/mol, respectively. PHBV-C1 and PHBV-C2 have dispersity values of 3.3 and 2.2, respectively.

The thermal properties of commercial and isolated PHB and PHBVs are given in Table 2.2. As expected, the T_m of PHBVs was lower than PHB homopolymer. The isolated PHBV-1 and PHBV-2 were shown to have higher 3HV molar fraction and lower T_m and T_g values than the commercial PHBV-C1, PHBV-C2 samples. An overall evaluation of PHBV samples shows that the thermal properties of copolymers highly correlate with the 3HV molar fraction, such as: (i) T_g decreases from 5.5 to -30.0 $^{\circ}$C with increasing 3HV fraction increases from 0.056to 0.72 mol/mol; (ii) T_m decreases when 3HV fraction <0.34 mol/mol, which has similar trends as reported by Reis et al. 2003; (iii) however, PHBV-1 and PHBV-2 with lower 3HV fraction were observed to have lower X_c % than the samples PHBV-R5 and PHBV-R6, having 0.71 and 0.72 mol/mol HV, respectively, and this may be attributed to the differences in D and higher HV monomeric unit chain length of these laboratory isolated samples (Table 2.2) (Avella et al., 2000; Dias et al., 2006; Doi, 1990; Reis et al., 2003). PHBV-1 and PHBV-2 were considerably more flexible (low Young's modulus) than the commercial PHB, PHBV-C1, and PHBV-C2 samples. If compared with solution casted films studied before (PHBV-R2 and -R4, -R5), the elongation to break also increases as the molar fraction of 3HV increases from 0 to 0.55 mol/mol; however, when the HV reaches to 0.71 mol/mol, the PHBV-R5 copolymer becomes as brittle as the PHB homopolymer (Doi, 1990). Values of Young's moduli and elongation to break of PHBV-1 and PHBV-2 were lower than the samples PHBV-R1 and PHBV-R2, respectively, with comparable HV molar fraction (0.34 mol/mol), and this may be due to differences in sample dimensions and preparation (Avella et al., 2000; Doi, 1990). Comparison of tensile properties of isolated PHBVs with other PHB, PHBV and common plastic indicates these copolyesters have comparable strength and flexibility to LDPE, and therefore these copolyesters obtained from

diary manure fermentation could be used as packaging materials, such as sealed and carry bags (Kulkarni et al., 2011; Rubin, 1990).

Table 2.2. Molecular weight, thermal and mechanical properties of PHBV and PHB samples

Sample	3HV molar fraction (mol/mol)		SEC		DSC			Tensile properties		
	GC-MS	^{1}H-NMR	M_w (x10^5 g/mol)	M_w/M_n	T_g (°C)	T_m (°C)	X_c (%)	Tensile strength(MPa)	Young's modulus(GPa)	Elongation to break (%)
PHB-C	0	0	4.1	1.9	2.5	175	60.2	22.5	1.31	2.80
PHBV-C1	0.064	0.056	3.0	3.3	5.5	160	44.3	17.0	0.990	10.7
PHBV-C2	0.189	0.197	4.2	2.2	0.9	156	36.2	20.6	1.07	8.77
PHBV-1	0.341	0.34	7.9	2.2	-3.2	147	2.1	15.0	0.299	58.8
PHBV-2	0.324	0.335	7.7	2.1	-2.1	148	1.9	14.8	0.289	57.6
PHBV-R1[a]	0.34	-	-	-	-9.0	97	-	18.0	1.20	970
PHBV-R2[b]	-	0.34	-	-	-8.0	97	-	18.0	-	970
PHBV-R3[c]	0.45	-	5.8	2.9	-	-	-	-	-	-
PHBV-R4[b]	-	0.55	-	-	10.0	77	-	16	-	>1200
PHBV-R5[b]	-	0.71	5.1	2.0	13.0	83	8.9	11	-	5
PHBV-R6[c]	0.72	-	3.5	1.4	30.0	99	7.0	-	-	-

[a, b, c] Data are cited from literatures (Avella et al., 2000; Dias et al., 2006; Doi, 1990).

2.4.3 ^{13}C-NMR comonomer sequence distribution analysis

The ^{13}C-NMR spectrum of PHBV-2 is shown in Figure 2.3. The peak assignments are in close agreement with those reported previously (Doi et al., 1986). Multiple peaks (Figure 2.3b) are assigned to carbonyl (B_1 and V_1) and methylene (B_2, V_2, and V_4) Cs from different sequence distributions of HB and HV units (Table 2.3). The carbonyl region is split into four peaks at δ=169.69, 169.51, 169.50, and 169.32 ppm, being assigned to different diad sequences: HV*HV, HV*HB, HB*HV, and HB*HB, respectively. The triad sequences were determined from a resonance of HV side-chain methylene C (V_4 and V_2) composed of four peaks assigned to HV-centered triads (HV-HV*HV, HB-HV*HV, HV-HV*HB, and HB-HV*HB) and consistent with those reported by Kamiya et. al. (Kamiya et al., 1989). The relative peak intensities obtained for the V_2 and V_4 resonances and the V_1, B_1, and B_2

resonances were determined to estimate the mole, diad, and HV-centered triad sequence distributions. Relative peak intensities of PHBV-1 and PHBV-2 are listed in Table 2.4.

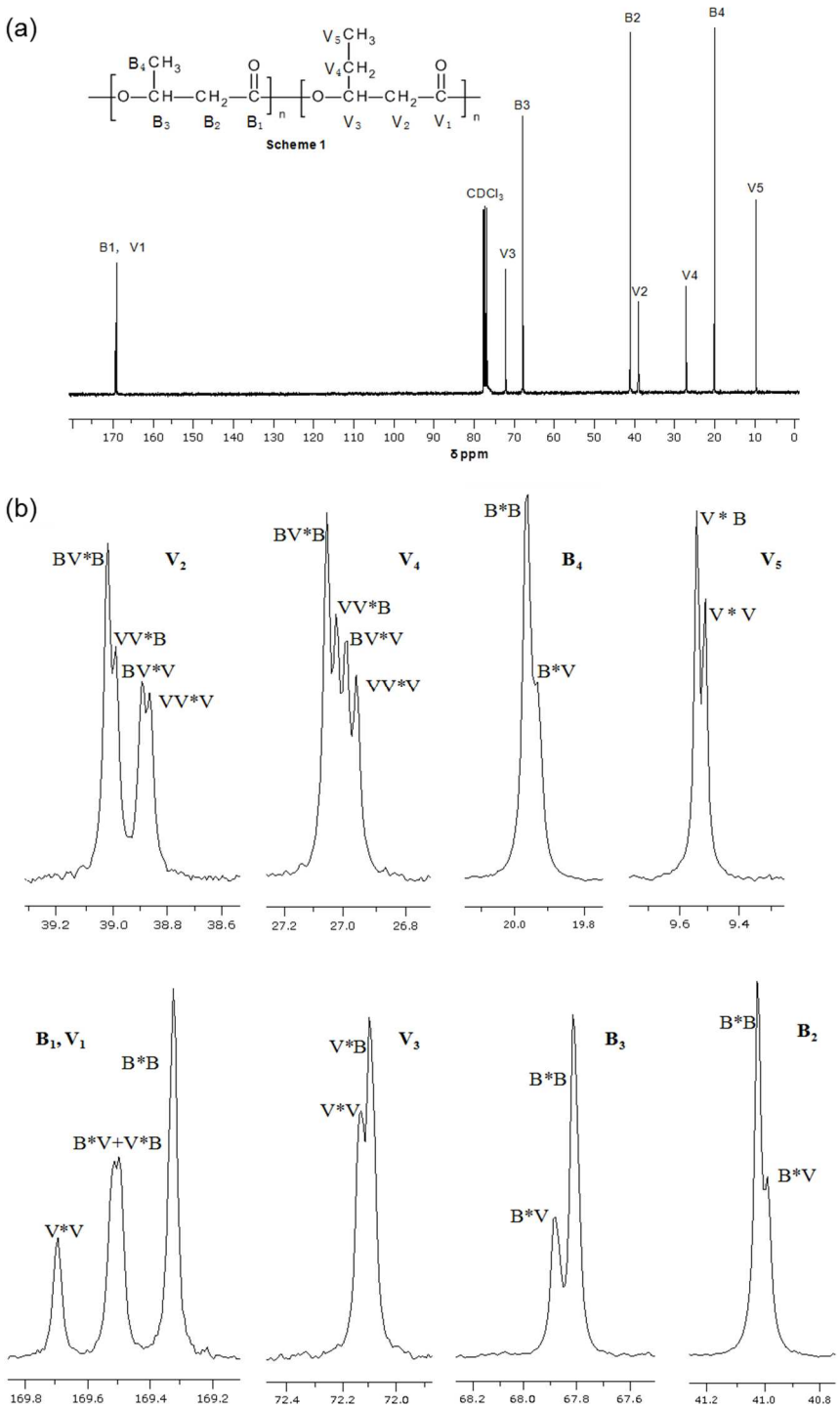

Figure 2.3. ^{13}C-NMR (a) full spectrum and (b) expanded region showing splitting of individual resonances of PHBV-2 sample.

Table 2.3. ^{13}C-NMR chemical shifts for carbonyl and methylene carbons in PHBV

Functional group	Chemical shift (δ, ppm)	Sequence
C=O (V_1, B_1)	169.69	3HV*3HV
	169.51	3HB*3HV
	169.50	3HV*3HB
	169.32	3HB*3HB
CH_2 (B_2)	41.02	3HB*3HB
	40.99	3HB*3HV
CH_2 (V_2)	39.02	3HB-3HV*3HB
	38.99	3HV-3HV*3HB
	38.89	3HB-HV*HV
	38.87	HV-HV*HV
CH_2 (V_4)	27.06	HB-HV*HB
	27.03	HV-HV*HB
	26.99	HB-HV*HV
	26.96	HV-HV*HV

Table 2.4. Experimental diad and HV-centered triad relative peak intensities for PHBV-1 and PHBV-2

Sample	Carbon	HV[a]	HV	HB	HV*HV	HV*HB	HB*HV	HB*HB	HV-HV*HV	HB-HV*HV	HV-HV*HB	HB-HV*HB
PHBV-1	V1,B1		0.360	0.640	0.134	0.226	0.221	0.419				
	B2			0.672			0.218	0.454				
	V2		0.328		0.132	0.196			0.195	0.208	0.244	0.352
	V4								0.191	0.222	0.247	0.340
	av	0.34	0.34	0.656	0.133	0.211	0.220	0.437	0.066	0.074	0.084	0.119
PHBV-2	V1,B1		0.352	0.648	0.145	0.208	0.193	0.455				
	B2			0.691			0.218	0.454				
	V2		0.309		0.118	0.191			0.205	0.177	0.257	0.360
	V4								0.239	0.236	0.210	0.314
	av	0.335	0.330	0.670	0.131	0.199	0.206	0.454	0.073	0.068	0.077	0.111

[a] Determined by ^{1}H-NMR spectroscopy.

The parameters statistical randomness (D) and coefficient R were used to estimate the degree of randomness of the copolymer based on experimental diad and triad level, respectively (Doi et al., 1986; Kamiya et al., 1989; Žagar et al., 2006). As shown in Table 2.5, D values were 1.25 and 1.40, whereas the R values were unity for PHBV-1 and PHBV-2, showing that the PHBVs were individual random copolymers not blocky or mixture of random copolymers. Within the experimental uncertainty of the diad and HV-centered triad fractions between these two samples are ±0.003 mol/mol. This result also supports that the copolymers exhibit only one T_m (Table 2.2), while other researchers found samples that are a mixture of random copolymers will show two or three T_m's (Žagar et al., 2006).

Table 2.5. Parameters D, R, experimental number average sequence lengths of HV units (L_V^E), number average sequence length of randomly distributed HV units in copolymer (L_V^R), ratio between the concentration of HV and HB units (k), four probabilities (Pij's) and the reaction index (r_1r_2) for PHBV-1 and PHBV-2

Sample	D[a]	R[b]	L_V^E	L_V^R	k	P_{VV}[c]	P_{VB}[c]	P_{BV}[c]	P_{BB}[c]	r_1r_2[d]	A	B	X	Model[e]	SD[f]
PHBV-1	1.25	1	0.85	1.52	1.91									exptl	R
														1	
						0.39	0.61	0.34	0.67	1.25				2	
											0.19	0.55	0.63	3	
PHBV-2	1.40	1	0.85	1.49	2.03									exptl	R
														1	
						0.39	0.60	0.31	0.68	1.45				2	
											0.17	0.59	0.65	3	

[a] $D = F_{VV}F_{BB}/F_{BV}F_{VB}$ (F_{vv}, F_{BB}, F_{BV} and F_{VB} are exptl values from Table 2.7). [b] $R = L_V^R/L_V^E$ [$L_V^E = (F_{VVV} + F_{VVB} + F_{BVV} + F_{BVB})/(F_{BVB} + F_{VVB})$, F_{VVV}, F_{VVB}, F_{BVV} and F_{BVB} are exptl values from Table 2.7]. [c] The estimated errors in the values of P_{ij}'s are <0.005. [d] $r_1 = P_{BB}/P_{BV}$ and $r_2 = P_{VV}/P_{VB}$. [e] exptl represent experimental data; 1, 2, and 3 are calculated values by Model 1, Model 2, and Model 3, respectively. [f] Sequence distribution; R indicates the copolymer is random.

The sequence distribution of diad and triad was calculated using three models (Kamiya et al., 1989; Yoshie et al., 1995). The equations are summarized in Table 2.6. Model 1 used Bernoullian statistics which is the simplest random copolymer model, and calculation were based on the experimental mole fraction of HV (F_V) (Kamiya et al., 1989). Model 2 is a

first-order Markovian model that was used to examine the possibility of block, random and alternative copolymers. As shown in Table 2.5, the four conditional probabilities P_{ij}'s (P_{VV}, P_{VB}, P_{BV}, and P_{BB}) of the probability matrix (P-matrix) were determined. From these P_{ij}'s, sequence distributions were derived (Doi et al., 1986; Ishihara et al., 1996). It was reported that the biosynthesis distributions of HB and HV units may be interpreted in terms of a binary copolymerization as shown in four propagation steps (Ishihara et al., 1996). Based on these steps, the selectivities of enzyme reactions of HB- and HV- terminals of PHBVs were evaluated by the reactivity index r_1r_2 calculated from P_{ij} values and listed in Table 2.5. It can be seen the values of r_1r_2 are near to unity, which indicates that the sequence distribution of HB and HV units follows an ideal random copolymerization procedure.

Model 3 was a simulation of a mix of two Bernoullian random copolymers (Kamiya et al., 1989). If two Bernoullian model copolymers with the HV mole fractions of A and B are mixed with a molar ratio of X:(1-X), then the three unknowns, *A*, *B*, and *X* can be calculated from the molar fractions of HV-centered triad sequences [A, B, X ∈ (0,1)] (Table 2.5) (Kamiya et al., 1989).

Table 2.7 gives the mole fractions of diad, and HV-centered triads of HB and HV in respective PHBV-1 and PHBV-2 samples. As stated above both PHBV samples with the D and R values close to 1, their experimental sequence distributions were found to be completely interpreted on the basis of model 1. Within the experimental uncertainty in the measured diad and triad fractions (±0.005) there was good agreement between the observed (experimental) values and calculated distributions based on Bernoullian model 1. Thus, it can be concluded that the comonomer distribution in PHBV produced by mixed microbial consortia was statistically a random copolymer. Considering that studies on both laboratory and commercial bacterial PHBV samples were shown to be random copolymers, this conclusion seems to be reasonable (Adamus et al., 2000; Doi et al., 1986; Feng et al., 2004; Mitomo et al., 1993; Žagar et al., 2006).

Table 2.6. Model 1, Model 2, Model 3, and equations used to calculate the diad and triad distributions

Model	Calculation[a]	Reference
Model 1	$F_{VV} = (F_V^E)^2$	
(Bernoulian Model)	$F_{VB} = F_{BV} = F_V^E (1- F_V^E)$	
	$F_{BB} = (1-F_v^E)^2$	(Kamiya et al., 1989; Montaudo and Montaudo, 1992; Inoue et al., 1989)
	$F_{VVV} = (F_V^E)^3$	
	$F_{BVV} = F_{VVB} = (F_V^E)^2 (1-F_V^E)$	
	$F_{BVB} = F_V^E (1-F_V^E)^2$	
Model 2	$P_{VV} = F_{VV}^E/F_V^E$	
(First-order Markovian Model)	$P_{VB} = F_{VB}^E/F_V^E$	
	$P_{BV} = F_{BV}^E/F_B^E$	
	$P_{BB} = F_{BB}^E/F_B^E$	
	$F_{VV} = P_{VV}P_{BV}/(P_{BV}+P_{VB})$	(Kamiya et al., 1989; Inoue et al., 1989)
	$F_{VB} = F_{BV} = P_{VB}P_{BB}/(P_{BV}+P_{VB})$	
	$F_{VVV} = P_{VV}^2P_{BV}/(P_{BV}+P_{VB})$	
	$F_{BVV} = F_{VB} = P_{VV}P_{VB}P_{BV}/(P_{BV}+P_{VB})$	
	$F_{BVB} = P_{VB}^2P_{BV}/(P_{BV}+P_{VB})$	
Model 3	$F_{VVV}^E = A^3X + B^3(1-X)$	
(Mixture of two Bernoullian models or Second-order Markovian Model)	$F_{BVV}^E = F_{VVB}^E = A^2(1-A)X + B^2(1-B)(1-X)$	
	$F_{BVB}^E = A(1-A)^2X + B(1-B)^2(1-X)$	
	$F_V=AX + B(1-X)$	
	$F_B= (1-A)X + (1-B)(1-X)$	(Kamiya et al., 1989; Yoshie et al., 1995; Inoue et al., 1989)
	$F_{VV} = A^2X + B^2(1-X)$	
	$F_{VB} = F_{BV} = A(1-A)X + B(1-B)(1-X)$	
	$F_{BB} = (1-A)^2X + (1-B)^2(1-X)$	
	$F_{VVV} = A^3X + B^3(1-X)$	
	$F_{BVV} = F_{VVB} = A^2(1-A)X + B^2(1-B)(1-X)$	
	$F_{BVB} = A(1-A)^2X + B(1-B)^2(1-X)$	

[a] Subscript E is values determined experimentally; F_X, F_{XY}, and F_{XVY} indicate mole fractions of sequence X, XY, and XVY, respectively, where X, Y=V or B; Four conditional probabilities P_{ij}'s (i,j=V or B) is conditional probability of j addition following the i unit at the propagation chain end with the relations that $P_{BV} + P_{BB} = 1$ and $P_{VB} + P_{VV} = 1$; A, B, X are following the convergence condition [F_{VVV}^E, F_{VVB}^E, F_{BVB}^E, A, B, X $\in$ (0,1)].

Table 2.7. Experimental and calculated mole, diad, and HV-centered triad sequence distributions of PHBV-1 and PHBV-2

Sample	Model[b]	Fv[c]	F_V	F_B	F_{VV}	F_{BV}	F_{BB}	F_{VVV}	$F_{BVV/VVB}$	F_{BVB}
PHBV-1	exptl	0.34	0.34	0.66	0.13	0.22	0.44	0.06	0.08	0.12
	1		0.34	0.66	0.12	0.22	0.43	0.04	0.08	0.15
	2		0.36	0.64	0.14	0.22	0.43	0.05	0.08	0.13
	3		0.32	0.68	0.13	0.19	0.49	0.07	0.07	0.12
PHBV-2	exptl	0.335	0.33	0.67	0.13	0.20	0.45	0.07	0.07	0.11
	1		0.33	0.67	0.11	0.22	0.45	0.04	0.07	0.15
	2		0.33	0.67	0.13	0.21	0.45	0.05	0.08	0.12
	3		0.31	0.69	0.14	0.18	0.51	0.07	0.06	0.11

[a] F_X, F_{XY}, and F_{XVY} indicate mole fractions of sequence X, XY, and XVY, respectively, where X, Y=V or B. [b] exptl represent experimental data; 1, 2, and 3 are calculated values by Model 1, Model 2, and Model 3, respectively. [c] Determined by ^{1}H-NMR spectroscopy.

2.4.4 ESI-MS^n analysis of PHBV and PHB

Controlled alkaline hydrolysis of PHB and PHBV samples was catalyzed by KOH/18-crown-6 ether complex. The comonomeric sequence distribution was characterized by ESI-MS^n analysis. Figure 2.4 shows the negative ion $[M-H]^-$ ESI-MS^n spectra of PHB and PHBV oligomers corresponding to the HB/HV oligomeric units and terminated by olefinic and carboxylic end groups from PHB after loss of the crown ether moiety. The PHB oligomers had differences of 86 m/z between HB units (Figure 2.4). The most abundant ion was m/z 515 which corresponds to HB_6 (hexamer) for both commercial PHB and PHBV samples (Figure 2.4a, b). Sets of fragment ions at m/z 429, 343, 257, and 171 were formed due to successive loss of crotonic acid. This shows evidence that the fragmentation of copolymers occurred due to partial depolymerization. The ESI-MS^n results of isolated PHBV oligomers allowed the identification of their chemical structure up to 22-mer (Figure 2.4c).

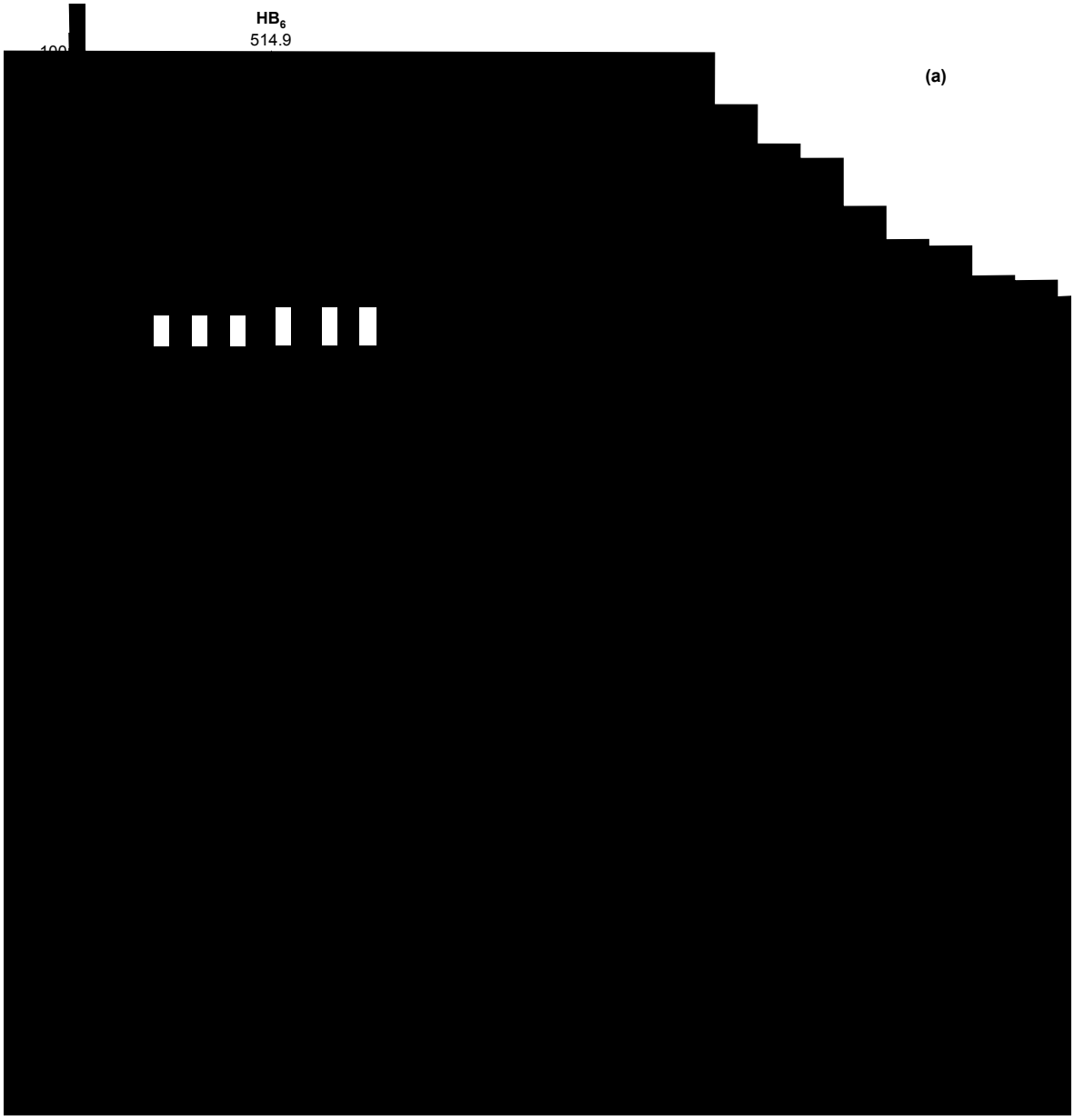

Figure 2.4. Negative ion ESI-MS spectra of partially hydrolyzed (a) PHB-C, (b) PHBV-C1, and (c) PHBV-1.

The expanded ESI-MS^n chromatogram of PHBV oligomers as well as peak assignments (pentamer to decamer clusters) is shown in Figure 2.5. The mass difference between HB and HV units is m/z 14 and shows a distribution of HB-HV oligomers. For example, the ions for the hexamer cluster gave peaks at m/z 515 (HB_6), 529 (HB_5HV_1), 543 (HB_4HV_3), 557 (HB_3HV_4), 571 (HB_2HV_5), 585 (HB_1HV_6), and 599 (HV_6) (Figure 2.5c) showing

composition and sequence distribution. It can be seen that the highest intensity of the signals in the hexamer decreased with increasing the molar fraction of 3HV for PHBV-C1. For the PHBV-1 (and -2) samples, the intensity of signals in the same oligomer cluster was higher than commercial PHBV (PHBV-C1), which was due to the higher 3HV content (Figure 2.5b, c).

The sequence distribution in the copolymer chains was determined from the relative ion peak intensities in the MS, and the experimental values were used to compare with theoretical values calculated for random copolymers of similar compositions (0.34-0.40 mol/mol of HV units) according to Bernoullian statistics (Adamus et al., 2000):

$$P_{x,y} = \binom{x+y}{y} P_B{}^x P_V{}^y \qquad \text{(eq. 2.1)}$$

Where, P_B and Pv are the molar fractions of HB and HV in the oligomers.

The differences between experimental and calculated values have been expressed in terms of error by means of the Hamilton agreement factor (AF) (Ballistreri et al., 1991):

$$AF = [\sum (I_{exp,i} - I_{calcd,i})^2 / \sum I_{exp,i}{}^2]^{1/2} \qquad \text{(eq. 2.2)}$$

Where, $I_{exp,i}$ and $I_{calcd,i}$ are the normalized experimental and calculated abundances of partially degraded copolymers (Adamus et al., 2000; Montaudo, 2002). The AF between the calculated and experimental values for each oligomer cluster (from dimer up to 15-mers) as a function of the ratio of P_B to P_V. The results for both commercial and laboratory PHBV samples are given in Figure 2.6. The best fit of the composition value of laboratory PHBV estimated from the ESI-MS^n characterization was found for the composition ratio around 66/34 (HB/HV) calculated for the random copolymer (Figure 2.6b), which is in good agreement with that of ^{1}H-NMR and GC-MS analysis at 0.32-0.34 mol/mol of HV in PHBV-1 and PHBV-2. However, the AF of PHBV-C1 oligomers show a more apparent minimum at 95-94 mol% HB units (Figure 2.6a). The results indicate that the PHBV-C1 was completely randomly distributed and consistent with ^{13}C-NMR spectroscopic data. For the PHBV-1 and -2 oligomers, the differences between the experimental and calculated oligomer distributions (Bernoullian chain statistics model) reflected by AF were slightly larger than that of commercial PHBV oligomers. Thus, it could be concluded that the

sequence distribution of PHBV copolymers determined by ESI-MS^n are consistent with those obtained by ^{13}C-NMR analysis.

To study the random composition and distribution of isolated PHBV comonomer units in each individual oligomer chain MS-MS fragmentation was conducted. The MS-MS experiments were on the ion at *m/z* 543 (HB_4HV_2) with two HV units being selected from hexamer cluster. This ion was selected since it was the most intense cluster (see Figure 2.4) and it has two HV units, which means it has 2 HV units randomly positioned along the macromolecular chain. The MS-MS spectrum of *m/z* 543 showed that the fragmentation induces a set of clusters containing 2 fragment ions in the first stage while 3 fragment ions in the following steps with the same degree of oligomerization but different HV molar fraction by successive loss of a crotonic acid (m/z 86) or 2-pentenoic acid (m/z 100) from the carboxylic end (Figure 2.7). Figure 2.8 shows visually the fragmentation pathways during the partial depolymerization procedure, which showed that two pentamers were generated: HB_3HV_2 (*m/z* 457) and HB_4HV (*m/z* 443). In the following steps, the clusters containing 3 fragment anions were formed successively. For example, the cluster of fragment ions corresponding to 4-mer (Figure 2.7: *m/z* 371, *m/z* 357, and *m/z* 343) the ion *m/z* 371 was generated by the pentamer *m/z* 457 (HB_3HV_2) when losing a crotonic acid; while 2-pentenoic acid is eliminated the *m/z* 357 ion was formed, and this ion might be coming from *m/z* 443 (HB_4HV) by loss a crotonic acid. The smallest fragment ion *m/z* 171 (HB_2) was possibly formed by either the fragment ion *m/z* 271 (HB_2HV) through losing 2-pentenoic acid or the *m/z* 257 (HB_3) by expulsion of a crotonic acid. This pathway was consistent with the MS-MS spectrum in Figure 2.7. This result confirmed that PHBV samples with relatively high 3HV molar fraction of this work have a random distribution of 3HB and 3HV units along the copolymer chain, which was comparable with other researches on commercial PHBV sample containing low 3HV fraction (0.056 mol/mol) (Adamus et al., 2000).

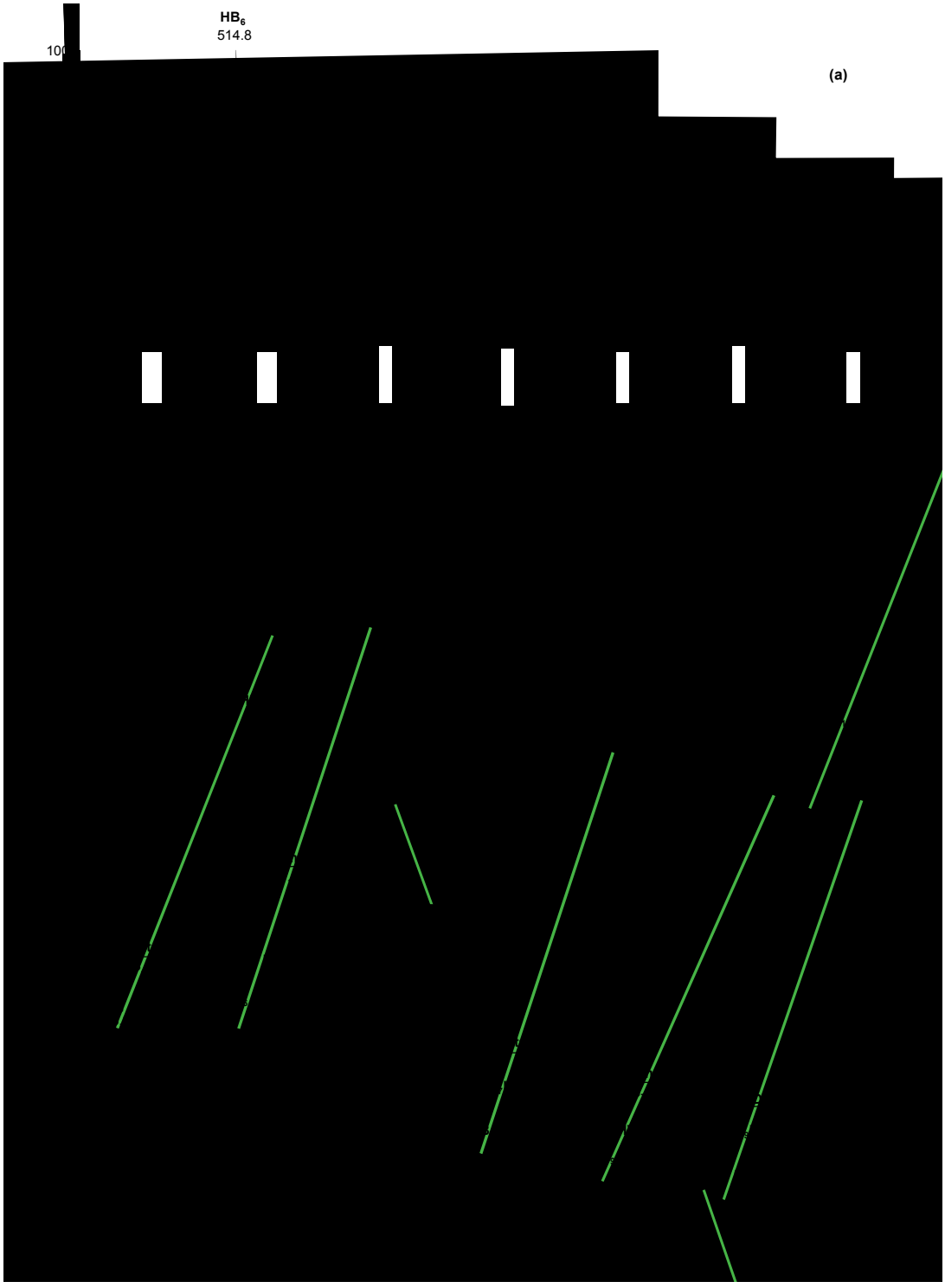

Figure 2.5. Expanded negative ion ESI-MS spectra of oligomers from partially hydrolyzed (a) PHB-C, (b) PHBV-C1, and (c) PHBV-1.

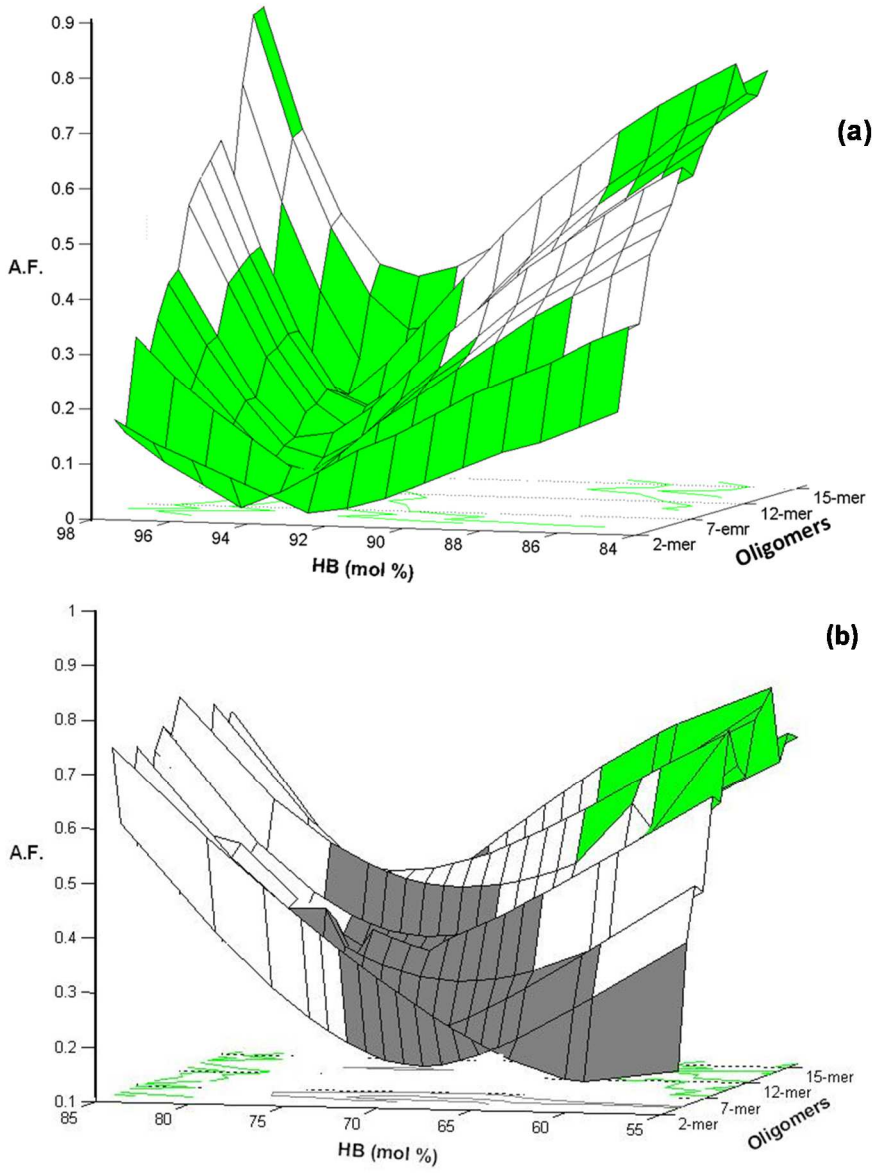

Figure 2.6. Calculated AF as a function of HB molar fraction (HB mol%) corresponding to individual PHBV oligomers for (a) PHBV-C1 and (b) PHBV-1 sample.

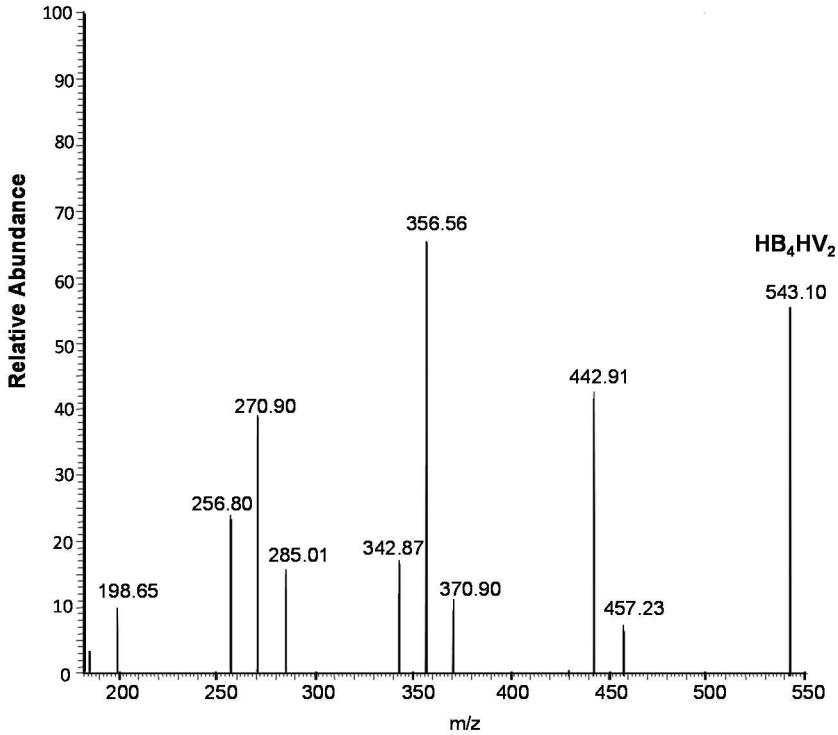

Figure 2.7. Sequence fragmentation spectrum (MS-MS, negative ion) obtained for isolated PHBV parent ion *m/z* 543.10 (hexamer cluster HB_4HV_2).

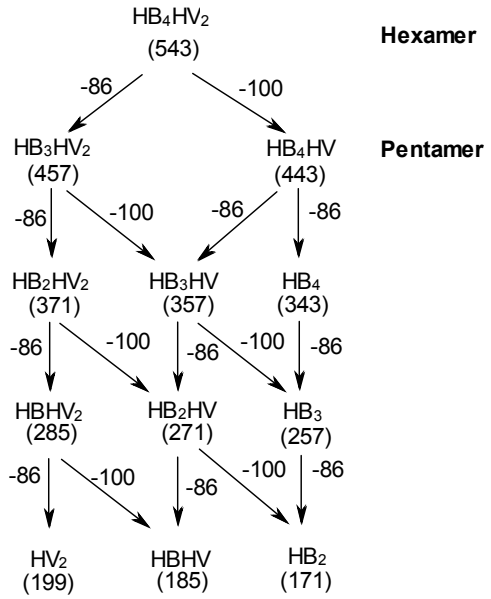

Figure 2.8. Fragmentation pathway as a result of MS-MS experiment for isolated PHBV parent ion *m/z* 543.10 (hexamer cluster HB_4HV_2).

2.5 Conclusions

In this study we successfully biosynthesized PHBV continuously for 12 months from VFA, obtained from fermented dairy manure, using a mixed microbial consortia. A comprehensive characterization of the isolated PHBV by a combination of mechanical and thermal properties, NMR spectroscopy and ESI-MS^n were done. The isolated PHBVs showed comparable mechanical properties as compared with other studies on PHBV copolymers with similar composition. The HV and HB sequence of isolated PHBVs were shown to be completely random copolymers based on Bernoullian and Markovian models using the diad and triad sequence distribution and comparable to commercial samples. These sequence distributions were interpretable on the basis of a model of individual random copolymers not a mixture of two or more random copolymers. This confirms that only a single T_m was observed for PHBVs. The NMR experiments required long acquisition times and sample throughput would be limited. While the controlled hydrolysis followed by ESI-MS^n analysis approach was relatively rapid and it could be easily automated for routine analysis of PHBV copolymers. We have developed these analytical tools for the future analysis of tailored PHBV polymers currently undertaken in our laboratory by (i) controlling the feeding regimes of VFA and (ii) cross-linking during processing.

2.6 References

Adamus, G., Sikorska, W., Kowalczuk, M., Montaudo, M., Scandola, M., 2000. Sequence distribution and fragmentation studies of bacterial copolyesters macromolecules characterization of PHBV macroinitiator by electrospray ion trap multistage mass spectrometry. Macromolecules 33, 5797-5802.

Avella, M., Martuscelli, E., Raimo, M., 2000. Properties of blends and composites based on poly(3-hydroxy)butyrate (PHB) and poly(3-hydroxybutyrate-hydroxyvalerate) (PHBV) copolymers. Journal of Matererials Science 35, 523– 545.

Ballistreri, A., Montaudo, G., Garozzo, D., Giuffrida, M., Montaudo, M.S., 1991. Microstructure of bacterial poly(β-hydroxybutyrate-co-β-hydroxyvalerate) by fast atom bombardment mass spectrometry analysis of the partial pyrolysis products. Macromolecules 24, 1231-1236.

Barham, P.J., Keller, A., Otun, E.L., 1984. Crystallization and morphology of a baterial thermoplastic: poly-3-hydroxybutyrate. Journal of Matererials Science 19, 2781-2794.

Bauer, H., Owen, A.J., 1988. Some structural and mechanical properties of bacterially produced poly-β-hydroxybutyrate-co-β-hydroxyvalerate. Colloid and Polymer Science 266, 241-247.

Bloembergen, S., Holden, D.A., Hamer, G.K., Bluhm, T.L., Marchessault, R.H., 1986. Studies of composition and crystallinity of bacterial poly(β–h-ydroxybutyrate-co-β-hydroxyvalerate). Macromolecules 19, 2865-2871.

Bluhm, T.L., Hamer, G.K., Marchessault, R.H., Fyfe, C.A., Veregin, R.P., 1986. Isodimorphism in bacterial poly(β-hydroxybutyrate-co-β-hydroxyvalerate). Macromolecules 19, 2871-2876.

Braunegg, G., Sonnleitner, B., Lafferty, R.M., 1978. A rapid gas chromatographic method for the determination of poly-*β*–hydroxybutyric acid in microbial biomass. European Journal of Applied Microbiology and Biotechnology 6, 29-37.

Coats, E.R., Gregg, M., Crawford, R.L., 2011. Effect of organic loading and retention time on dairy manure fermentation. Bioresource Technology 102, 2572-2577.

Coats, E.R., Loge, F.J., Smith, W.A., Thompson, D.N., Wolcott, M.P., 2007. Functional stability of a mixed microbial consortium producing PHA from waste carbon sources. Applied Biochemistry and Biotechnology 136-140, 909-925.

Dias, J.M.L., Lemos, P.C., Serafim, L.S., Oliveira, C., Eiroa, M., Albuquerque, M.G.E., Ramos, A.M., Oliveira, R., Reis, M.A.M., 2006. Recent advances in polyhydroxyalkanoate production by mixed aerobic cultures: from the substrate to the final product. Macromolecular Bioscience 6, 885-906.

Dobroth, Z.T., Hu, S., Coats, E.R., McDonald, A.G., 2011. Polyhydroxybutyrate synthesis on biodiesel wastewater using mixed microbial consortia. Bioresource Technology 102, 3352-3359.

Doi, Y., 1990. Microbial polyesters. VCH Publishers: New York, Chapter 7, pp.118-126.

Doi, Y., Kanesawa, Y., Kunioka, M., Saito, T., 1990. Biodegradation of microbial copolyesters: poly(3-hydroxybutyrate-co-3-hydroxyvaleratea) and poly(3-hydroxybutyrate-co-4-hydroxybutyrate). Macromolecules 23, 26-31.

Doi, Y., Kunioka, M., Nakamura, Y., Soga, K., 1986. Nuclear magnetic resonance studies on poly(β-hydroxybutyrate) and a copolyester of β-hydroxybutyrate and β-hydroxyvalerate isolated from *Alcaligenes eutrophus* H16. Macromolecules 19, 2860-2864.

Feng, L., Yoshie, N., Asakawa, N., Inoue, Y., 2004. Comonomer-unit compositions, physical properties and biodegradability of bacterial copolyhydroxyalkanoates. Macromolecular Bioscience 4, 186-198.

Hu, S., McDonald, A.G., Coats, E.R., 2013. Characterization of polyhydroxybutyrate biosynthesized from crude glycerol waste using mixed microbial consortia. Journal of Applied Polymer Science 129, 1314-1321.

Inoue, Y., Kamiya, N., Yamamoto, Y., chujo, R., 1989. Microstructures of commercially available poly(3-hydroxybutyrate-*co*-3-hydroxyvalerate)s. Macromolecules 22, 3800-3802.

Ishihara, Y., Shimizu, H., Shioya, S., 1996. Mole fraction control of poly(3-Hydroxbutyric-co-3-Hydroxyvaleric) acid in fed-batch culture of *Alcaligenes eutrophus*. Journal of Fermentation and Bioengineering 81, 422-428.

Iwata, T., Doi, Y., Kasuya, K.-i., Inoue, Y., 1997. Visualization of enzymatic degradation of poly[(R)-3-hydroxybutyrate] single crystals by an extracellular PHB depolymerase. Macromolecules 30, 833-839.

Jedlinski, Z., Kowalczuk, M., Adamus, G., Sikorska, W., Rydz, J., 1999. Novel synthesis of functionalized poly(3-hydroxybutanoic acid) and its copolymers. International Journal of Biological Macromolecules 25, 247–253.

Kamiya, N., Sakurai, M., Inoue, Y., Chujo, R., 1991. Isomorphic behavior of random copolymers: Thermodynamic analysis of cocrystallization of poly(3-hydroxybutyrate-co-3-hydroxyvalerate). Macromolecules 24, 3888-3892.

Kamiya, N., Yamamoto, Y., Inoue, Y., Chujo, R., Doi, Y., 1989. Microstructure of bacterially synthesized poly(3-hydroxybutyrate-*co*-3-hydroxyvalerate). Macromolecules 22, 1676-1682.

Kulkarni, S.O., Kanekar, P.P., Jog, J.P., Patil, P.A., Nilegaonkar, S.S., Sarnaik, S.S., Kshirsagar, P.R., 2011. Characterisation of copolymer, poly (hydroxybutyrate-co-

hydroxyvalerate) (PHB-co-PHV) produced by Halomonas campisalis (MCM B-1027), its biodegradability and potential application. Bioresource Technology 102, 6625-6628.

Kunioka, M., Tamaki, A., Doi, Y., 1989. Crystalline and thermal properties of bacterial copolyesters: poly(3-hydroxybutyrate-co-3-hydroxyvaleratea) and poly(3- hydroxybutyrate-co-4-hydroxybutyrate). Macromolecules 22, 694-697.

Lemos, P.C., Viana, C., Salgueiro, E.N., Ramos, A.M., Crespo, J.P.S.G., Reis, M.A.M., 1998. Effect of carbon source on the formation of polyhydroxyalkanoates (PHA) by a phosphate-accumulating mixed culture. Enzyme and Microbial Technology 22, 662–671.

Madison, L., Huisman, G.W., 1999. Metabolic engineering of poly(3-Hydroxyalkanoates): from DNA to plastic. Microbiology and Molecular Biology Reviews 63, 21-53.

McChalicher, C., Srienc, F., 2007. Investigating the structure–property relationship of bacterial PHA block copolymers. Journal of Biotechnology 132, 296-302.

Mitomo, H., Morishita, N., Doi, Y., 1993. Composition range of crystal phase transition of isodimorphism in poly(3-hydroxybutyrate-co-thydroxyvalerate). Macromolecules 26, 5809-5811.

Montaudo, M.S., 2002. Mass spectra of copolymers. Mass Spectrometry Reviews 21, 108-144.

Montaudo, M.S., Ballistreri, A., Montaudo, G., 1991. Determination of microstructure in copolymers. Statistical modeling and computer simulation of mass spectra. Macromolecules 24, 5051-5057.

Montaudo, M.S., Montaudo, G., 1992. Further studies on the composition and microstructure of copolymers by statistical modeling of their mass spectra. Macromolecules 25, 4264-4280.

Montaudo, M.S., Puglisi, C., Samperi, F., Montaudo, G., 1998. Structural characterization of multicomponent copolyesters by mass spectrometry. Macromolecules 31, 8666-8676.

Pederson, E.N., McChalicher, C.W.J., Srienc, F., 2006. Bacterial synthesis of PHA block copolymers. Biomacromolecules 7, 1904-1911.

Reis, M.A.M., Serafim, L.S., Lemos, P.C., Ramos, A.M., Aguiar, F.R., Van Loosdrecht, M.C.M., 2003. Production of polyhydroxyalkanoates by mixed microbial cultures. Bioprocess and Biosystems Engineering 25, 377-385.

Rubin, I.I., 1990. Handbook of plastic materials and technology. Wiley, New York.

Sudesh, K., Abe, H., Doi, Y., 2000. Synthesis, structure and properties of polyhydroxyalkanoates: biological polyesters. Progress in Polymer Science 25, 1503-1555.

Wei, L., McDonald, A.G., Freitag, C., Morrell, J.J., 2013. Effects of wood fiber esterification on properties, weatherability and biodurability of wood plastic composites. Polymer Degradation and Stability 98, 1348-1361.

Yoshie, N., Menju, H., Sato, H., Inoue, Y., 1995. Complex composition distribution of poly(3-hydroxybutyrate-co-3-hydroxyvalerate). Macromolecules 28, 6516-6521.

Yu, L., Dean, K., Li, L., 2006. Polymer blends and composites from renewable resources. Progress in Polymer Science 31, 576-602.

Žagar, E., Kržan, A., Adamus, G., Kowalczuk, M., 2006. Sequence distribution in microbial poly(3-hydroxybutyrate-co-3-hydroxyvalerate) co-polyesters determined by NMR and MS. Biomacromolecules 7, 2210-2216.

Chapter 3. Thermophysical analysis of bacterial poly(3-hydroxybutyrate) by TMA, DSC and TMDSC

3.1 Abstract

The melting, isothermal and nonisothermal crystallization behaviors of poly(3-hydroxybutyrate) (PHB) have been studied by means of temperature modulated differential scanning calorimetry (TMDSC) and conventional DSC. Various experimental conditions including isothermal/annealing temperatures (80, 90, 100, 105, 110, 120, 130 and 140 °C), cooling rates (2, 5, 10, 20 and 50 °C/min) and heating rates (5, 10, 20, 30, 40 and 50 °C/min) have been investigated. The lower endothermic peak (T_{m1}) representing the original crystals prior to DSC scan, while the higher one (T_{m2}) is attributed to the melting of the crystals formed by recrystallization. Thermomechanical analysis (TMA) was used to evaluate the original melting temperature (T_{melt}) and glass transition temperature (T_g) as comparison to DSC analysis. The multiple melting phenomenon was ascribed to the melting-recrystallization-remelting mechanism of the crystallites with lower thermal stability showing at T_{m1}. Different models (Avrami, Jeziorny-modified-Avrami, Liu and Mo, and Ozawa model) were utilized to describe the crystallization kinetics. It was found that Liu and Mo's analysis and Jeziorny-modified-Avrami model were successful to explain the nonisothermal crystallization kinetic of PHB. The activation energies were estimated in both isothermal and nonisothermal crystallization process, which were 102 and 116 kJ/mol in respective condition.

3.2 Introduction

Polyhydroxyalkanoates (PHAs) is a family of renewable bioplastics which are produced by microbial biosynthesis and stored by bacteria as energy reserves (Madison and Huisman, 1999). Poly(3-hydroxybutyrate) (PHB), the predominate biopolymer of PHAs, has been studied most extensively and considered as rigid material with thermal properties close to polypropylene (Khanna and Srivastava, 2005; Wei and McDonald, 2015). Its biodegradation but low permeability for water vapor have great potential in food packaging industry (Wei et al., 2014). However, its high degree of crystallinity (~60%) resulting in the formation of

large crystal spherulites and the mechanical properties are poor if the size of these spherulites exceed a critical level, and therefore PHB is always considered as brittle thermoplastic (Tri et al., 2013; Wei and McDonald, 2015; Wei et al., 2015). Therefore, improving the thermomechanical properties of PHB and/or its blends with other natural/synthetic polymers is a popular subject, especially in the field of crystallization studies in relation to its semi-crystalline structure (Chen et al., 2003b; Roa et al., 2013; Wang et al., 2008; Wang et al., 2003).

The crystallization behavior of a polymer tells whether the polymer crystals can be present under certain external conditions, while its speed to finish crystallization is determined by the kinetics of the crystallization process (Long et al., 1995). To summarize the studies of crystallization of different polymers in the past, there are two main conditions: (i) the isothermal crystallization, keeping the external environments (i.e. cooling/heating rates and thermal gradients) constant and (ii) the nonisothermal crystallization as a compensation to (i), considering the changes of external conditions which can reflect industrial processing situation. Most studies on PHB just focused on a relatively narrow range of isothermal temperatures that is close to or just slightly above its cold crystallization onset temperature (T_c) in case (i) (An et al., 1999). However, in the processing of PHB (or its copolymer) products from melt, such as injection molding and extrusion, the temperature of the mold is set far lower or higher than the T_c (Wang et al., 1996). In other words, isothermal crystallization of the injection molded PHB products always occurred at temperatures much lower or higher than its T_c. Therefore, to understand the kinetics of isothermal crystallization in a wider temperature range is necessary to give guidance to process PHB effectively. In either (i) or (ii) of conditions of different classes of polymers including PHB, various theories/models have been proposed, modified and reviewed (Liu et al., 1997; Long et al., 1995). Generally, in these studies the samples are quenched below their glass transition temperature (T_g) from melt then heated to melt the sample again, which is namely known as cold crystallization process. Nevertheless, in the industrial scale polymers are usually processed in the molten state and the properties of polymer are determined by the resulting crystalline structure of the product from melt, while the melting behavior is influenced by the crystallization process history (Tri et al., 2013). To explain the phenomena models are

developed such as the classic Avrami model to evaluate the kinetics of isothermal crystallization; while the Ozawa analysis model is widely used for nonisothermal crystallization of polymers but always failed because it neglects secondary crystallization (An et al., 1999). Other models have been developed to improve model predictability. For example, Liu and Mo's model was found to be successful to explain the nonisothermal crystallization of the bioplastic, poly(lactic acid) (PLA)/PHB blends (Tri et al., 2013), while Jeziorny-modified-Avrami model was applicable to poly(butylene terephthalate) (PBT) and its composite (Deshmukh et al., 2014). Hence, nonisothermal crystallization behavior of semi-crystalline PHB is also expected to be explained by these models.

Meantime, the subsequent melting behavior after crystallization can attract more attention in the fields of both academia and industry. Double or multiple melting endothermic behaviors are usually found in semicrystalline polymers melts by differential scanning calorimetry (DSC), which are crystallized isothermally at selective crystallization temperatures or nonisothermal conditions at various cooling rates (Qiu et al., 2003b). However, the documented data on multiple or double melting behavior of PHB following the isothermal or nonisothermal crystallization processes is limited. Temperature modulated DSC (TMDSC) experiments can obtain more accurate heat capacity measurements and separate thermodynamic phenomena (e.g. glass transition, crystallization and melting behavior) with better resolution and sensitivity. This techniques was used to examine the crystallization and multiple melting behavior of PHB by Guanratne et al. (2006c). In their study, the effects of isothermal crystallization and crystallization rates on the multiple melting behavior of PHB were determined, but conducted in a relatively small temperature range (100-120 $^{\circ}$C) and the kinetics was not addressed. Whereas many industrial processes, such as injection molding and extrusion, involve isothermal crystallization in the mold or die in which the temperature was generally set beyond the range studied for PHB (Rizk et al., 2013).

Isothermal/nonisothermal crystallization processes were also shown to play a crucial role in the melting behavior of other semicrystalline polymers, such as poly(butylene succinate) (PBSU) and poly(ethylene succinate) (PES) (Qiu et al., 2003b), poly(ethylene terephthalate) (PET) and poly(ethylene 2,6-naphthalene dicarboxylate) (PEN) (Montserrat et al., 2003), and isotactic polystyrene (iPS) (Liu and Petermann, 2001). Various reasons have been

attributed to the multiple melting behavior of semicrystalline polymers, such as the melting, recrystallization and remelting (MRR) during DSC heating scans, resulting in the presence of crystal modifications and different molecular species present in the polymer systems (Qiu et al., 2003a). However, controversies still exist as to the exact origins of the multiple melting behavior of PHB.

The aim of this study was to investigate the influence of isothermal annealing of PHB (over a wide temperature range) on the nonisothermal cold crystallization process from melt at different cooling rates by DSC and TMDSC. Meanwhile, the cold crystallization behavior and the kinetics were studied using different models including the Liu and Mo's and Jeziorny-modified-Avrami models to evaluate the nonisothermal crystallization kinetics of PHB for the first time. The developed models will give insight as to the mechanism of the crystallization process for PHB and its multiple melting behaviors; especially the nonisothermal crystallization induced multiple melting phenomenons. Thermal mechanical analysis (TMA) was employed to identify the original (or true) melting temperature (T_{melt}) as a comparison to the DSC and TMDSC melting transitions.

3.3 Experimental

3.3.1 Materials and sample preparation

The commercial grade PHB was obtained from Tianan Biopolymer Inc. (Ningbo, China). The PHB was purified to remove any additives in the commercial preparation before analysis. PHB powder was dissolved in chloroform, precipitated in cold petroleum ether (boiling point range 35-60 $^{\circ}$C), recovered by filtration and dried under vacuum for at least one week prior to use in order to remove any excess moisture/solvent. The weight average molecular weight (M_w) = 290, 000 g/mol and polydispersity (PD) = 2.3 was determined by size exclusion chromatography (SEC) (Hu et al., 2013).

3.3.2 Thermomechanical analysis (TMA)

The thermomechanical properties were characterized using Perkin Elmer TMA7 instrument equipped with a penetration probe (0.01 N applied load). PHB sample was molded into a

rectangular bar using a Dynisco Lab Mixer Extruder. For the TMA analysis a small piece (in triplicate, 2 x 1 x 1 mm^3) was cut from the molded bar and heated from -50 to 190 ˚C at a rate of 5 ˚C/min. The T_g and T_{melt} were determined from the onset point of softening.

3.3.3 Differential scanning calorimetry (DSC) and temperature modulated DSC (TMDSC)

Conventional DSC and TMDSC were performed on PHB (4-6 mg, in triplicate) using a TA Instruments model Q200 DSC with refrigerated cooling. All the samples were heated rapidly at 100 ˚C/min to 180 ˚C to remove any thermal history.

For the isothermal crystallization kinetics study, samples were held isothermally at 180 ˚C for 5 min to allow for complete melting to occur, followed by rapid cooling (50 ˚C/min) to the target isothermal crystallization temperature (T_{iso} = 80, 90, 100, 105, 110, 115, 120, 130 and 140 ˚C). All samples were held at T_{iso} for 1 h after which PHB crystallization was believed to be complete. The relative degree of crystallinity, $X_{t\text{-}iso}$, after time t, was determined according to the equation:

$$X_{t-iso} = \int_0^t (dH/dt)dt / \int_0^\infty (dH/dt)dt \qquad \text{(eq. 3.1)}$$

where, the first integral is the heat released after time t and the second integral is the total heat of the whole crystallization process, for $t = \infty$; the activation energy of crystallization, E_{iso}, was calculated as follows:

$$V_c = A \exp(-E_{iso}/RT_{iso}) \qquad \text{(eq. 3.2)}$$

where V_c is the crystallization rate determined from the slop of the linear region of $X_{t\text{-}iso}$ vs. t plot, A is an arbitrary pre-exponential factor, R is the gas constant.

In order to investigate the effect of isothermal annealing on the subsequent melting behavior of PHB, a wider range of isothermal annealing temperature (T_a = 80, 90, 100, 105, 110, 120, 130 and 140 ˚C) was selected. In this study, PHB melts were rapidly cooled to T_a at -50 ˚C/min and held for 1 h followed by the heating TMDSC measurements to 200 ˚C, at an average heating rate of 2 ˚C/min with a period of 60 s and modulation amplitudes of ±0.6 ˚C.

The control (unannealed) sample was treated with a similar procedure in that the polymer melt was cooled to -50 ˚C and then heated to 200 ˚C directly without being annealed.

The nonisothermal crystallization test of PHB melts was performed at various cooling rates (ϕ) of 2, 5, 10, 20 and 50 ˚C/min, respectively, to -50 ˚C. The T_c, crystallization peak temperature (T_p) and the temperature at which crystallization was complete (T_e) were determined from the cooling scan. The effects of nonisothermal crystallization on the melting behavior of PHB were investigated by reheating the samples from -50 to 200 ˚C at a heating rate of 10 ˚C/min by either the conventional DSC or TMDSC measurements with an average heating rate of 2 ˚C/min with a period of 60 s and modulation amplitudes of ±0.6 ˚C. From the heating scan the T_g was determined.

The effect of heating rate (Φ) on the multiple melting behaviors was investigated after polymer melts were cooled down to -50 ˚C rapidly at a cooling rate of 80 ˚C/min and held for 5 mins, and then heated to 200 ˚C at Φ = 5, 10, 20, 30, 40 and 50 ˚C/min. Both conventional DSC and TMDSC data were analyzed using TA Universal Analysis v4.4A software.

3.4 Results and discussion

3.4.1 Melting temperature obtained by TMA

TMA penetration provides excellent means of assessing T_g and T_{melt} of material in the compression mode by recording the displacement (%) as function of temperature. Below the T_{melt} of PHB the sample undergoes a slight expansion, while the temperature was above the T_g the sample softens and if the temperature was above T_{melt} the sample melts and the lightly loaded probe penetrates the sample and a rapid decrease in the thickness of the sample was observed. The T_g and T_{melt} of the PHB were determined to be about 5 ± 1 ˚C and 167 ± 0.5 ˚C, respectively (Figure 3.1). These values were in close agreement with the literature (He et al., 2001).

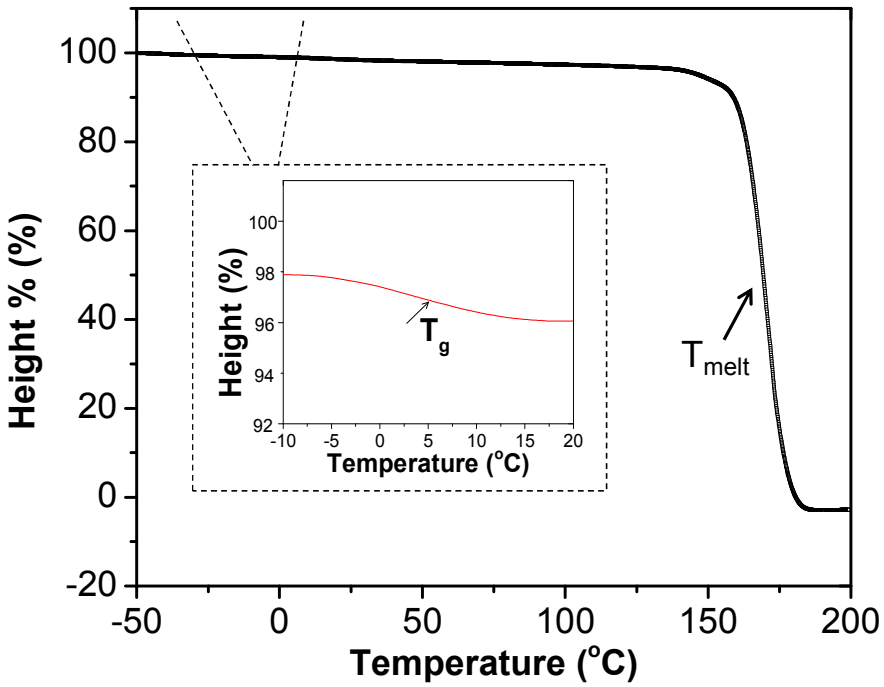

Figure 3.1.TMA thermograms of PHB samples. Note: arrows pointed to T_g and T_{melt}.

3.4.2 Isothermal crystallization behavior and kinetics

One property of a polymer that will have an impact on processing or end use of the final product is the crystallization behavior of the polymer. The primary method used to understand the crystallization of polymer is isothermal crystallization, especially the kinetics involved. Therefore, in this section, the isothermal crystallization kinetics of PHB was studied at selected temperatures (T_{iso}). A conventional DSC was used by following the classical scans that the polymer was first heated to the molten state and then quench-cooled rapidly to the desired T_{iso} and held for sufficient time (1 h) for the crystallization process to be complete and the heat flow signal reaches the baseline. Figure 3.2a shows the relative crystallization evolution ($X_{t\text{-}iso}$ vs. time t) of PHB. The crystallization rate (V_c), crystallization half time ($t_{cry\text{-}1/2}$) and activation energy (E_{iso}) were determined and summarized in Table 3.1. When the T_{iso} was increased from 80 to 140 ˚C, the crystallization rate was reduced significantly, hence the $t_{cry\text{-}1/2}$ was increased and a longer overall time was required to complete the crystallization process. The activation energy (E_{iso}) of the isothermally crystallized PHB in this study was 102 kJ/mol. Previous kinetic studies of

commercial PHB (Sigma-Aldrich, US) on the isothermal crystallization at a narrower temperature range (100-120 °C) showed a lower activation energy of 87.3 kJ/mol with M_w = 230, 000 g/mol and PD = 2.6 (Gunaratne and Shanks, 2006b). The higher M_w (290, 000 g/mol) in this study suggests longer polymer chains present in the polymer system and the more tangled up they will get, and hence a lot more energy will be required to diffuse these long chains into the crystalline lattice during crystallization process.

The isothermal crystallization kinetics of PHB and its copolymer (polyhydroxybutyrate-co-hydroxyvalerate, PHBV) in a relatively narrower temperature range have been explained successfully by Avrami equations (Gunaratne and Shanks, 2005; Hu et al., 2013):

$$1 - X_{t\text{-}iso} = \exp(-kt^n) \qquad \text{(eq. 3.3)}$$

Eq. (3.3) can be written in double-logarithmic form as:

$$\ln[-\ln(1 - X_{t\text{-}iso})] = \ln k + n\ln t \quad \text{(eq. 3.4)}$$

where k and n are the Avrami rate constant and Avrami exponent at time t, respectively, which depend on both the nucleation mechanism and the growth geometry (Hu et al., 2013; Hu et al., 2006).

The Avrami plot ($\ln[-\ln(1 - X_{t\text{-}iso})]$ vs. $\ln t$) of the data from Figure 3.2a and Table 3.1 is shown in Figure 3.2b. The experimental data fitted very well with the Avrami equation at different T_{iso} = 80, 90, 100, 105 and 110 °C. However, when the T_{iso} was increased to ≥ 115 °C the initial linear relationship was observed followed by a slight leveling off. This phenomenon could be contributed to the secondary crystallization of PHB due to slow crystallization of the crystal defects, or the spherulite impingement in the later stage of the whole crystallization process at higher T_{iso}. From the slope and intercept of each fitted line from Figure 3.2b, the Avrami parameters, the Avrami exponent (n) and overall crystallization rate constant (k), were determined respectively. In addition, the half time, $t_{Avrami\text{-}1/2}$, to complete the crystallization process was obtained by the equation (Gunaratne and Shanks, 2006b):

$$t_{Avrami\text{-}1/2} = (\ln 2/k)^{1/n} \quad \text{(eq. 3.5)}$$

and the overall rate of crystallization was evaluated by $k^{1/n}$. These values are summarized in Table 3.1. The $k^{1/n}$ values decreased with increasing T_{iso}, suggesting the whole crystallization process can be finished in a shorter time period, which was supported by lower $t_{Avrami-1/2}$ and $t_{cry-1/2}$ values at lower T_{iso}. The calculated $t_{Avrami-1/2}$ values were close to the data from $t_{cry-1/2}$. For example, the $t_{cry-1/2}$ at T_{iso} = 80 and 90 °C was only seconds, while 40 min was required to reach 50% crystallization at T_{iso} = 140 °C. These values were slightly higher than other studies, which may be attributable to its higher M_w in this study resulting in the relative lower crystallization rates. At different T_{iso}'s the n values varied between 1.8 to 4.8, which could be attributed to the heterogeneous nucleation mechanism and geometry of PHB crystal growth (Hu et al., 2013; Hu et al., 2006).

Table 3.1. The crystallization rate (V_c, determined from $\ln V_c$ vs. $1/T_{iso}$), crystallization half time ($t_{cry-1/2}$, determined from X_{t-iso} vs. t plot), isothermal activation energy (E_{iso}), crystallization half time ($t_{Avrami-1/2}$, calculated from Avrami parameters, n and k), and the overall rate of crystallization, $k^{1/n}$

T_{iso} (°C)	V_c (min^{-1})	$t_{cry-1/2}$ (min)	E_{iso} (kJ/mol)	$t_{Avrami-1/2}$ (min)	n	$k^{1/n}$ x 10^{-4} (min^{-1})
80	3.8	<1.0		0.1	2.09	42177
90	3.3	<1.0		0.2	2.01	39634
100	0.38	1.2		1.1	1.82	7479
105	0.34	3.6	102	2.2	1.83	3678
110	0.16	6.1		3.7	2.01	2252
115	0.13	10.1		8.7	2.00	956
120	0.10	15.4		14.4	2.08	583
130	0.05	27.2		28.8	2.22	294
140	0.04	38.8		38.6	4.80	240

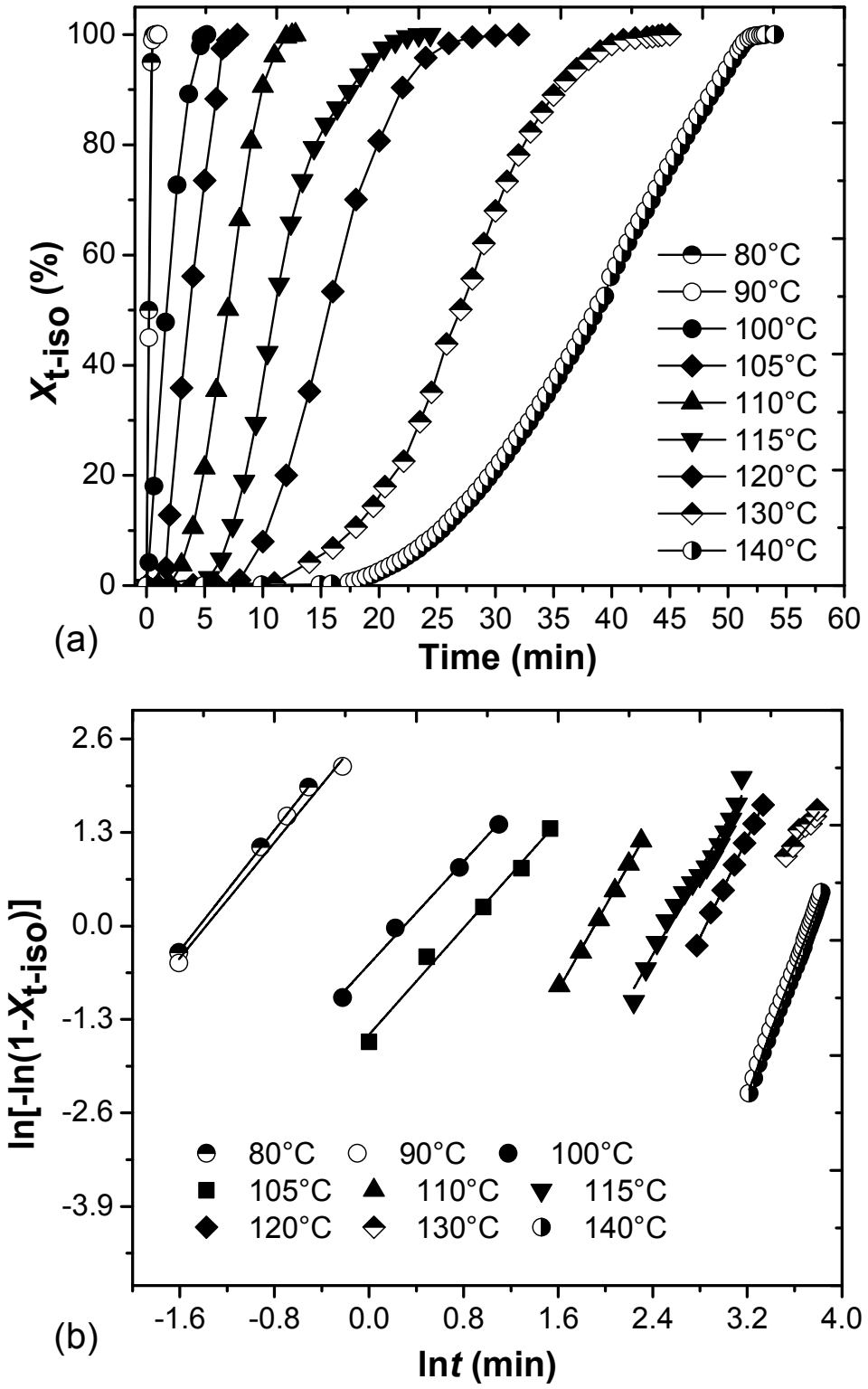

Figure 3.2. (a) Plot of relative crystallinity, $X_{t\text{-iso}}$ (%), as function of time, t, and (b) Avrami plot of ln[-ln(1 – $X_{t\text{-iso}}$)] vs. ln$t$ at different isothermal temperatures (T_{iso} = 80, 90, 100, 105, 110, 115, 120, 130 and 140 °C) as determined by conventional DSC.

3.4.3 Influence of isothermal annealing temperatures to melting behavior of PHB

Isothermal annealing temperatures have a significant impact on the melting behavior of PHB. Figure 3.3 shows the melting curves of total and reversing heat flow curves by TMDSC for samples annealed at different temperatures. The annealing time was 1 h. The results show clearly that the melting behavior was different for different annealing temperatures at the same fixed annealing time and identical cooling/heating rate. The melting enthalpy was higher after annealing as compared with the control sample. From Figure 3.3, three endothermic peaks were observed after annealing (labeled as T_{ap}, T_{m1} and T_{m2} in the order of temperature from low to high). T_{m1} and T_{m2} were easier to be identified in the reversing heat flow curve (Figure 3.3b) than in the total heat flow curve (Figure 3.3a). The annealing peak (T_{ap}) shifted to higher temperature with increasing T_a and the T_{ap} was always at ca. 15-20 $^{\circ}$C above T_a. The similar phenomenon was observed for isothermally crystallized PET (Kong and Hay, 2003; Minakov et al., 2004). They concluded that the annealing peak was associated with the fusion of defective secondary lamellae, which melt earlier because of their lower stability.

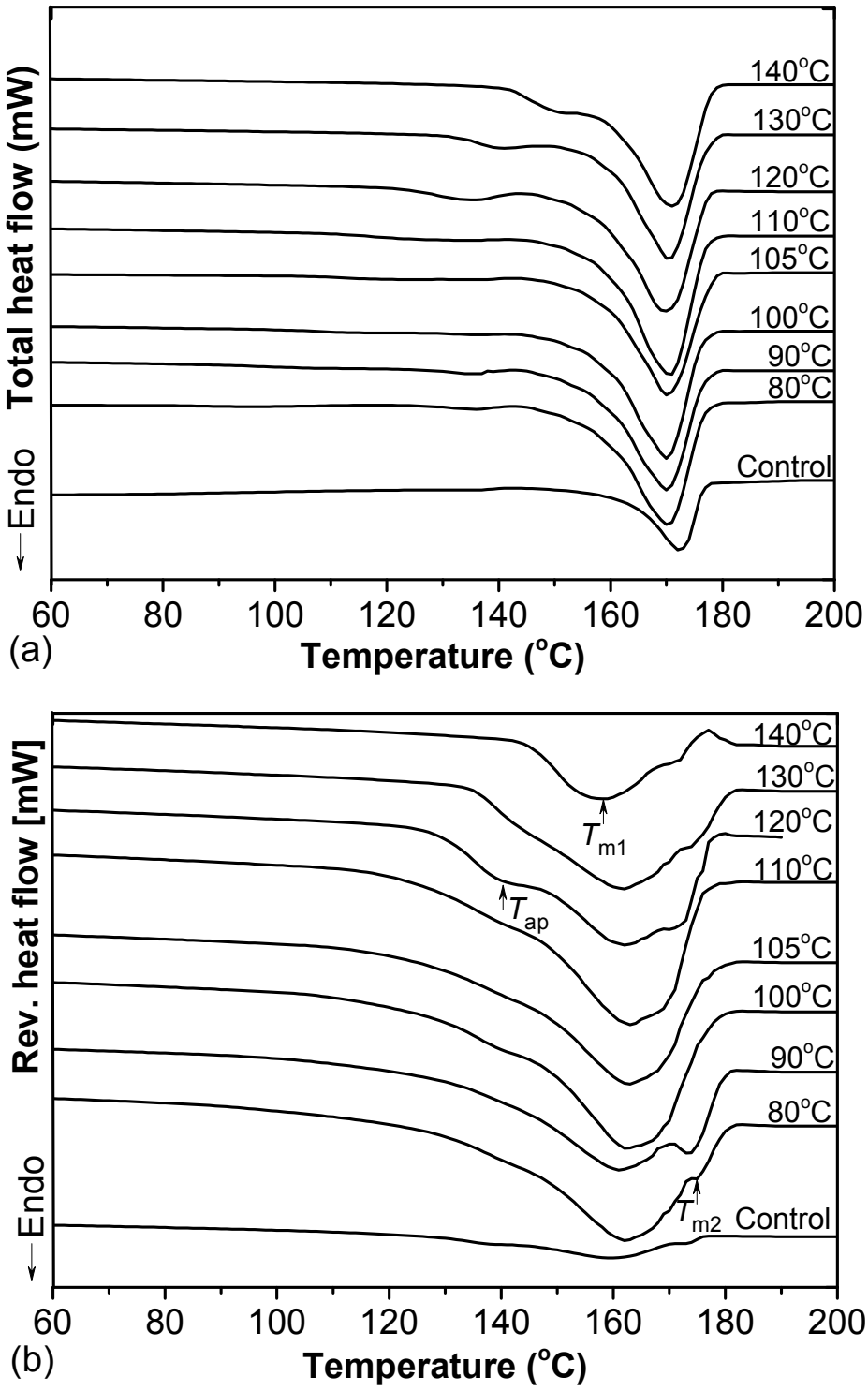

Figure 3.3. (a) TMDSC total heat flow curves and (b) reversing (Rev.) heat flow curves of control sample and samples isothermally annealed at different temperatures. The curves are shifted vertically for clarity.

The variations of the melting transition (T_{m1} and T_{m2}) with T_a are shown in Figure 3.4. T_{m1} decreased to a minimum value when T_a <100 °C; when T_a >100 °C, with increasing T_a, the T_{m1} shifts to higher temperatures and finally merges into the highest endotherm (T_{m2}). With an increase of T_a, T_{m2} remains constant at ca. 170 °C. T_{m1} was attributed to the melting of original crystals formed before the DSC scan, and the T_{m2} was associated with the melting of the recrystallized components during heating scan (Wellen et al., 2013). The origin of double melting was probably due to the MRR mechanism during the TMDSC reheating scan (Liu and Petermann, 2001; Qiu et al., 2003a), whereas the initial decrease of T_{m1} could be attributed to the thicker crystal lamella formed at lower T_a (<100 °C) in this study. These results are in agreement with the isothermally induced multiple melting behavior of PET (Kong and Hay, 2003). When measuring the crystallinity of a polymer, TMDSC observes the formation of crystalline structures as soon as the sample starts to melt, and this phenomenon is known as recrystallization and might not be detected by conventional DSC (Kampert and Sauer, 2001; Sauer et al., 2000). The recrystallization process is evaluated by the degree of undercooling, $\Delta T = T_m^0 - T_m$, where the T_m^0 is the ideal equilibrium melting temperature of PHB. According to the method of Hoffman and Weeks (Hoffman, 1982) the T_m^0 was obtained by plotting the T_m versus T_a, extrapolation of experimental data (used T_{m2} for T_a >100 °C) to the intersection of $T_m = T_a$ yields T_m^0 which was estimated to be 177.3 °C (Figure 3.4). T_m was the experimental melting temperature (T_{m1} was used). The ΔT is interpreted as the driving force of recrystallization in semicrystalline polymers (Pogodina and Winter, 1998; Qiu et al., 2003a). At higher T_a, T_{m1} was shown to increase, resulting in a decrease of ΔT so that less driving force was available to move PHB towards recrystallization. Hence, the double melting peaks started to merge gradually when T_a increased from 100 °C to 140 °C; while two melting endotherms were clearly observed for T_a <100 °C. In other words, at higher T_a, the rate at which the equilibrium state is reached will be faster. Therefore, higher isothermal annealing temperature will inhibit the recrystallization behavior.

Montserrat and coworkers showed that the total heat flow was a suitable parameter to be used to calculate the crystallinity for PET by TMDSC (Montserrat et al., 2003). Hence, the

degree of crystallinity (X_c %) for PHB in the isothermal crystallization study was calculated using the equation (Wei et al., 2014):

$$X_c\ \% = \Delta H_m/\Delta H_0 \times 100 \qquad \text{(eq. 3.6)}$$

where ΔH_m is the melting enthalpy obtained from the total heat flow curve (Figure 3.3a) and ΔH_0 is melting enthalpy of 100% crystalline PHB (146 J/g) (Wei et al., 2014). The results of X_c% versus different T_a's, as given in Figure 3.5, indicate (i) when the T_a is <100 °C the degree of crystallinity (X_c %) of PHB decreases from 63.3% to 60.5% with an increase of T_a from 80 to 100 °C; (ii) when 100 °C < T_a > 120 °C, the crystallinity seems to be around 60%; if (iii) the T_a is >120 °C the degree of crystallinity decreases significantly from 59.3% to 45.6% with increasing the respective annealing temperature from 120 to 140 °C. This shows that at higher T_a, a greater driving force was required to align polymer chains and crystallize accordingly. This result would provide a profound insight into the relationship between thermal history during processing and the property of end product (especially the crystallinity and mechanical properties). In other words, in the manufacturing of PHB products such as injection molding, different mold temperatures can be selected to tailor the crystallinity of the final products, which will affect their corresponding thermophysical properties accordingly.

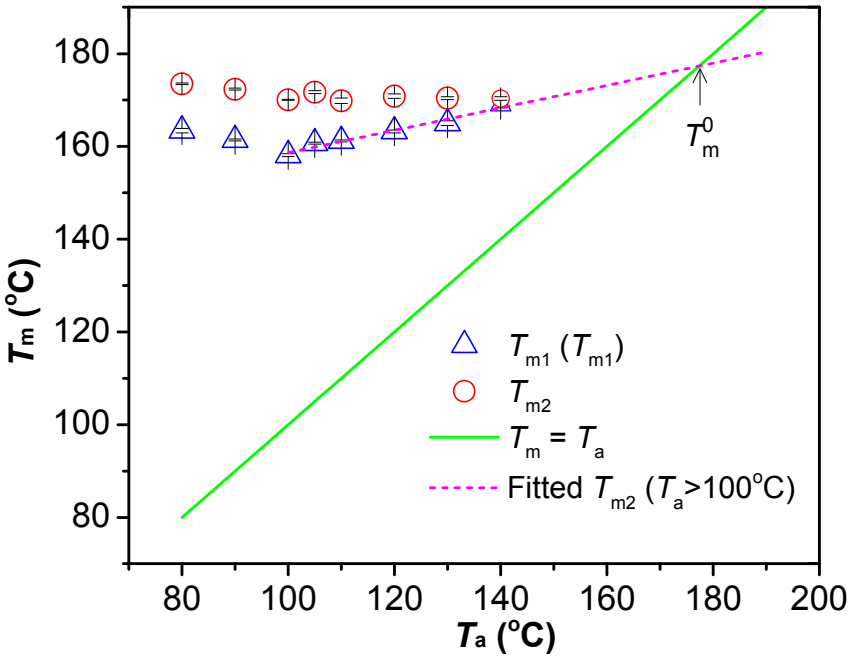

Figure 3.4. Plot of melting temperatures (T_{m1} and T_{m2}) vs. different T_a's for PHB. The transition temperatures were determined and averaged from triplicate TMDSC reversing heat flow curves as shown in Figure 3.3b with standard deviation showed as error bars. Extrapolation of T_m^0 from the melting temperature as a function of T_a's of PHB.

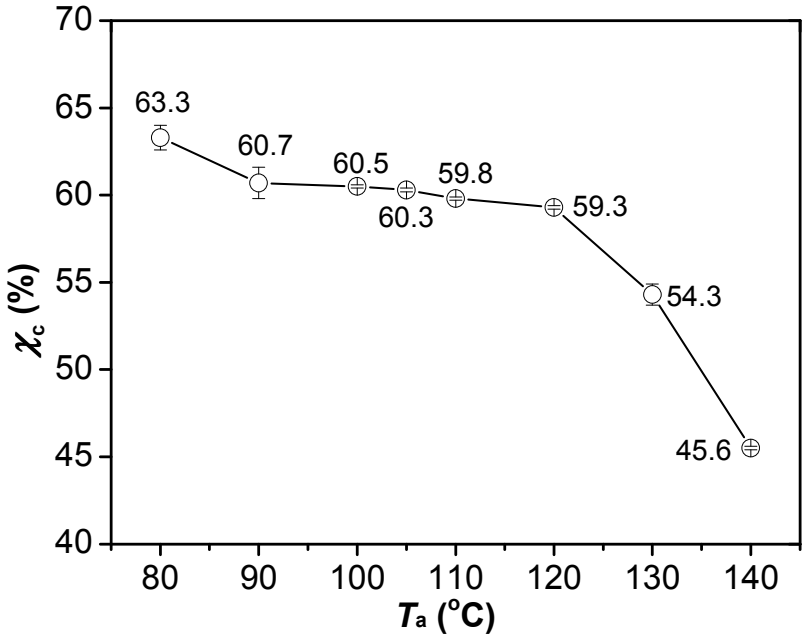

Figure 3.5. Plot of PHB crystallinity, X_c (%), vs. annealing temperature, T_a, and the averaged values from triplicates are labeled with standard deviation was shown as error bars.

3.4.4 Influence of nonisothermal crystallization

Figure 3.6 shows nonisothermal crystallization exothermic DSC curves versus temperature at various ϕ for PHB from the melt. It was seen that increasing ϕ resulted in a smaller exothermic peak and this was consistent with another study using a narrower temperature range (2.5 to 40 $^{\circ}$C/min) (An et al., 1998). This resulted in less time being available for PHB crystallization to occur and less perfect crystals tended to develop at higher ϕ. The onset starting temperature of crystallization (T_0), crystallization peak temperature (T_p), the end crystallization temperature (T_e) and the crystallization enthalpy (ΔH_c) evolved were determined and the results given in Table 3.2. It was clearly observed that as the ϕ increased both the T_0 and T_p shifted towards lower temperature, as expected. For example, T_0 and T_p decreased from 119 to 94 $^{\circ}$C and 113.3 to 76.4 $^{\circ}$C, respectively, when ϕ was increased from 2 to 50 $^{\circ}$C/min. A similar phenomenon was observed for a PHB/layered nanocomposite and PHBV copolymer (Liu et al., 2010; Yuan et al., 2006). If the molten PHB was cooled down at a higher ϕ, there was insufficient time to overcome the nucleation energy barriers and more enthalpy was required for PHB chains to align orderly. Hence, the nucleation was being activated at lower temperature, which resulted in the delay of initiation of crystallization, lowering of T_0 and T_e values, and increasing ΔH_c (J/g) accordingly (Hsu et al., 2007). Whereas, upon slower cooling, the polymer chains have sufficient time to take on a more orderly configuration, hence the crystallization was initiated at an early stage so that higher T_0 values were observed (Kim et al., 2006).

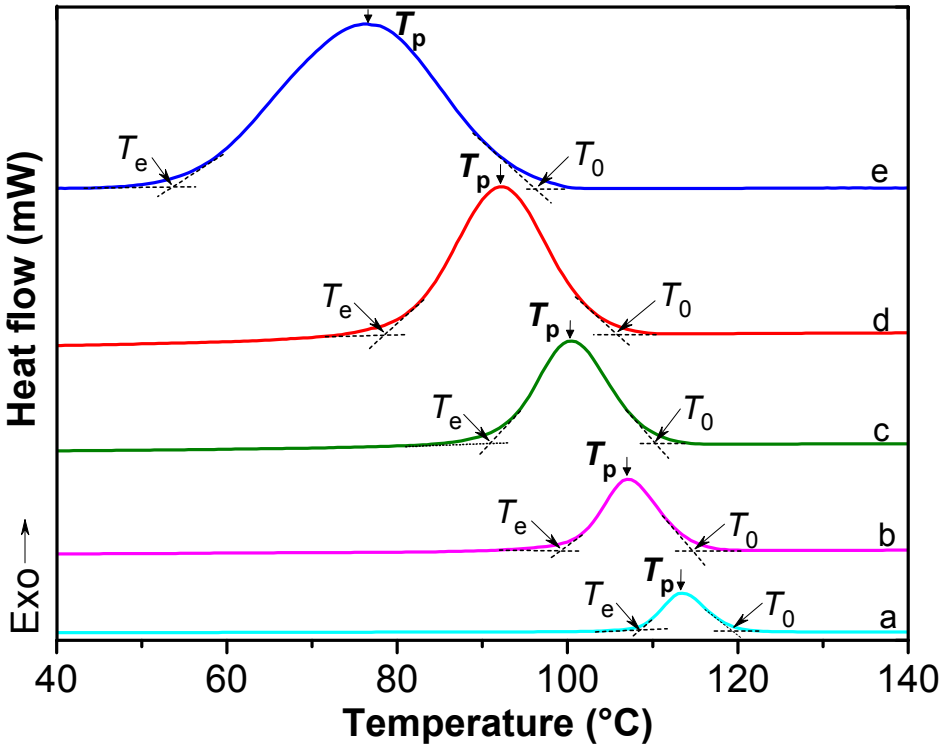

Figure 3.6. DSC curves showing exothermic curves in nonisothermal crystallization process at various cooling rates (a: 2; b: 5; c: 10; d: 20, and e: 50 ˚C/min). The curves are shifted vertically for clarity.

Table 3.2. Values of the heat evolved during nonisothermal crystallization (ΔH_c, J/g), the T_0, T_c, T_p and the half-time of the crystallization ($t_{noniso\text{-}1/2}$) for PHB determined from Figure 3.7a, and Z_c values obtained by the Jeziorny-modified-Avrami analysis

Cooling rate (˚C/min)	T_0 (˚C)	T_p (˚C)	T_e (˚C)	$t_{noniso\text{-}1/2}$ (min)	ΔH_c (J/g)	Z_c
2	119.1	113.3	107.2	7.4	59.9	0.7424
5	114.3	106.8	99.4	3.0	72.4	0.7803
10	109.3	100.4	92.9	2.5	77.9	0.7943
20	103.1	92.2	78.3	1.4	84.2	0.8122
50	94.1	76.4	52.7	1.0	86.4	0.8831

3.4.4.1 Nonisothermal crystallization kinetics analysis by different models

Previous nonisothermal crystallization kinetic studies of PHB were focused on a relatively narrow cooling rate range or used limited models (An et al., 1998). Therefore, this study used a wider range of cooling rates and developed models based on Liu and Mo's analysis and Jeziorny-modified-Avrami models to investigate PHB. In order to obtain more systematic kinetic information, the raw data such as those shown in Figure 3.7 was presented as the relative crystallinity ($X_{\text{t-noniso}}$) as a function of temperature as follows (Liu et al., 2010):

$$X_{\text{t-noniso}} = \int_{T_0}^{T}(\mathrm{d}H_c/\mathrm{d}T)\mathrm{d}T \,/\, \int_{T_0}^{T_\infty}(\mathrm{d}H_c/\mathrm{d}T)\mathrm{d}T \quad \text{(eq. 3.7)}$$

where T_0 and T are the initial crystallization temperature and an arbitrary temperature, respectively. T_∞ was the end crystallization temperature and $\mathrm{d}H_c/\mathrm{d}T$ was the heat flow rate. Once this relation was constructed the conversion from raw data into the $X_{\text{t-noniso}}$ as function of time, t, was obtained by transforming the temperature scale into a time scale according to:

$$t = (T_0 - T)/(\phi) \quad \text{(eq. 3.8)}$$

where T is the temperature at time t, T_0 is the temperature at which crystallization begins (t = 0).

Figure 3.7a shows the plots of relative degree of crystallinity ($X_{\text{t-noniso}}$ %) as function of crystallization time at various ϕ. From this plot the half-time of crystallization, $t_{\text{noniso-1/2}}$, was obtained (Table 3.2). It was clearly shown that by increasing ϕ, $t_{\text{noniso-1/2}}$ values were reduced. For example, at ϕ = 50 °C/min, $t_{\text{noniso-1/2}}$ was only 1 min, suggesting that such a high ϕ can encourage the crystallization to occur faster.

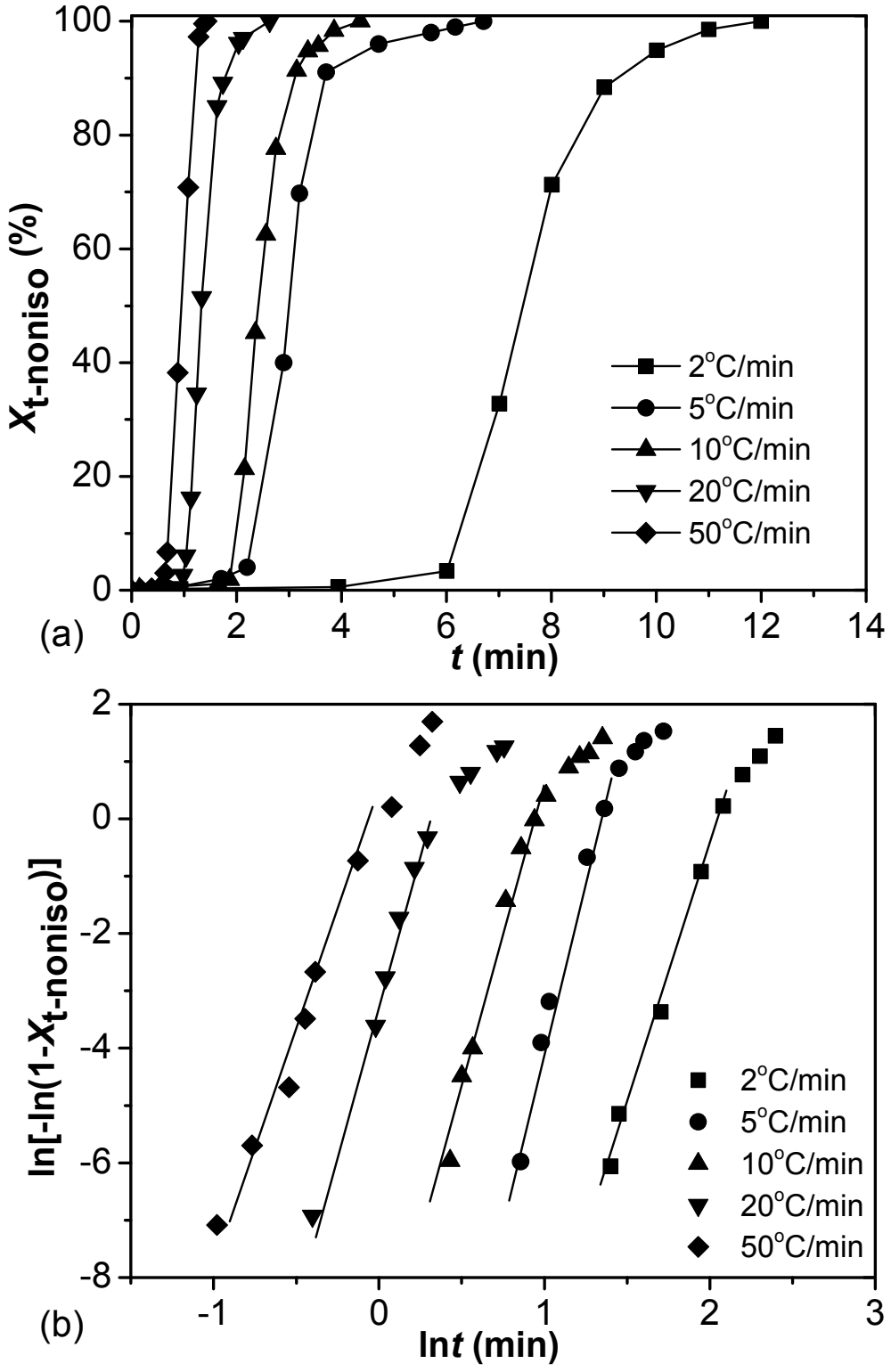

Figure 3.7. (a) Plot of relative crystallinity, $X_{t\text{-noniso}}$ (%), as function of time, t, and (b) plot of $\ln[-\ln(1 - X_{t\text{-iso}})]$ vs. $\ln t$ of nonisothermal crystallization at different cooling rates (labeled in plot).

As mentioned above, the Avrami equation was applied to explain the isothermally induced crystallization, whereas during the nonisothermal crystallization process the parameters k and n will depend upon both the rates of nucleation and crystal growth process (Li et al., 2013). This was further confirmed by the straight line obtained from the plot of $\ln[-\ln(1-X_{t\text{-noniso}})]$ vs. $\ln t$ at the early stage of crystallization followed by a large deviation (Figure 3.7b). Jeziorny modified this model to describe the non-isothermal crystallization process with changing ϕ. Most recently Deshmukh and his coworkers successfully used this model to investigate the nonisothermal crystallization kinetics of PBT (based composites) (Deshmukh et al., 2014). Hence, semi-crystalline PHB was expected to be explained by Jeziorny-modified-Avrami model. To consider the effect of ϕ on the rate constant, k was corrected by assuming a constant, Z_c, and then the modified form of the parameter to characterize the kinetics of non-isothermal crystallization was established (Deshmukh et al., 2014):

$$\ln Z_c = \ln k/(\phi) \qquad \text{(eq. 3.9)}$$

where Z_c is the Jeziorny constant.

From Table 3.2, Z_c values reflecting the crystallization rate were increased with increasing ϕ. The crystallization rate depends on the rates of nucleation and nuclei growth (Vyazovkin and Sbirrazzuoli, 2004). Higher ϕ induces a higher extent of undercooling, resulting in an increase of nucleation density, and hence the crystallization rate will be increased accordingly. Thus, the Avrami model did not describe the kinetics of nonisothermal crystallization observed. However, the Jeziorny-modified-Avrami theory was able to describe successfully the kinetic behavior of nonisothermal crystallization of PHB.

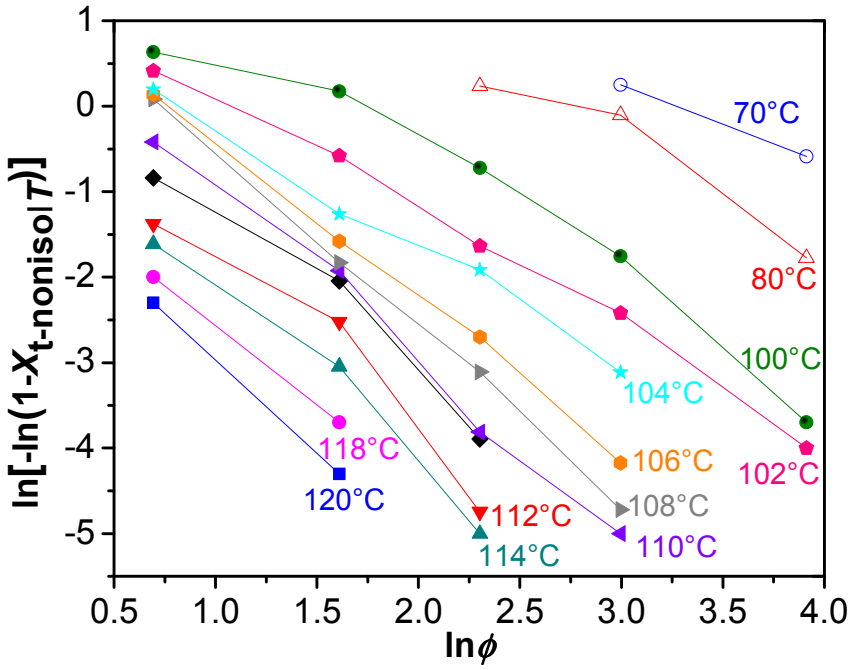

Figure 3.8. Ozawa plots of $\ln[-\ln(1-X_{\text{t-noniso}\,|\,T})]$ vs. $\ln\phi$ for nonisothermal crystallization of PHB.

By simple modification, Ozawa extended the Avrami equation to describe the nonisothermal crystallization kinetics (Ziaee and Supaphol, 2006). Based on his assumption, the nonisothermal crystallization process was to be comprised of infinitesimally small isothermal crystallization steps at a conditional temperature (T) and expressed as:

$$1 - X_{\text{t-noniso}\,|\,T} = \exp[-K(T)/(\phi)^m] \qquad \text{(eq. 3.10)}$$

and this equation can be rearranged to be in double-logarithmic form:

$$\ln[-\ln(1 - X_{\text{t-noniso}\,|\,T})] = \ln[K(T)] - m\ln(\phi) \qquad \text{(eq. 3.11)}$$

where $K(T)$ is the cooling function and m is the Ozawa exponent depending on the crystal growth. If the Ozawa model is valid, the explanation of the nonisothermal crystallization of PHB in this study would give a straight line for the plot of $\ln[-\ln(1 - X_{\text{t-noniso}\,|\,T})]$ versus $\ln(\phi)$, from which the $K(T)$ and m can be obtained. The Ozawa plot based on eq. 3.11 at specific temperatures of PHB is shown in Figure 3.8. The Ozawa plots clearly shows deviation from linearity and m varies at various ϕ, suggesting the Ozawa analysis was not successful in

explaining the nonisothermal crystallization kinetics of PHB. This may be ascribed to either a change in crystallization mechanism or secondary crystallization which has been ignored in Ozawa's model (Deshmukh et al., 2014; Li et al., 2013).

To further explain the nonisothermal crystallization kinetics of PHB, a new model was proposed by Liu and Mo which combined the Avrami and Ozawa's equations as follows (Liu et al., 1997):

$$\ln\phi = \ln F(T) - \alpha \ln t \qquad \text{(eq. 3.12)}$$

where $F(T) = [K(T)/k)^{1/m}]$ is the ϕ that needs to reach a defined degree of crystallinity at a unit of crystallization time, α is the ratio between the Avrami exponent, n, and the Ozawa exponent, m, namely n/m. By plotting $\ln\phi$ vs. $\ln t$ at selected relative degree of crystallinity ($X_{\text{t-noniso}}$), the $F(T)$ and α can be obtained from the intercept and slope of the fitted straight line, respectively. These values are listed in Table 3.3. It can be seen that PHB exhibits a linear relationship between $\ln\phi$ and $\ln t$ at given $X_{\text{t-noniso}}$ values of 20%, 40%, 60% and 80%, and α values varies from 1.50 to 1.59. The variation in α was small, indicating that the Liu and Mo's model was appropriate to describe the nonisothermal crystallization kinetics of PHB. The value of $F(T)$ increased with an increase of $X_{\text{t-noniso}}$, suggesting that at a unit crystallization time a higher degree of crystallinity will be achieved with a higher ϕ. Similar findings were reported for polylactic acid (Li et al., 2013), polybutyleneterphalate (Deshmukh et al., 2014), and polypropylene (Yuan et al., 2006). This result is consistent with the Jeziorny-modified-Avrami analysis. It can be concluded that the Liu and Mo's analysis is a suitable model to explain the nonisothermal crystallization behavior of PHB in this study.

Table 3.3. Nonisothermal crystallization kinetic parameters at different degree of relative crystallinity ($X_{t\text{-noniso}}$) determined from Liu and Mo's analysis and activation energy values based on Kinsinger's ($\Delta E_{noniso\text{-Kinsinger}}$) and Friedman ($\Delta E_{noniso\text{-Friedman}}$) models.

$X_{t\text{-noniso}}$ (%)	$F(T)$	α	$\Delta E_{noniso\text{-Kinsinger}}$ (kJ/mol)	$\Delta E_{noniso\text{-Friedman}}$ (kJ/mol)
20	10.01	1.50	115.6	96.1
40	13.02	1.55		97.6
60	14.44	1.57		98.3
80	18.92	1.59		100.8

3.4.4.2 Activation energy in nonisothermal crystallization process

To evaluate the activation energy involved during the nonisothermal crystallization process with different ϕ, the Kissinger's method was primarily used (Liu et al., 2010):

$$d[\ln(\phi/T_p^2)]/d(1/T_p) = \text{Constant} - \Delta E_{noniso\text{-Kinsinger}}/RT_p \qquad \text{(eq. 3.13)}$$

where R is the universal gas constant, and $\Delta E_{noniso\text{-Kinsinger}}$ is the activation energy of crystallization. From the plot of $\ln(\phi/T_p^2)$ vs. $1/T_p$ (Figure 3.9a), the $\Delta E_{noniso\text{-Kinsinger}}$ was determined from slope of the fitted straight line as 115.6 kJ/mol (Table 3.3). This value was 20% higher than the result of 92.6 kJ/mol reported by An et al. (1998), which might be caused by differences of M_w and molecular weight distribution.

Recently, the differential isoconversional method of Friedman and the advanced integral isoconversional method of Vyazovkin were found to be more appropriate than the Kissinger's method (Papageorgiou et al., 2005). In this study, the method of Friedman was used to validate the activation energy of the nonisothermal crystallization process.

The Friedman equation is expressed as follows:

$$\ln[dX_{t\text{-noniso}}/dt] = \text{constant} - \Delta E_{noniso\text{-Friedman}}/RT_p \quad \text{(eq. 3.14)}$$

where $dX_{t\text{-noniso}}/dt$ is the instantaneous crystallization rate as a function of time at a given conversion $X_{t\text{-noniso}}$. The $dX_{t\text{-noniso}}/dt$ was obtained by integrating the $X_{t\text{-noniso}}$ with respect to the time that needed to reach to a relative degree of crytallinity ($X_{t\text{-noniso}}$).

The Friedman plot of $\ln[dX_{t\text{-noniso}}/dt]$ vs. $1/T_p$ for PHB at different relative crystallinities ($X_{t\text{-noniso}}$ = 20, 40, 60, and 80%) is shown in Figure 9b. The $\Delta E_{noniso\text{-Friedman}}$ values determined from the straight lines ($R^2 = 0.99$) at selected $X_{t\text{-noniso}}$ are shown in Table III. It can be seen that $\Delta E_{noniso\text{-Friedman}}$ ranges from 96.1 to 100.8 kJ/mol. This is slightly lower than the activation energy obtained from Kinsinger's model.

Crystallization activation energy was a good indicator for the crystallization ability of polymers; hence the higher ΔE_{noniso} values reveal that it was more difficult for PHB to transport polymer chains segments to grow on the surfaces of previously formed crystals. However, apart from the higher activation energy obtained, the other kinetics parameters such as $t_{noniso\text{-}1/2}$ and Z_c clearly showed that the higher ϕ could enhance the PHB crystallization rate.

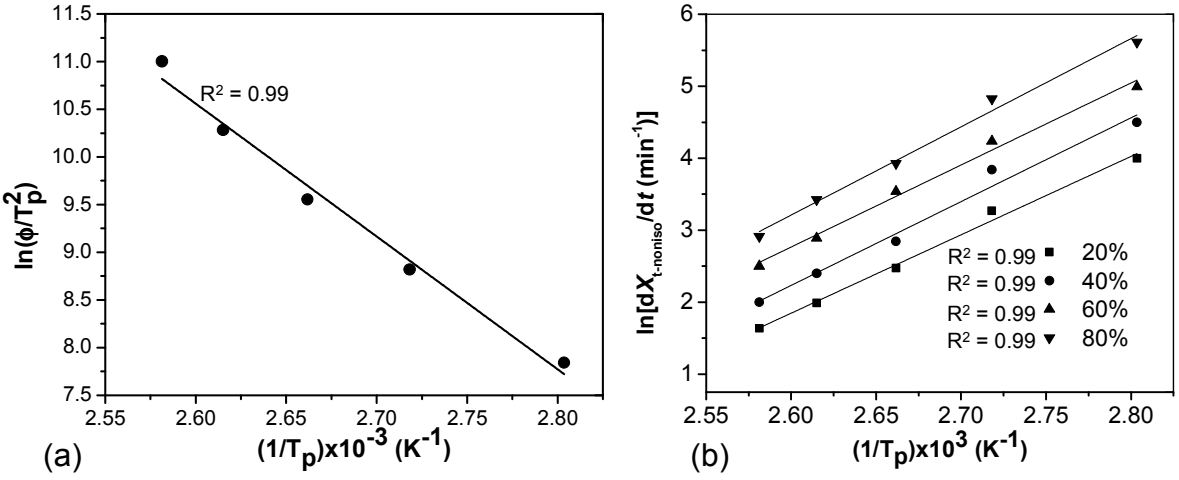

Figure 3.9. (a) Kissinger's ($\ln(\phi/T_p^2)$ vs. $1/T_p$) and (b) Friedman ($\ln(dX_{noniso}/dt$ vs. $1/T_p$) plot for nonisothermal crystallization of PHB.

3.4.4.3 Effect of cooling rate on the melting behavior

Semicrystalline polymers are usually processed nonisothermally from melt; hence it was important to investigate the subsequent melting behavior of PHB after it had finished nonisothermal crystallization at different ϕ. The DSC curves of the melting behavior of PHB are shown in Figure 3.10. After the nonisothermal crystallization process from melt at different ϕ, ranging from 2 to 50 °C/min, the conventional DSC heating scans were recorded

at Φ of 10 °C/min (Figure 3.10a). If the ϕ was set at 2 °C/min, only one broad melting peak was observed. Whereas by increasing the ϕ to 5 °C/min or higher, two endothermic peaks (labeled as T_{m1} and T_{m2} in the order of low to high temperature) started showing up and the higher endotherm (T_{m2}) was more clearly to be seen at higher ϕ (10 to 50 °C/min). The T_{m1} values shifted from 165.0 to 161.5 °C when ϕ was increased from 5 to 50 °C/min, while T_{m2} was not changed and located at 170 °C that is close to the T_{melt} obtained by TMA. The similar multiple melting behavior was also observed in other nonisothermally crystallized semicrystalline polymers from melt, such as PBSU and PES which was regarded as the evidence for the melting-recrystallization mechanism (Qiu et al., 2003b). The effect of ϕ on the degree of crystallinity ($X_{noniso\text{-melt}}$) of PHB was determined according to equation 6 from the melting enthalpies of the endothermic curves (Figure 10a). The $X_{noniso\text{-melt}}$ values were 54%, 56%, 58%, 60%, and 63%, respectively, when ϕ = 2, 5, 10, 20, and 50 °C/min. This confirmed that the higher ϕ results in more crystalline PHB, which agrees with the kinetic study by Liu and Mo's model.

Although the MRR was assumed to occur during DSC heating scans, the exothermic peak was hard to detect by conventional DSC due to superposition of the recrystallization and the melting endotherms (Qiu et al., 2003a). Therefore, TMDSC was employed to prove the melting-recrystallization behavior during the heating scan; meantime, the T_g (~ 5 °C) was obtained from the heating scans. Figure 3.10b shows an example of TMDSC melting scans of PHB following the nonisothermally crystallization at ϕ = 10 °C/min. The total heat flow (T) curve was separated into the non-reversing (Non-Rev) and reversing (Rev) curves. Unlike the conventional DSC traces shown in Figure 3.10a where no recrystallization exotherm was seen at a heating rate of 10 °C/min, one crystallization exotherm (Figure 10b, labeled as Exo) was observed by TMDSC between the two endothermic peaks in the Rev curve because the time was long enough for crystallites involved in low melting endotherm with low thermal stability to experience the melting and recrystallization at a heating rate of 2 °C/min. The higher endotherm was the dominant peak which was in accordance with conventional DSC and similar finding was observed in literature (Wellen et al., 2013). All these results confirmed the assumption that the multiple melting behavior observed in the nonisothermally crystallized PHB was ascribed to the MRR mechanism of crystallites of the

low melting endotherm with low thermal stability. This finding was in good agreement with studies on different polymers (Qiu et al., 2003b).

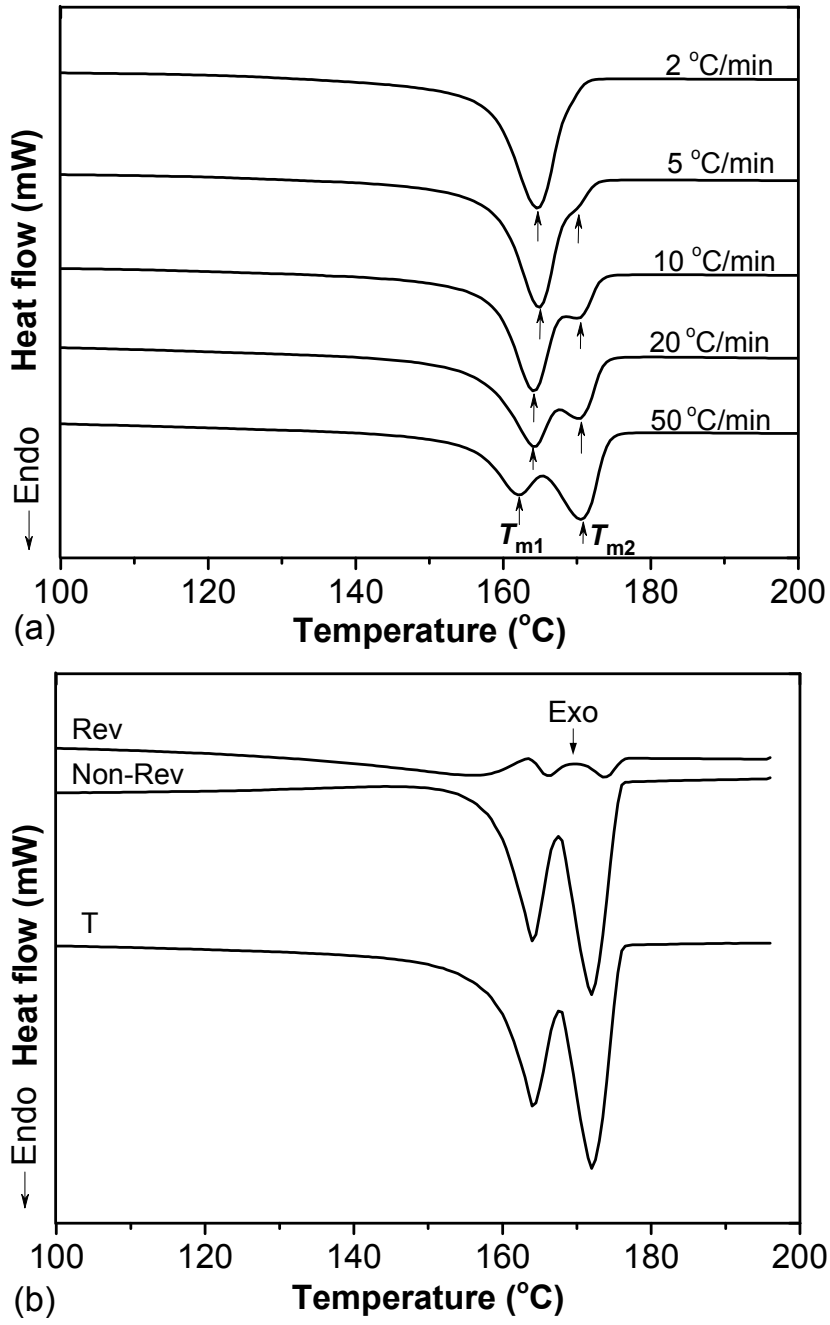

Figure 3.10. (a) Conventional DSC and (b) TMDSC curves of the melting behavior of PHB after nonisothermal (ϕ = 10 °C/min) crystallization.

3.4.5 Effects of heating rate on the melting behavior of PHB studied by DSC

From the literature, the MRR model is often used to explain the multiple melting behavior depending on the heating scan rates (Liu and Petermann, 2001; Qiu et al., 2003a). In this study, heating scans as function of different Φ were recorded after PHB samples were quenched to -50 °C, and then heated to 200 °C using conventional DSC (Figure 3.11a). It can be seen that two melting endotherms appear when Φ was <30 °C/min, and when the Φ was increased >40 °C/min, the two melting endotherms merged into one broad peak. The peak values of these two endotherms (labeled as T_{m1} and T_{m2} in the order of temperature from low to high) and their corresponding enthalpies associated were determined and plotted in Figure 3.11b. With an increase in Φ the T_{m1} shifted slightly from 164 to 164.5 °C, while T_{m2} was decreased slightly from 172 to 168 °C, and the magnitude of T_{m1} was increased as indicated by the increase of ΔH_{m1}. Whereas, ΔH_{m2} was shown to decrease significantly as Φ increased from 5 to 30 °C. At higher Φ, recrystallization was limited by less time available to align chains and form new crystals, consequently the amount and perfection of the reorganized crystals will be reduced, resulting in a slight decrease of T_{m2} (Liu and Petermann, 2001). This further confirms the assumption that the MRR model can explain the multiple/double melting behavior of PHB.

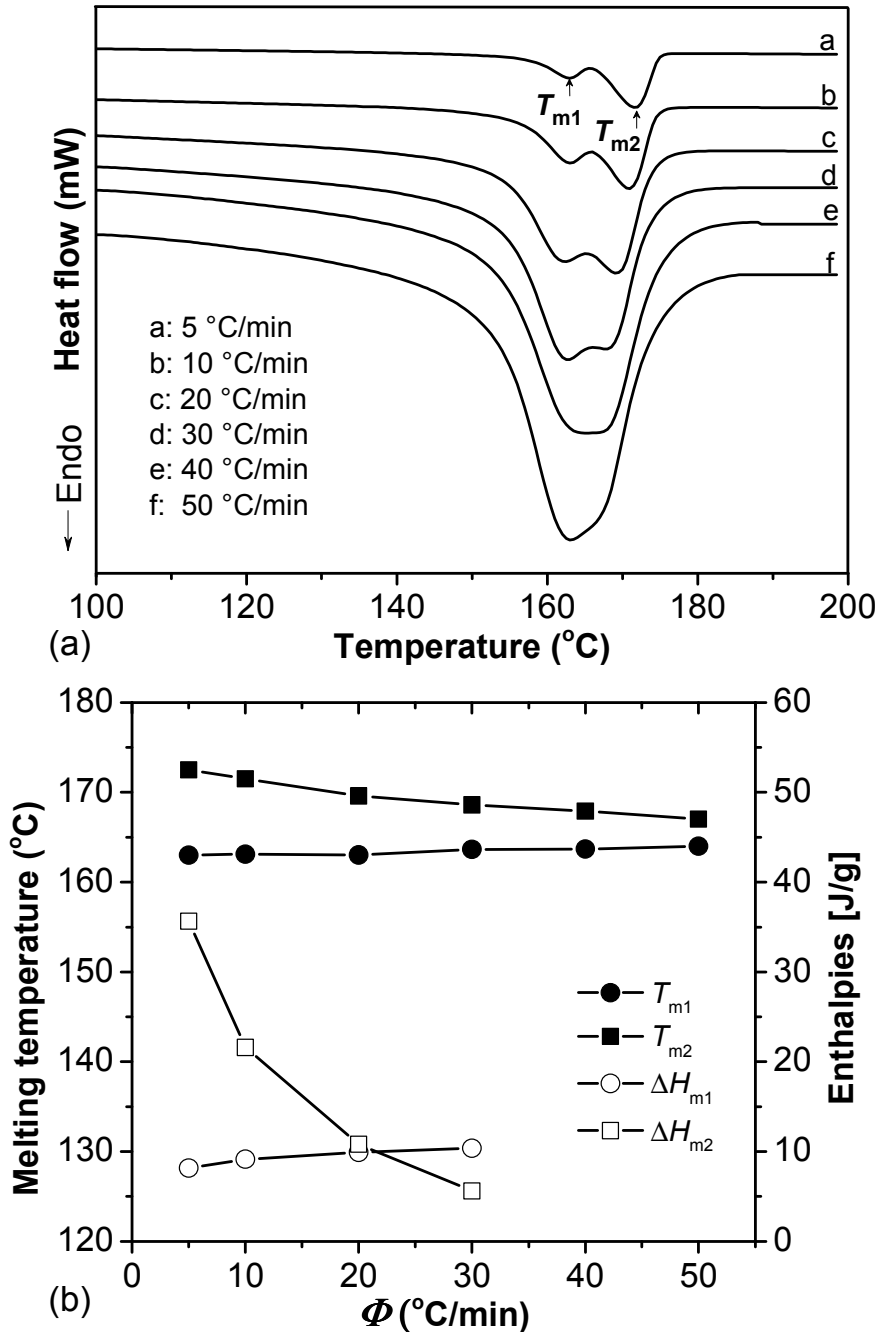

Figure 3.11. (a) DSC heating scans and (b) melting temperatures (T_{m1} and T_{m2}) and their corresponding enthalpies (ΔH_{m1} and ΔH_{m2}) for PHB performed at different heating rates (Φ).

3.5 Conclusions

The annealing-temperature-dependent multiple melting and recrystallization behavior of PHB was studied by conventional DSC and TMDSC. It was found that PHB showed multiple melting peaks, annealing peak (T_{ap}) and two melting peaks (T_{m1} and T_{m2}), after being annealed at different temperatures (T_a) and same time. The T_{m1} was not influenced by T_a, but the T_{m2} was associated with T_a. The degree of crystallinity (χ_c%) was shown to depend on annealing temperature. When T_a was <100 °C and >120 °C the χ_c% decreased with increasing T_a, but only showed a slight change when 100 °C < T_a <120 °C. It could be expected that lower annealing temperature will result in higher crystallinity end products and more amorphous PHB will be obtained if higher annealing temperature will be applied in the PHB manufacturing procedure. The higher isothermal annealing temperature will inhibit the recrystallization behavior, resulting in a single melting endotherm. It was concluded that T_a = 100 °C was a suitable isothermal T_a for PHB. Wider isothermal temperature range (T_{iso} = 80 to 140 °C) was selected to investigate the isothermal crystallization kinetics of PHB. Nonisothermal crystallization studies showed dual melting peaks at high cooling rates (ϕ) ~10 °C/min. The Jeziorny-modified-Avrami method and Liu-Mo's analysis were successful in describing the nonisothermal crystallization kinetics of PHB, while the Ozawa model was not. The multiple melting behaviors were also heating-rate-dependent and at a high heating rate (Φ, 40 °C/min) the multiple melting peaks merged into one. The higher endothermic peak (T_{m2}) was not affected by ϕ and T_{m2} decreased slightly with increasing Φ. T_{m1} was considered to be related to the original crystals before analysis while the T_{m2} was ascribed to the recrystallization of crystals with lower thermal stability showing an endotherm at T_{m1}. In brief, the higher melting peak induced by either isothermally or nonisothermally was mainly ascribed to melting-recrystallization-remelting mechanism (MRR) during DSC heating scans, and the TMDSC technique allows the observation of the recrystallization present in the heating process more clearly. The activation energies were estimated in isothermal and nonisothermal crystallization process to be 102 and 116 kJ/mol, respectively. This study has provided insight into the thermal history and property (especially the crystallinity involved in the isothermal/nonisothermal process)

relationship, giving theoretical guidance to the PHB industrial processing (e.g., injection molding and extrusion) and product applications.

3.6 References

An, Y., Dong, L., Li, L., Mo, Z., Feng, Z., 1999. Isothermal crystallization kinetics and melting behavior of poly(β-hydroxybutyrate)/poly(vinyl acetate) blends. European Polymer Journal 35, 365-369.

An, Y., Dong, L., Mo, Z., Liu, T., Feng, Z., 1998. Nonisothermal Crystallization Kinetics of Poly(β-hydroxybutyrate). Journal of Polymer Science Part B: Polymer Physics 36, 1305-1312.

Branciforti, M.C., Corrêa, M.C.S., Pollet, E., Agnelli, J.A.M., Nascente, P.A.d.P., Avérous, L., 2013. Crystallinity study of nano-biocomposites based on plasticized poly(hydroxybutyrate-co-hydroxyvalerate) with organo-modified montmorillonite. Polymer Testing 32, 1253-1260.

Bruno Rocha e Silva, M., Tavares, M.I.B., Oliveira da Silva, E., Neto, R.P.C., 2013. Dynamic and structural evaluation of poly(3-hydroxybutyrate) layered nanocomposites. Polymer Testing 32, 165-174.

Deshmukh, G.S., Peshwe, D.R., Pathak, S.U., Ekhe, J.D., 2014. Nonisothermal crystallization kinetics and melting behavior of poly(butylene terephthalate) (PBT) composites based on different types of functional fillers. Thermochimica Acta 581, 41-53.

Di Lorenzo, M.L., Righetti, M.C., 2013. Evolution of crystal and amorphous fractions of poly[(R)-3-hydroxybutyrate] upon storage. Journal of Thermal Analysis and Calorimetry 112, 1439-1446.

Di Lorenzo, M.L., Silvestre, C., 1999. Non-isothermal crystallization of polymers. Progress in Polymer Science 24, 917-950.

El-Hadi, A., Schnabel, R., Straube, E., Müller, G., Riemschneider, M., 2002. Effect of melt processing on crystallization behavior and rheology of PHB and its blends. Macromolecular Materials and Engineering 287, 363-372.

Galego, N., Rozsa, C., Sánchez, R., Fung, J., Vázquez, A., Santo Tomas, J., 2000. Characterization and application of poly(β-hydroxyalkanoates) family as composite biomaterials. Polymer Testing 19, 485-492.

Gunaratne, L.M.W.K., Shanks, R.A., 2005. Multiple melting behaviour of poly(3-hydroxybutyrate-co-hydroxyvalerate) using step-scan DSC. European Polymer Journal 41, 2980-2988.

Gunaratne, L.M.W.K., Shanks, R.A., 2006a. Isothermal crystallisation kinetics of poly(3-hydroxybutyrate) using step-scan DSC. Journal of Thermal Analysis and Calorimetry 83, 313-319.

Gunaratne, L.M.W.K., Shanks, R.A., 2006b. Thermal memory of Poly(3-hydroxybutyrate) using temperature-modulated differential scanning calorimetry. Journal of Polymer Science Part B: Polymer Physics 44, 70-78.

Gunning, M.A., Geever, L.M., Killion, J.A., Lyons, J.G., Chen, B., Higginbotham, C.L., 2014. The effect of the mixing routes of biodegradable polylactic acid and polyhydroxybutyrate nanocomposites and compatibilised nanocomposites. Journal of Thermoplastic Composite Materials.

Hoffman, J.D., 1982. Role of reptation in the rate of crystallization of polyethylene fractions from the melt. Polymer 23, 656-670.

Hsu, S.-F., Wu, T.-M., Liao, C.-S., 2007. Nonisothermal crystallization behavior and crystalline structure of poly(3-hydroxybutyrate)/layered double hydroxide nanocomposites. Journal of Polymer Science Part B: Polymer Physics 45, 995-1002.

Hu, S., McDonald, A.G., Coats, E.R., 2013. Characterization of polyhydroxybutyrate biosynthesized from crude glycerol waste using mixed microbial consortia. Journal of Applied Polymer Science 129, 1314-1321.

Hu, Y., Zhang, J., Sato, H., Futami, Y., Noda, I., Ozaki, Y., 2006. C-H-O=C Hydrogen Bonding and Isothermal Crystallization Kinetics of Poly(3-hydroxybutyrate) Investigated by Near-Infrared Spectroscopy. Macromolecules 39, 3841-3847.

Kampert, W.G., Sauer, B.B., 2001. Temperature Modulated DSC Studies of Melting and Recrystallization in Poly(oxy-l,4-phenyleneoxy-l,4-phenylenecarbonyl-I ,4-phenylene) (PEEK). Polymer Engineering and Science 41, 1714-1730.

Khanna, S., Srivastava, A.K., 2005. Recent advances in microbial polyhydroxyalkanoates. Process Biochemistry 40, 607-619.

Kim, J.Y., Park, H.S., Kim, S.H., 2006. Unique nucleation of multi-walled carbon nanotube and poly(ethylene 2,6-naphthalate) nanocomposites during non-isothermal crystallization. Polymer 47, 1379-1389.

Kong, Y., Hay, J.N., 2003. Multiple melting behaviour of poly(ethylene terephthalate). Polymer 44, 623-633.

Li, Y., Han, C., Zhang, X., Dong, Q., Dong, L., 2013. Effects of molten poly(d,l-lactide) on nonisothermal crystallization in stereocomplex of poly(l-lactide) with poly(d-lactide). Thermochimica Acta 573, 193-199.

Liu, Q., Deng, B., Tung, C.-H., Zhu, M., Shyr, T.-W., 2010. Nonisothermal crystallization kinetics of poly(ε-caprolactone) blocks in double crystalline triblock copolymers containing poly(3-hydroxybutyrate-co-3-hydroxyvalerate) and poly(ε-caprolactone) units. Journal of Polymer Science Part B: Polymer Physics 48, 2288-2295.

Liu, T., Mo, Z., Wang, S., Zhang, H., 1997. Nonisothermal Melt and Cold Crystallization Kinetics of Poly(Aryl Ether Ether Ketone Ketone). Polymer Engineering and Science 37, 568-575.

Liu, T., Petermann, J., 2001. Multiple melting behavior in isothermally cold crystallized isotactic polystyrene. Polymer 42, 6453-6461.

Long, Y., Shanks, R.A., Stachurski, Z.H., 1995. Kinetics of polymer crystallisation. Progress in Polymer Science 20, 651-701.

Madison, L., Huisman, G.W., 1999. Metabolic Engineering of Poly(3-Hydroxyalkanoates): from DNA to Plastic. Microbiology and Molecular Biology Reviews 63, 21-53.

Montserrat, S., Roman, F., Colomer, P., 2003. Study of The Crystallization and Melting Region of PET and PEN and Their Blends by TMDSC. Journal of Thermal Analysis and Calorimetry 72, 657-666.

Pogodina, N.V., Winter, H.H., 1998. Polypropylene Crystallization as a Physical Gelation Process. Macromolecules 31, 8164-8172.

Qiu, Z., Ikehara, T., Nishi, T., 2003a. Melting behaviour of poly(butylene succinate) in miscible blends with poly(ethylene oxide). Polymer 44, 3095-3099.

Qiu, Z., Komura, M., Ikehara, T., Nishi, T., 2003b. DSC and TMDSC study of melting behaviour of poly(butylene succinate) and poly(ethylene succinate). Polymer 44, 7781-7785.

Rizk, S., Connelly, D.W., Bernasconi, M., Carter, A.J., Martin, D.P., Williams, S.F., 2013. Injection Molding of Poly-4-Hydroxybutyrate, U.S. Patent 20130309166 A1, USA.

Vyazovkin, S., Sbirrazzuoli, N., 2004. Isoconversional Approach to Evaluating the Hoffman–Lauritzen Parameters(U* and K_g) from the Overall Rates of Nonisothermal Crystallization. Macromolecular Rapid Communications 25, 733-738.

Wei, L., Guho, N.M., Coats, E.R., McDonald, A.G., 2014. Characterization of poly(3-hydroxybutyrate-co−3-hydroxyvalerate) biosynthesized by mixed microbial consortia fed fermented dairy manure. Journal of Applied Polymer Science 131.

Wellen, R.M.R., Rabello, M.S., Fechine, G.J.M., Canedo, E.L., 2013. The melting behaviour of poly(3-hydroxybutyrate) by DSC. Reproducibility study. Polymer Testing 32, 215-220.

Yuan, Q., Awate, S., Misra, R.D.K., 2006. Nonisothermal crystallization behavior of polypropylene–clay nanocomposites. European Polymer Journal 42, 1994-2003.

Ziaee, Z., Supaphol, P., 2006. Non-isothermal melt- and cold-crystallization kinetics of poly(3-hydroxybutyrate). Polymer Testing 25, 807-818.

Chapter 4. Peroxide induced cross-linking by reactive melt processing of two biopolyesters: poly(3-hydroxybutyrate) and poly(L-lactic Acid) to improve their melting processability

4.1 Abstract

Poly(3-hydroxybutyrate) (PHB) and poly(L-lactic acid) (PLLA) were individually cross-linked with dicumyl peroxide (DCP) (0.25 to 1 wt%) by reactive melt processing. The cross-linked structures of the polymer gel were investigated by nuclear magnetic resonance (NMR) and Fourier transform infrared (FTIR) spectroscopies. The size of the polymer crystal spherulites, glass transition temperature (T_g), melting transition temperature (T_m) and crystallinity were all decreased as a result of cross-linking. Cross-linking density (ν_e) was shown to increase with DCP concentration. Based on parallel plate rheological study (dynamic and steady shear), elastic and viscous modulus (G'' and G'), complex viscosity (η^*) and steady shear viscosity (η) were all shown to increase with cross-linking. Cross-linked PHB and PLLA showed broader molar mass distribution and formation of long chain branching (LCB) as estimated by RheoMWD. Improvements in melt strength offer bioplastic processors improved material properties and processing options, such as foaming and thermoforming, for new applications.

4.2 Introduction

Recently, biodegradable and renewably derived polymers have attracted much attention due to the environmental awareness and sustainability issues associated with petroleum-based polymers (Rasal et al., 2010). Aliphatic polyesters such as poly($_{D,L}$-lactic acid) (PLA) and bacterial poly(3-hydroxyalkanoates) (PHAs) including poly(3-hydroxybutyrate) (PHB) and its copolymer [poly(3-hydroxybutyrate-co-3-hydroxyvalerate (PHBV)] are gaining interest due to their renewability, biocompatibility and biodegradability (Groot et al., 2010; Yu et al., 2006). Rather, PLA and PHB are linear polymers, lacking in branches which contributes to their poor melt elasticity as evidenced by low die swell and “neck in”, low thermodegradation temperature, and high crystallinity (Lunt, 1998; Yamaguchi and Arakawa, 2006). These features, especially the low melt elasticity, limit their processability

in cast film extrusion, foaming, blown-film manufacture, thermoforming, and fiber spinning, etc. (Lunt, 1998; Rasal et al., 2010). Long chain branching (LCB) and polymer chain entanglement in PHB and PLAs can improve their processability (D'Haene et al., 1999). Various methods have been used to introduce cross-links into linear polymer such as copolymerization/blend with other biodegradable polymer blocks (Roa et al., 2013; Wang et al., 2008), radiation induced cross-linking, and peroxide induced cross-linking (D'Haene et al., 1999; Dean et al., 2012; Nijenhuis et al., 1996; Ryan et al., 1997; Sijdergard et al., 1995; Takamura et al., 2010). Some of these methods have improved the polymer foaming ability and blown film processability (Jandas et al., 2013; Yu et al., 2013), and the resultant products modified by some of these methods are still biodegradable (Fei et al., 2004; Jandas et al., 2013).

Practical cross-linking involves the use of peroxides, which, when used at very low levels, can result in significant increases in melt elasticity. Furthermore, cross-linking, can alter their physical properties such as the crystallinity and transition temperatures (Rasal et al., 2010). Studies on dicumyl peroxide (DCP) induced cross-linking in carbon black polyethylene and poly(ε-caprolactone) were dependent on reaction temperature, peroxide concentration, and extrusion residence time (Nijenhuis et al., 1996). Recently the effect of type and amount of peroxide with high-, moderate- and low-decomposition rate on cross-linking of PLLA during extrusion was investigated (Takamura et al., 2008). For the slowly decomposed peroxide, e.g. DCP, the lifetime is relatively close to the residence time of extrusion. DCP has relatively high H abstraction ability, which makes it ideal as a cross-linking agent for plastics. When DCP is exposed to high temperature, it will decompose into cumyloxy radicals, of which 60% formed methyl radicals and acetophenone by β-scission (Takamura et al., 2008). These free radicals are capable of abstracting H atoms from any tertiary –CH along the PLLA or PHB backbone. The corresponding H abstraction mechanism of PHB and PLLA resulting in cross-linking and chain extension are simplified in Figure 4.1. This cross-linking may be expected to occur primarily in the amorphous regions. Melt and rheological properties of the rapidly decomposed lauroyl peroxide and dibenzoyl peroxide cross-linked PLLA were studied (Dean et al., 2012). The reductions in crystallinity and improved melt strength of cross-linked PLLA were suitable to be used in

conventional melt processing operations including film and foam formation. A PHBV cross-linking study indicated that extensive branching occurred at a DCP concentration above 0.2 wt% (D'Haene et al., 1999). The thermophysical properties such as crystallinity, melting behavior and tensile properties of high-density polyethylene (HDPE) were shown to be influenced by di-tert butyl cumyl peroxide (BCUP) induced cross-linking (Khonakdar et al., 2003). The generally accepted process of peroxide induced cross-linking of polymers follows three key steps: (i) the primary radical formation from the thermal decomposition of peroxide, (ii) H abstraction from polymer backbone by free radicals of peroxide generated in step (i), and (iii) the bimolecular radical recombination of polymer radicals from step (ii) to generate C-C cross-links (Figure 4.1) (Takamura et al., 2010). Whereas, there is limited information on the chemical position(s) associated with cross-linked molecular chains to form a gel network structure. Moreover, the documentation on the melt rheological properties of PLA and PHAs, especially for peroxide cross-linked PHAs, is limited and therefore instigated this study.

The aims of this study were to cross-link two commercial biopolyesters (PHB and PLLA) by reactive melt processing with DCP, to improve their melt properties and to understand the cross-linking reaction. The cross-linking site of the PLLA and PHB was investigated by ^{13}C NMR spectroscopy. The thermal, viscoelastic, rheological and morphological properties were evaluated by FTIR spectroscopy, DSC, DMA, HS-POM, dynamic rheometry and TGA. To the authors' knowledge, a limited number of reports have used RheoMWD to estimate the molar mass distribution of polymers. This study would provide a profound insight into the structure-property (especially the rheological properties) relationship, induced by cross-linking to improve the industrial processability of PHB and PLLA, broadening the potential applications for these biopolymers.

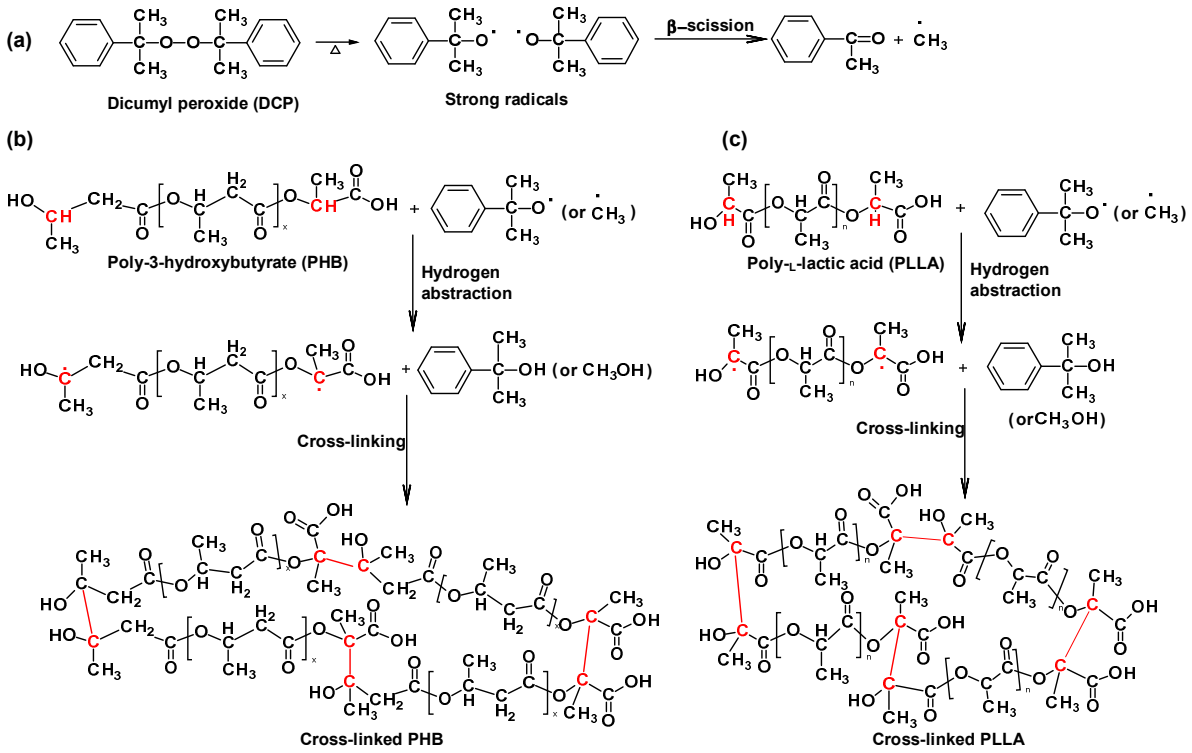

Figure 4.1. Schematic illustration of DCP induced cross-linking: (a) thermal decomposition of DCP into primary radicals when exposed to heat and then hydrogen abstraction from polymer chains by primary radicals and bimolecular recombination of polymer radicals of PHB (b) and PLLA (c).

4.3 Experimental

4.3.1 Materials

Dicumyl peroxide (DCP) (98%) was purchased from Sigma-Aldrich Co. LLC (USA). PHB powder was from Tianan Biopolymer Inc. (China) and poly(L-lactic acid) (PLLA) was supplied by Purac Biochem Inc. (The Netherlands). The weight average molar mass (M_w) and polydispersity (PD) of PHB and PLLA were determined by size exclusion chromatography (SEC) (PHB: M_w = 290,000 g/mol, PD_{SEC} = 2.3; PLLA: M_w = 121,000 g/mol, PD_{SEC} = 1.41). SEC separation was performed using a mixed bed Jordi DVB column on elution with $CHCl_3$ (1 mL/min) with triple detection system [refractive index (Waters model 2414), low-and right-angle laser light scattering and differential viscometer (Viscotek model 270, Viscotek Corporation)].

4.3.2 Cross-linking via reactive melt processing

PHB and PLLA were dried under vacuum for at least one week prior to use. Dried PHB powder or PLLA granules (2 g) were placed in a Dynisco laboratory mixing extruder/molder operating at 175 °C for PHB and 190 °C for PLLA and melt was mixed (100 revolutions/min) for 5 min, to which DCP (0, 0.25, 0.5, 1 wt%) was added and mixed for a defined reaction time. All samples were then either injected into a mold (discs or rectangular bars: PHB samples were coded PHB_0, $PHB_{0.25}$, $PHB_{0.5}$ and PHB_1; PLLA samples were coded $PLLA_0$, $PLLA_{0.25}$, $PLLA_{0.5}$ and $PLLA_1$) or extruded into a strand (1 mm Ø).

4.3.3 Gel fraction and degree of swelling in solvent

Cross-linked polymer networks were not readily soluble in an organic solvent but swelled into a gel. The gel fraction was determined on extruded strands that were refluxed in $CHCl_3$ for 48 h in order to remove the soluble "sol" fraction by filtration (nylon mesh, 27 μm). The un-dissolved gels induced by 0.25, 0.5 and 1.0 wt% DCP of PHB and PLLA were respectively coded as $PHB_{0.25gel}$, $PHB_{0.5gel}$ and PHB_{1gel}, and $PLLA_{0.25gel}$, $PLLA_{0.5gel}$ and $PLLA_{1gel}$. The cross-linked gel fractions were collected and vacuum dried for 48 h and yields were calculated gravimetrically as follows:

$$\text{Gel fraction (\%)} = (W_{gel}/W_0) \times 100 \qquad \text{(eq. 4.1)}$$

where W_0 is the dry weight of the cross-linked polymer, W_{gel} is the weight of dry gel fraction.

Swelling experiments of dry gels (50 mg) were performed in $CHCl_3$ (50 mL) at room temperature (21 °C) for 48 h. The degree of swelling (DS, cm^3/cm^3) was calculated by:

$$DS = [(W_s - W_{gel})/W_{gel}] \times (\rho_{ap}/\rho_{chloroform}) \qquad \text{(eq. 4.2)}$$

where W_{gel} is the weight of dry gel in the cross-linked polymer sample, W_s is the weight of swollen gel sample (W_s), while ρ_{ap} and $\rho_{chloroform}$ are densities of amorphous polymers (1.248 g/cm^3 for PLA; 1.179 g/cm^3 for PHB) (De Koning and Lemstra, 1993; Nijenhuis et al., 1996) and $CHCl_3$ (1.48 g/cm^3), respectively.

4.3.4 NMR spectroscopy

Cross-linked $PHB_{0.25gel}$ and $PLLA_{0.25gel}$ gels were partially depolymerized by methanolysis (3% H_2SO_4 in CH_3OH (3 mL) + $CHCl_3$ (1 mL) at 100 ˚C for 8 h) without cleaving the C-C cross-links. The resulting methyl esters were soluble in $CDCl_3$ for NMR analysis. Standard ^{13}C and DEPT-135 (distortionless-enhancement-by-polarization-transfer) NMR spectra were obtained on a Bruker Avance 500 spectrometer.

4.3.5 FTIR spectroscopy

Vacuum dried PHB_0, $PLLA_0$, $PHB_{0.25\text{-}1gel}$ and $PLLA_{0.25\text{-}1gel}$ samples were characterized by FTIR spectroscopy (Avatar 370 FTIR spectrometer, ThermoNicolet) using a ZnSe attenuated total reflection (ATR) probe. Absorbance spectra (in triplicate) were averaged and ATR and baseline corrected using Omnic v9.0 software (Thermo scientific).

For the quantitative analysis, the spectra were normalized and curve-fitted using Igor Prof 6.03 software (WaveMetrics, Inc) (Wei et al., 2013). The area (A) of each band found by curve fitting was integrated by the software. The carbonyl index ($I_{C=O}$) was calculated as the ratio of the areas (A) under carbonyl (C=O) bands at 1720 to 1740 cm^{-1} of PHB:

$$I_{C=O} = A_{1720}/A_{1740} \qquad \text{(eq. 4.3)},$$

while the –CH stretching index ($I_{C\text{-}H}$) was determined by the ratio of areas of –CH (~2882 cm^{-1}) to $–CH_3$ (asym, ~2946 cm^{-1}) bands of PLLA:

$$I_{C\text{-}H} = A_{2882}/A_{2946} \qquad \text{(eq. 4.4)}$$

4.3.6 Differential scanning calorimetry

Temperature modulated DSC (TMDSC) measurements were conducted on PHB_0, $PLLA_0$, $PHB_{0.25\text{-}1gel}$ and $PLLA_{0.25\text{-}1gel}$ samples using a TA Instruments model Q200 DSC with refrigerated cooling. All samples were first rapidly heated to 200 ˚C (100 ˚C/min) to remove thermal history followed by a cooling scan (-20 ˚C/min) to -50 ˚C. Then TMDSC measurements were obtained for heating scans from -50 to 200 ˚C, at an average heating rate of 2 ˚C/min with a period of 60s and modulation amplitudes of ±0.6 ˚C. The data were

analyzed using TA Universal Analysis v4.4A software. The cold crystallization temperature (T_c) was determined from the cooling scan curve. From the heat capacity data curve, T_g, T_m and enthalpy of fusion (ΔH_m) were determined. The degree of crystallinity (X_c %) of PHB and PLLA were calculated based on eq. 4.5 (Solarski et al., 2005):

$$X_c\ \% = (\Delta H_m - \Delta H_{crys+recrys})/\Delta H_0 \times 100 \qquad \text{(eq. 4.5)}$$

where ΔH_m is the melting enthalpy (reversing curve), the $\Delta H_{crys+recrys}$ is the sum of exotherms of crystallization (reversing) and recrystallization (non-reversing), and ΔH_0 is melting enthalpy in J/g of 100% crystalline PHB (146 J/g) and PLLA (93.6 J/g) (Solarski et al., 2005; Wei et al., 2014). The heat flow data from the TMDSC scans were used to calculate the variation of specific heat capacity (ΔC_p, J/g/˚C) close to the glass state at which T_g was determined.

4.3.7 Hot stage-polarized optical microscopy (HS-POM)

PHB_0 and $PLLA_0$ films (cast from $CHCl_3$ solution ~ 1 mg/mL) and the cross-linked $PHB_{0.25\text{-}1gel}$ and $PLLA_{0.25\text{-}1gel}$ films were prepared by hot pressing at 180 ˚C. Films were used for morphological studies on isothermally formed crystals using an Olympus BX51 microscope [10x objective, polarized light filters and digital camera (Olympus DP70)] equipped with a Mettler Toledo FP900 Thermosystem (FP90 central processor and FP84 hot stage). Samples were first heated at 20 ˚C/min to 190 ˚C, held for 2 min, then cooled at -20 ˚C/min to the desired temperature (90 ˚C), and held isothermally for 1 h (Hu et al., 2013). All images were processed using the Olympus MicroSuite (TM)-SE 3.2 software.

4.3.8 Thermogravimetric analysis (TGA)

Thermal stability of PHB_0, $PLLA_0$, $PHB_{0.25\text{-}1gel}$ and $PLLA_{0.25\text{-}1gel}$ samples (3-5 mg) were characterized using a Perkin Elmer TGA 7 instrument (50-900 ˚C at 20 ˚C/min under N_2 flow) and data were analyzed using Pyris v8 software.

4.3.9 Dynamic mechanical analysis (DMA)

The flexural properties of molded bars (60 mm x 4 mm x 2 mm) for PHB_{0-1} and $PLLA_{0-1}$ samples were dried under vacuum for 24 h and then conditioned (25 ˚C, 50% relative humidity) for 7 days. DMA was carried out using a DMA model Q800 instrument (TA instrument) to determine the viscoelastic properties in 3-point bending mode (50 mm span) from -50 to 150 ˚C at 3 ˚C/min, 0.5% strain, and 1 Hz.

4.3.10 Parallel plate rheometry

Steady shear (η) and dynamic measurements (G', G'' and η^*) were determined using a Bohlin Instuments CVO 100 rheometer, parallel plate (25 mm Ø), in oscillating shear mode with an ETC module on molded discs (2 mm x 25 mm Ø) samples (PHB_{0-1} and $PLLA_{0-1}$). Experiments were performed in the linear viscoelastic region. For PHB measurements these were carried out at 170, 175 and 180 ˚C, while for PLLA these were performed at 180, 190 and 200 ˚C. Steady shear measurements were undertaken at shear rates (γ) from 0.1 to 100 s^{-1}, while dynamic measurements were conducted in the frequency range of 0.1 to 100 rad/s at an applied strain of 0.5%. Data was analyzed using the Bohlin rheology v6.51 software.

An estimation of molecular PD was determined by RheoMWD 1.5 software (Polydynamics Inc., Canada) using a viscosity function method from dynamic rheology data (G' and G'' as function of frequency). Four PD measures were recorded: the crossover point index (CPI), global distribution index (GDI), high elasticity index (HEI) and Dow rheology index (DRI). In this analysis, the temperature dependence factor (TDF) for same material was required. Step one is to calculate PD measures for all materials using the same value of the TDF at 3 different temperatures (listed above). If the calculated PD measures were almost the same as the correct TDF value then TDF will be changed and PD measures recalculated until the calculated PD measures are the same. The viscosity function method uses the steady shear viscosity data [viscosity (η) vs. shear rate at a single temperature] to estimate the PD ($=M_w/M_n$) as a molar mass distribution indicator.

4.4 Results and discussion

4.4.1 PLLA and PHB cross-linking via reactive melt processing with dicumyl peroxide

Cross-linked PHB and PLLA materials form covalently tied networks, are insoluble gels, and are only swollen in contact with solvents (Figure 4.2a) (Liu et al., 2012). Factors that influence cross-linking in the gel fraction are reaction time and DCP concentration. Experiments showed that the gel fraction increased with reaction time up to 8 min for PHB and 10 min for PLLA. However, when reaction time was extended, the gel fraction decreased. The gel fraction for PHB increased from 4 to 58%, while for PLLA increased from 5 to 59% when DCP concentration increased from 0.25 to 1 wt% (Figure 4.2b). The DS is a good indicator of cross-linking density of polymers. The DS of both PHB and PLLA decreased with DCP concentration (Figure 4.2b). These results support that cross-linking occurred and the extent of cross-linking was DCP concentration dependent.

At 175 ˚C for PHB and 190 ˚C for PLLA chain scission will accompany cross-linking reactions and at long reactions times the gel fraction will decrease. The efficiency of cross-linking can be determined from the Charlesby-Pinner equation (eq. 4.6), when there are both cross-linking and chain scissioning present, as follows (Takamura et al., 2008):

$$S + S^{0.5} = p_0/q_0 + (2M_n[I])^{-1} (E_c)^{-1} \qquad \text{(eq. 4.6)}$$

where S is the soluble fraction, p_0 and q_0 are the fractions of the repeat units of polymer undergoing scissioning and cross-linking, respectively, M_n is the number-average molar mass of the polymer before cross-linking, $[I]$ is the decomposed peroxide in mol/g polymer, $(2M_n[I])^{-1}$ is the mole ratio of radicals to polymer chains in our work, and E_c is the cross-linking efficiency. The Charlesby-Pinner plot of $S + S^{0.5}$ against $(2M_n[I])^{-1}$ for different levels of DCP are shown in Figure 4.3. The intercept of $S + S^{0.5}$ axis gives the ratio of the chain scissioning and cross-linking, p_0/q_0, which are 0.48 for PHB and 0.36 for PLLA, indicating chain scissioning occurs under their corresponding processing temperatures. It was possible that some chain scissioning was attributed to thermal instability of the linear polymer (El-Hadi et al., 2002). The E_c is given by 1/slope which was calculated at 7.88 for

PHB and 2.28 for PLLA. These data suggest that a higher DCP concentration is required for PLLA than PHB if a comparable cross-linking density is to be obtained.

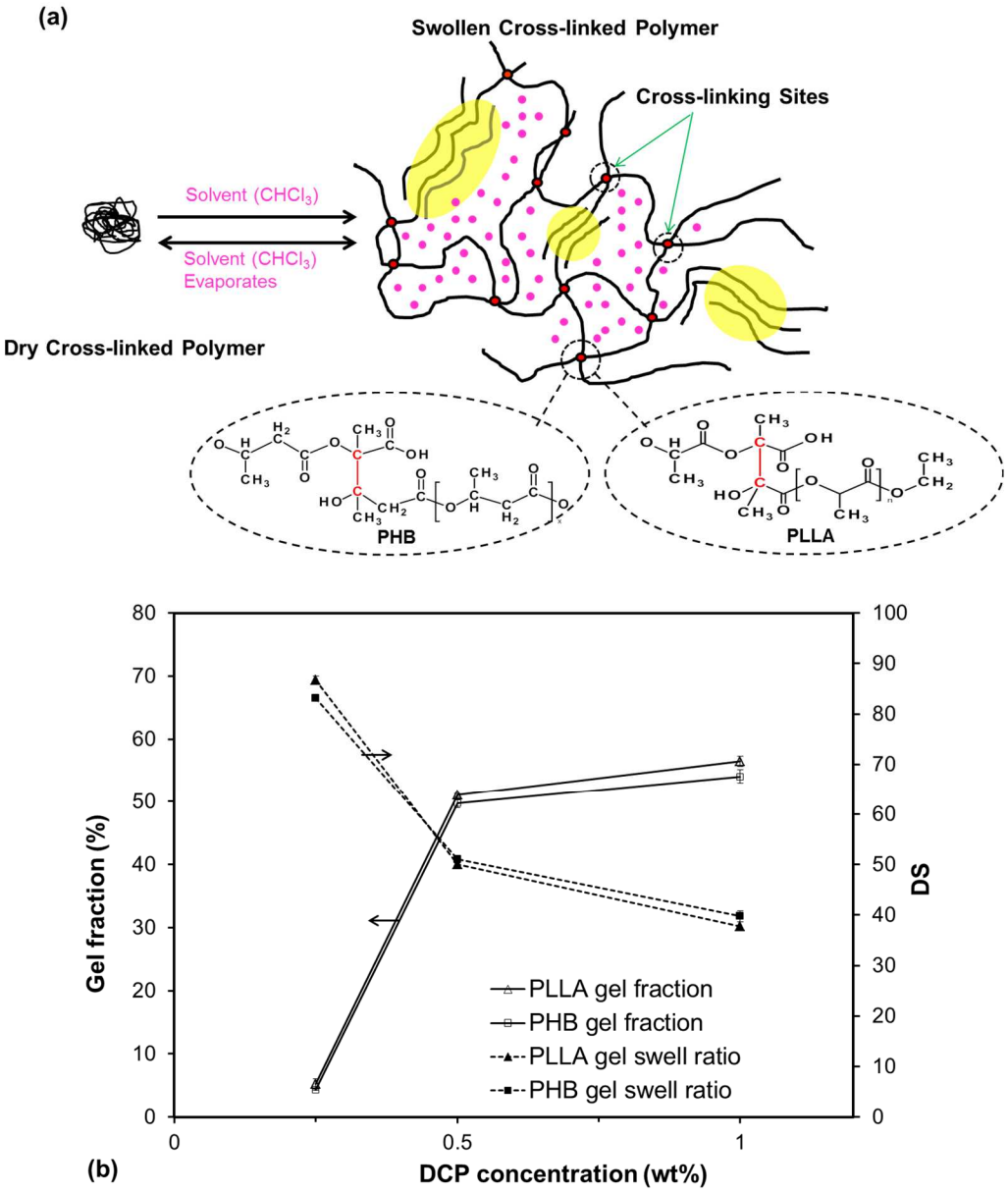

Figure 4.2. (a) A model of cross-linked polymer gels swelling in solvent (note: polymer chains (black) comprising crystalline (yellow shadow) and amorphous domains cross-linked at sites (red) allow the cross-linked network to expand in contact with the solvent (e. g. $CHCl_3$) and will be incorporated with solvent molecules (pink); (b) Gel fraction (%) and DS of cross-linked $PHB_{0.25\text{-}1}$ (8 min) and $PLLA_{0.25\text{-}1}$ (10 min) extruded strands as function of DCP concentration (0.25, 0.5 and 1wt%). (Note: the results were averaged from 3 replicates with standard error showed as error bars).

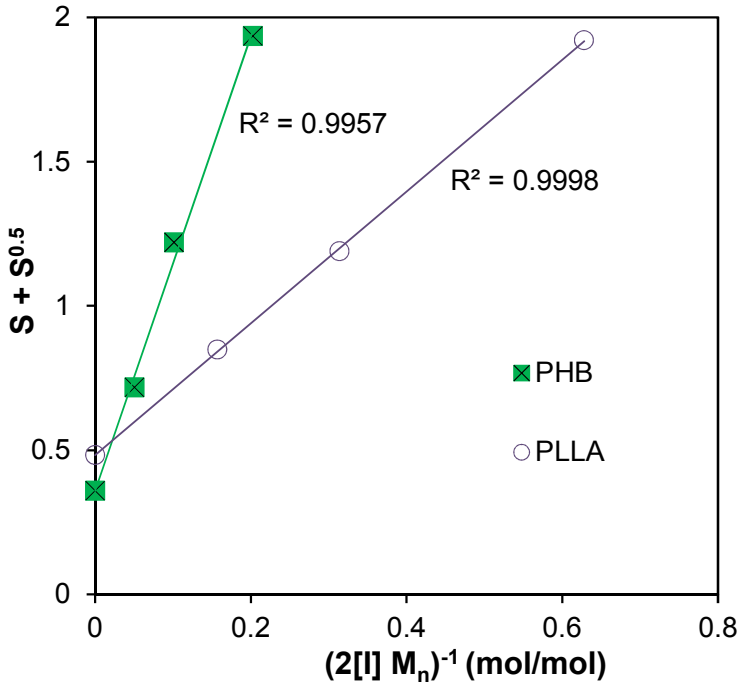

Figure 4.3. (a) Charlesby-Pinner plot of the cross-linking of PHB at 175 ˚C for 8 min and PLLA at 190 ˚C for 10 min with DCP concentration.

4.4.2 Characterization by NMR

The cross-linking sites for PHB and PLLA were investigated by ^{13}C NMR experiments on the methanolyzed $PHB_{0.25gel}$ and $PLLA_{0.25gel}$. As proposed (Figure 4.1), for both PHB and PLLA cross-linking would occur at the tertiary C to form a quaternary C. A standard ^{13}C NMR spectrum of cross-linked PHB showed two quaternary C signals at δ 172.2 ppm (C=O) and 70.5 ppm which disappeared in DEPT-135 spectrum (Figure 4.4a), supports the PHB cross-linking site outlined in Figure 4.1. The methanolyzed $PLLA_{0.25gel}$ showed quaternary C signals at δ 176.0 ppm (C=O) and 97.0 ppm in the ^{13}C spectrum and disappeared in the DEPT-135 (Figure 4.4b) which supports the PLLA cross-linking site (Figure 4.1). Therefore it is concluded that the cross-linking did occur for PHB and PLLA polymers with DCP.

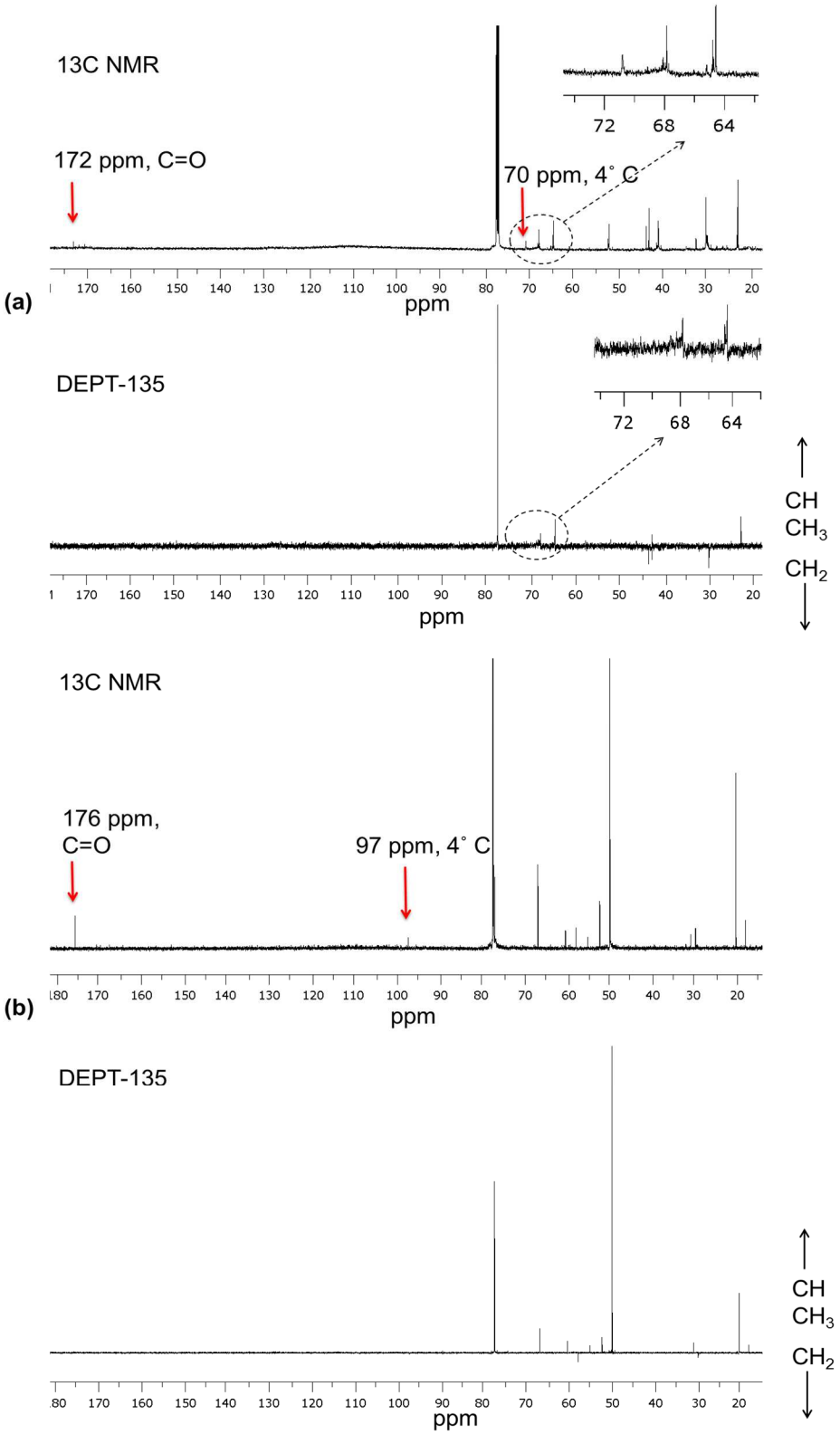

Figure 4.4. ^{13}C NMR and DEPT-135 spectra of methanolyzed (a) $PHB_{0.25gel}$ and (b) $PLLA_{0.25gel}$.

4.4.3 Quantitative analysis by FTIR

The crystallinity of PHB and PLLA will decrease due to cross-linking and this was monitored by FTIR spectroscopy (Figure 4.5). The intensities of bands at 980, 1226, 1278 cm^{-1} from the PHB crystalline phase were shown to decrease with cross-linking, the band at 1181 cm^{-1} associated with the amorphous phase was shown to increase (Figure 4.5a) (El-Hadi et al., 2002). The broad band between 1800 and 1650 cm^{-1} was assigned to carbonyl stretching of the PHB polymer and was processed by peak fitting to obtain better band assignments (Figure 4.5a). The fitted bands at 1720 and 1740 cm^{-1} were assigned to the stretching vibration of the crystalline and amorphous ester carbonyl groups, respectively (Figure 4.5a) (El-Hadi et al., 2002). Due to cross-linking the band intensity increased at 1720 cm^{-1} and the shoulder at 1740 cm^{-1} increased relative to 1720 cm^{-1} band. These results show that the amorphous PHB level increased with the extent of cross-linking. To quantify this change related to crystallinity, the FTIR spectra were imported into Igor Pro software, peak fitted and $I_{C=O}$ was calculated with results summarized in Table 4.1. It can be seen that $I_{C=O}$ values decreased from 1.30 (PHB_0) to 0.39 for PHB_{1gel}.

For PLLA strong IR bands at 2997, 2946, and 2882 cm^{-1} were assigned to the –CH stretching region ($–CH_{3(asym)}$, $–CH_{3(sym)}$, and –CH modes) (Gonçalves et al., 2010). Due to different levels of cross-linking by DCP the intensity of all these samples were higher than $PLLA_0$ (Figure 4.5b). For quantitatively analysis, the region of CH stretching between 3050 and 2800 cm^{-1} was peak-fitted (Figure 4.5b). The ratio of the areas of –CH and $–CH_3$ (sym), I_{C-H}, was obtained (Table 4.1). It was determined that I_{C-H} was 2.27 for $PLLA_0$. When the DCP levels increased to 1 wt% the I_{C-H} value was significantly reduced to 0.06. This verified that with more PLLA chains were cross-linked together at the methine sites. In other words, less methine groups were present in the cross-linked networks as compared to the methyl groups as outlined in Figure 4.1.

Table 4.1. The $I_{C=O}$, I_{C-H}, crystallinity and thermal properties of PHB_0, $PLLA_0$, $PHB_{0.25\text{-}1gel}$ and $PLLA_{0.25\text{-}1gel}$ samples

	PHB_0	$PHB_{0.25gel}$	$PHB_{0.5gel}$	PHB_{1gel}	$PLLA_0$	$PLLA_{0.25gel}$	$PLLA_{0.5gel}$	$PLLA_{1gel}$
$I_{C=O}$	1.30	1.23	0.97	0.39				
I_{C-H}					2.27	0.16	0.07	0.06
T_g (˚C)	5.5	4.4	2.2	0.5	62.0	59.0	57.3	52.0
T_{2nd} (˚C)	-20.4	-22.0	-24.1	-29.3				
ΔC_p (J/g/˚C)[a]	0.43	0.64	0.70	0.88	0.29	0.37	0.43	0.51
T_c (˚C)	93.9	89.0	88.9	86.9	103.0	100.8	95.6	94.9
$\Delta H_{crys+recrys}$ (J/g)[b]	0.36	0.51	4.19	4.29	29.31	13.17	11.08	10.55
T_m (˚C)[c]	174.0	170.0	158.1	151.0	176.8	164.0	160.0	159.0
ΔH_m (J/g)[d]	59.48	21.75	8.91	7.94	58.03	18.6	13.48	10.84
X_c (%)[e]	40.49	14.55	3.23	2.50	31.93	6.43	0.96	0.31

[a] Variation of heat capacity (C_p). [b] Exothermal enthalpy of crystallization and recrystallization. [c] Melting temperature determined from the second melting peak (higher temperature) of total heat flow curve (T) as shown in Figure 4.6. [d] Melting enthalpy.

[e] Degree of crystallinity determined by eq. 4.5.

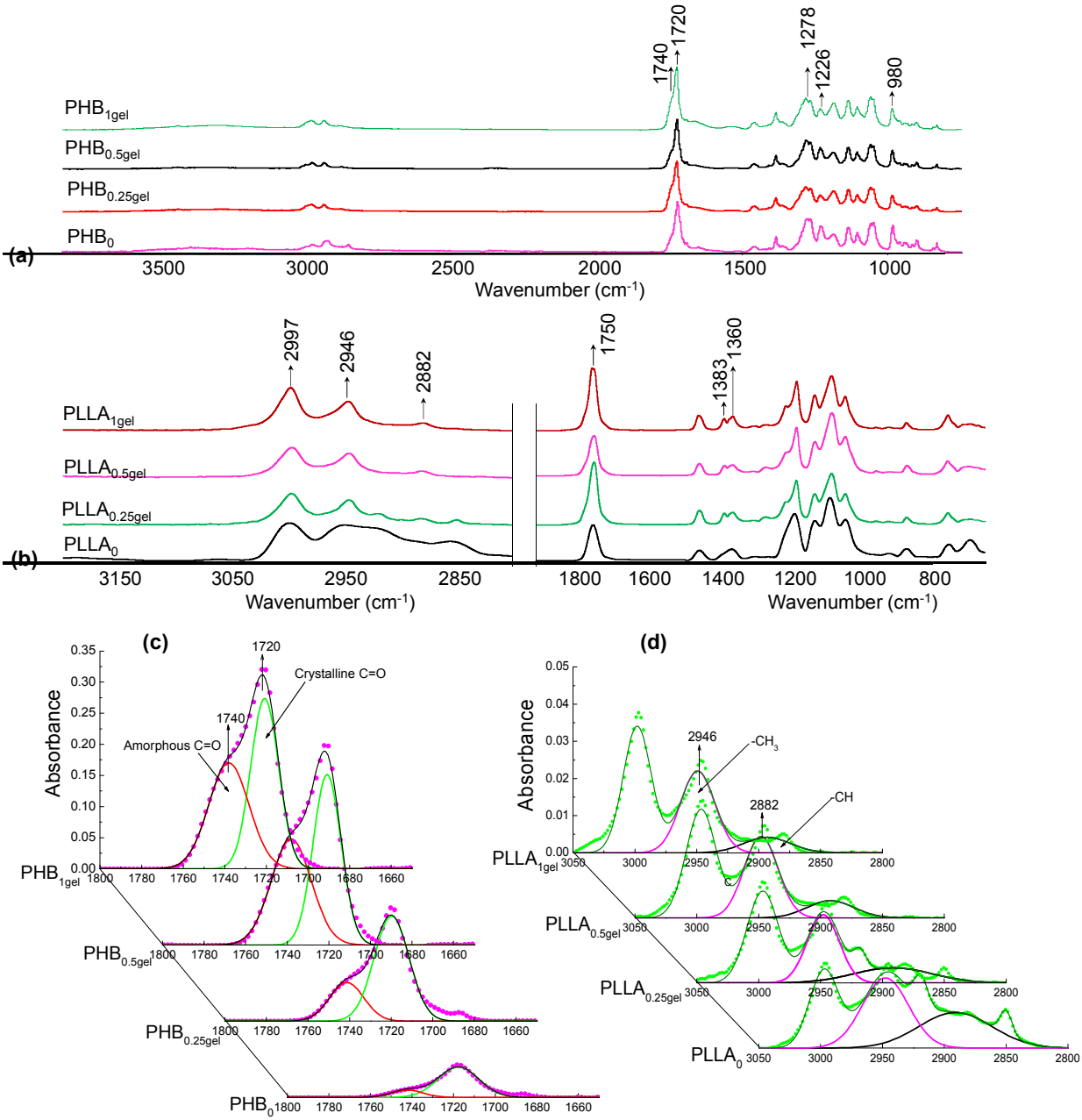

Figure 4.5. FTIR spectra of (a) $PHB_{0\text{-}1gel}$, (b) $PLLA_{0\text{-}1gel}$, (c) curve fitting of carbonyl (C=O) band (1800-1650 cm^{-1}) of $PHB_{0\text{-}1gel}$ samples, and (d) curve fitting of –C–H stretching band (3050-2800 cm^{-1}) of $PLLA_{0\text{-}1gel}$ samples.

4.4.4 DSC analysis

The polymers were analyzed by TMDSC which allowed for observing the formation of crystalline structures as soon as the polymer starts to melt (recrystallization). The thermal properties of the polymers are listed in Table 4.1. The total heat flow curve (T) of all samples was separated into non-reversing (Non-Rev) and the reversing flow (Rev) curves (Figure 4.6) (Solarski et al., 2005). The T_g was clearly visible in Rev curves followed by the cold crystallization (exotherm) region after which a melting endotherm peak was observed. From the Non-Rev curves a recrystallization exothermal peak was observed.

The T_g of PHB and PLLA were influenced by DCP concentration (Table 4.1). The PHB_0 and $PLLA_0$ have a T_g at 5.0 and 62.0 ˚C, respectively. The T_g was shown to decrease with the extent of cross-linking. For example, the T_g decreased by 5 ˚C for PHB_{1gel} and 10 ˚C for $PLLA_{1gel}$ as compared to controls. To note, one more transition/relaxation of PHB system (T_{2nd}) was observed at the region below T_g and the onset temperature (T_{2nd}) shifted to lower values (Figure 4.6a and b). This T_{2nd} was probably attributed to an increased amount of side macromolecular chains of the cross-linked PHB gels. The precise original X_c% of PHB_{1gel} and $PLLA_{1gel}$ reduced significantly to 2.5% and 0.31%, respectively. The decrease of crystallinity (or amorphous phase increase) observed by DSC were supported by FTIR (Table 4.1). Since T_g is directly related to the macromolecular mobility of polymer chains, hence, lower X_c% the lower the energy required to move the polymer chains in the amorphous phase (Kurniawan et al., 2007). In other word, cross-linked polymers show higher chain mobility. Therefore, the temperature to transit the polymer from a glassy to a rubbery state (T_g) will be lowered. For cross-linked PHB and PLLA, the X_c% was low, which explains why T_g and peak of cold crystallinity appeared more clearly than controls (Figure 4.6). The similar thermal behavior changes were observed for cross-linked PE by BCUP and PHBV by DCP respectively (Fei et al., 2004; Khonakdar et al., 2003). Hence, DCP concentration can be adjusted to tune the extent of cross-linking in PHB and PLLA to meet various requirements for T_g and X_c% for different applications.

The heat capacity (ΔC_p) was shown to increase for both PHB (0.43 to 0.88 J/g/˚C) and PLLA (0.29 to 0.51 J/g/˚C) with increasing DCP concentration or cross-linking density (0.25

to 1%) (Table 4.1). These changes of ΔC_p due to cross-linking also indicate that more polymer chains entered into amorphous state (Scandola et al., 1988). This was further verified by the large crystallization peak observed for cross-linked PHB and PLLA (Figure 4.6), because molecular chains with higher mobility tend to align and recrystallize with melting proceeded. In addition, the T_m and ΔH_m were determined from the endotherm peak of the total and rev heat flow curves, respectively. For PHB_0 and $PLLA_0$, multiple/double melting peaks were observed, suggesting PHB samples experienced secondary crystallization during TMDSC heating scans under the experimental condition (using cooling rate = 20 ˚C/min) employed (Gunaratne and Shanks, 2006c). The peak at higher temperature was considered to be the true melting peak (T_m) representing the original polymer before the DSC experiment. These multiple peaks merged into one single melting peak with an increase of DCP concentration. T_m and ΔH_m (crystalline fraction) for PHB and PLLA were shown to decrease with the extent of cross-linking. The cold crystallization temperature (T_c) of cross-linked PHB and PLLA was also shown to decrease slightly, since the formation of cross-linking networks will disturb the reorganization and chain folding during crystallization process (Khonakdar et al., 2003). This phenomenon will result in the formation of small crystallites and thus T_c will decrease accordingly.

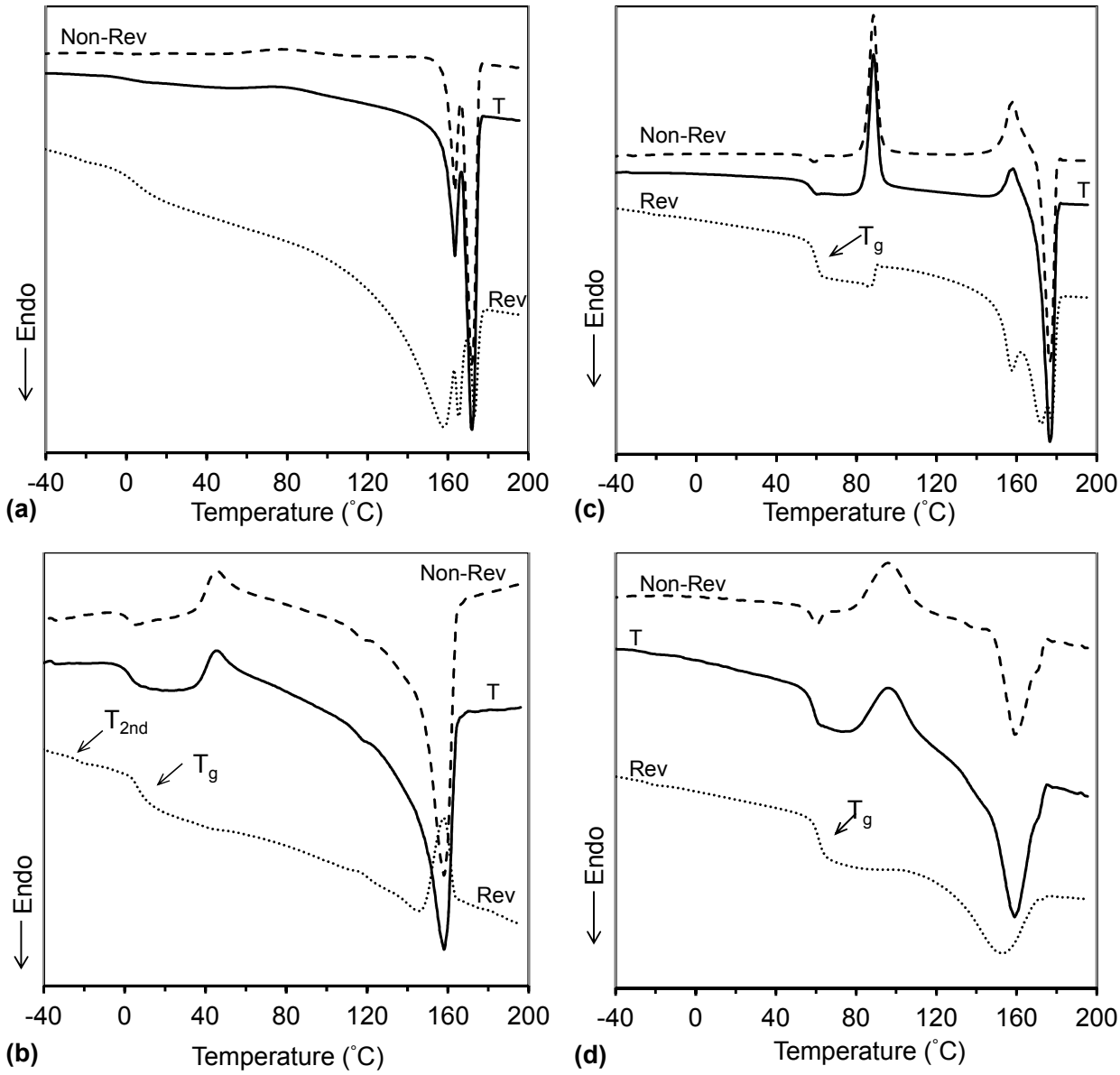

Figure 4.6. TMDSC thermograms of (a) PHB_0, (b) PHB_{1gel}, (c) $PLLA_0$ and (d) $PLLA_{1gel}$. Three curves for each sample are total heat flow (T), non-reversing (Non-Rev) and reversing (Rev) heat flow.

4.4.5 Morphology

The crystalline morphologies of PHB and PLLA samples were analyzed by HS-POM after isothermal crystallization from the melt at 90 ˚C (above their T_c as shown in Table 4.1). Figures 4.7a and 4.8a show micrographs of solvent casted PHB and PLLA films showing

spherulites with typical birefringent Maltese cross pattern (Hu et al., 2013). The control $PLLA_0$ has smaller spherulites (radius about 240 μm) than PHB_0 (radius about 560 μm), while straight boundaries were observed between neighboring spherulites for both of them, indicating the spherulite growth follows the heterogeneous nucleation mechanism (Hu et al., 2013). If the isothermal temperature was set about 30 °C higher than the T_c then the diameter of PHB_0 spherulite tends to reach to 3000 μm before they impinge each other because the nuclei site are limited. Cross-linking tends to reduce the size of PHB and PLLA spherulites (Figures 4.7b-d and 4.8b-d), because those numerous cross-linking sites performed as nucleation sites. With the increase of cross-linking the polymer chains are constrained against diffusion and conformational rearrangement, hence, higher peroxide loadings give rise to a reduced X_c% and crystal size. Therefore, it could be suggested that cross-linked PHB, and PLLA, will be less brittle than the original polymers due to the decrease in the size of crystals which minimizes crack formation between the spherulites (Hinüber et al., 2010). In other words, the cross-linking partial would play a plasticizer or nucleation agent role in the final products.

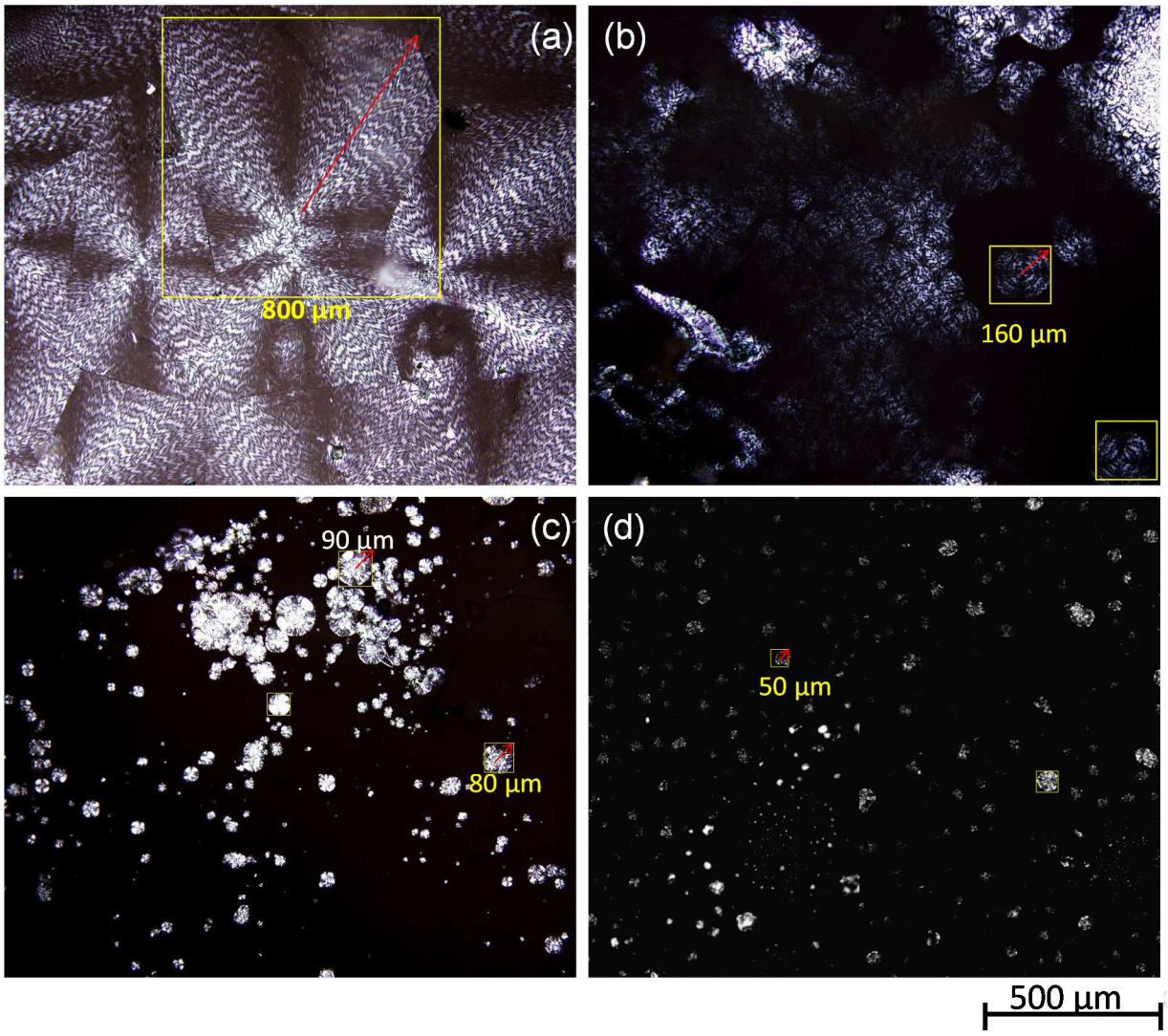

Figure 4.7. HS-POM micrographs (100 x) at 90 ˚C of: (a) solvent cast PHB_0 film, and hot pressed (b) $PHB_{0.25gel}$, (c) $PHB_{0.5gel}$ and (d) PHB_{1gel} films. All the images have the same scale and marked area showed the sizes of spherulites (note: arrow shows the approximate radius).

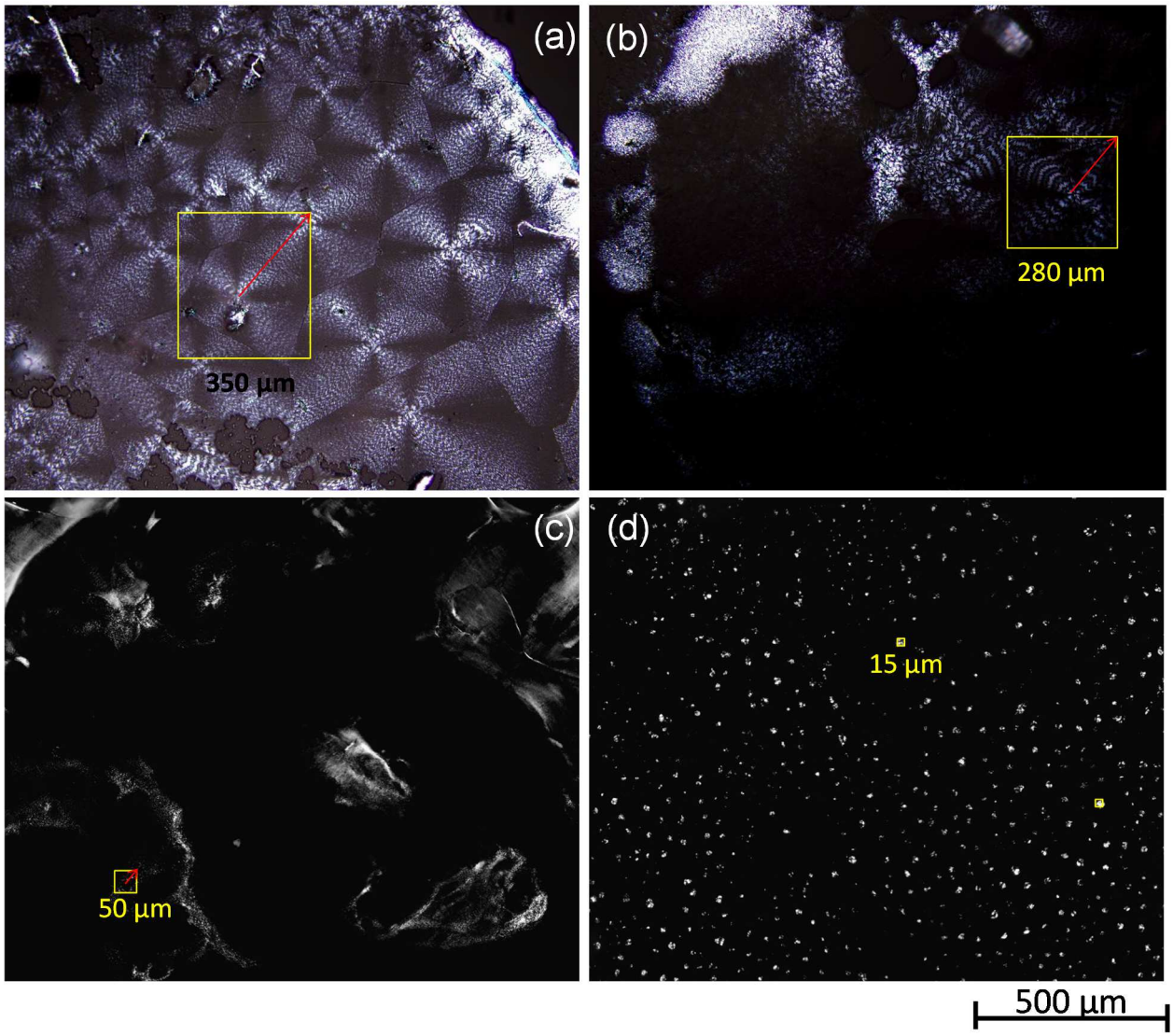

Figure 4.8. HS-POM micrographs (100 x) at 90 ˚C of: (a) solvent cast $PLLA_0$ film, and hot pressed (b) $PLLA_{0.25gel}$, (c) $PLLA_{0.5gel}$ and (d) $PLLA_{1gel}$ films. All the images have the same scale and marked area showed the sizes of spherulites (note: arrow shows the approximate radius).

4.4.6 Thermal stability

Table 4.2 reports the starting (onset) decomposition temperature (T_{onset}) and their complete degradation temperature (T_{comp}) for all control and cross-linked PLLA and PHB samples.

Degradation (98% mass loss) occurred in one step for all polymers. PHB_0 and $PLLA_0$ started to decompose at 270 and 344 °C, respectively. However, cross-linked gels started degradation at higher temperature (>10 °C) for both PHB and PLLA. These observations indicate that cross-linked structures improve the thermal stability of PHB and PLLA to some extent, especially for PHB since its thermal instability is one of its drawbacks (Yamaguchi and Arakawa, 2006). Since cross-linking occurred at the tertiary carbons this makes the polymer more prone to thermal decomposition as found for HDPE (Khonakdar et al., 2003). Therefore, the observed thermal stability for PHB and PLLA is cross-link dependent and results in fewer tertiary C's for scission.

Table 4.2. Decomposition temperatures of PHB_0, $PLLA_0$, $PHB_{0.25\text{-}1gel}$ and $PLLA_{0.25\text{-}1gel}$ samples obtained by TGA

Samples	T_{onset} (°C)	T_{comp} (°C)
PHB_0	270	295
$PHB_{0.25gel}$	281	300
$PHB_{0.5gel}$	284	311
PHB_{1gel}	291	313
$PLLA_0$	344	383
$PLLA_{0.25gel}$	356	390
$PLLA_{0.5gel}$	359	391
$PLLA_{1gel}$	361	392

4.4.7 Viscoelastic properties

The results of three point bending test of cross-linked PHB and PLLA samples by DMA are shown in Figure 4.9 and Table 4.3. For both PHB and PLLA only one transition (glass transition or α transition) were seen from the tan δ peak (Figure 4.9b and d), and the transition temperature [tan δ_{max} (°C)] shifted to lower temperatures with the increase of DCP concentration (Table 4.3), indicating the cross-linked PHB became more flexible and the same trend was seen in PLLA. In addition, the maximum values of tan δ (tan δ_{max}) were higher due to cross-linking for both PHB and PLLA (Table 4.3), suggesting higher mobility

of cross-linked polymers (reduction in degree of crystallinity) with more side branches were introduced with an increase of DCP concentration and broader polymer structural distribution (Kurniawan et al., 2007). The loss modulus (E'') of all cross-linked PHB were shown to have two transitions (α or T_g and β) (Figure 4.9a and c), while the low temperature β transition (around -25 °C) was very close to the T_{2nd} of cross-linked gels (around -22 to -29.3 °C) as obtained by TMDSC (Table 4.1). The β transition is associated with side chain branching effect in the cross-linked polymer and not observed in PHB_0 (Kurniawan et al., 2007). No β transition was observed in $PLLA_0$, however for the cross-linked $PLLA_1$ sample only showed a β transition (between 20 and 35 °C). If compared with TMDSC data (Table 4.1), positions of α transitions detected by DMA seemed to be reasonable (Table 4.3). These results support the findings obtained from the Charlesby-Pinner plot (Figure 4.3) that higher concentration of DCP is required for cross-linking PLLA than PHB.

To confirm these observations, the cross-linking density (ν_e) for the obtained networks was calculated (Table 4.3). In this study, the ν_e was calculated by the equation derived from the theory of rubber elasticity (Worzakowska, 2010):

$$E' = 3\nu_e RT \qquad \text{(eq. 4.7)}$$

where E' is the storage modulus in the rubbery plateau region from DMA test, R is the gas constant, and T is the absolute temperature. The ν_e increased from 1.32 for $PHB_{0.25}$ to 1.88 for PHB_1 (Table 4.3). This illustrated why lower DS was observed with higher DCP concentration. For PLLA samples a similar trend was seen in that the ν_e was positively dependent on DCP concentration. The higher E' values were observed for all cross-linked samples within the glassy region of PHB and PLLA as well (Table 4.3), which attributed to the higher ν_e and the extra high strength of C-C bonds formed within the cross-linked networks (Nair et al., 2009).

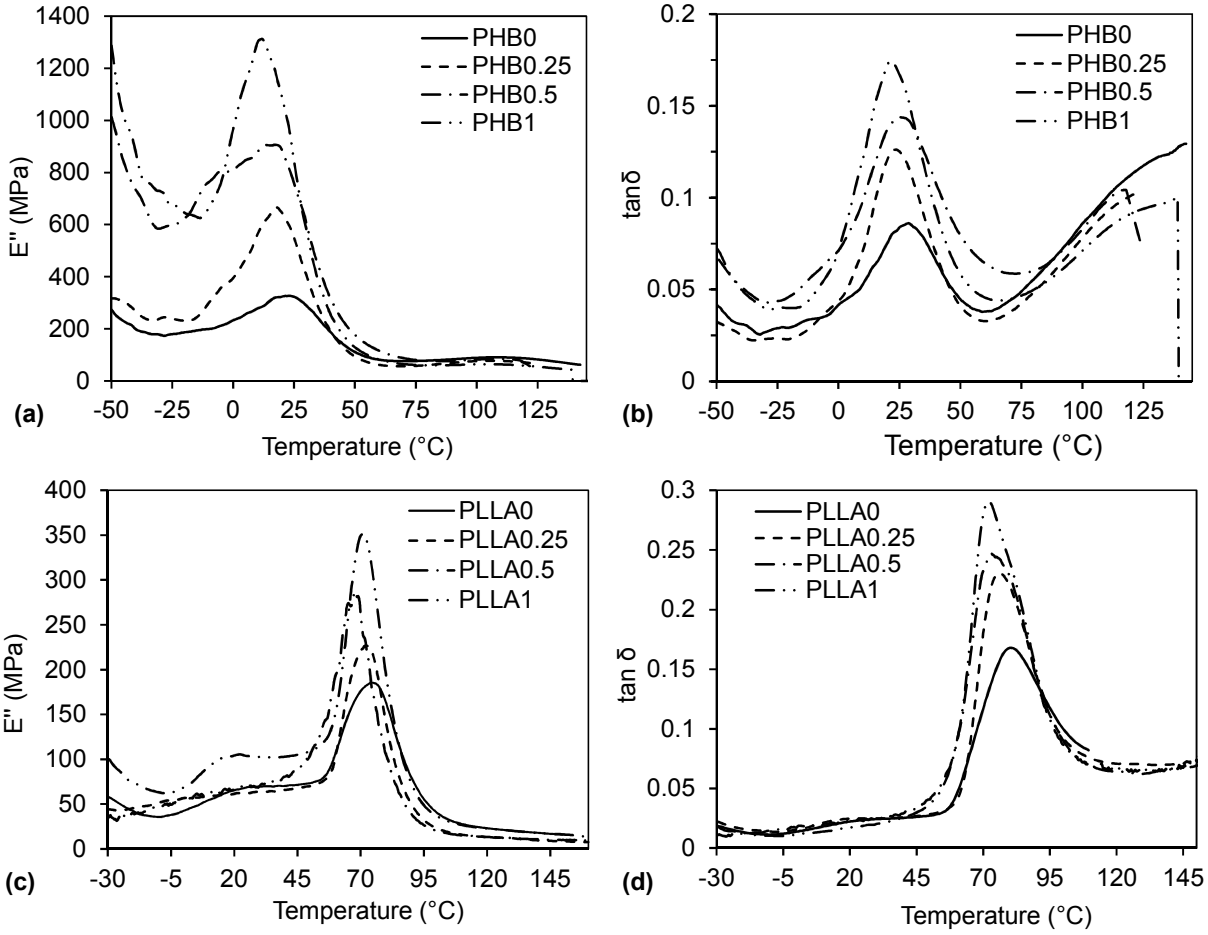

Figure 4.9. DMA thermograms showing the effect of cross-linking on the (a) loss modulus (E'') and (b) tan δ for $PHB_{0\text{-}1}$ samples; (c) loss modulus (E'') and (d) tan δ for $PLLA_{0\text{-}1}$ samples.

Table 4.3. Viscoelastic properties obtained by DMA on three point bending tests for molded PHB_{0-1} and $PLLA_{0-1}$ disc samples

Sample	tan δ_{max}	tan δ_{max} (°C)	α transition (°C)[a]	β transition (°C)[a]	E' (MPa)	ν_e x 10^{-3} (mol/cm^3)
PHB_0	0.08	29	22	None	5644	0.83
$PHB_{0.25}$	0.12	24	20	-26	8968	1.32
$PHB_{0.5}$	0.14	24	10	-28	11459	1.68
PHB_1	0.18	21	6	-29	12838	1.88
$PLLA_0$	0.18	77	75	None	2372	0.29
$PLLA_{0.25}$	0.20	73	73	None	2739	0.34
$PLLA_{0.5}$	0.24	71	68	-30	2942	0.37
$PLLA_1$	0.28	70	70	-29	3613	0.45

[a] α (T_g) and β transitions were determined from E'' as shown in Figure 4.10a and c; None: no transition was observed.

4.4.8 Melt strength and rheological properties

Figure 4.10 shows the dynamic moduli (G' and G") of PLLA (190 °C) and PHB (180 °C) and their cross-linked materials under isothermal conditions. For both PLLA and PHB, elasticity (G') and loss modulus (G") were shown to increase upon cross-linking. For instance, the G' for PHB_0 was shown to increase from 10 to 200 Pa (PHB_1) at 1 rad/s. At lower frequency (ω, rad/s) the G' was lower than G", indicating that the polymers were liquid-like. The cross-over point of G' and G'' ($G_c = G' = G''$) was shown to occur at a lower frequency for the cross-linked polymers than for PHB_0 and $PLLA_0$. The G_c decreased from 90 rad/s for PHB_0 to 10 rad/s for PHB_1 (Figure 4.10a). A similar trend was observed between $PLLA_0$ to $PLLA_{0.5}$ while $PLLA_1$ had a much lower G_c value (Figure 4.10b). Positive correlations between G_c and D (or M_w/M_n and M_z/M_n) has previously been reported for other linear polymers (Cocchini and Nobile, 2003). The G' and G'' values of cross-linked $PHB_{0.25-1}$ and $PLLA_{0.25-1}$ were higher than PHB_0 and $PLLA_0$ polymers which clearly show that melt strength was significantly increased by a higher level of LCB and cross-linking density (D'Haene et al., 1999). The low levels of elasticity for PHB_0 and $PLLA_0$ compared to cross-

linked polymers was caused by their higher chain stiffness and this phenomenon is in accordance with higher T_g and T_m for the linear polymers.

The viscosity (η and η^*) of PLLA and PHB were shown to increase significantly with the extent of cross-linking (Figure 4.11). For example, η^* for PHB increased from 30 (PHB_0) to 1000 Pa·s for PHB_1 (at 0.1 rad/s) upon cross-linking. For PHB_0 and $PLLA_0$, the viscosity curves (η and η^*) show a Newtonian plateau when γ <10 Hz, while the γ >10 Hz, shear thinning was observed (Figure 4.11a). The cross-linked $PHB_{0.25\text{-}1}$ polymers have a higher PD and therefore have a broad transition range (shear rate) where shear thinning occurs. This trend was similar to the cross-linked PLLA samples (Figure 4.11b). Since the shear thinning behavior is associated with a decrease of entanglement and network density and/or polymer chains dissociation by shear during extrusion, PHB experienced more shear thinning than PLLA (Ramkumar and Bhatacharya, 1998).

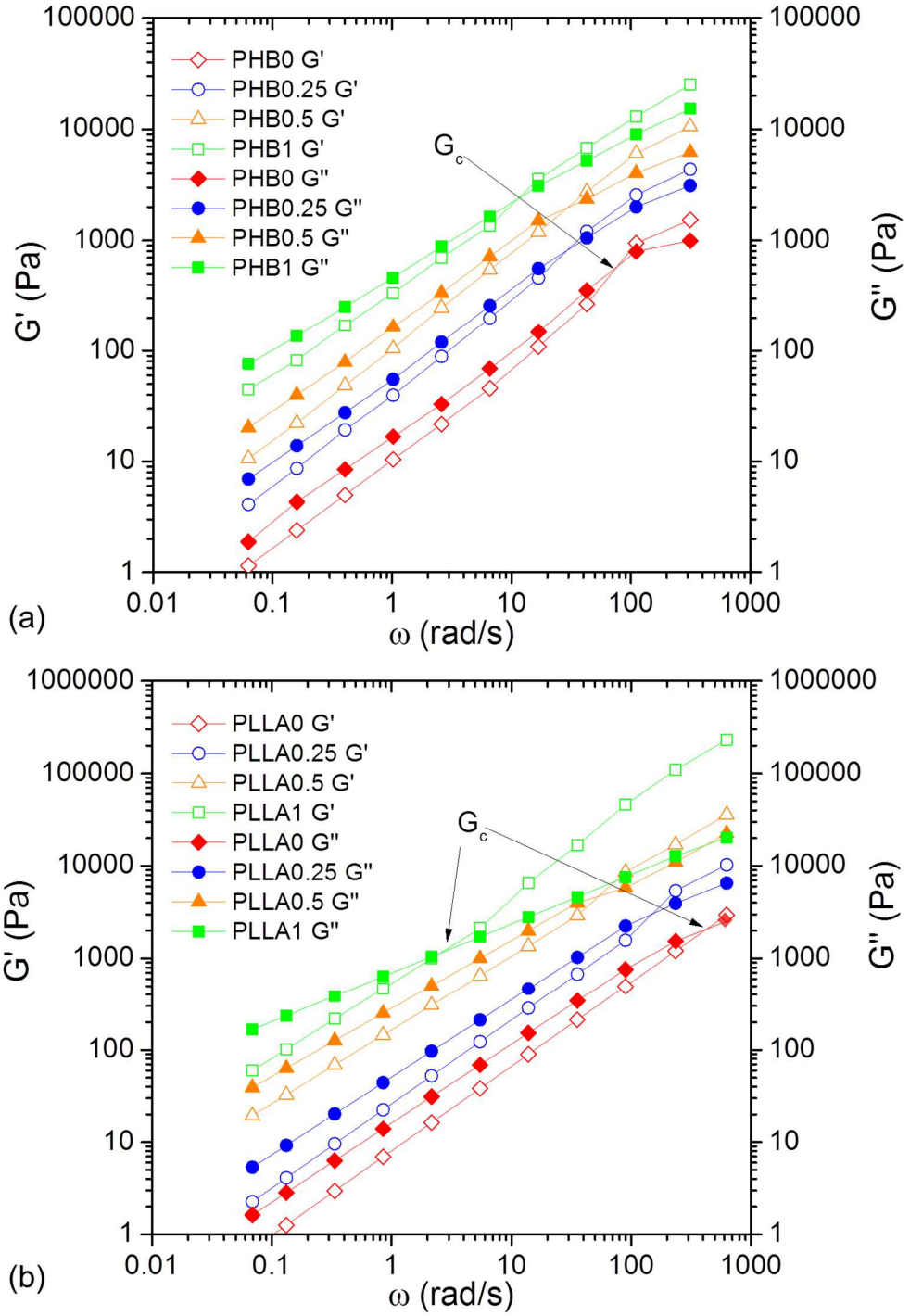

Figure 4.10. Effect of DCP concentration on dynamic rheology storage ($G^{'}$) and loss ($G^{''}$) moduli of (a) $PHB_{0\text{-}1}$ samples at 180 °C and (b) $PLLA_{0\text{-}1}$ samples at 190 °C.

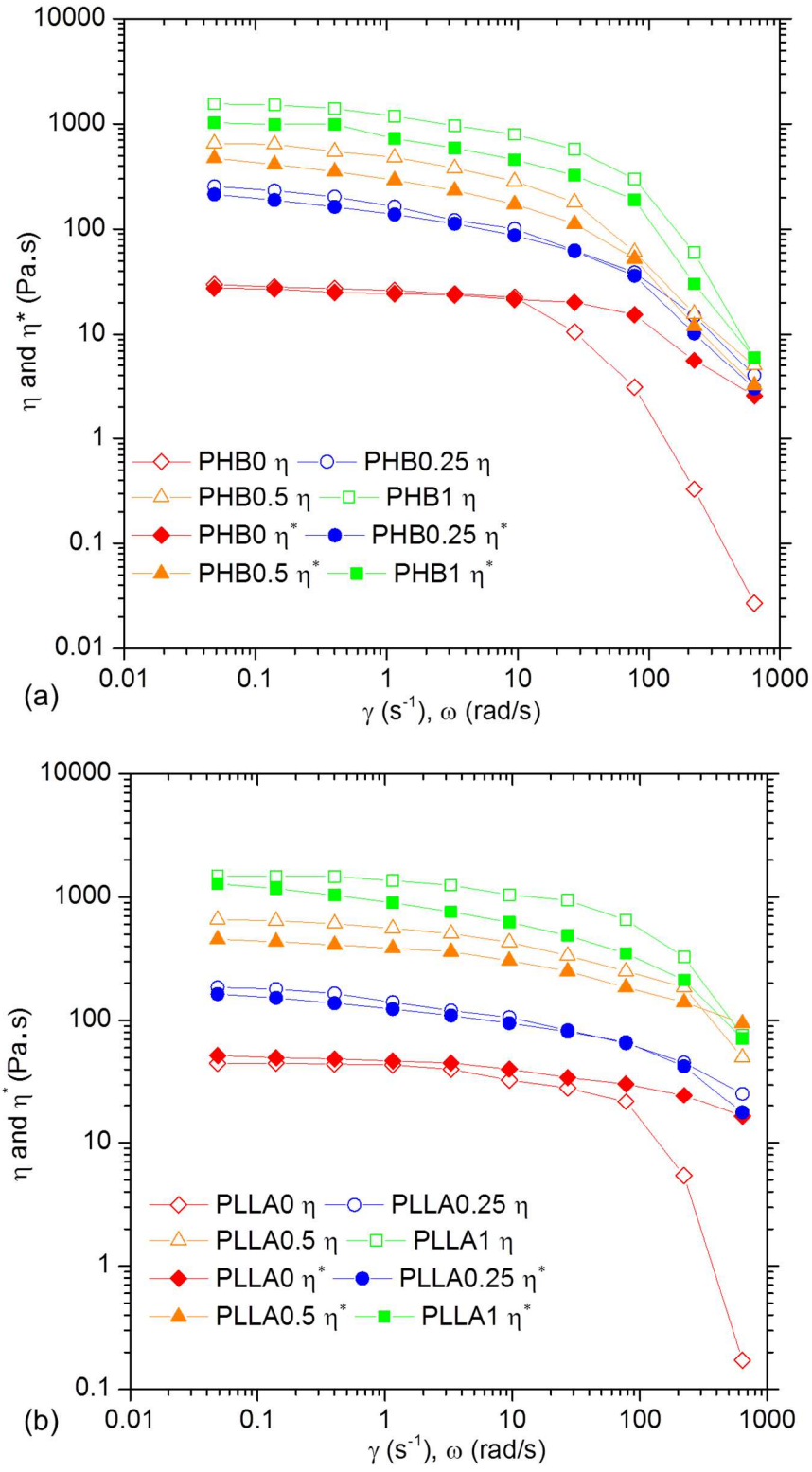

Figure 4.11. Dynamic rheology showing complex viscosity (η*) as a function of frequency (ω, rad/s) and steady shear viscosity (η) as a function of shear rate (γ, s^{-1}) of (a) $PHB_{0\text{-}1}$ samples at 180 ˚C and (b) $PLLA_{0\text{-}1}$ samples at 190 ˚C.

Dynamic rheological data were analyzed using the RheoMWD Polydispersity Measures software to further understand polymer chain entanglement. TDF values for PHB and PLLA were estimated to be 0.99 and 0.9, respectively. The RheoMWD incorporates four measures of PD, which are CPI, HEI, GDI and DRI. Each of these indices was derived from frequency data in the linear viscoelastic region and calculated values are given in Table 4.4. The HEI values were higher for cross-linked $PHB_{0.25\text{-}1}$ and $PLLA_{0.25\text{-}1}$ samples compared to linear PHB_0 and $PLLA_0$. The HEI term was introduced specifically for characterizing the breadth of molar mass distribution. Note: HEI was designed to quantify high molar mass PD and/or the LCB at the higher molar mass end, and HEI has no contributions at low molar mass (Shroff and Mavridis, 1995). Therefore, these results indicate that cross-linked PHB and PLLA have broader MWD at the high molar mass end than linear PHB and PLLA, respectively. The GDI term was affected by both the high molar mass component (M_z/M_w) as well as the low molar mass component (M_w/M_n). From the HEI values it was found that the M_z/M_w was larger for cross-linked PHB and PLLA samples. However, the GDI values were significantly larger for cross-linked samples indicating that not only do they have a larger high molar mass component, but they also have a broader MWD at the low molar mass end (M_w/M_n). Therefore, it was important to examine HEI and GDI together, since both of these measures were sensitive to high molar mass fractions. The CPI was determined from G_c. CPI values have been reported to be in a good correlation with M_w/M_n for polypropylenes (Zeichner and Patel, 1981). CPI, GDI and HEI values of cross-linked PHB and PLLA, respectively, all increased with the extent of cross-linking. These data shows that DCP increased LCB (Ryan et al., 1997). Since the LCB favors chain entanglement over short chain branching (SCB) the melt elasticity is proportional to the degree of chain entanglement. Therefore, both G' and G'' were shown to increase significantly with DCP concentration (Figure 4.10) and LCB. The DRI is a measure of the shear sensitivity of viscosity, introduced by the Dow Chemical Company to characterize LCB for copolymers of ethylene and α-olefins made with INSITE technology metallocene catalysts (Pannier and Chai, 2013), and was not a meaningful measure for polymers whose viscosity was influenced by both MWD and LCB. DRI seems to fail for PHB_0 and $PLLA_0$ and their cross-linked polymers (Table 4.4).

Table 4.4. Computed PD measures and MWD for $PHB_{0\text{-}1}$ and $PLLA_{0\text{-}1}$ samples by RheoMWD

Sample	M_w/M_n	TDF	CPI	GDI	HEI	DRI
PHB_0	2.01	0.99	7.78	2.15	2.11	120
$PHB_{0.25}$	3.23	0.99	14.1	10.0	2.53	165
$PHB_{0.5}$	3.45	0.99	41.1	30.0	4.34	132
PHB_1	4.56	0.99	50.5	40.1	6.21	353
$PLLA_0$	1.46	0.90	6.72	2.42	1.18	109
$PLLA_{0.25}$	4.56	0.90	9.99	4.54	3.75	14.9
$PLLA_{0.5}$	4.98	0.90	13.47	13.3	4.84	500
$PLLA_1$	5.22	0.90	15.2	37.3	5.04	361

All $PHB_{0\text{-}1}$ and $PLLA_{0\text{-}1}$ samples were also analyzed using the M_w/M_n viscosity function method on the steady shear viscosity data (as function of shear rate (γ)) at different temperatures. For these calculations the zero-shear viscosity (η_0) was estimated by the software program and not entered explicitly (Table 4.4). The two other parameters, polynomial order for the high γ fit and final slope magnitude, were set for all materials to be 2 and 0.75, respectively. The final slope magnitude was determined by decreasing its value from 1.0 until the weight distribution normalization values for all materials was as close as possible to 1.0. The η_0 of cross-linked PHB and PLLA were higher and increased with DCP concentration. D'Haene et al. had shown that DCP level < 0.3% resulted in cross-linked PHBV with a decreased η_0 and was similarly observed for low density polyethylene (LDPE) as a result of high branching and a considerable decrease in the radius of gyration compared to the linear polymer (D'Haene et al., 1999). Hence, it could be concluded the LCB formed in cross-linked PHB and PLLA polymer networks that would not lead to a decrease in the radius of gyration as compared with their linear polymers. The calculated values of M_w/M_n are given in Table 4.4. The M_w/M_n values were positively correlated with η_0 values. The computed M_w/M_n ratios of linear polymers were very close to SEC determined values. The values of M_w/M_n for both PHB and PLLA were shown to increase with DCP concentration or extent of cross-linking. In other words, the DCP induced cross-linking result in the

broader MWD and higher degree of LCB, which is consistent with the results of PD measures (HEI, GDI and CPI). The computed results show that PHB cross-linked with 1% DCP increased M_w/M_n two-fold, while for PLLA the M_w/M_n increased four-fold. The increase of the M_w/M_n with increasing peroxide concentration may be caused by an increasing amount of side chains and cross-links, resulting in a change in the weight average molar mass but not in the number average molar mass (Sijdergard et al., 1995). For many polymers especially the ones with linear or short chain branching structures, the temperature dependence of rheological behavior can be described using a time shift factor, a_T, over a series of specific temperature, and a modulus shift factor, b_T, also known as time-temperature superposition (TTS). The time shift factor often follows the Arrhenius relation (Wood-Adams and Costeux, 2001).

$$a_T = \exp[(E_a/R)\,(1/T\text{-}1/T_0)] \qquad \text{(eq. 4.8)}$$

where T is the absolute temperature, E_a is the activation energy of polymer melt, R is the gas constant and the subscript, "0", refers in all further discussion to an arbitrary reference temperature (T_0 = 180 and 200 ˚C respectively for PHB and PLLA).

The RheoMWD analysis showed that LCBs formed upon DCP based cross-linking. TTS was shown to fail in the case of LCB materials with thermorhelogical complex behavior, which means that the effect of temperature cannot be described by a single time shift factor, and different shift factor is required at each time; hence the zero shear viscosity was employed by Wood-Adams and Costeux for the LCB based polyethylene:

$$\eta_0(T) = \eta_0(T_0)\exp\left[(\hat{E}_a/R)(1/T - 1/T_0)\right] \qquad \text{(eq. 4.9)}$$

where $\hat{E}_a$ is the apparent zero shear rate activation energy, a weighted average of the material E_a (Wood-Adams and Costeux, 2001). The η_0 was estimated by RheoMWD at T = 170, 175 and 180 ˚C for PHB, and T = 180, 190 and 200 ˚C for PLLA. Using this approach the E_a based on η_0 were estimated by fitting the linearized form of eq. 4.9. The E_a was determined from the slope (slope=$\hat{E}_a/R$) versus 1/T of the fitted trend-line for LCB PHB and PLLA (Figure 4.12). Cross-linked PHB and PLLA polymers have higher E_a compared with

their linear polymers. According to rheological studies there is a positive relationship between E_a and LCB for polyethylene (Wood-Adams and Costeux, 2001). Hence, it seems to be concluded that the higher LCB levels existed in the cross-linked polymer network, especially when >0.5% DCP were employed. Since LCB will enhance the shear thinning of a polymer melt (Figure 4.11), cross-linked $PHB_{0.25\text{-}1}$ and $PLLA_{0.25\text{-}1}$ showed more severe shear thinning than PHB_0 and $PLLA_0$. However, they also proposed that the combination of LCB with SCB also contribute to the thermorheological complex behavior. Therefore, the future work will be aimed at understanding the index of LCB and SCB, and how these will influence PHB and PLLA melt properties.

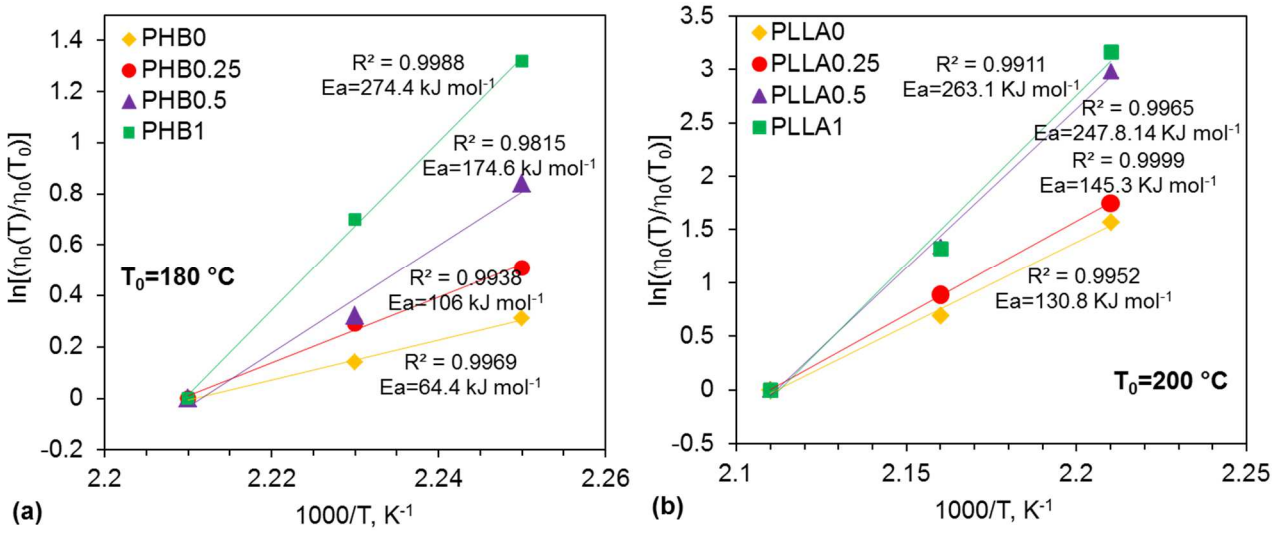

Figure 4.12. The effect of DCP concentration on the activation energy (E_a) of (a) PHB and (b) PLLA.

4.5 Conclusions

Free radical initiated cross-linking with DCP in the molten state proved to be an effective approach for modifying PHB and PLLA. The cross-linking reaction was verified to occur at tertiary carbon along the polymer chain. During cross-linking some chain scissioning also occurred, hence, to control the reaction time seems to be crucial to limit polymer degradation. Cross-linking resulted in a ductile material by lowering the polymer T_g, T_m and X_c %, as well as reducing spherulite sizes. The cross-linked polymers were more thermally stable than linear polymers. Furthermore, the cross-linked PHB and PLLA materials had a

broader MWD and LCB and thus showed improved melt strength. The cross-linked PHB and PLLA polymers could be potentially run at the higher line speeds and throughputs on industrial extrusion or foaming lines with minimum thermal degradation at lower cost because of lower heat input due to decrease of T_m and reduce the levels of plasticizers.

4.6 References

Cocchini, F., Nobile, M.R., 2003. Constrained inversion of rheological data to molecular weight distribution for polymer melts. Rheologica Acta 42, 232–242.

D'Haene, P., Remsen, E.E., Asrar, J., 1999. Preparation and characterization of a branched bacterial polyester. Macromolecules 32, 5229-5235.

De Koning, G.J.M., Lemstra, P.J., 1993. Crystallization phenomena in bacterial poly[(R)-3-hyd roxybutyrate]: 2. Embrittlement and rejuvenation. Polymer 34, 4089-4094.

Dean, K.M., Petinakis, E., Meure, S., Yu, L., Chryss, A., 2012. Melt strength and rheological properties of biodegradable poly(lactic acid) modified via alkyl radical-based reactive extrusion processes. Journal of Polymers and the Environment 20, 741-747.

El-Hadi, A., Schnabel, R., Straube, E., Müller, G., Riemschneider, M., 2002. Effect of melt processing on crystallization behavior and rheology of PHB and its blends. Macromolecular Materials and Engineering 287, 363-372.

Fei, B., Chen, C., Chen, S., Peng, S., Zhuang, Y., An, Y., Dong, L., 2004. Crosslinking of poly[(3-hydroxybutyrate)-co-(3-hydroxyvalerate)] using dicumyl peroxide as initiator. Polymer International 53, 937-943.

Gonçalves, C., Coutinho, J., Marrucho, I., 2010. Optical properties, in: Auras, R., Lim, L.-T., Selke, S.E.M., Tsuji, H. (Eds.), Poly(lactic acid): Synthesis, Structures, Properties, Processing, and Applications. John Wiley & Sons, Inc.: Hoboken, New Jersey, p.97.

Groot, W., van Krieken, J., Sliekersi, O., de Vos, A.S., 2010. Production and purification of lactic acid and lactide, in: Auras, R., Lim, L.-T., Selke, S.E.M., Tsuji, H. (Eds.), Poly(Lactic Acid): Synthesis, Structures, Properties, Processing, and Applications. John Wiley & Sons, Inc.: Hoboken, New Jersey, Chap.1, pp. 3-18.

Gunaratne, L.M.W.K., Shanks, R.A., 2006. Thermal memory of Poly(3-hydroxybutyrate) using temperature-modulated differential scanning calorimetry. Journal of Polymer Science Part B: Polymer Physics 44, 70-78.

Hinüber, C., Häussler, L., Vogel, R., Brünig, H., Werner, C., 2010. Hollow Poly(3-hydroxybutyrate) Fibers Produced by Melt Spinning. Macromolecular Materials and Engineering 295, 585-594.

Hu, S., McDonald, A.G., Coats, E.R., 2013. Characterization of polyhydroxybutyrate biosynthesized from crude glycerol waste using mixed microbial consortia. Journal of Applied Polymer Science 129, 1314-1321.

Jandas, P.J., Mohanty, S., Nayak, S.K., 2013. Sustainability, compostability, and specific microbial activity on agricultural mulch films prepared from poly(lactic acid). Industrial and Engineering Chemistry Research 52, 17714-17724.

Khonakdar, H.A., Morshedian, J., Wagenknecht, U., Jafari, S.H., 2003. An investigation of chemical crosslinking effect on properties of high-density polyethylene. Polymer 44, 4301-4309.

Kurniawan, L., Qiao, G.G., Zhang, X., 2007. Chemical modification of wheat protein-based natural polymers: grafting and cross-linking reactions with poly(ethylene oxide) diglycidyl ether and ethyl diamine. Biomacromolecules 8, 2909-2915.

Liu, B., Png, R.-Q., Zhao, L.-H., Chua, L.-L., Friend, R.H., Ho, P.K.H., 2012. High internal quantum efficiency in fullerene solar cells based on crosslinked polymer donor networks. Nature Communications 3, 1321.

Lunt, J., 1998. Large-scale production, properties and commercial applications of polylactic acid polymers. Polymer Degradation and Stability 59, 145-152.

Nair, T.M., Kumaran, M.G., Unnikrishnan, G., Pillai, V.B., 2009. Dynamic mechanical analysis of ethylene-propylene-diene monomer rubber and styrene-butadiene rubber blends. Journal of Thermal Analysis and Calorimetry 112, 72-81.

Nijenhuis, A.J., Grijpma, D.W., Pennings, A.J., 1996. Crosslinked poly(L-lactide) and poly(ε-caprolactone). Polymer 37, 2783-2791.

Pannier, G., Chai, C.K., 2013. Novel polymers. European Patent 2012/074792.

Ramkumar, D.H.S., Bhatacharya, M., 1998. Steady shear and dynamic properties of biodegradable polyesters. Polymer Engineering and Science 38, 1426-1435.

Rasal, R.M., Janorkar, A.V., Hirt, D.E., 2010. Poly(lactic acid) modifications. Progress in Polymer Science 35, 338-356.

Roa, J.P., Patrício, P.S.D.O., Oréfice, R.L., Lago, R.M., 2013. Improvement of the thermal properties of poly(3-hydroxybutyrate) (PHB) by low molecular weight polypropylene glycol (LMWPPG) addition. Journal of Applied Polymer Science 128, 3019-3025.

Ryan, C.M., Hartmann, M.H., Nangeroni, J.F., 1997. Branching of PLA to increase melt strength for extrusion coating, Polymers Laminations and Coatings Conference TAPPI Proceedings, pp. 139-144

Scandola, M., Pizzoli, M., Ceccorulli, G., Cesaro, A., Paoletti, S., L.Navarini, 1988. Viscoelastic and thermal properties of baterial poly(D-(-)-β-hydroxybutyrate). International Journal of Biological Macromolecules, 373-377.

Shroff, R., Mavridis, H., 1995. New measures of polydispersity from rheological data on polymer melts. Journal of Applied Polymer Science 57, 1605-1626.

Sijdergard, A., Niemi, M., Selin, J.-F., Ngisman, J.H., 1995. Changes in peroxide melt-modified poly(L-lactide). Industrial and Engineering Chemistry Research 34, 1203-1207.

Solarski, S., Ferreira, M., Devaux, E., 2005. Characterization of the thermal properties of PLA fibers by modulated differential scanning calorimetry. Polymer 46, 11187-11192.

Takamura, M., Nakamura, T., Kawaguchi, S., Takahashi, T., Koyama, K., 2010. Molecular characterization and crystallization behavior of peroxide-induced slightly crosslinked poly(L-lactide) during extrusion. Polymer Journal 42, 600-608.

Takamura, M., Nakamura, T., Takahashi, T., Koyama, K., 2008. Effect of type of peroxide on cross-linking of poly(l-lactide). Polymer Degradation and Stability 93, 1909-1916.

Wang, L., Zhu, W., Wang, X., Chen, X., Chen, G.-Q., Xu, K., 2008. Processability modifications of poly(3-hydroxybutyrate) by plasticizing, blending, and stabilizing. Journal of Applied Polymer Science 107, 166-173.

Wei, L., Guho, N.M., Coats, E.R., McDonald, A.G., 2014. Characterization of poly(3-hydroxybutyrate-co−3-hydroxyvalerate) biosynthesized by mixed microbial consortia fed fermented dairy manure. Journal of Applied Polymer Science 131. DOI: 10.1002/app.40333, in press.

Wei, L., McDonald, A.G., Freitag, C., Morrell, J.J., 2013. Effects of wood fiber esterification on properties, weatherability and biodurability of wood plastic composites. Polymer Degradation and Stability 98, 1348-1361.

Wood-Adams, P., Costeux, S.p., 2001. Thermorheological Behavior of Polyethylene Effects of Microstructure and Long Chain Branching. Macromolecules 34, 6281-6290.

Worzakowska, M., 2010. Succinic or glutaric anhydride modified linear unsaturated (epoxy) polyesters. Journal of Thermal Analysis and Calorimetry 101, 685-693.

Yamaguchi, M., Arakawa, K., 2006. Effect of thermal degradation on rheological properties for poly(3-hydroxybutyrate). European Polymer Journal 42, 1479-1486.

Yu, L., Dean, K., Li, L., 2006. Polymer blends and composites from renewable resources. Progress in Polymer Science 31, 576-602.

Yu, L., Toikka, G., Dean, K., Bateman, S., Yuan, Q., Filippou, C., Nguyen, T., 2013. Foaming behaviour and cell structure of poly(lactic acid) after various modifications. Polymer International 62, 759-765.

Zeichner, G.R., Patel, P.D., 1981. A comprehensive evaluation of polypropylene melt rheology, The 2nd World Congress of Chemical Engineering, Montreal, Canada, pp. 333-337.

Chapter 5. Grafting of bacterial poly(3-hydroxybutyrate) (PHB) onto cellulose via *in-situ* reactive extrusion with dicumyl peroxide

5.1 Abstract

Poly(3-hydroxybutyrate) (PHB) was grafted onto cellulose fiber by dicumyl peroxide (DCP) radical initiation via *in-situ* reactive extrusion. The yield of the grafted (cellulose-*g*-PHB) copolymer was recorded and grafting efficiency was found to be dependent on the reaction time and DCP concentration. The grafting mechanism was investigated by electron spin resonance (ESR) analysis and showed the presence of radicals produced by DCP radical initiation. The grafted copolymer structure was determined nuclear magnetic resonance (NMR) spectroscopy. Scanning electronic microscopy (SEM) showed that the cellulose-*g*-PHB copolymer formed a continuous phase between the surfaces of cellulose and PHB as compared to cellulose-PHB blends. The relative crystallinity of cellulose and PHB were quantified from Fourier transform infrared (FTIR) spectra and X-ray diffraction (XRD) results, while the absolute degree of crystallinity was evaluated by differential scanning calorimetry (DSC). The reduction of crystallinity indicated the grafting reaction occurred not just in the amorphous region but also slightly in crystalline regions of both cellulose and PHB. The smaller crystal sizes suggested the brittleness of PHB was decreased. Thermogravimetric analysis (TGA) showed that the grafted copolymer was stabilized relative to PHB. By varying the reaction parameters the compositions (%PHB and %cellulose) of resultant cellulose-*g*-PHB copolymer are expected to be manipulated to obtain tunable properties.

5.2 Introduction

Cellulose is the most abundant naturally occurring biopolymer and has received a great deal of attention due to its good mechanical properties, chemical reactivity, and being a renewable resource (Carlmark et al., 2012; Roy et al., 2009). The physical and chemical properties of cellulose greatly depend on its specific structure. Cellulose is a homopolymer of repeating 1→4 glycosidic linked β-D-glucopyranose units (Kadla and Gilbert, 2000). The hydroxyl groups on cellulose contribute to the high chemical reactivity of the

glucopyranosyl rings and also tend to form extensive intra- and inter-molecular C−H···O hydrogen bonds (Klemm et al., 2005; Roy et al., 2009). The hydrogen bonding is responsible for the crystalline nature of cellulose fibers resulting in its high tensile strength (~18 GPa) and modulus (~138 GPa) (Nishino et al., 2004). The properties of cellulose make it a suitable reinforcement in biocomposite materials when the density of that is not a concern and become an attractive environmentally friendly material towards a sustainable/green society (Nishino et al., 2004; Wambua et al., 2003; Wittek, 2008). Meantime, the lack of thermoplasticity and highly hydrophilicity make it not desirable for some applications.

Great efforts have been carried out to modify the properties of cellulose by imparting the desired and targeted properties of polymers onto cellulose (or its derivatives) through the method, namely "grafting copolymerization". The graft copolymerization approaches are summarized into two classes, "grafting-onto" and "grafting-from" (Carlmark et al., 2012; Roy et al., 2009). The later strategy, such as the ring-opening copolymerization of poly(lactic acid) (PLA) or poly(ε-caprolactone) (PCL) with cellulose (Habibi et al., 2008; Lönnberg et al., 2006), radical (irradiation initiation) initiated by *in-situ* polymerization of monomer onto cellulose (Liu and Sun, 2008; Oh et al., 2009; Zoppe et al., 2010), and ion-initiated polymerization (Gupta and Khandekar, 2003; Gupta et al., 2002), has been extensively studied and reported. However, the former strategy is scarcely studied due to the low reactivity of solid cellulose and relatively low grafting density, and the characterization is difficult (Carlmark et al., 2012; Roy et al., 2009).

Poly(3-hydroxybutyrate) (PHB) and poly(3-hydroxybutyrate-co-3-hydroxyvalerate) (PHBV) are the two major members of the polyhydroxyalkanoate (PHA) family, known for good biodegradability, biocompatibility and being bio-derived from renewable resources by bacterial synthesis (Chen and Patel, 2012; Chen and Wu, 2005). Therefore, PHAs have been used for biomedical applications including tissue engineering and bone replacement materials and also used in packaging materials and personal disposable articles (Chen and Wu, 2005; Mekonnen et al., 2013). However PHAs have some drawbacks, such as poor melt strength, low thermal stability, relatively high brittleness and production cost (Mekonnen et al., 2013). Our previous work using dicumyl peroxide to initiate the cross-linking of PHB

between tertiary carbon radicals found this method is successful to improve the melting processability and thermal stability, and meantime to reduce the crystallinity of the resultant cross-linked PHB by long-chain branching (Wei and McDonald, 2015). The degree of crystallinity was reduced significantly via this method; whereas documentation of grafting PHAs onto cellulose via grafting copolymerization is scarce. Samain and coworkers prepared PHA grafted onto cellulose by first transforming PHA into lower molecular weight oligomers (telechelic diols) and converted them into chloride oligomers which were then grafted onto cellulose in solution (Samain et al., 2011). Hence, developing an alternative grafting method which can easily be incorporated into an industrial process (e.g. extrusion) to retain their intrinsic properties, and enhance the compatibility between the polymer phases, triggered the research interest of this study.

In this work, low concentrations of dicumyl peroxide (DCP) radicals were generated at higher temperature and performed as initiator to graft PHB onto cellulose powder via *in-situ* reactive extrusion. Grafting parameters were calculated to evaluate the effects of reaction time and DCP concentration on the yield of grafted products. The radicals produced and chemical structures of resultant grafted copolymer were characterized by ESR and nuclear NMR spectroscopies, respectively, to investigate the possible grafting mechanism. FT-IR spectroscopy and XRD were used to investigate the crystallinity changes due to grafting, while thermal properties were characterized by DSC and TGA. The morphology of the polymeric materials was examined by SEM.

5.3 Experimental

5.3.1 Materials

Commercial cellulose fiber (CF1: Ø, 15–30 μm; length, 124–400 μm, Whatman), poly(3-hydroxybutyrate) (PHB: M_w = 290,000 g/mol, Tianan Biopolymer Inc., China), dicumyl peroxide (DCP) (98%, Sigma-Aldrich, USA), trifluoroacetic anhydride (TFAA, Oakwood Products, USA), acetone (99.5%, Macron Fine Chemicals, USA), $CHCl_3$ (J.T. Baker, USA), and $CDCl_3$ (D: 99.8%; Cambridge Isotope Labs. Inc., USA) were used as received.

5.3.2 Preparation of CF1-*g*-PHB and CF1-PHB blend

Vacuum dried PHB and CF1 were separately coated with DCP in acetone (4-8 mg/mL) for 30 min. To limit the formation of PHB homopolymers (Figure 5.1) a smaller portion of DCP was coated onto PHB as compared to CF1.

PHB (80%, 1.6 g) and CF1 (20%, 0.40 g) were dried and premixed in a beaker, resulting in a total DCP content between 2 and 5% (sample formulations are listed in Table 5.1). The CF1-*g*-PHB copolymer was prepared in a Dynisco Lab Mixer Molder/Extruder (LMM) by the reactive extrusion process. The blended materials were placed in the LMM at 175 $^{\circ}$C and mixed for a defined period of reaction time (t_R, 5 to 15 min) and then extruded into strands (1 mm Ø) or injection molded into rectangular bars (60 x 9 x 2 mm^3). Blends of CF1 and PHB (CF1-PHB, without addition of DCP) were prepared as control strand and rectangular bar samples. To optimize the reaction conditions, the extruded copolymerized strands were Soxhlet extracted with $CHCl_3$ for 24 h to dissolve any non-reacted PHB, and then filtered through a nylon screen to collect the crude gel products. The pore size of the screen was about 450 μm which was sufficient to allow the non-reacted CF1 to pass through, and the gel left on the screen was considered to be the true CF1-*g*-PHB copolymer. The gel was vacuum dried and gel yield (gel%) was calculated from:

$$\text{gel\%} = W_{drygel}/W_0 \times 100 \qquad \text{(eq. 5.1)}$$

where W_{drygel} and W_0 are the dry weights of the isolated copolymer gel and the strand samples before extraction, respectively. The t_R will be optimized based on maximum gel% and that time will be called t_{max}.

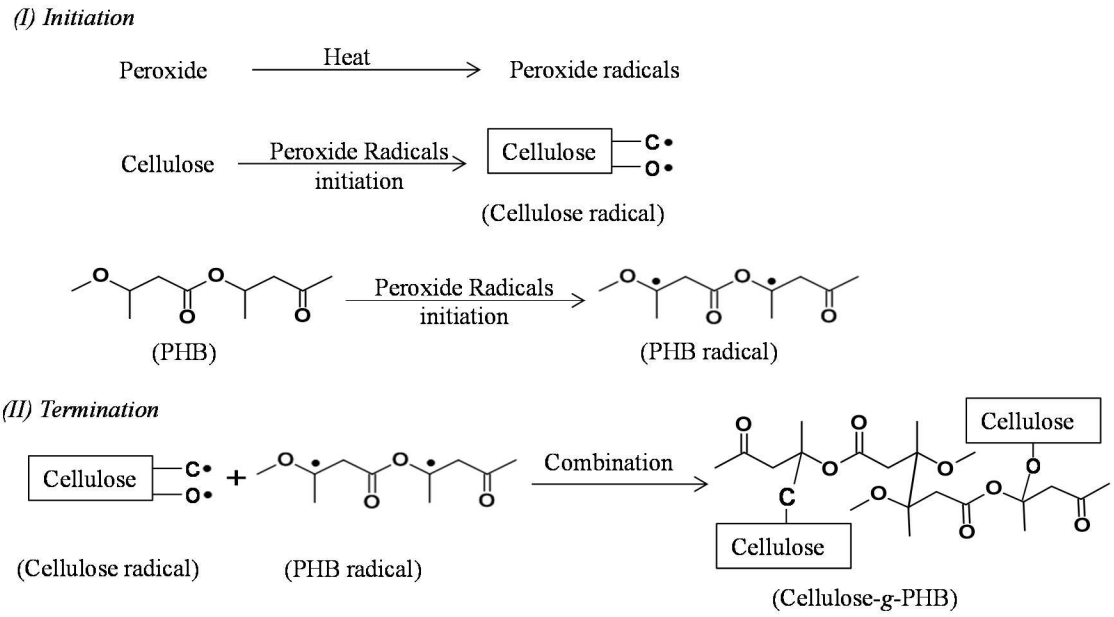

Figure 5.1. The general mechanism of peroxide radical initiated grafting of PHB onto cellulose.

Table 5.1. Summary of conditions for PHB and cellulose treatment and reaction parameters

Sample[a]	DCP in CF1 (wt%)	DCP in PHB (wt%)	Total DCP (wt%)	t_R (min)
2CGP5	1	1	2	5
2CGP10	1	1	2	10
2CGP15	1	1	2	15
3CGP5	2	1	3	5
3CGP10	2	1	3	10
3CGP15	2	1	3	15
4CGP5	3	1	4	5
4CGP10	3	1	4	10
4CGP15	3	1	4	15
5CGP5	3	2	5	5
5CGP10	3	2	5	10
5CGP15	3	2	5	15

[a] XCGPY, where X is the concentration of total DCP (2, 3, 4 and 5 %); CGP: CF1-*g*-PHB; Y is reaction time (5, 10 and 15 min).

5.3.3 Grafting parameters

The graft percentage (%GP), weight percent of grafted polymer with respect to initial weight of cellulose; the graft efficiency (%GE), weight % of PHB grafted onto cellulose backbone; and weight conversion (%WC), weight % of cellulose grafted were calculated according to eqs. 5.2 to 5.4:

$$\%GP = (W_{gf} - W_{CF1})/W_{CF1} \times 100 \quad \text{(eq. 5.2)}$$

$$\%GE = (W_{gf} - W_{CF1})/W_{PHB} \times 100 \quad \text{(eq. 5.3)}$$

$$\%WC = W_{gf}/W_{PHB} \times 100 \quad \text{(eq. 5.4)}$$

where, W_{gf}, W_{CF1} and W_{PHB} are the weights of the grafted copolymer recovered after Soxhlet extraction,

5.3.4 ESR spectroscopy

Radicals present in cellulose and PHB were studied by ESR spectroscopy (Bruker EMX Plus Spectrometer (X-band)). Extruded strands were immediately placed in liquid nitrogen and ground in a mortar and particles transferred into an ESR tube standing in liquid nitrogen. ESR spectra were recorded at room temperature after thawing the samples. The instrumental parameters were as follows: microwave power, 2 mW; microwave frequency, 9.87 GHz; modulation frequency, 100 kHz; time constant, 5 ms. Data were acquired and processed using WinEPR software.

5.3.5 Acetylation of CF1 and CF1-*g*-PHB

CF1 (1 g) and CF1-*g*-PHB (1 g) were acetylated with acetic acid (1 mL) and TFAA (2 mL) at 50 $^{\circ}$C for overnight. The acetylated CF1 and CF1-*g*-PHB products were precipitated out with cold ethanol, filtered and dried under vacuum until constant weight.

5.3.6 NMR spectroscopy

Acetylated CF1 and CF1-*g*-PHB samples were dissolved in $CDCl_3$, and ^{1}H, ^{13}C NMR, DEPT-135 and ^{1}H-^{13}C HSQC spectra were recorded on an Advance Bruker 500 MHz

spectrometer at 27 °C. TMS was used as the internal reference for chemical shift. Spectra were analyzed using SpinWorks v3.1.7 software.

5.3.7 Scanning electron microscopy

The copolymerized CF1-*g*-PHB and CF1-PHB blend bar samples were microtomed into 100 μm thick specimens and lightly coated with carbon (bottom layer) and gold (surface layer) and analyzed at 3-4.5 kV at 500x on a LEO Gemini field emission SEM.

5.3.8 X-ray diffraction

CF1, PHB and ground CF1-*g*-PHB samples were characterized by XRD (Siemens D5000 diffractometer). The system was set up with a rotating Cu Kα2 X-ray tubes operating at 40 kV with a current density of 30 mA at room temperature. Scanning was performed over the 2θ ranging from 5 to 50° with steps of 0.2°. The diffractograms were analyzed using IGOR Pro v6 software. The crystallinity index of cellulose CF1 (CrI_{CF1}) was determined from the ratio of the integral intensities of crystalline portions to the total intensity of sample according to the method of Segal et al. (Segal et al., 1959):

$$CrI_{CF1} = (1 - (I_{am}/I_{002})) \times 100 \qquad \text{(eq. 5.5)}$$

where I_{am} is the intensity of the peak at $2\theta = 18^{\circ}$, I_{002} is the maximum intensity of the (002) plane diffraction, respectively.

The PHB crystallinity index was calculated according to:

$$CrI_{PHB} = I_{17}/I_{total} \times 100 \qquad \text{(eq. 5.6)}$$

where I_{17} is the intensity of the peak close to $2\theta = 17^{\circ}$, I_{total} is the total intensity of all crystalline peaks of PHB.

The crystal size dimension D_{hkl} was evaluated by Scherrer's formula (Alexander, 1969):

$$D_{hkl} = K \times \lambda / (\beta_{1/2} \times \cos\theta) \qquad \text{(eq. 5.7)}$$

Where K is the crystal shape constant, λ is the X-ray wavelength (λ = 0.1542 nm, $\beta_{1/2}$ is the

peak full width at half of maxima intensity (FWHM = 2 Deg.) obtained by IGOR Pro, when peak fitting was conducted with Gaussian function, and θ is the diffraction angle.

5.3.9 FTIR spectroscopy

CF1, PHB and CF1-*g*-PHB were characterized by FTIR spectroscopy using a Thermo Nicolet IS5 FTIR spectrometer (ZnSe attenuated total reflection (ATR) probe (iD5)). Samples (in triplicate) were analyzed after vacuum drying. The absorbance spectra were averaged and baseline corrected using Omnic v9.0 software (Thermo scientific).

Total crystallinity index (TCI) of CF1, the PHB carbonyl index ($I_{PHB/C=O}$) and PHB crystallinity index ($I_{PHB/C-O}$) of PHB before and after grafting were calculated as follows:

$$TCI = A_{1370}/A_{2900} \quad \text{(eq. 5.8)}$$

$$I_{PHB/C=O} = A_{1720}/A_{1740} \quad \text{(eq. 5.9)}$$

$$I_{PHB/C-O} = A_{1230}/A_{1453} \quad \text{(eq. 5.10)}$$

where A_{1370} and A_{2900} are the areas of cellulose CF1 peaks at 1370 and 2900 cm^{-1}, respectively, and A_{1230}, A_{1453}, A_{1720} and A_{1740} are the areas of the peaks at 1230, 1453, 1720 and 1740 cm^{-1} from PHB molecular chains, respectively. All band areas were determined by peak fitting processing using IGOR Pro software (Wei et al., 2013). Gaussian functionality was employed for peak fitting using a peak width at half height value of 19 cm^{-1}.

5.3.10 Thermal analysis

DSC was performed using a TA Instruments model Q200 DSC with refrigerated cooling. The samples were (i) equilibrated at 40 ˚C (3 min) then ramped to 180 ˚C at 10 ˚C/min, held isothermally for 5 min to remove any thermal history (ii) cooled to -50 ˚C at the rate of -10 ˚C/min and held isothermally for 3 min and (iii) reheated to 180 ˚C at 10 ˚C/min to record the heating scan. Data were analyzed using TA Universal Analysis v4.4A software.

TGA was conducted using a Perkin-Elmer TGA-7 instrument at a heating rate of 10 ˚C/min under nitrogen atmosphere (30 mL/min). The energy of activation for the decomposition of

samples will be calculated with fraction (α) decomposed at different temperatures from the derivative thermogravimetric (DTG) results based on the eq. 5.11 (Gupta et al., 2002):

$$\ln \ln(1-\alpha)^{-1} = 100\ E_a/(R T_s^2)/(T_f - T_i)(\theta) + C \qquad \text{(eq. 5.11)}$$

where T_i and T_f are the initial and final decomposition temperatures and have been taken as points of deviation from baseline in the differential temperature (DTG) curve above the dehydration temperature. The θ is the difference of decomposition temperature (T) and temperature of reference (T_s). The plot between the reciprocal of the double logarithmic (1-α) versus temperature deference (T-T_s) enabled calculation of the value of activation energy of the sample.

5.4 Results and discussion

5.4.1 Reaction time optimization and grafting efficiency

The CF1-*g*-PHB sample formulations are given in Table 5.1. The influence of two factors (DCP concentration and t_R) was investigated to allow us to tailor the grafting efficiency between PHB and CF1 through controlling the initiator (free peroxide radicals) density on the surface (Table 5.2). The copolymer was extracted with $CHCl_3$ to remove any non-reacted PHB or smaller homopolymers, and then filtered to remove non-grafted CF1. The dry weight of the gels was recorded and the gel% calculated and used to optimize the reaction parameters (t_R and DCP concentration). The 3D plot of gel% (Figure 5.2), t_R and DCP concentration showed the gel% was decreased dramatically with time (from 5 to 15 min) because the peroxide radical's half-life is short (< 3 min at 175°C) (Dannenberg et al., 1958). Another possible reason to cause this reduction could be the degradation/dissociation of PHB with time. The grafted sample 2CGP5 gave the highest gel content of 48% followed by 2CGP10 (gel%=40.0), 4CGP5 (gel%=35.3) and 5CGP5 (gel%=31.6). Similar trends have been seen for %GP, %GE and %WC which are summarized in Table 5.2. The grafting efficiencies through this method were comparable to the grafting of low molecular weight PHBV onto chitosan via a condensation reaction in solvent (Arslan et al., 2007). The values of %GP, %GE and %WC were shown to decrease with DCP concentration (> 2%), indicating that the grafting takes place just primarily at the surface of cellulose and PHB. At

2% DCP sufficient quantities of radicals were available to graft PHB and CF1. Another possible explanation for this decrease in gel content with DCP concentration is that a higher level of cross-linking may occur between PHB chains than grafting between cellulose and PHB, contributing to DCP's higher mobility with PHB when melting.

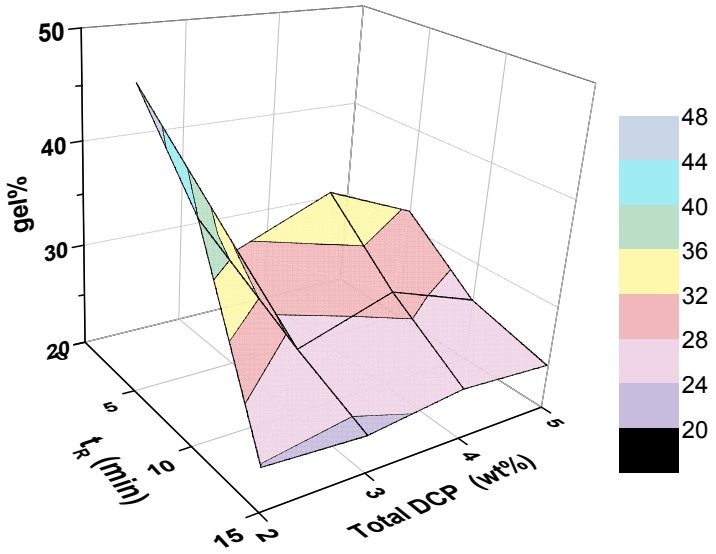

Figure 5.2. Effect of t_R (min) and total DCP concentration on the graft yield (gel%) of CF1 and PHB (CF1, 0.5g; PHB, 2g; temperature = 175 °C).

Table 5.2. Summary of grafting parameters (graft percentage (%GP), graft efficiency (%GE) and weight conversion (%WC)) for the CF1-*g*-PHB copolymers (the standard deviation values from three replicated is shown in the parentheses)

Sample	%GP	%GE	%WC
2CGP5	139.3 (3.4)	34.8 (0.8)	59.8 (0.8)
2CGP10	100.2 (2.4)	25.0 (0.5)	50.0 (0.6)
2CGP15	19.6 (6.4)	4.9 (0.6)	29.9 (1.6)
3CGP5	57.0 (2.5)	14.3 (0.6)	39.3 (0.6)
3CGP10	31.3 (1.5)	7.8 (0.5)	32.8 (0.6)
3CGP15	17.1 (0.5)	4.3 (0.1)	29.3 (0.1)
4CGP5	76.4 (5.9)	19.1 (1.5)	44.1 (1.5)
4CGP10	46.6 (4.4)	11.7 (1.0)	36.6 (1.1)
4CGP15	23.5 (0.9)	5.9 (1.5)	30.9 (1.5)
5CGP5	58.1 (0.2)	14.5 (0.0)	39.5 (0.0)
5CGP10	31.0 (2.8)	7.7 (0.6)	32.8(0.6)
5CGP15	20.9 (4.3)	5.2 (0.6)	30.2 (1.1)

5.4.2 Reaction mechanism, structure and morphology characterization

From Figure 5.2 and Table 5.2 the grafting reaction primarily occurred in the first 5 min (t_{max} = 5 min), due to the short life of DCP radicals and the grafting efficiency was dependent on DCP content. Hence, a moderate peroxide content (5% DCP) was used and the grafted sample was collected at time t = 4 min (< t_{max}). It is worth noting that the samples collected in this way were expected to contain sufficient amounts of both cellulose and PHB radicals to be readily detected by ESR. For comparison purposes PHB + DCP (2%) and CF1 + DCP (2%) were each heated to 175 °C (4 min), then quenched in liquid nitrogen, and analyzed by ESR. Figure 5.3 shows the ESR spectra of radical species in PHB, CF1 and CF1-*g*-PHB (5CGP4: 5% DCP & reaction for 4 min). The observation of signals confirms the free radicals were formed. The major signals of the CF1-*g*-PHB sample (Figure 5.3c, pointed •) were similar to that of PHB + DCP (Figure 5.3a), but were of higher relative intensity (by 20%). This increase was most likely from the addition of cellulose radicals in the sample. The proposed free radical sites on PHB and CF1 based on ESR spectral analysis are shown in Figure 5.3d-2f. For PHB, the peroxide radicals preferentially attack the tertiary protons (Takamura et al., 2008; Zhou and Zhu, 1997), which will show hyperfine splitting from 2 H_{β}'s and 3 $H_{\beta'}$'s; however, weak splitting (mixture of triplet + quartet, highlighted in Figure 5.3a and 2c as ○, Δ and ♦) were seen. As for the cellulose radical sites (Figure 5.3e), they are classified in two major groups: (i) carbon radicals formed on the glucopyranose ring (C_1 to C_6 positions) and (ii) alkoxy groups formed when the protons of –OH groups were abstracted (Saiki et al., 2011). Hence, the cellulose ESR spectrum showed a more complicated pattern. Whereas the weak splitting pattern of the signal centered at g = 2.003 looks like a triplet; it was therefore speculated that the C_6 radical was the dominant species (Figure 5.3f). Although the ESR simulations are typically used to confirm and determine the radicals environments, in this study the hyperfine coupling constant (Hfcc) could not be obtained precisely due to the weak minor signals. Furthermore, it should also point out that the radical concentration decays more rapidly at room temperature, and thus simulation was not performed. Further efforts are required to monitor the grafting reaction by ESR at high temperature (e.g. 175 °C). Therefore, ESR results confirmed the mechanism postulated in Figure 5.1 that DCP radicals formed at high temperature were capable to initiate the

cellulose and PHB radical formation in the solid state.

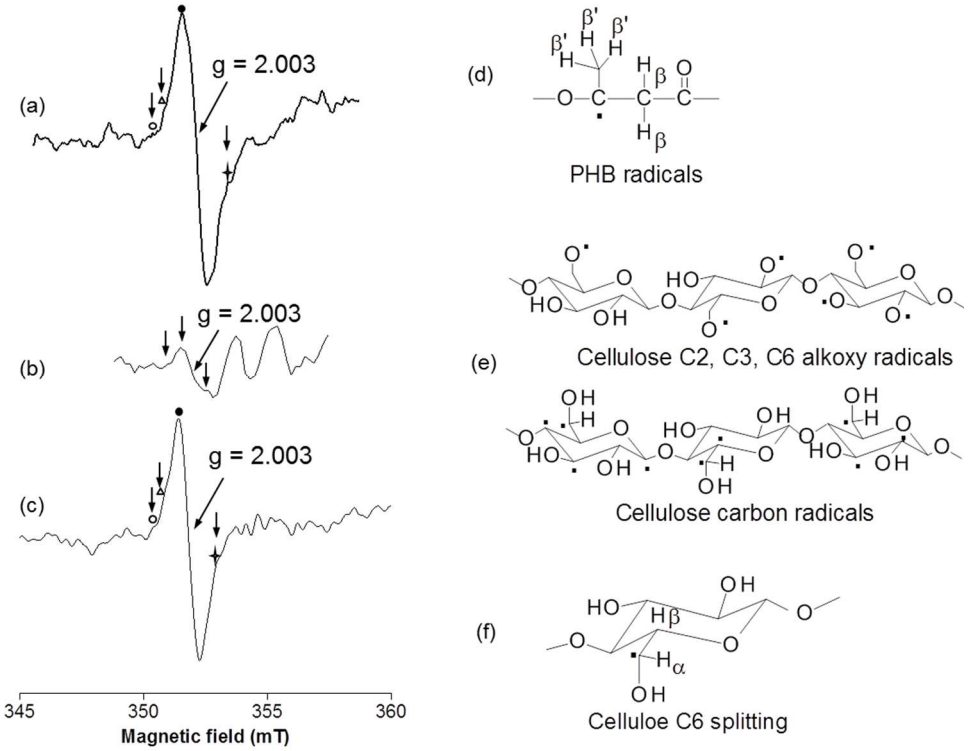

Figure 5.3. ESR spectra of (a) PHB + DCP (2%), (b) CF1 + DCP (2%), (c) PHB + CF1 + DCP (5%). The peak positions are marked (major peak: ●; minor peaks: Δ, ○, and ♦).

The chemical structures of CF1 and CF1-*g*-PHB, after acetylation, were also characterized by NMR spectroscopy. The ^{13}C NMR spectrum of acetylated CF1 (Figure 5.4a) showed the characteristic peaks of cellulose triacetate (VanderHart et al., 1996). The signals at δ = 100.70, 72.11, 72.75, 76.30, 73.09 and 62.27 ppm were assigned to the carbons on the glucopyranosyl ring at position C_1, C_2, C_3, C_4, C_5 and C_6, respectively. The CF1-*g*-PHB sample 2CGP10 was selected for structural analysis (Figure 5.4b). The spectrum of acetylated 2CGP10 showed all signals of acetylated CF backbone (C_1 to C_6) and C's of PHB chains at δ = 169.35, 67.84, 41.03 and 19.97 ppm corresponding to C_A, C_B, C_C and C_D, respectively, were observed. The strong DCP radicals generated at higher temperature have strong hydrogen abstraction ability, and then could attack the cellulose at different positions, for example, to assume that OH groups attached to C_2, C_3 and C_6 are attacked alkoxy radicals (C_2O•, C_3O• and C_6O•) will be produced, while scission of the cellulose 1,4-

glycosidic bond will form alkoxy and carbon radicals ($C_4O\bullet + C_1\bullet$), and if dehydrogenation occurred at C_1, C_5 and C_6 positions then $C_1\bullet$, $C_5\bullet$ and $\bullet C_6$,H−OH radicals will be produced. Tertiary carbons (−CH) on PHB will be attacked to form $C_B\bullet$ radicals. The free radicals formed on PHB and cellulose readily undergo secondary/binary terminations that new C_B−OC bonds (e.g., C_B−OC_2, C_B−OC_3, C_B−OC_4 and C_B−OC_6) and C_B-C bonds (e.g., C_B−$C_1\bullet$, C_B−C_5 and C_B−C_6,HOH) will be formed. However, the –OH groups at position C_3 on cellulose are involved in intramolecular H bonding (−C_3−OH) with the pyranose ring oxygen, O_5, of the neighboring glucose ring, and similarly between −C_6−OH and O_2 of the neighboring ring. The intermolecular H bonding is formed between the hydroxyl groups on C_6 (−C_6−OH) and C_3 (−C_3−OH) of cellulose molecules that are located adjacently on the same plane (Roy et al., 2009). These –OH groups in the crystalline regions are less likely to be accessed by radicals; in other words, only hydroxyl groups and carbons in the amorphous regions or surfaces from the crystalline region will be initiated. ^{13}C NMR spectroscopic analysis of the acetylated CF1-*g*-PHB material will help establish possible sites of grafting. Figure 5.4b shows the ^{13}C spectrum of acetylated CF1-*g*-PHB containing the characteristic signals for cellulose triacetate (C_1 to C_6) plus signals for PHB. A new signal was observed at δ = 50.99 ppm possibly assigned to a carbon signal attached to alkoxy groups of CF1, giving a new carbon environment C−O. This newly produced carbon signal could be derived from two possible groups: (i) associated with the C_B signal of PHB position of C_B−OC_2, C_B−OC_3, C_B−OC_4 or C_B−OC_6, and therefore signal shift for grafted PHB would be observed; otherwise (ii) contributed by C_6, of C_B−C_6,H−OH.

To confirm the structure 2D HSQC (^1H-^{13}C) and DEPT-135 experiments were performed on acetylated 2CPG10 (Figure 5.5). The spectra indicated the new carbon signal (δ = 50.99 ppm) was directly attached to the strong proton signal at δ = 3.44 ppm. Furthermore, the DEPT-135 showed this carbon could be a tertiary carbon (−CH), meanwhile only when –CH is attached to a –OH group can give the proton signal showing at such high field (δ = 3.44 ppm). To summarize these pieces of information together the chemical structure of this new carbon should be contributed by C_6, of partial structure C_B−C_6,H−OH of the acetylated CF1-*g*-PHB (Figure 5.4b). This further provides evidence that one of the H's attached to C_6 of CF1 was attacked by peroxide radical that was postulated by ESR spectra (Figure 5.3) and

then to combine with C_B• of PHB to give the general copolymer structure (Figure 5.4b). This was reasonable because the atoms of –C_6H_2–OH has higher flexibility/movability in comparison to C_1 to C_5 of the glucopyranose ring (Hon and Shiraishi, 2001). From these results it was concluded that the *in-situ* peroxide radicals initiated copolymerization of PHB chains onto cellulose backbone was successful.

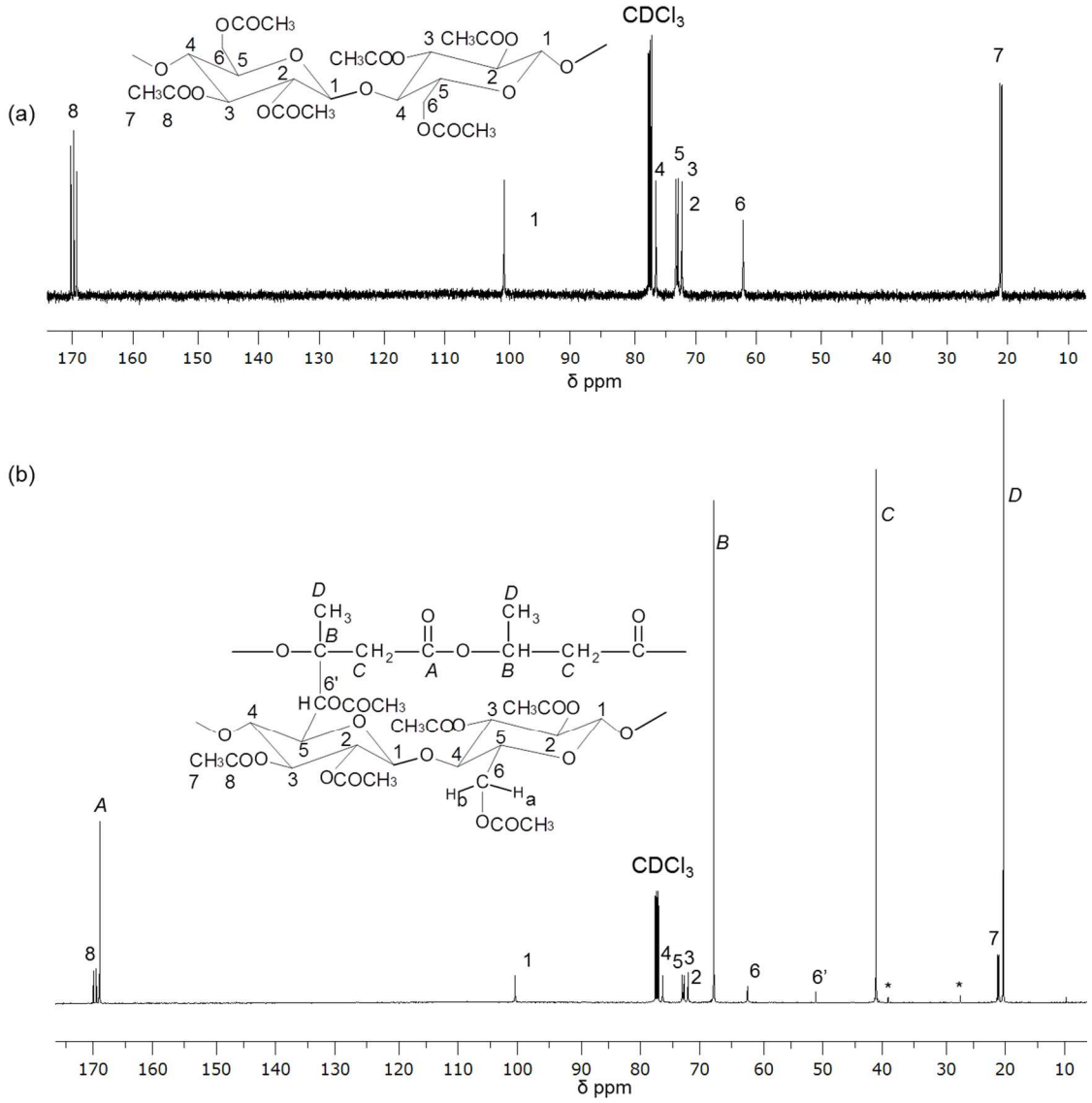

Figure 5.4. ^{13}C NMR spectra of (a) acetylated CF1 and (b) acetylated CF1-*g*-PHB (2CGP10). Note: the signals shown at δ = 38.9 and 27.1 ppm are from impurities of commercial PHB used.

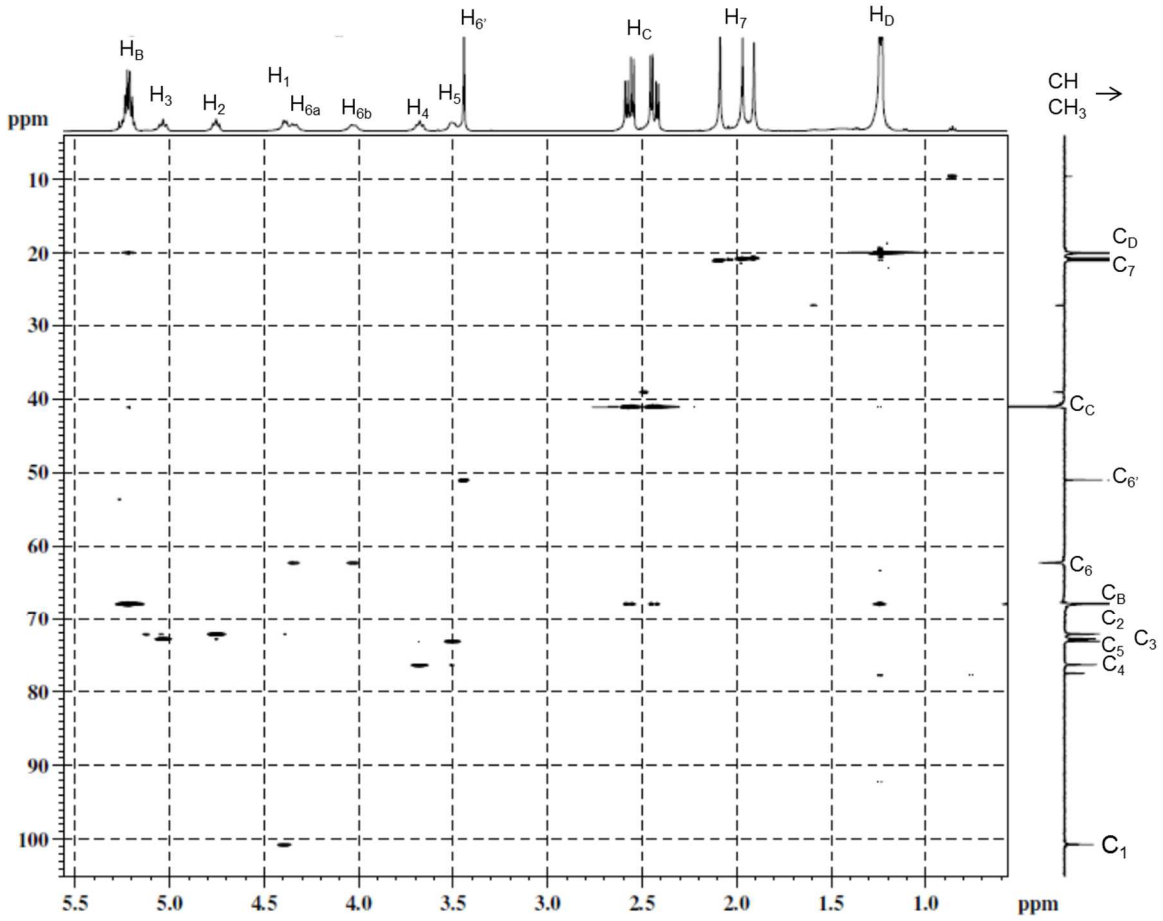

Figure 5.5. HSQC (^{1}H-^{13}C (DEPT-135)) spectra of acetylated CF1-*g*-PHB (2CGP10).

The SEM micrographs of the CF1 fiber showed a smooth surface (Figure 5.6a). After DCP treatment for 10 min (Figure 5.6b), the CF1 surface became slightly rougher, which may provide access for PHB to attach onto during reactive extrusion. The reactive extruded CF1-*g*-PHB (2CGP10) showed CF1 fibers encapsulated with a smooth layer of PHB suggesting that the PHB had grafted onto the cellulose surface (Figure 5.6c). In contrast, blends of CF1-PHB, as a non-grafted control, showed discrete zones of PHB and CF1 which was evidence of poor interfacial compatibility (Figure 5.6d). The literature indicated peroxide treated sisal cellulose fibers had better compatibility with a polyethylene matrix.(Joseph and Thomas, 1996)

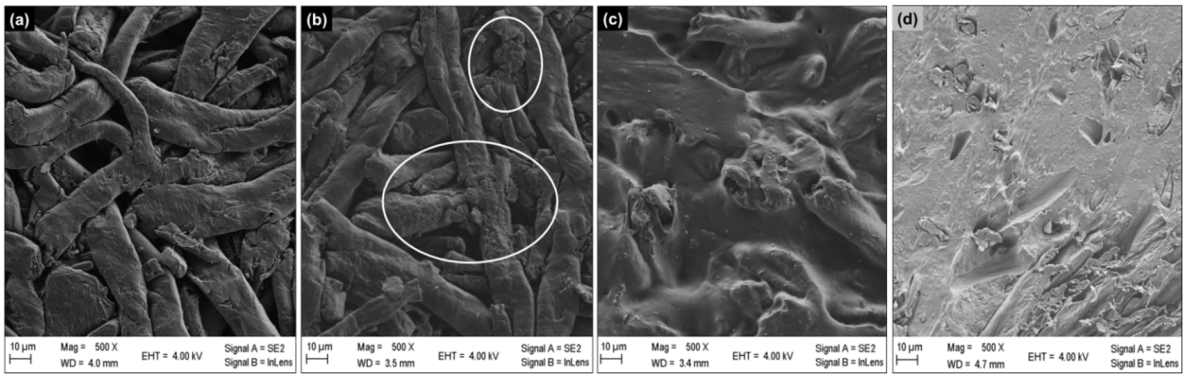

Figure 5.6. SEM micrographs (500x) of (a) CF1, (b) DCP treated CF1, (c) CF1-*g*-PHB (2CGP10), and (d) melt blended CF1-PHB control biocomposite.

5.4.3 Thermal analysis

The thermal stability of CF1-*g*-PHB was found to be higher than PHB and CF1-PHB blend as shown in TG and DTG curves (Figure 5.7). The onset temperature (T_{onset}) of degradation for the CF1-*g*-PHB (2CGP10) sample was 22 $^{\circ}$C higher than that of PHB (275 $^{\circ}$C). The T_{onset} for the CF1-PHB blend was close to PHB, and 80% of the sample degraded in the first stage contributed to the degradation of PHB which agrees to the formulation (CF1:PHB = 1:4). This indicated the simple blending of these two materials didn't improve the thermal stability of PHB. The temperature of maximum decomposition rate (T_{max}) in sample 2CGP10 was 20 $^{\circ}$C higher than T_{max} of PHB (300 $^{\circ}$C). During this degradation stage, PHB was completely decomposed at T = 313 $^{\circ}$C, while ca. 70% of the 2CGP10 sample was degraded at T $\leq$ 349 $^{\circ}$C followed by the second stage (349 $^{\circ}$C to 380 $^{\circ}$C) due to the degradation of cellulose CF side (Figure 5.7: TG curves). The final decomposition temperature (T_f) of the CF1-*g*-PHB was also increased to 478 $^{\circ}$C due to grafting. However, the 2CGP10 copolymer was less stable than CF1, which may be attributable to having low cellulose content and/or some degradation or modification to the cellulose structure during grafting. As discussed above the sample 2CGP10 only has 8% cellulose content, but showed a significantly improved thermal stability as compared to PHB and it could be postulated that the thermal stability of the grafted copolymer was increased with the increasing of cellulose content. This was further confirmed from the activation energy of decomposition of CF1, PHB and CF1-*g*-PHB copolymer calculated from eq. 5.11 with decomposed fraction

was obtained from DTG curves (Figure 5.7). The plot of $\ln[\ln(1-\alpha)^{-1}]$ vs. $(T-T_s)$ is shown in Figure 5.8. The activation energy (E_a) of CF1-*g*-PHB was 174 kJ/mol and was higher than PHB (108 kJ/mol) and CF1-PHB blend (135 kJ/mol), but lower than cellulose (202 kJ/mol). This provided more evidence that the grafted copolymer increased the thermal stability of PHB. Through grafting more C-C bonds formed required higher energy input to activate the decomposition mechanism of the resultant copolymer.

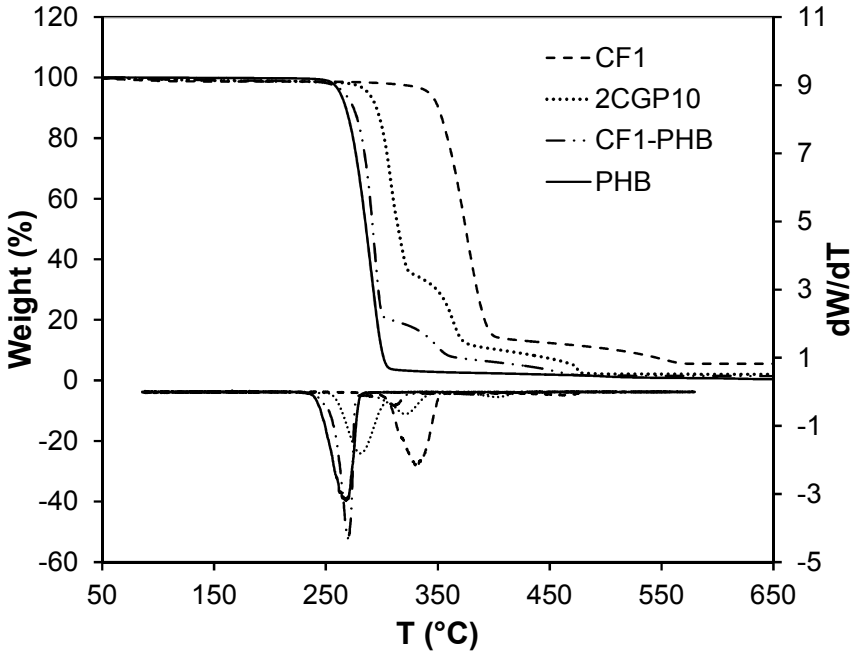

Figure 5.7. TGA and DTG curves of cellulose CF1, PHB, CF1-PHB blend, and CF1-*g*-PHB (2CGP10).

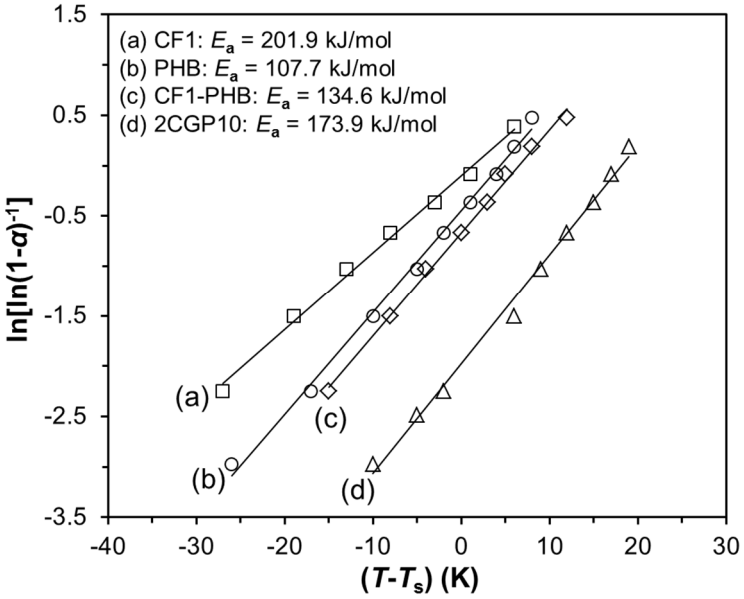

Figure 5.8. Plots of $\ln[\ln(1-\alpha)^{-1}]$ vs. $(T-T_s)$ of CF1, PHB, CF1-PHB blend and CF1-*g*-PHB (2CGP10) to determine their E_a from DTG data.

PHB showed a glass transition (T_g) at about 4.5 °C, while the T_g's of all the CF1-*g*-PHB copolymers shifted to between 7 and 11 °C and varied slightly among samples initiated at different DCP contents. This increase in T_g was contributed to the restriction of PHB chains by the CF1 fiber surfaces and newly formed C-C bonds between amorphous PHB side chains and cellulose as well. Meantime, the ΔC_p was determined from DSC endothermic curves for each glass transition; using ΔC_p of pure PHB as a reference, the percentage of PHB (%PHB) present in the grafted copolymer was estimated by ΔC_p values (Table 5.3). The trend was similar to the grafting parameters results (Table 5.2) that 2CGP5 showed highest %PHB (88%) followed by 2CGP10 (87%), 4CGP5 (73%), 5CGP5 (69%) and 3CGP5 (60%). For the CF1-PHB blend the ΔC_p was 0.40 J/g/°C, close to 75% of the ΔC_p value of bulk PHB, which is consistent to the formulation (CF1:PHB = 1:4). This method was successfully used to estimate the poly(*N*-isopropylacrylamide) content in its grafted copolymer with cellulose nanocrystals (Zoppe et al., 2010). This indicated the composition of the grafted copolymer can be controlled by varying the reaction time and DCP concentration, and therefore the thermal stability, crystallinity and other properties are expected to be tunable.

Melting enthalpy, ΔH_m, was contributed to PHB fragment in the copolymer; hence the melt enthalpy used for the calculation of the degree of crystallinity was normalized, and then the absolute degree of crystallinity (X_c%) was calculated (see Table 5.3) according to Wei et. al. (2014). X_c% was lowered by grafting, indicating the PHB molecular chains aligned to form crystal structures which were hindered either by cellulose or by the slightly long chain branching of PHB homopolymer (Wei and McDonald, 2015). This agrees with an increased cold crystallization temperatures (T_c) of all grafted copolymers as compared to bulk PHB. A lower X_c%, requires less energy to move the polymer chains in the amorphous phase (Kurniawan et al., 2007), hence the crystallization of grafted copolymers from melts were initiated at higher temperature. However, for CF1-PHB blends a slight decrease in X_c% was observed, which would contribute to an increase of molecular motions of the amorphous phase of PHB and thus lead to a decrease in T_g. CF1-PHB blends showed double melting peaks as bulk PHB, and both of them shifted to higher temperatures, which could be attributed to the physical interaction between CF1 and PHB polymer matrix (Bengtsson et al., 2005). Unlike the bulk PHB and the CF1-PHB blend, only a single melting peak was observed at the lower endothermic position for all CF1-*g*-PHB copolymers. The double melting behavior was attributed to the lower stability of crystals showing at lower endothermic would recrystallize and remelt at higher temperature (Qiu et al., 2003a). Therefore, the grafting of PHB onto cellulose backbone reduced the recrystallization of original crystals with lower stability or defects. These thermal properties of the resulting grafted copolymer were tunable by varying the DCP content and reaction time.

Table 5.3. DSC results of PHB, CF1-PHB blends, and CF1-*g*-PHB copolymers

Sample[a]	T_g (°C)	ΔC_p (J/g/°C)	%PHB	ΔH_m (J/g)	X_c (%)	T_c (°C)	T_{m1} (°C)	T_{m2} (°C)
PHB	4.5	0.52	100	84.1	57.6	84.4	157.5	169.7
CF1-PHB	3.2	0.40	80	63.9	54.7	104.1	165.5	171.2
2CGP5	11.0	0.46	88	51.1	39.8	109.1	155.2	-
2CGP10	9.5	0.45	87	51.4	40.5	106.4	152.7	-
3CGP5	6.6	0.31	60	45.3	51.7	104.5	151.7	-
4CGP5	8.2	0.38	73	47.7	44.8	102.7	152.4	-
5CGP5	7.5	0.36	69	47.1	46.7	104.2	150.6	-

[a] Only CF1-*g*-PHB samples with %GE > 14% are listed.

5.4.4 Crystallinity Changes Due to Grafting

The degree of crystallinity of polymers and composite materials significantly affect their mechanical properties and processability as well, hence the crystalline nature of materials is important and can be obtained by a combination of FTIR and XRD techniques. Figure 5.9a showed the FTIR spectrum of the grafted copolymer (2CGP10) sample with characteristic absorbance peaks arising from either CF1 or PHB. The absorbance bands at 980, 1230, 1720 cm^{-1} were assigned to crystalline PHB (Xu et al., 2002), and intensities were reduced due to grafting. Whereas the shoulder showing at 1740 cm^{-1} of the band at 1720 cm^{-1} assigned to the carbonyl (C=O stretching) from amorphous region became more intense of grafted copolymer as compared to PHB (see Figure 5.9b). This observation further indicated the grafting of PHB onto cellulose hindered the crystallization of PHB from melts, resulting in more amorphous PHB. In addition, the band at 1429 cm^{-1} (symmetric $–CH_2$ bending) was characteristic of amorphous cellulose CF1, which appeared in the grafted copolymer, again supporting that grafting had occurred. The quantitative analyses of the FTIR spectra for PHB and cellulose were performed to further confirm that their crystallinity was reduced due to the grafting reaction. The spectral ratio of 1370/2900 cm^{-1} bands (total crystallinity index, TCI) was shown to be proportional to the crystallinity degree of cellulose (Åkerholm et al., 2004), while the band ratios 1720/1740 cm^{-1} (carbonyl index, $I_{PHB/C=O}$) (Yu et al., 2012) and 1230/1450 cm^{-1} (C-O index, $I_{PHB/C-O}$) reflect the crystallinity of PHB (Xu et al., 2002). Quantitative analysis of the infrared crystallinity ratios calculated from the peak fitted spectra of the carbonyl region (1800-1680 cm^{-1}) for PHB and the –C–H bending (centered at 1370 cm^{-1} from crystalline region, Figure 5.9c) for CF1. The analyzed data for PHB, CF1, CF1-PHB blend, and CF1-*g*-PHB copolymers (2CGP5 and 2CGP10) are given in Table 5.4. The incorporation of CF1 caused a reduction in PHB crystallinity of the CF1-PHB blend slightly, while grafting reduced all the three crystallinity indices significantly and these values are correlated to the graft efficiency. Grafting between cellulose and PHB acts as a coupling agent in these CF1-*g*-PHB materials, which would improve the stress transfer between the two phases.

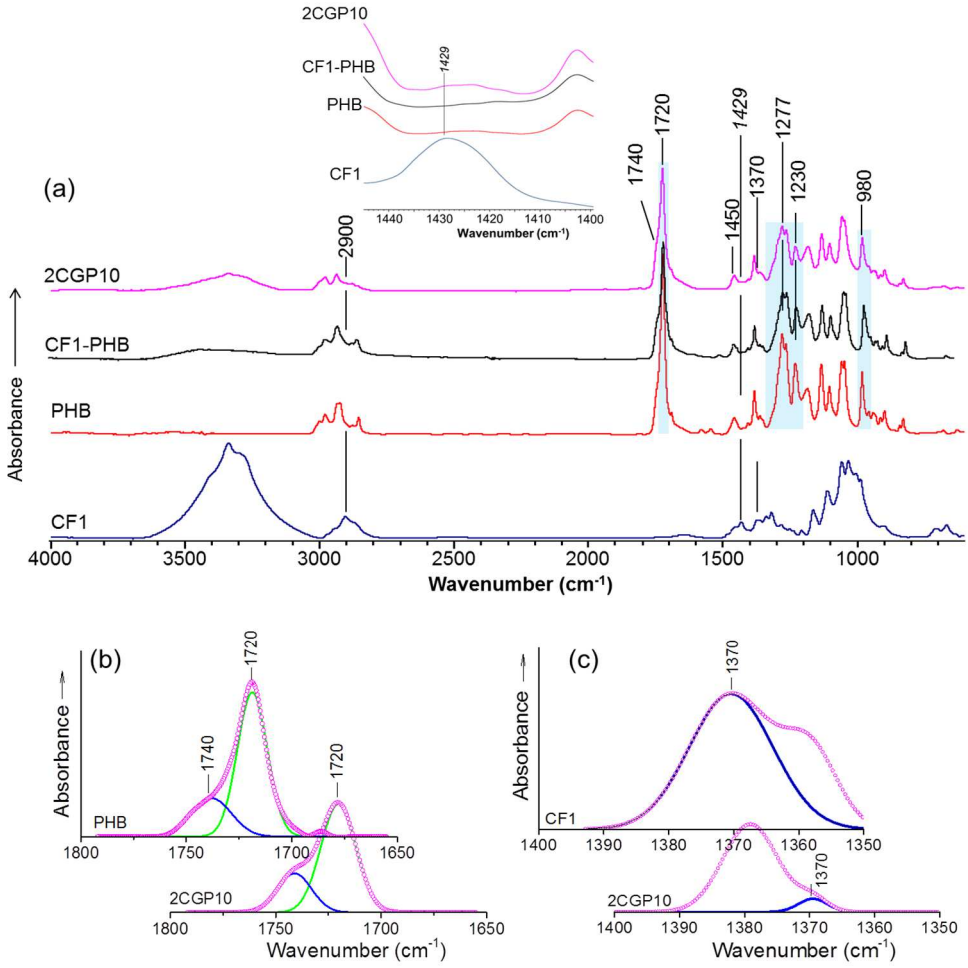

Figure 5.9. (a) Full and expanded region FTIR spectra for CF1, PHB and CF1-*g*-PHB sample 2CGP10; (b) carbonyl (C=O) fitted peaks for PHB and 2CGP10, and (c) –C–H bending (1370 cm^{-1}) fitted peaks for CF1 and 2CGP10.

The effect of the grafting on the crystalline structures of PHB and cellulose segments was further investigated. Vacuum dried samples were subjected to XRD analysis. The XRD diffractograms are shown in Figure 5.10. CF1 showed typical patterns of cellulose I; peaks showing at 2θ scale at 14.6˚, 16.8˚ and 22.8˚ were assigned to the planes of (101), (10-1) and (002), respectively. PHB had crystalline peaks at 13.7˚, 16.5˚, 20.2˚, 21.4˚, 22.4˚, 25.8˚ and 27.2˚, respectively, corresponding to planes of (020), (110), (021), (101), (121), (040), and (200) (Medvecky, 2012). All of these peaks appeared in the CF1-PHB blends and CF1-*g*-PHB products (2CGP5 and 2CGP10) only with lower intensity as compared to native cellulose and PHB. A similar behavior has been observed for bacterial cellulose and PHB

composite membrane in that the cellulose and PHB crystallinity were shown to affect each other (Barud et al., 2011). The Gaussian function was used for peak fitting of the XRD diffractograms, and therefore the FWHM values were obtained accordingly. Crystallinity indices were calculated from the ratios of fitted peak intensities, and crystal sizes according to Scherrer's formula using a shape constant $K = 0.9$ for both PHB and cellulose. These parameters are summarized in Table 5.4. Crystallinity index and average crystal width were 69% (CrI_{CF1}) and 267 Å (D_{002}) for CF1, and 62% (CrI_{PHB}) and 1309 Å (D_{020}) for PHB, respectively. For the CF1-PHB blend both the CF1 and PHB components showed lower crystallinity indices and crystal sizes. After grafting both crystallinity indices and crystal dimensions were reduced significantly and varied with grafting time (or efficiency) as highlighted between samples 2CGP5 and 2CGP10. This is consistent with the findings from FTIR and DSC analyses, which therefore further confirmed the crystallinity of PHB and cellulose were both reduced during this grafting approach. Smaller crystal sizes of the grafted products suggests that the formation of large crystals of either PHB or cellulose was hindered by each other, because the large crystal size of PHB was one of the most accepted reasons leading to its brittleness (De Koning and Lemstra, 1993). The decrease in cellulose crystallinity in sample 2CGP10 may be caused by the disruption of surface chains of the crystalline regions due to formation of radicals and reaction with PHB. To note, the CF1-PHB blend also had lower PHB and CF1crystallinity, which may be due to the hindrance of crystallization between them or the amorphous components of both cellulose and PHB with 2θ near to 17°. The similar trend was observed in bacterial cellulose and PHB composites (Barud et al., 2011). Nevertheless, the decreasing trend was more significant as a result of grafting suggesting that the grafted sites (C-C bonding) could limit the numbers of PHB chains involved in crystallization except for the physical interruption between them. It is therefore speculated that a limited number of peroxide radicals formed on surfaces of the crystalline phase of CF1 could be attached by PHB, resulting in more amorphous CF1.

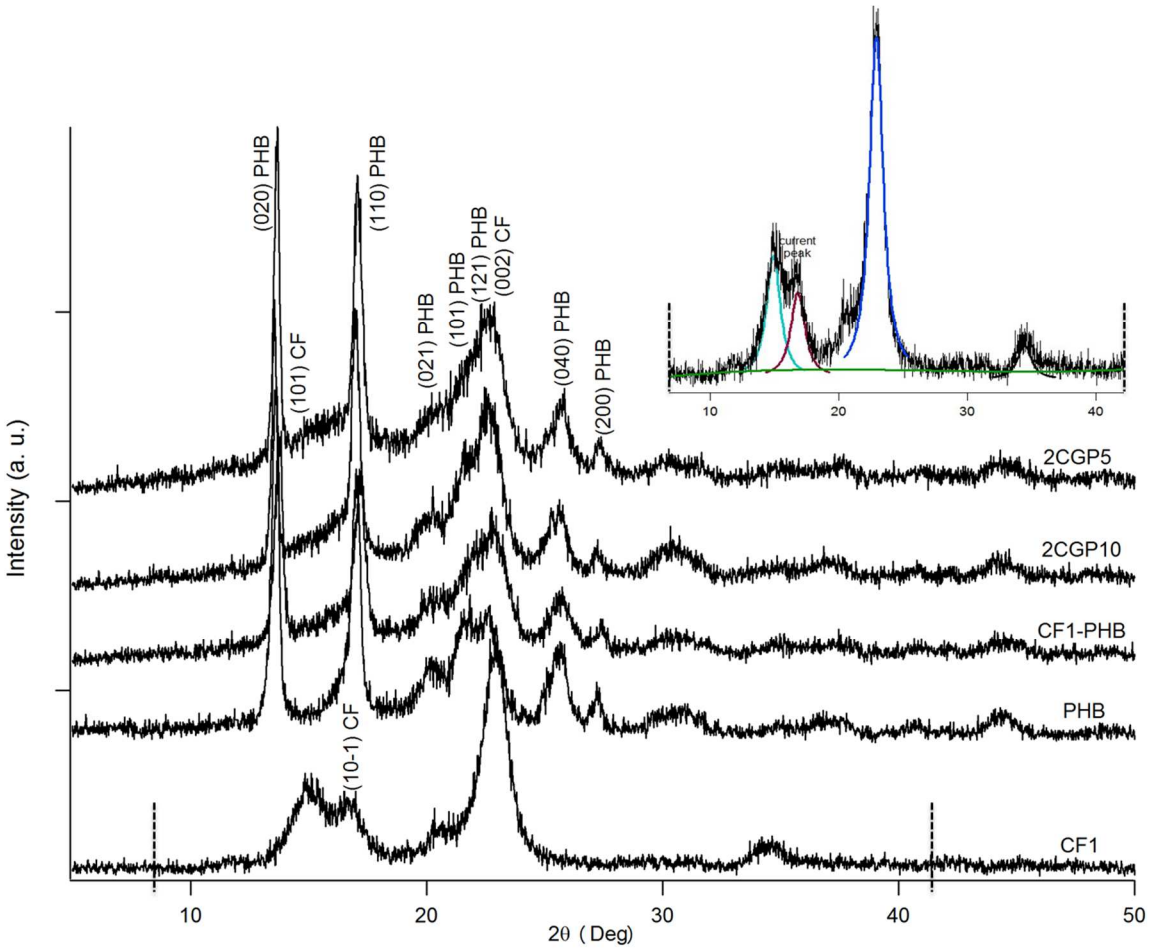

Figure 5.10. XRD diffractograms of CF1, PHB, CF1-PHB blend, and CF1-*g*-PHB (2CGP5 and 2CGP10) samples. The inset-plot shows an example (CF1) of peak fitting using IGOR Pro.

Based on the crystallinity changes, the possible grafted sites of CF1-*g*-PHB are proposed: (a) CF1 and melted PHB radicals are produced first (Figure 5.11a); (b) the radicals tend to be combined at the possible grafted sites and meantime PHB will crystallize when cools (Figure 5.11b). These grafted sites would impede or limit the crystallization of PHB from melts; thus, molecular chains with fewer grafted sites would crystallize when cooled from melts and accounted for the crystalline fraction, whereas molecular chains with more grafted sites would contribute to the amorphous component due to inhibited crystallization. As for CF1, the highly crystalline material with less mobility, only radicals generated on its surface of the crystalline and amorphous regions would be accessible to the molten PHB (with

radicals) would be able to produce the CF1-*g*-PHB copolymer. Hence, the grafting density was higher in the CF1 amorphous region. In addition, those grafted sites located on the surfaces of crystalline CF1 would also reduce the crystallinity index of the resultant CF1-*g*-PHB, which agrees with the SEM finding that peroxide treated CF1 surfaces looked different with the original cellulose.

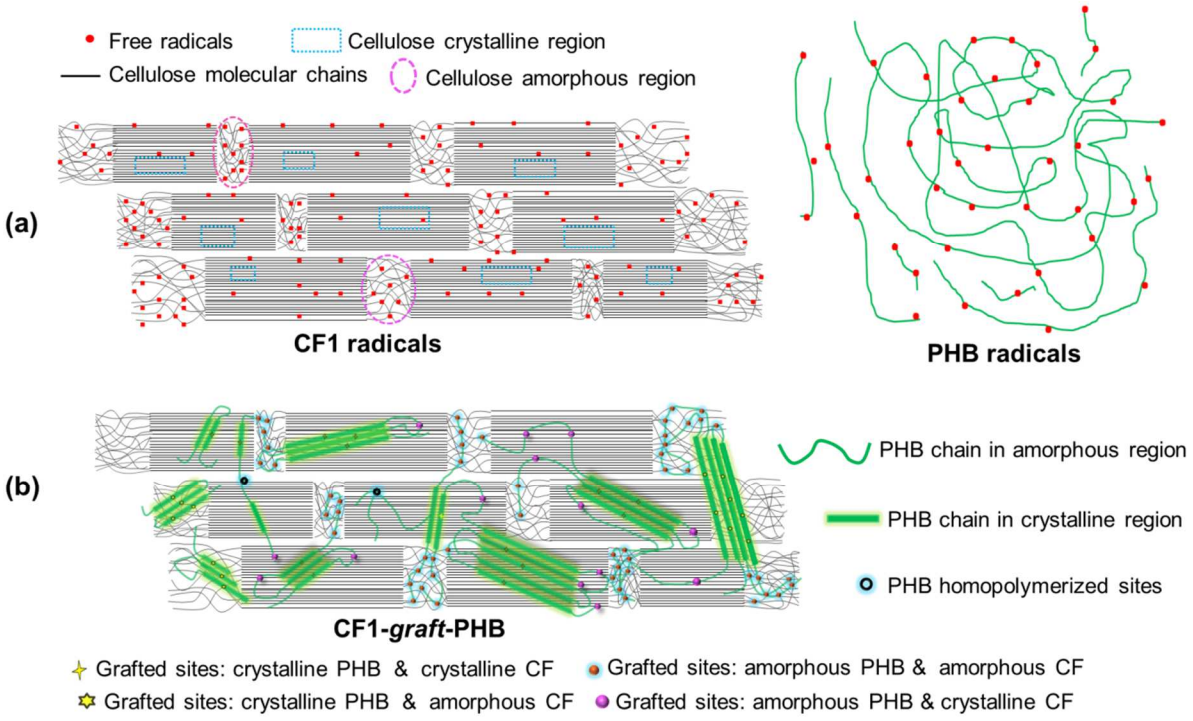

Figure 5.11. Schematic illustration of (a) possible structures showing radicals formed of CF1 and PHB melts, and (b) possible structure showing grafted sites (crystalline/amorphous) between CF1 and PHB of CF1-*g*-PHB. Note: PHB molecular chains with fewer grafted sites tend to crystallize from melt.

Table 5.4. Crystallinity parameters characterized by FTIR and WAXD[a].

Sample	TCI	$I_{PHB/C=O}$	$I_{PHB/C-O}$	CrI_{CF1}	CrI_{PHB}	D (002) (Å)	D (020) (Å)
CF1	0.30			69.2		267	
PHB		6.94	2.40		61.9		1309
CF1-PHB	0.27	5.69	1.95	50.9	47.9	245	1269
2CGP10	0.13	3.51	1.52	47.5	36.9	227	948
2CGP5	0.10	2.47	1.30	41.1	34.0	197	455

[a] Crystal sizes were determined in the direction perpendicular to the planes of (002) and (020) for cellulose CF and PHB, respectively.

5.5 Conclusions

In-situ radical initiation via reaction extrusion of PHB was successfully able to graft onto cellulose in a simple process. This "grafting-onto" strategy gave a reasonable grafting efficiency and the grafting efficiency (density) and copolymer composition were dependent on the reaction time and DCP concentration. The highest yield of grafted copolymer was obtained in 5 min with 2% DCP. ESR was used to confirm the presence of radical species on PHB-cellulose materials. The sites of grafting between PHB and cellulose were supported by NMR and confirmed the reaction mechanism as proposed from ESR findings. SEM indicated that the grafting reaction occurred between the surfaces of cellulose and PHB. Due to new bonds formed via grafting the thermal stability of PHB was improved. The crystallinity of the cellulose-PHB material was modified through grafting, which could introduce more flexibility to both cellulose and PHB. The properties of the CF1-*graft*-PHB materials (crystallinity and thermal stability) could be tuned by varying reaction conditions. This approach afforded cellulose reinforced bioplastic composite materials with improved properties by chemically linking the fibers with the matrix to improve stress transfer. This simple reactive extrusion process broadens the processing window for PHB and PHB based biocomposites and ultimately the applications these biomaterials can be used such as packaging and semi-structural profiles.

5.6 References

Åkerholm, M., Hinterstoisser, B., Salmén, L., 2004. Characterization of the crystalline structure of cellulose using static and dynamic FT-IR spectroscopy. Carbohydrate Research 339, 569-578.

Alexander, L.E., 1969. X-ray diffraction method in polymer science. Wiley-Interscience, New York.

Arslan, H., Hazer, B., Yoon, S.C., 2007. Grafting of poly(3-hydroxyalkanoate) and linoleic acid onto chitosan. Journal of Applied Polymer Science 103, 81-89.

Barud, H.S., Souza, J.L., Santos, D.B., Crespi, M.S., Ribeiro, C.A., Messaddeq, Y., Ribeiro, S.J.L., 2011. Bacterial cellulose/poly(3-hydroxybutyrate) composite membranes. Carbohydrate Polymers 83, 1279-1284.

Bengtsson, M., Gatenholm, P., Oksman, K., 2005. The effect of crosslinking on the properties of polyethylene/wood flour composites. Composites Science and Technology 65, 1468-1479.

Carlmark, A., Larsson, E., Malmström, E., 2012. Grafting of cellulose by ring-opening polymerisation – A review. European Polymer Journal 48, 1646-1659.

Chen, G.-Q., Patel, M.K., 2012. Plastics derived from biological sources: present and future: A technical and environmental review. Chemical Reviews 112, 2082-2099.

Chen, G.-Q., Wu, Q., 2005. The application of polyhydroxyalkanoates as tissue engineering materials. Biomaterials 26, 6565-6578.

Dannenberg, E.M., Jordan, M.E., M, H., 1958. Peroxide crosslinked carbon black polyethylene compositions. Journal of Polymer Science 31, 127-153.

De Koning, G.J.M., Lemstra, P.J., 1993. Crystallization phenomena in bacterial poly[(R)-3-hyd roxybutyrate]: 2. Embrittlement and rejuvenation. Polymer 34, 4089-4094.

Gupta, K.C., Khandekar, K., 2003. Temperature-responsive cellulose by ceric(IV) ion-initiated graft copolymerization of N-isopropylacrylamide. Biomacromolecules 4, 758-765.

Gupta, K.C., Sahoo, S., Khandekar, K., 2002. Graft copolymerization of ethyl acrylate onto cellulose using ceric ammonium nitrate as initiator in aqueous medium. Biomacromolecules 3, 1087-1094.

Habibi, Y., Goffin, A.-L., Schiltz, N., Duquesne, E., Dubois, P., Dufresne, A., 2008. Bionanocomposites based on poly(ε-caprolactone)-grafted cellulose nanocrystals by ring-opening polymerization. Journal of Materials Chemistry 18, 5002-5010.

Hon, D.N.-S., Shiraishi, N., 2001. Wood and cellulosic chemistry, Second Edition, Revised, and Expanded. Marcel Dekker, Inc., New York.

Joseph, K., Thomas, S., 1996. Effect of chemical treatment on the tensile properties of short sisal fibre-reinforced polyethylene composites. Polymer 37, 5139-5149.

Kadla, J.F., Gilbert, R.D., 2000. Cellulose structure: A review. Cellulose Chemistry and Technology, 197-216.

Klemm, D., Heublein, B., Fink, H.-P., Bohn, A., 2005. Cellulose: fascinating biopolymer and sustainable raw material. Angewandte Chemie International Edition 44, 3358-3393.

Kurniawan, L., Qiao, G.G., Zhang, X., 2007. Chemical modification of wheat protein-based natural polymers: grafting and cross-linking reactions with poly(ethylene oxide) diglycidyl ether and ethyl diamine. Biomacromolecules 8, 2909-2915.

Liu, S., Sun, G., 2008. Radical graft functional modification of cellulose with allyl monomers: Chemistry and structure characterization. Carbohydrate Polymers 71, 614-625.

Lönnberg, H., Zhou, Q., III, H.B., Teeri, T.T., Malmström, E., Hult, A., 2006. Grafting of cellulose fibers with poly(ε-caprolactone) and poly($_L$-lactic acid) via ring-opening polymerization, Biomacromolecules, pp. 2178-2185.

Medvecky, L., 2012. Microstructure and properties of polyhydroxybutyrate-chitosan-nanohydroxyapatite composite scaffolds. Scientific World Journal 2012, 1-8.

Mekonnen, T., Mussone, P., Khalil, H., Bressler, D., 2013. Progress in bio-based plastics and plasticizing modifications. Journal of Materials Chemistry 1, 13379-13398.

Nishino, T., Matsuda, I., Hirao, K., 2004. All-Cellulose composite. Macromolecules 37, 7683-7687.

Oh, J.K., Lee, D.I., Park, J.M., 2009. Biopolymer-based microgels/nanogels for drug delivery applications. Progress in Polymer Science 34, 1261-1282.

Qiu, Z., Ikehara, T., Nishi, T., 2003. Melting behaviour of poly(butylene succinate) in miscible blends with poly(ethylene oxide). Polymer 44, 3095-3099.

Roy, D., Semsarilar, M., Guthrie, J.T., Perrier, S., 2009. Cellulose modification by polymer grafting: A review. Chemical Society Reviews 38, 2046-2064.

Saiki, S., Nagasawa, N., Hiroki, A., Morishita, N., Tamada, M., Kudo, H., Katsumura, Y., 2011. ESR study on radiation-induced radicals in carboxymethyl cellulose aqueous solution. Radiation Physics and Chemistry 80, 149-152.

Samain, X., Langlois, V., Renard, E., Lorang, G., 2011. Grafting biodegradable polyesters onto cellulose. Journal of Applied Polymer Science 121, 1183-1192.

Segal, L., Creely, J.J., Martin, A.E., Conrad, C.M., 1959. An empirical method for estimating the degree of crystallinity of native cellulose using the X-ray diffractometer. Textile Research Journal 29, 786-794.

Takamura, M., Nakamura, T., Takahashi, T., Koyama, K., 2008. Effect of type of peroxide on cross-linking of poly(l-lactide). Polymer Degradation and Stability 93, 1909-1916.

VanderHart, D.L., Hyatt, J.A., Atalla, R.H., Tirumalai, V.C., 1996. Solid-State ^{13}C NMR and Raman studies of cellulose triacetate: Oligomers, polymorphism, and inferences about chain polarity. Macromolecules 29, 730-739.

Wambua, P., Ivens, J., Verpoest, I., 2003. Natural fibres: can they replace glass in fibre reinforced plastics? Composites Science and Technology 63, 1259-1264.

Wei, L., Guho, N.M., Coats, E.R., McDonald, A.G., 2014. Characterization of poly(3-hydroxybutyrate-co−3-hydroxyvalerate) biosynthesized by mixed microbial consortia fed fermented dairy manure. Journal of Applied Polymer Science 131. DOI: 10.1002/app.40333, in press.

Wei, L., McDonald, A.G., 2014. Peroxide induced cross-linking by reactive melt processing of two biopolyesters: poly(3-hydroxybutyrate) and poly(L-lactic acid) to improve their melting processability. Journal of Applied Polymer Science. DOI: 10.1002/app.41724, in press.

Wei, L., McDonald, A.G., Freitag, C., Morrell, J.J., 2013. Effects of wood fiber esterification on properties, weatherability and biodurability of wood plastic composites. Polymer Degradation and Stability 98, 1348-1361.

Wittek, T., 2008. Mechanical properties and fire retardancy of bidirectional reinforced composite based on biodegradable starch resin and basalt fibres. Express Polymer Letters 2, 810-822.

Xu, J., Guo, B., Yang, R., Wu, Q., Chen, G., Zhang, Z., 2002. In situ FTIR study on melting and crystallization of polyhydroxyalkanoates. Polymer 43, 6893-6899.

Yu, H.-Y., Qin, Z.-Y., Wang, L.-F., Zhou, Z., 2012. Crystallization behavior and hydrophobic properties of biodegradable ethyl cellulose-g-poly(3-hydroxybutyrate-co-3-hydroxyvalerate): The influence of the side-chain length and grafting density. Carbohydrate Polymers 87, 2447-2454.

Zhou, W., Zhu, S., 1997. ESR study on peroxide modification of polypropylene. Industrial and Engineering Chemistry Research 36, 1130-1135.

Zoppe, J.O., Habibi, Y., Rojas, O.J., Venditti, R.A., Johansson, L.-S., Efimenko, K., Österberg, M., Laine, J., 2010. Poly(N-isopropylacrylamide) brushes grafted from cellulose nanocrystals via surface-initiated single-electron transfer living radical polymerization. Biomacromolecules 11, 2683-2691.

Chapter 6. Conclusion

6.1 Summary

Petroleum-based plastics are derived from non-renewable resources and require millennia to fully break down, and therefore the drive to develop more environmentally friendly bioplastic materials. The class of bioplastics, polyhydroxyalkanoates, has gained considerable attention due to being both bioderived and biodegradable. However, these bioplastics have some material property and processing limitations and this dissertation aims to correct some of these issues.

As a typical semicrystalline thermoplastic, these bioplastics can be processed into different shapes and realize different applications demands, including the biomedical field. However, it is believed that they also possess shortcomings, especially for PHB, such as high crystallinity characteristic, narrow melt processing window due to the low melt elasticity (strength), low thermodegradation temperature, poor interaction with natural fibers, high cost, and most crucially the brittleness.

To overcome some of these inherent material limitations of PHB and broaden its processing window and applications as well, several strategies have been attempted in this study (Figure 6.1). It was found that processing conditions can influence the final product properties significantly. Therefore, modeling studies of the crystallization process and investigation of the origins of multiple melting behavior of PHB were successfully conducted. Different analytical techniques were employed to provide experimental data to compliment the theoretical model of the PHB melting processes for applications such as injection molding and extrusion. For example, the temperatures of the mold or die and the residence time of specimens are highly dependent on the crystalline kinetics (crystallization rate) and melting behaviors (melting temperatures) of polymers including PHB. Therefore, by varying/modifying the processing parameters the properties of final products are expected to be manipulated.

In addition to adjusting processing parameters to change PHB properties, polymer modifications via (i) long chain branching (LCB) by cross-linking; and (ii) introduction of

fiber reinforcement by grafting to the original polymer system were successfully achieved. To note that similar limitations for PHB homopolymers are also encountered with PLA, such as the poor melt strength and thermal stability, which narrowed its processing window and limits its applications in some areas accordingly. In the former modification approach, PHB and PLLA were individually cross-linked with a small amount of DCP radicals via reactive melt processing, extrusion. The melt strength was improved by cross-linking. Cross-linked PHB and PLLA showed lower degree of crystallinity and smaller crystal sizes (less brittle/more flexible), and better thermal stability due to formation of LCB. All these improvements offered bioplastic processors better material properties and more processing options for PHB and PLA, such as foaming and thermoforming, for new applications.

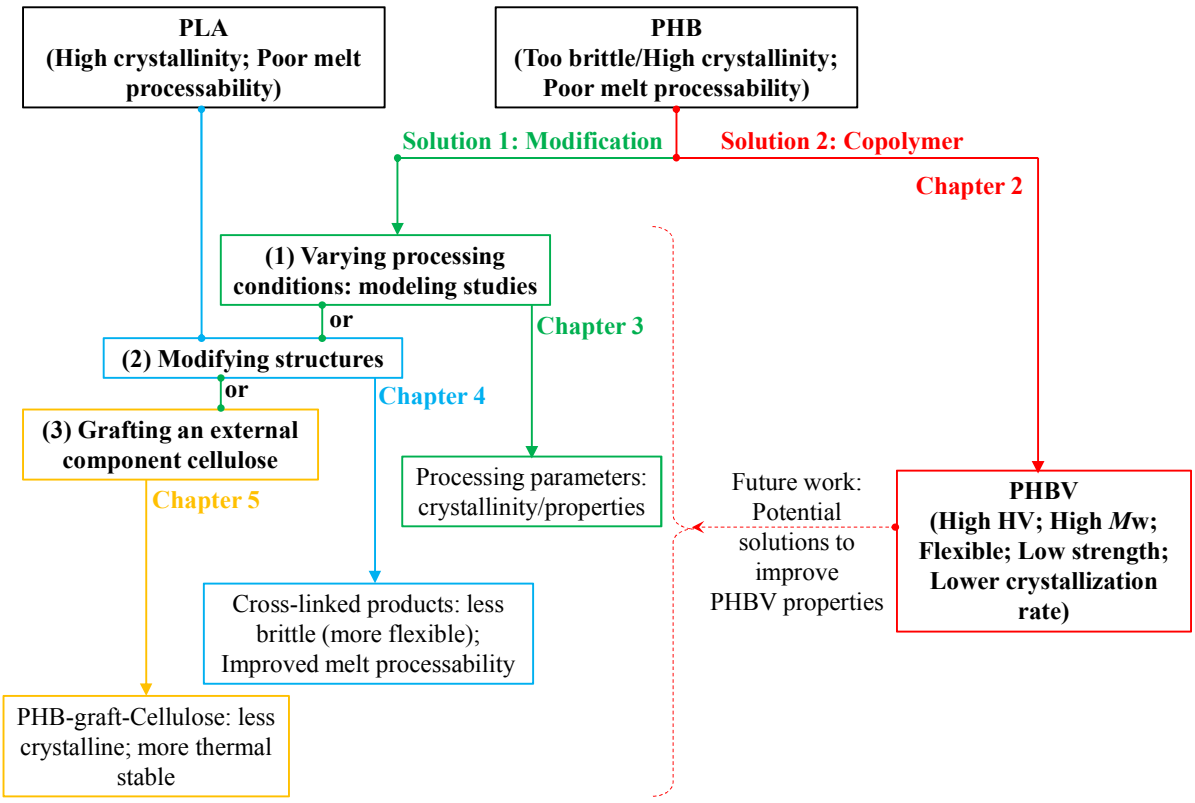

Figure 6.1. Schematic diagram showing the linkages of each chapter of this dissertation.

Apart from modifying PHB structure by cross-linking, cellulose fibers can be added to impart reinforcement. Furthermore, the cellulose fibers were grafted onto PHB to improve their compatability. In order to understand the grafting mechanism occurring between PHB (and other PHA) and cellulose interfaces, PHB was grafted onto cellulose fiber by DCP radical initiation via *in-situ* reactive extrusion method. Spectroscopic (ESR, NMR, and FTIR), morphological (SEM) and crystalline structural (FTIR, DSC, and XRD) studies showed by varying the reaction conditions the resulting copolymerized biocomposites with tunable properties. Grafting between cellulose and PHB, acted as a coupling agent in the resultant biocomposites materials and improved the stress transfer between the two phases. This study clearly showed the potential of reinforcing PHAs with cellulose fibers.

As compared to PHB homopolymers, the PHBV copolymer has different properties, such as better flexibility/ductility, especially those with higher HV content. A unique PHBV with high HV content (~ 35%) and M_w was biosynthesized by mixed microbial consortia fed fermented dairy manure and its properties determined. To establish the relationship between its chemical structure and properties, NMR and ESI-MS were used to determine its comonomeric distribution. Results showed random copolymer PHBV was synthesized. The isolated PHBV was flexible due to low crystallinity which was attributed to its high HV content and M_w as compared to most commercial PHBV (with HV = 0 - 20%). This bioplastic can be used for packaging applications (i.e. garbage bags for short-term uses). Despite these advantages of PHBV as compared to PHB homopolymers, still has poor thermal stability, low mechanical strength (modulus), slow crystallization rate, and poor interaction with hydrophilic fibers still require potential modifications. The aforementioned modification means for PHB (or PLA) are applicable for PHBV to broaden its property range and applications.

6.2 Future work

After isolating PHAs from dry biomass, the residual bacterial biomass (~60 wt%) is usually discarded as waste. Pyrolysis and/or hydrothermal treatment are attractive processes to convert this residual biomass into sugars and chemicals which can then be reutilized in a

fermenter to generate VFAs. This approach will use and remaining carbon and nitrogen sources to biosynthesize PHA from the VFA.

A logical step forward is to improve PHBV properties by cross-linking and grafting onto cellulose fibers as outlined respectively in chapters 4 and 5. Cellulose fibers and cellulose nanocrystals can be generated from low value small diameter (thinnings) trees such as *lodgepole pine*. Using these forest residues can improve forest health by reducing forest fuels caused by overstocked stands in the Inland-Northwest forestland.